NASA CR-73394
(AVAILABLE TO THE PUBLIC)
TRW ER-7256-20

AIRCREW OXYGEN SYSTEM DEVELOPMENT

WATER ELECTROLYSIS SUBSYSTEM REPORT

BY

A. D. BABINSKY AND T. P. O'GRADY

PREPARED UNDER CONTRACT NO. NAS-2-4444

BY

TRW INC.
CLEVELAND, OHIO

FOR
AMES RESEARCH CENTER
NATIONAL AERONAUTICS AND
SPACE ADMINISTRATION

MAY 1970

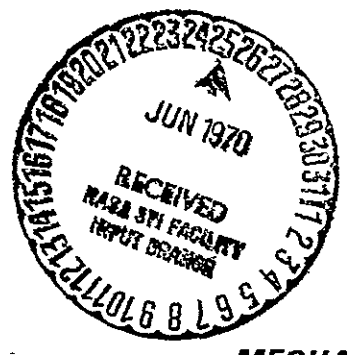

TRW®
MECHANICAL PRODUCTS DIVISION

NASA CR-73394
(Available to the Public)

AIRCREW OXYGEN SYSTEM DEVELOPMENT
WATER ELECTROLYSIS SUBSYSTEM REPORT

by

A. D. Babinsky and T. P. O'Grady

May 1970

Prepared under Contract No. NAS2-4444

by

TRW INC.
Cleveland, Ohio

for

AMES RESEARCH CENTER
NATIONAL AERONAUTICS AND SPACE ADMINISTRATION

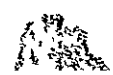

TABLE OF CONTENTS

LIST OF FIGURES

LIST OF FIGURES
(Cont.)

LIST OF FIGURES
(Cont.)

LIST OF FIGURES
(Cont.)

LIST OF FIGURES
(Cont.)

LIST OF TABLES

SUMMARY

Liquid oxygen systems (LOX) currently used in military aircraft present a significant logistics problem. To replace these LOX systems a program was initiated under Contract No. NAS2-4444 to develop a closed loop aircrew oxygen system which generates oxygen on-board the aircraft as required. A water electrolysis module is used as the oxygen generator while the amount of oxygen required is decreased significantly under open-loop requirements through the use of a closed loop rebreather subsystem.

The Water Electrolysis Module (WEM) was designed as a laboratory type module utilizing air-cooled fins for heat removal and a static water feed system such that the module is capable of operation in all degrees of rotation. The physical characteristics of the cells and modules are summarized as follows:

Electrode Area:	33 in^2 (per cell)	No. Cells per Module:	10
Electrode Type:	AB-6	Module Size (Overall):	7.75x11.0x4.39
Electrolyte Matrix:	Asbestos	Module Weight:	50 Pounds
Cell Material:	Polysulfone	Module Voltage:	20 Volts
Cell Size (Overall):	7.75x11.0x0.36	Module Power:	$\leq$460 Watts
Current Density:	100 ASF	O_2 Generation Rate:	0.15 lb/hr

The individual cell structural components were machined from extruded polysulfone sheets. Endplates were machined of 3/8 inch thick stainless steel plate. Current collectors were formed by nickel plating copper sheets, followed by drilling and shearing to size after the plating operation. Electrodes, asbestos matrices and plastic screens were hand-cut to size. Module assembly was accomplished by stacking the individual components for ten cells on an assembly fixture. Insulated drawbolts, torqued in a predetermined pattern complete the module assembly.

A test stand was designed and assembled to provide all the services, controls and instrumentation required for operation of the Water Electrolysis Module test plan including parametric, cyclic and extended life testing. Several modifications were made to increase the test rig reliability including removal of solenoid valves from shutdown circuitry, installation of a four-day capacity water feed tank and increased water capacity in condenser-filter trap assemblies.

Parametric testing was accomplished to determine the performance of the module over a range of operating conditions including temperatures up to 182°F, pressures up to 65 psig, and $\pm$5.0 psi pressure differential across the cell matrix. Water balance studies were conducted over a 121-hour test period indicating a range of electrolyte concentrations of 0 to 13% KOH in the oxygen compartment and 22% KOH in the hydrogen cavity. Initial charge concentration was 25% KOH. Oxygen purity was shown to be over 99.5% by volume as measured by a Beckman E-2 Analyzer. Water feed tests demonstrated the applicability of the static feed concept using non-degassed water. Overcapacity was demonstrated by

operation at 150 ASF for 8.5 hours. Typical polarization data, with cell operating at 175°F and 67 psig, is as follows:

Current Density, Amps/Ft^2	Cell Voltage, Volts
25	1.58
50	1.64
75	1.67
100	1.71
125	1.73
150	1.76

Total parametric test time was 280 hours.

Module life testing consisted of cyclic tests to demonstrate short-term cold start operation and long-term tests to demonstrate long term operational stability and materials stability. The cyclic tests consisted of nineteen module startup-shutdown sequences with approximately ten hours of operation per run. Module operating conditions for these tests (total test time - 200 hours) were as follows:

Current Density, amps/ft^2	100
Stack Temperature, °F	174-185
O_2 Pressure, psig	50-67
O_2 to H_2 ΔP, psid	1.0-2.8
Stack Voltage, range, VDC	17.9-23.0
Cycle Duration, range, hrs.	5.3-10.2

Long-term life testing started in August at 480 hours module test time and continued through to December 1969 accumulating an additional 10,014 hours to yield a total test time of 10,494 hours. During the life of the module the assembly was exposed to electrolyte for a total of 13,607 hours. During the life test a number of shutdowns were encountered due to reasons as summarized:

No. of Shutdowns	Cause of Shutdown
11	Test rig service
32	Test rig malfunction
4	Operator error
6	Service interruption
5	Module malfunction
1	Module recharge

Module malfunctions consisted of two separate failures of water feed matrix support screens, two incidences of electrolyte leakage through epoxied access port plugs and one failure of cell matrix. The last failure occurred several days prior to scheduled shutdown. This failure of the cell matrix was the only such failure of WEM #1 during the entire test period of 10,494 hours spanning a period of 16 months.

The major conclusions relative to the water electrolysis module development based on information derived from the NAOS development program are:

1. The long-term operational capability of the WEM as designed was demonstrated in the life test in which WEM #1 was operated for 10,494 hours.

2. The ability to maintain design performance capability for extended periods of continuous operation was demonstrated.

3. The module proved capable of immediate full operation after long storage periods in the charged (electrolyte) condition.

4. Additional study is required to establish more suitable materials for use in supporting the water feed matrix.

Based on NAOS program experience it is recommended that a Water Electrolysis Module Development Program should be continued, incorporating the following:

- Provision of a liquid-gas separator for degassing the feed water cavity
- Improved water feed matrix support
- Decrease the number of cell components and number of seals per cell
- Provide more integral structure for metal components to reduce electrical losses due to formation of metal oxides
- Improve sealing design
- Elimination of expoxied access ports
- More suitable selection of cell electrolyte concentration
- Selection of oxygen electrode more specifically designed for application
- Incorporation of internal liquid cooling passages
- Submodule construction to improve ease of assembly, check-out and repair

Several appendices are included to provide additional details in the following three areas:

1. A study of the degree of effectiveness of the use of aqueous glycol, aqueous methanol and tap water feed in a static water feed electrolysis system.

2. Thermal analysis to determine most effective means of heat removal for a water electrolysis subsystem as designed for use in the F-111 aircraft.

3. Detailed results of the photographic and visual study of the component parts of WEM #1 by post-test disassembly inspection.

INTRODUCTION

TRW, under NASA Contract NAS2-4444, developed an aircrew oxygen system using electrochemical oxygen generation and carbon dioxide removal. The objective of the program was to develop a feasibility demonstration model of a safe, reliable, compact system which could replace the presently used LOX systems.

Aircraft oxygen systems are currently limited to the use of stored supplies of oxygen in the form of liquid oxygen or high pressure gaseous oxygen. Use of oxygen from these sources limits the duration of a mission to the amount of stored gases and creates somewhat of a problem in logistics and service to provide the needed oxygen.

A means of avoiding these problems is the provision of a method of continuously generating oxygen on board the aircraft as oxygen is required. This can be accomplished electrochemically by electrolysis of water or concentration of oxygen from the ambient air. The size and power requirements of these electrochemical oxygen generators would be prohibitive when coupled to an open loop aircraft oxygen system. If, however, a rebreather loop is provided such that the oxygen used corresponds to the pilot's metabolic consumption, the size of the oxygen generator and rebreather loop becomes competitive with a present-day LOX converter system.

The rebreather loop functions to recondition the exhaled gas such that it can be reused in the breathing cycle. The rebreather thus removes exhaled carbon dioxide, nitrogen, water vapor and heat.

Generation of oxygen by water electrolysis was selected to make the system independent of air source (high altitude or space application). The water is presently replenished by refill of a water tank between missions. The basic electrolysis cell consists of an electrolyte containing asbestos matrix sandwiched between two catalyzed screen electrodes, producing oxygen by the following electrode reactions:

$$\text{Cathode:} \quad 4H_2O + 4e^- \longrightarrow 4OH^- + 2H_2$$

$$\text{Anode:} \quad 4OH^- \longrightarrow 2H_2O + O_2 + 4e^-$$

* Water is added to each cell in the hydrogen compartment by a static feed mechanism, as required.

The design philosophy was to develop a water electrolysis module of laboratory type (non-optimized with respect to weight, volume, or performance) design, with the capability for operation independent of gravitational orientation. The development of the Water Electrolysis Subsystem (WES) consisted of the following subtasks:

- Design of the Water Electrolysis Module (WEM), the static water feed system, module pressure controls and the Water Electrolysis Module Test Stand.

- Fabrication of WEM, water feed tank, test stand and accessory components.

- Conduct parametric testing of WEM to establish operating characteristics over a range of operating conditions, i.e., determine cell voltage as a function of current density, as a function of cell operating temperature, pressure and pressure differentials across cell matrices. Additional tests included oxygen purity measurements and moisture balance and feed water quality checks.

- Conduct a series of cold startup, short-term cyclic tests to determine applicability of WEM design to aircraft type use profiles.

- Long-term life tests to demonstrate long-term performance stability and materials suitability for extended use when exposed to electrolyte-temperature-pressure-voltage-gas operating environment.

- Perform feed water studies using small cell hardware to determine the suitability of using tap water and anti-freeze-water mixtures as emergency water supplies for WEM feed water -- this data reported in Appendix A.

- Perform a thermal balance study on WEM to determine most suitable cooling mode for application to a system installed in an F-111 aircraft -- reported in Appendix B.

- Perform post-test inspection of WEM #1 components following completion of life test to determine the condition of materials selected and used in the WEM #1 design, fabrication and test.

The Water Electrolysis Module design used in the above tasks was used in fabricating three additional modules which were used in the Laboratory Breadboard System and Flight Breadboard System test programs.

Performance of WEM #1 was generally satisfactory in all test phases, meeting and, in many instances, exceeding design specifications. Significant information concerning changes to be made in improving future module design was obtained in all program test phases.

WATER ELECTROLYSIS MODULE DESIGN

Design Objectives

One of the objectives in the development of the on-board aircrew oxygen generating system was to design, fabricate and test a full-scale laboratory model of the 0.15 lb/hr oxygen generating water electrolysis cell, utilizing air-cooled fins to remove the heat and the associated static water feed system having a ten-hour flight capacity.

The design philosophy was to verify design concepts and module performance and, therefore, current density was not maximized nor were cell thickness and weight minimized.

Parametric testing of the electrolysis module included investigation of the following parameter ranges: current density variation from 0 to 100 amps/ft^2; operating temperature to 180^{o}F; and an operating pressure range from atmospheric to 80 psia. Cell design was therefore governed by those parameter ranges.

General Cell Configuration and Operation

The schematic presented in Figure 1 illustrates the basic cell construction chosen for the electrolytic oxygen generator. The electrolyte is held in a porous matrix, sandwiched between two catalytically active (platinized) electrodes. A water feed membrane separates the feed water cavity (containing electrolyte) from the gaseous hydrogen compartment. This type of configuration

(a) permits relatively large pressure differentials to exist between the individual compartments (3-5 psia is the anticipated operating differential);

(b) allows the cell electrodes to be spaced close together (within 0.03 inches) which reduces the cell size and weight and lowers the internal resistance (power requirements);

(c) avoids bulk electrolyte in the gas compartment that would ultimately require bulky (large capacity) zero gravity, gas/liquid separators;

(d) prevents electrolyte aerosol from forming and being carried out of the cell with the evolved gases (by maintaining oxygen cavity pressure > hydrogen cavity pressure > feed water cavity pressure); and

(e) prevents contamination of the oxygen with hydrogen (by maintaining oxygen cavity pressure above hydrogen cavity pressure).

Cell operation is, as follows: When power is applied to the electrodes, water from the cell electrolyte is decomposed. As a result, the concentration of the electrolyte in the cell matrix increases above its initial value of 25% KOH, and thus its vapor pressure is reduced to a level below that of electrolyte in the water feed cavity which theoretically remains at the 25% KOH concentration

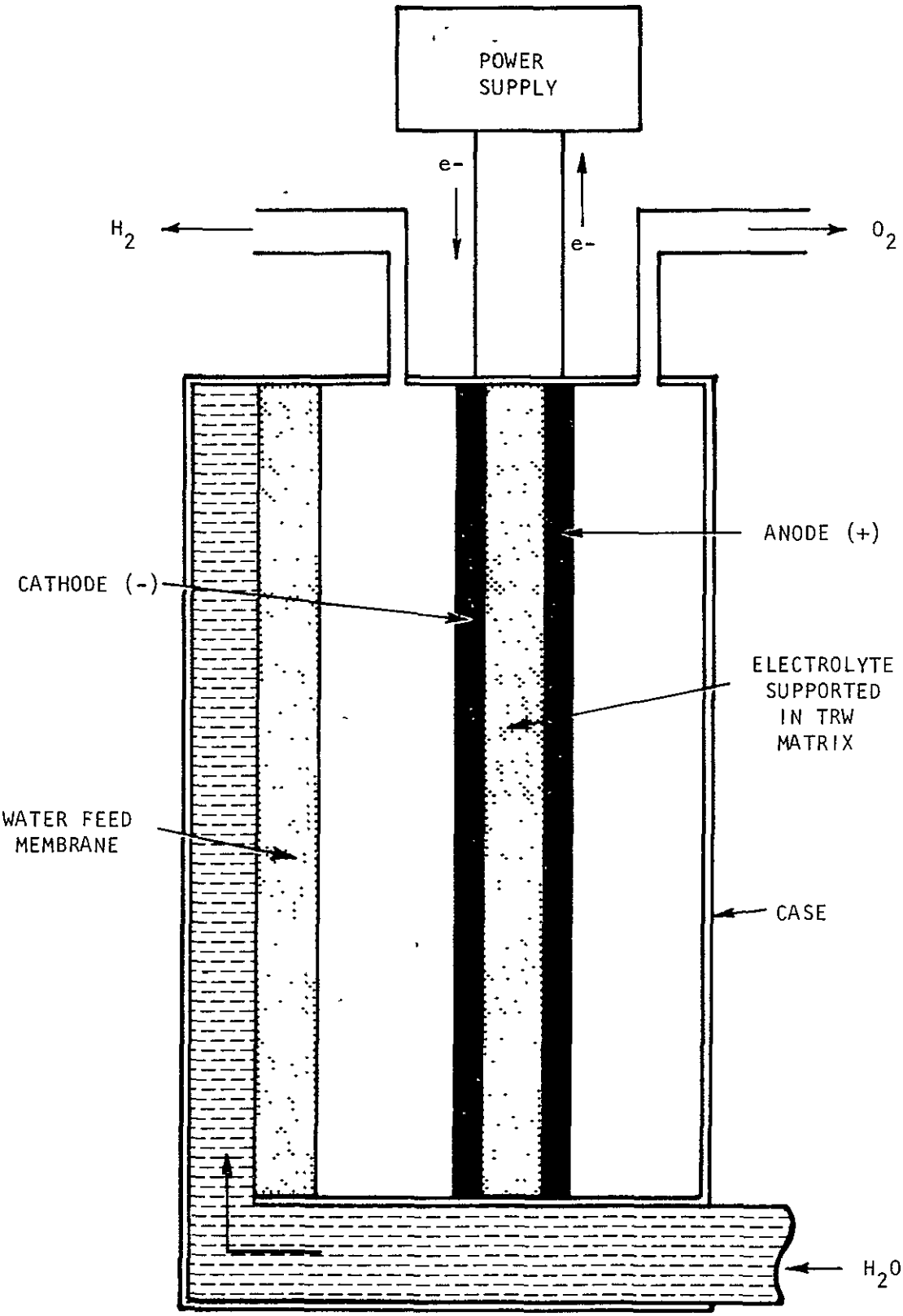

FIGURE 1 WATER ELECTROLYSIS CELL SCHEMATIC

equilibrium condition. The vapor pressure differential produced by the increase in cell matrix electrolyte concentration causes water to diffuse from the water cavity feed membrane through the hydrogen cavity and electrode into the cell electrolyte. This diffusion process continues as long as the cell electrolyte vapor pressure is maintained at a value below that of the water feed matrix electrolyte by electrolytic decomposition of cell matrix water. The transfer of water from the water feed cavity to the cell matrix tends to reduce the water volume in the feed compartment. However, the resulting drop in pressure level in the feed compartment offsets this tendency by drawing make-up water from an external reservoir into the feed compartment.

Design Details

To generate 0.15 lb/hr of oxygen requires 228 amperes. At a current density of 100 amps/ft^2 (at 2 volts, a conservative performance level based on past test experience) an active electrode area of 330 in^2 is required. To keep current level to a minimum, but above the maximum available voltage level of 20 VDC, a ten-cell stack, electrically connected in series, was selected. The active electrode area per cell is, therefore, 33 in^2 with a stack current of approximately 23 amps and a nominal stack voltage of 20 VDC.

The plane dimensions of the active electrode area and also water feed compartment are 4.75 inches wide by 7.00 inches long with 0.25 inch radius corners. These dimensions were based on a partial optimization with respect to heat removal, since going from a square to a rectangular opening allows for more optimum heat removal when using air-cooled external fins. (See Appendix A)

Based on power requirements for water decomposition and materials compatibility considerations, an aqueous solution of KOH was selected as the cell electrolyte.

One of the foremost considerations that governed the cell and stack design was to electrically isolate the feed water manifolding and compartments from any cell potential. This is essential for cells with static water feed systems since generation of gases, due to electrolysis, in these passages causes an increase in electrolyte concentration (by liquid displacement) in the feed compartments which can lead to eventual cell dry-up.

Based on structural and compatibility requirements, the basic materials selected were polysulfone structural components, ethylene propylene gaskets and seals, polypropylene screens and nickel (or nickel-plated) current collector heat removal plates.

Figure 2 shows a cross-section of a unit cell of the module. Table I identifies the numbered items, including material of construction. The laboratory module consists of ten such cell units stacked in series and held between two 3/8 inch thick stainless steel end plates by twenty-six #10-32 drawbolts.

As can be seen from Figure 2, intercavity sealing is accomplished by compressing the cell and feed asbestos matrices (items 7 and 13). O-rings (items 1 and 4) seal cavities and manifolds from the environment.

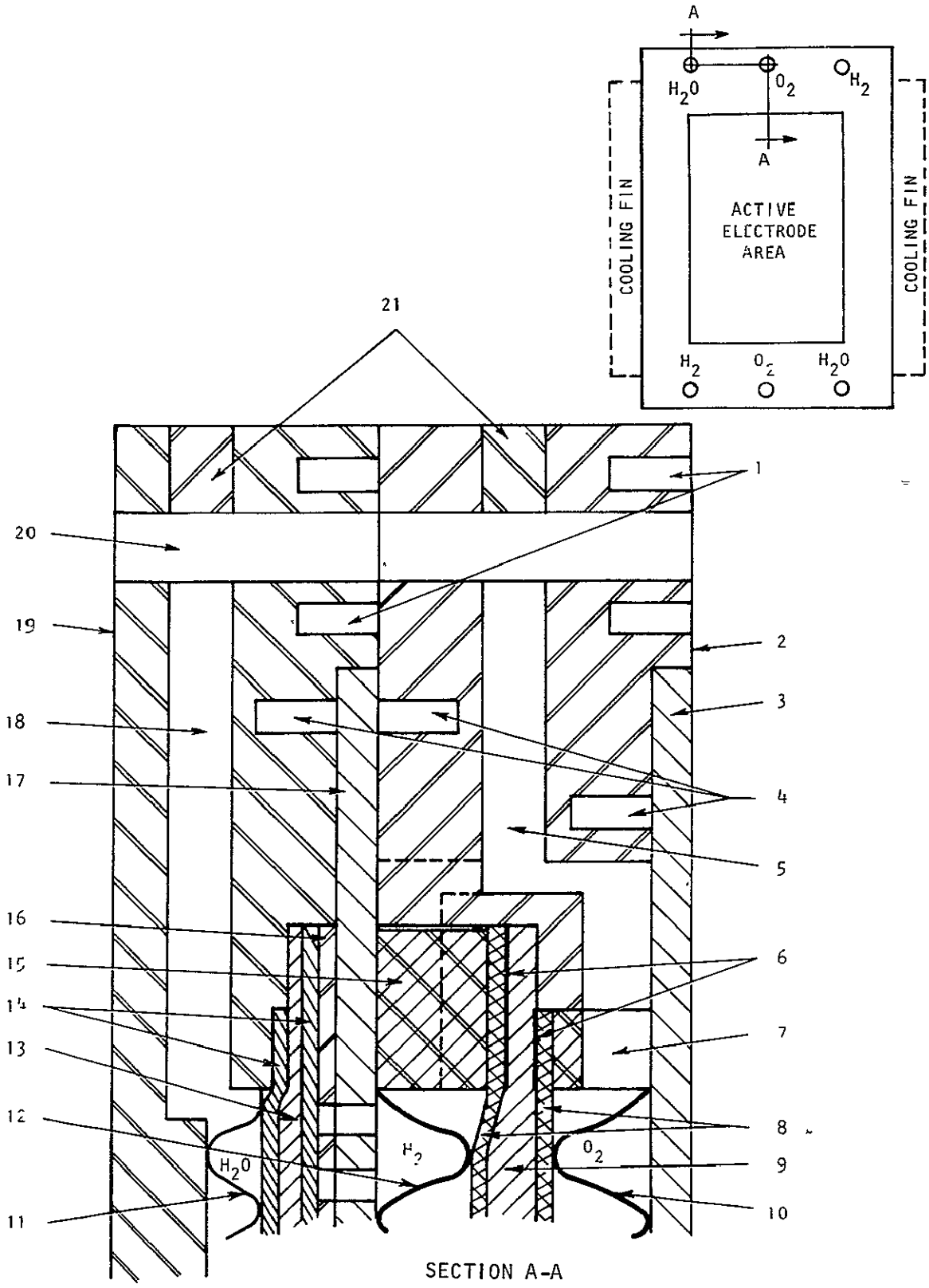

FIGURE 2 NAOS ELECTROLYSIS CELL - SECTION THROUGH MANIFOLD AREA

TABLE I

ELECTROLYSIS CELL COMPONENTS

Item		
1	Manifold O-Rings	Ethylene Propylene
2	H_2 - O_2 Frame	Polysulfone
3	Current Collector, Plain	Nickel-Plated Copper
4	Cavity Sealing O-Rings	Ethylene Propylene
5	.042" Dia. O_2 Passage	N/A
6	Insulating Tape	Teflon
7	Support Spacer	Nickel 270
8	Electrodes	AB-6
9	Cell Matrix	.030" Asbestos
10	O_2 Cavity Spacer	Expanded Nickel
11	H_2O Cavity Spacer	12 Mesh, .020" Threads, Polypropylene Screen
12	H_2 Cavity Spacer	Expanded Nickel
13	Feed Matrix	.015" Asbestos
14	Feed Matrix Support Screens	ASTM #70 Mesh, Polypropylene Screen
15	Support Spacer	Nickel 270
16	Insulator	Polysulfone
17	Current Collector, Slotted	Nickel-Plated Copper
18	.042" Dia. H_2O Feed Passage	N/A
19	H_2O Feed Compartment Frame	Polysulfone
20	Gas or Liquid Manifold	N/A
21	Plug	Polysulfone

All manifolding for liquid and gas flow is internal, connecting respective cell compartments in parallel. Each individual cell cavity (water feed, hydrogen, oxygen) is connected to two separate, internal stack manifolds located on opposing ends of each cavity.

The current collectors (items 3 and 17) have two functions: first, they provide electrical continuity and, second, they conduct the heat, generated by cell inefficiencies (activation, concentration and ohmic polarization) from the cell interior to external air-cooled (forced convection) fins. The finning is simply accomplished by extending the current collectors past the outer edges (on two sides only) of items 2 and 19. The finning is limited to the two 7 inch dimension sides only, thus avoiding manifold-current collector sealing problems. The loss of the short side (4.75 inch) cooling is negligible due to the larger heat paths. Based on an average internal temperature gradient of 8°F, a plate thickness times thermal conductivity product of 0.367 btu/hr-°F was needed. To keep current collector thickness to a minimum, copper sheet (0.020 inches thick), nickel-plated for corrosion protection (0.0025 inches each side), was selected.

The nickel frames, items 7 and 15, serve as compression rings for oxygen to hydrogen cavity sealing plus providing positive current paths (in parallel with items 10 and 12) from the current collectors to the electrodes.

The teflon tape, item 6, eliminates electrolysis in the compressed areas of the cell matrix, thus avoiding buildup of high concentration electrolyte.

Table II summarizes the cell and module physical characteristics.

TABLE II

PHYSICAL CHARACTERISTICS OF CELLS AND MODULES

Electrode Area (per cell)	33 in^2
Electrode Type	AB-6
Electrolyte Matrix	Asbestos
Cell Material (frames)	Polysulfone
Cell Size (overall)	7.75 x 11 0 x .36
Cell Voltage	≤ 2 0 Volts
Current Density	100 ASF
Number Cells per Module	10
Module Size (overall)	7.75 x 11.0 x 4.39
Module Weight	50 Pounds
Module Voltage	20 Volts
Module Power	≤460 Watts
O_2 Generation Rate	0.15 Lb/Hour

STATIC WATER FEED DESIGN

Design Objectives

The function of the static water feed device is to replace the water that is evaporated from the feed matrices while maintaining the maximum feed compartment pressure level below that of the hydrogen compartment. The capacity of the feed reservoir for the laboratory electrolysis module is sufficient to supply enough water to generate 0.15 lb/hr of oxygen for ten hours, plus account for the humidification of the generated gases.

Materials of construction are compatible with the cell electrolyte (KOH).

Maximum operating pressure levels reach 80 psia.

Design Details

The feed water system consists of a water reservoir, pressure regulating devices and interconnecting lines. The pressure regulating devices employ the oxygen product gas supply in maintaining the water cavity at a reference pressure level 0 to 5 psi less than that of the hydrogen compartment.

Figure 3 shows a section through the water feed reservoir. The reservoir consists of a cylindrical container with the internal volume divided into liquid and gas compartments by a flexible diaphragm. The gas compartment is connected to the low pressure end of the pressure reduction devices (oxygen flow side). The liquid compartment is filled with water and is connected to the feed water manifold of the electrolysis cell. As water is decomposed in the cell and is replaced by flow out of the reservoir, water volume displacement in the reservoir is continuously replaced with oxygen gas flow.

Transparent cast acrylic tubing is used for the cylindrical side wall to enable visual observation during testing. The flexible diaphragm is sufficient in size to traverse from endplate to endplate. Total useful volume is 89 in^3 (3.2 lbs of water) and is sufficient to sustain oxygen generation at 0.15 lbs/hr for seventeen hours (including humidification requirements at 80 psia and 150^{o}F).

A full size, all plastic (acrylic) model of the water reservoir was fabricated and tested with a multi-cell electrolysis module. The tests verified the design concept. Reservoir orientation with respect to gravity had no effect on its operation.

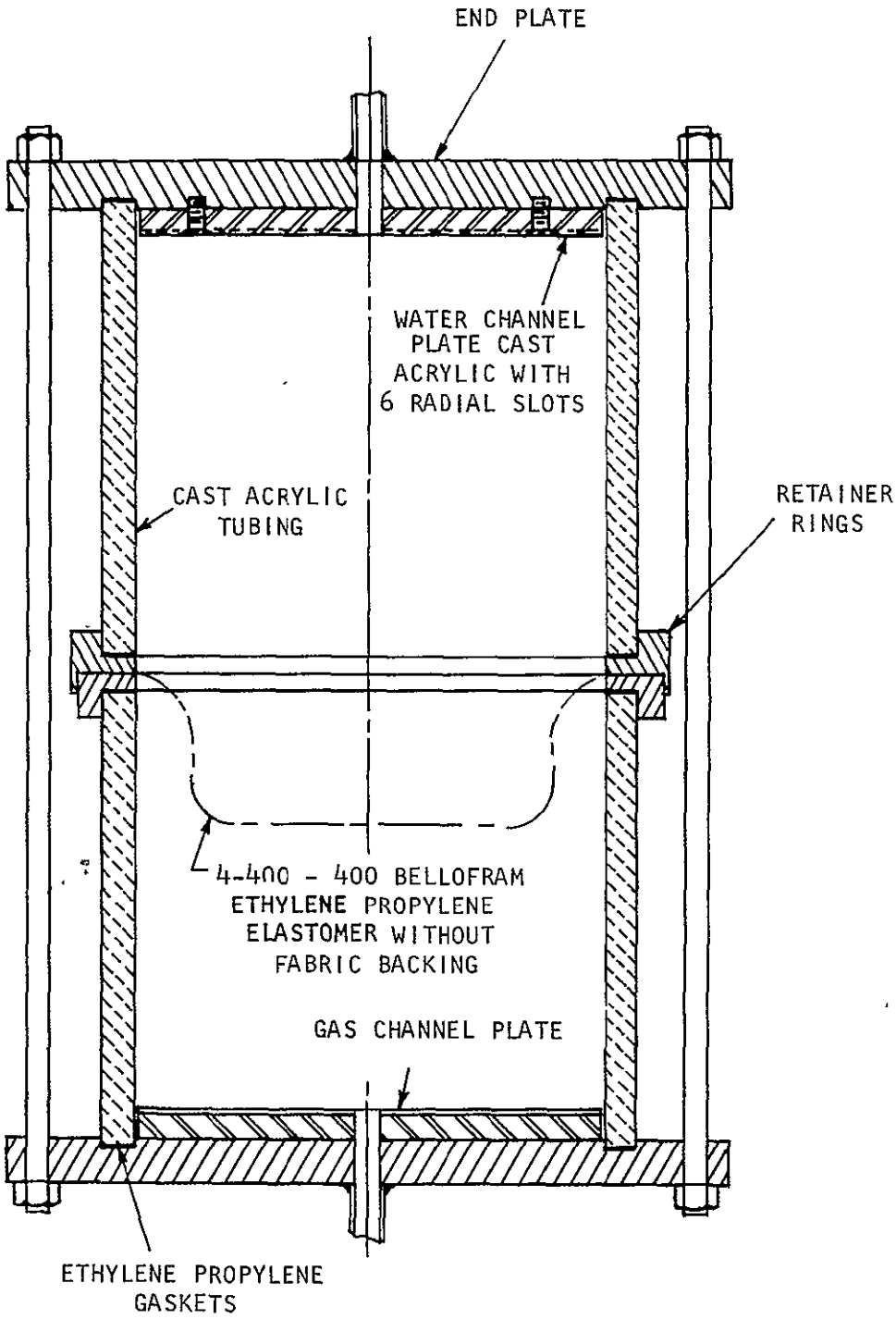

FIGURE 3 WATER FEED TANK FOR TEST RIG

MODULE FABRICATION AND ASSEMBLY

The main structural components of a unit cell of the water electrolysis module are the water cavity plate and hydrogen-oxygen plate. Both are shown in Figure 4. The plates were machined from extruded polysulfone sheets. Bolt and manifold holes were drilled with the aid of a specially designed drill fixture. The water cavity plate subassembly shown in Figure 5 consists of the water cavity plate, a water cavity spacer (12 x 13 mesh, 20 mil yarn polypropylene screen), two support screens (70 mesh polypropylene), the asbestos feed matrix (15 mil fuel cell paper) and a slotted 10 mil polysulfone spacer. Both the water cavity spacer and its adjacent support screen are resin-bonded to the water plate. The polysulfone slotted spacer is resin-bonded to its adjacent support screen and, after the feed matrix is positioned, the spacer and screen are in turn resin-bonded to the water plate.

Figure 6 shows the structural endplates for the multi-cell electrolysis module and the components that compose a unit cell. The endplates were machined from 3/8 inch thick, 316 stainless steel plate (final thickness is 0.360 inches). One-fourth inch O.D. stainless steel tube stubs, heliarc welded to the plates, serve as water and gas manifold extensions.

The slotted and plain current collectors consist of nickel plated, 0.020 inch thick, half-hard copper sheet. Plating thickness is 0.0025 inches. Sample plating had shown that excessive nickel buildup occurred around bolt holes and along the plate edges. The center configuration of the slotted current collector, however, had a self-shading effect and uniform plating was achieved. Since the bolt holes and plate edges are not exposed to a corrosive environment during module operation, oversized (approximately two inches in each plane dimension) copper sheets were plated and the hole drilling operation and shearing to final dimensions was performed after the plating operation. This sequence of fabrication eliminated special taping and/or shading techniques during plating.

The compression rings were made from standard gage 200 nickel strips, tack welded at the corners to form the required rectangular shapes. Later modules used compression rings milled from nickel sheets in one piece.

Both the hydrogen and oxygen cavity spacers were made from 5 mil thick nickel, expanded to form 60 mil thick separators. The expanded form allows gas flow in the perpendicular and lateral directions. The electrodes are American Cyanamid type AB-6 and the cell matrix consists of 30 mil FCB (Fuel Cell Board).

The O-rings, made from ethylene propylene compound, seal the water, hydrogen and oxygen cavities and the manifolds from the environment.

Module assembly was accomplished with the aid of an assembly stand. Figure 7 shows the stand with a partially assembled stack. Assembly is made cell by cell starting with the water cavity assembly on the metal endplate, then the slotted current collector, and cell assembly with solid current collector.

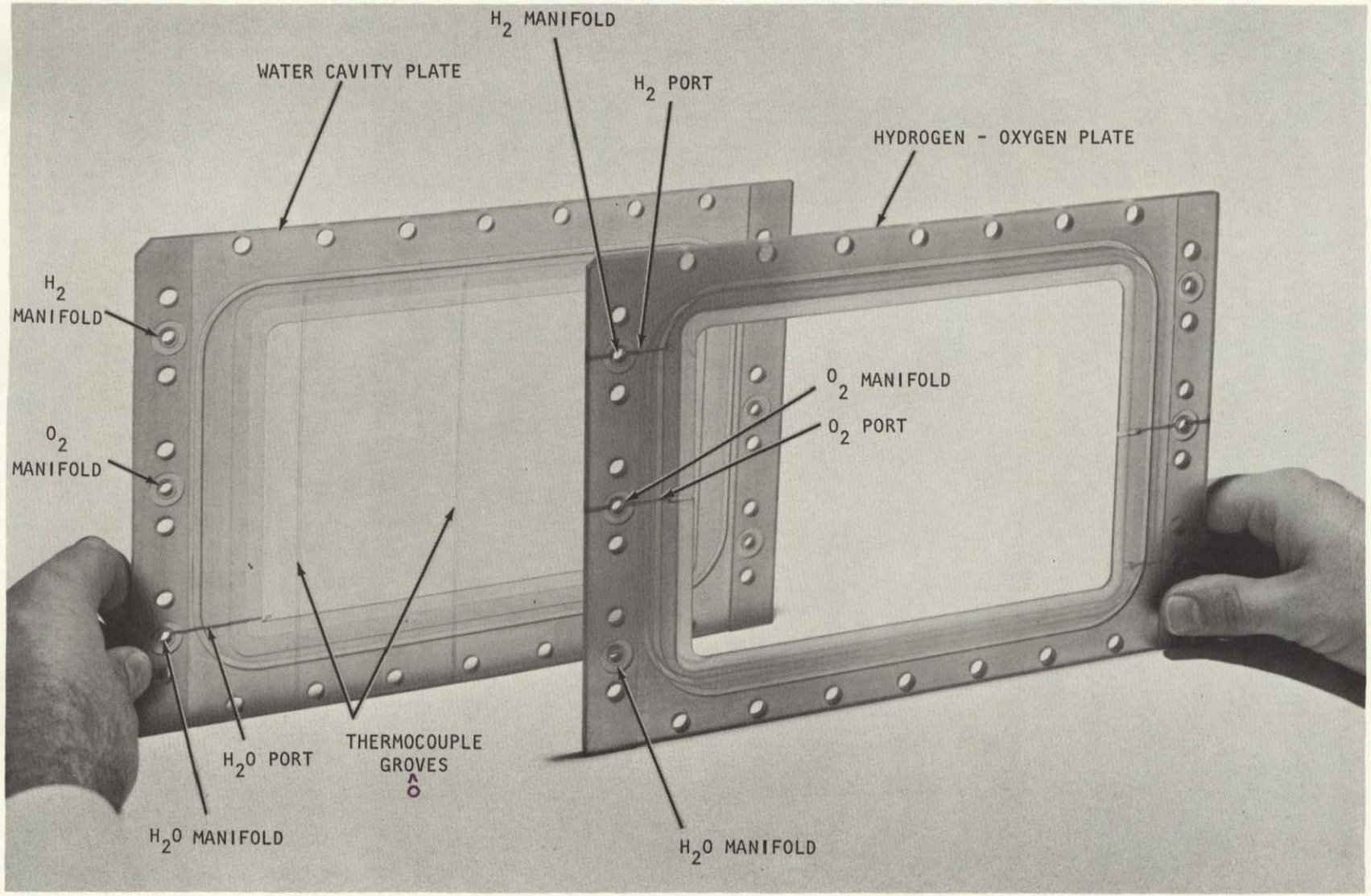

FIGURE 4 WATER ELECTROLYSIS CELL PLATES

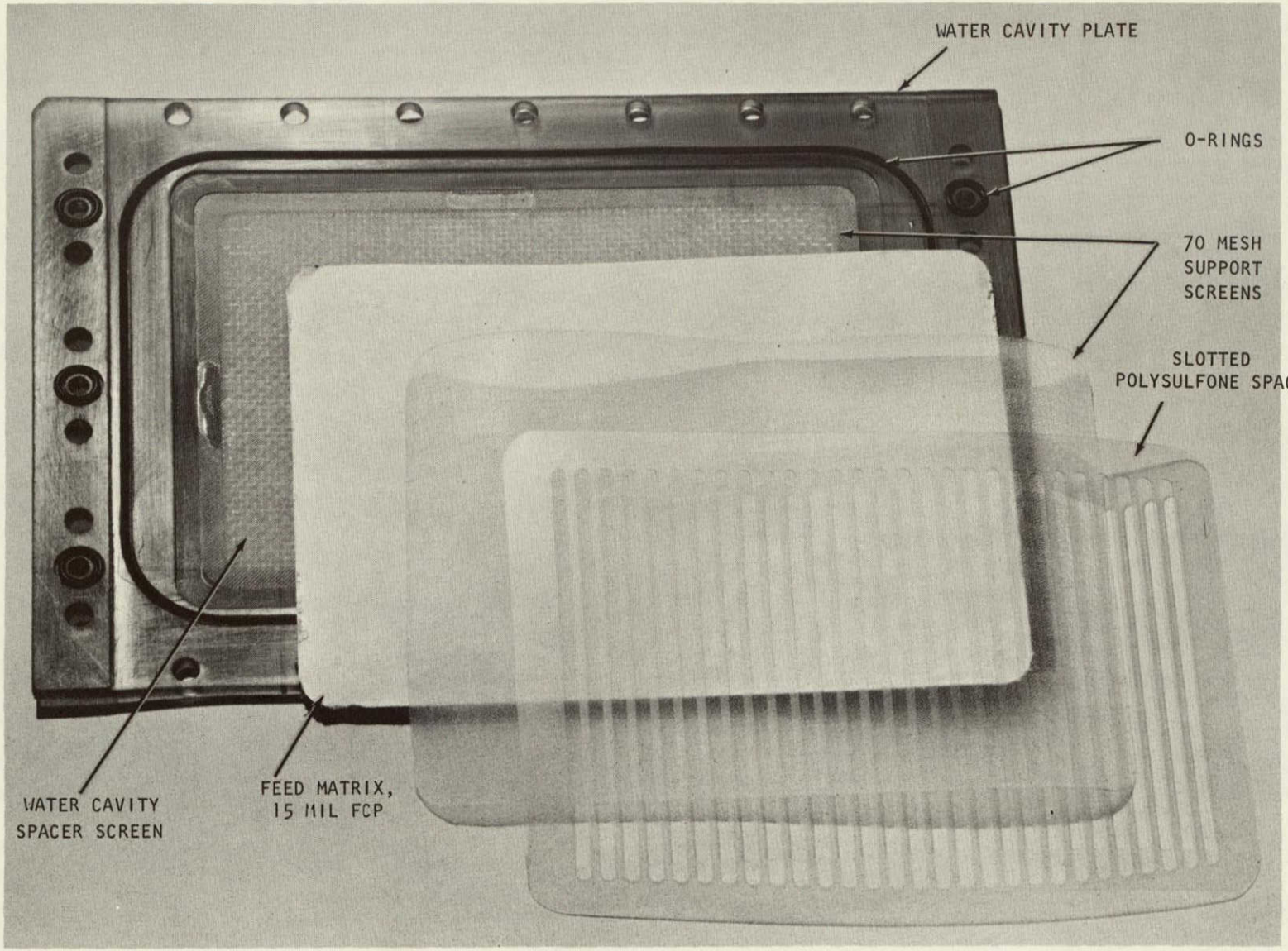

FIGURE 5 WATER CAVITY PLATE SUBASSEMBLY

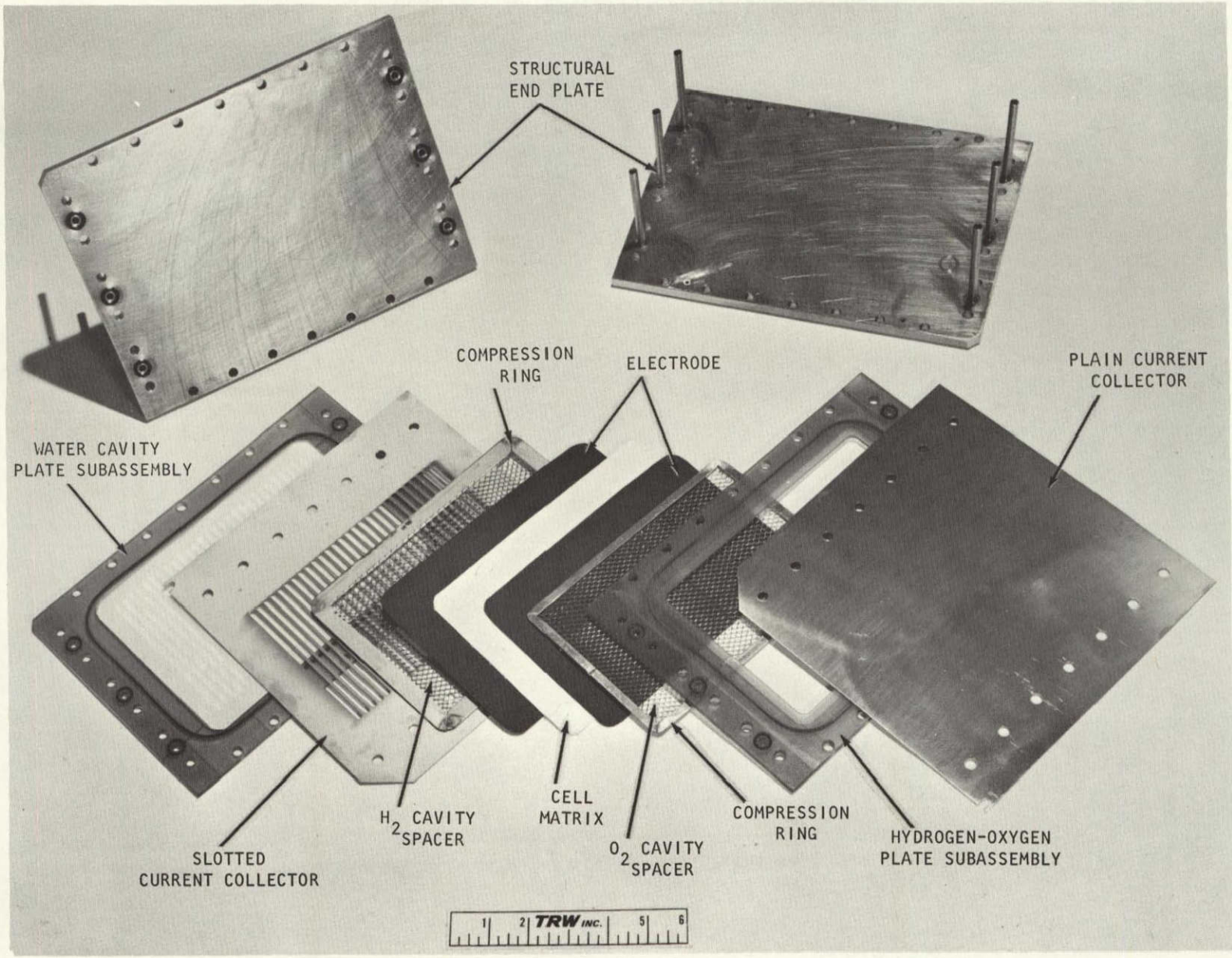

FIGURE 6 WATER ELECTROLYSIS CELL - STACK END PLATES AND UNIT CELL COMPONENTS

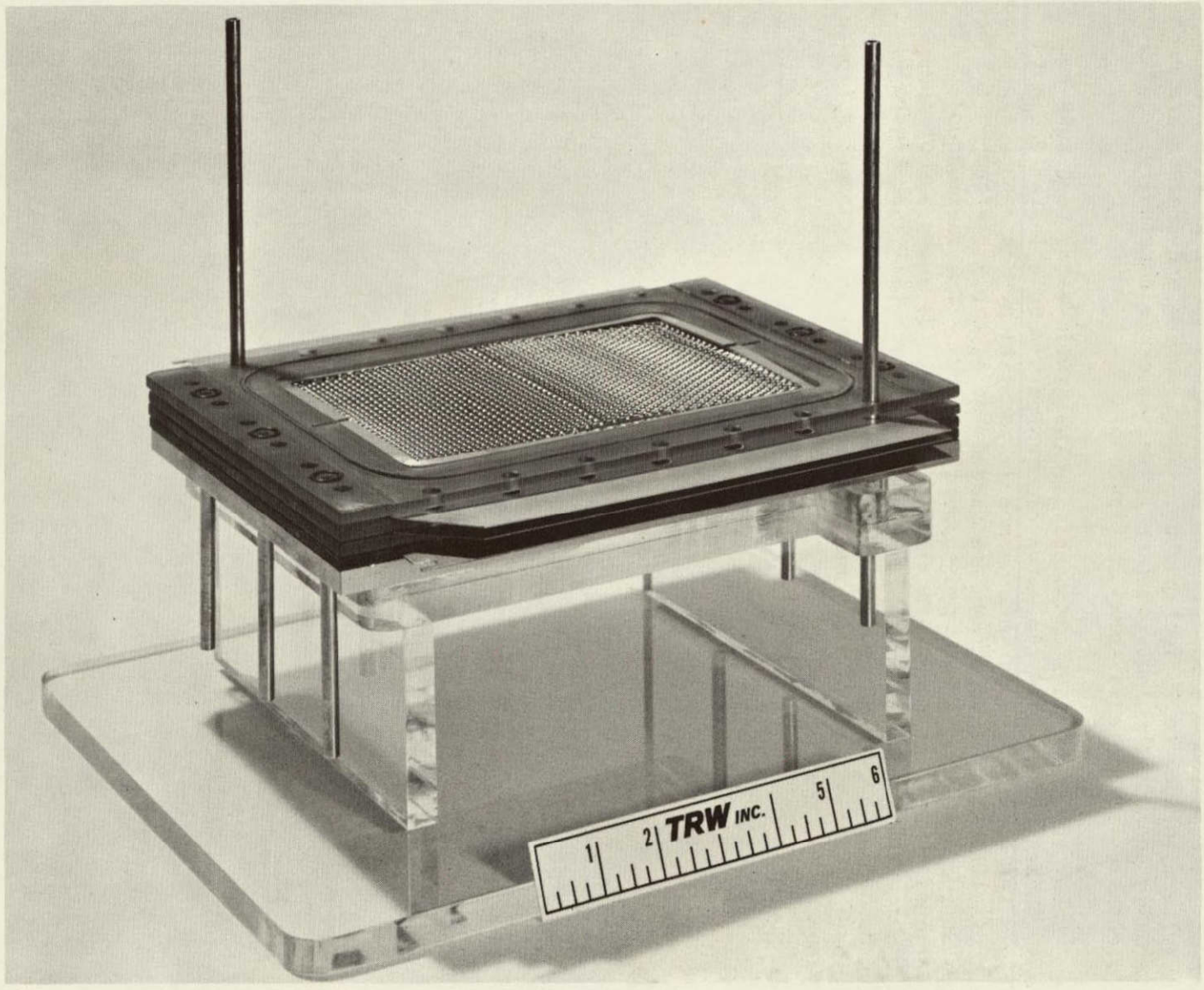

FIGURE 7 WATER ELECTROLYSIS ASSEMBLY STAND WITH PARTIALLY ASSEMBLED STACK

This is repeated until the desired number of cells are stacked on the stand. The other stainless steel endplate is then added. The 26 bolt holes in the stack assembly are lined with teflon tubing to electrically insulate the current collectors from the bolts. The 26 drawbolts (10-32 NF with elastic stop nuts) are torqued to 25 inch-pounds. Brass screws and spacers are used to externally connect the individual cells in series (electrically). A 10-cell water electrolysis module is shown in Figure 8.

Figure 9 shows the individual components of the static water feed tank and Figure 10 shows the tank and the water electrolysis module installed in the test rig. The cooling shroud for the module consists of 3/8 inch resin-bonded acrylic plastic. Only four screws are needed for assembly. Attached to the cooling shroud are the thermocouple support fixtures. The thermocouples can be positioned to any desired depth within the module by using any of the three thermocouple grooves in each water plate of each cell (see Figure 4). The thermocouples have ungrounded junctions within a 0.020 inch O.D. stainless steel sheath. The stainless steel endplates are shown uninsulated in Figure 10 to show module positioning in the test rig.

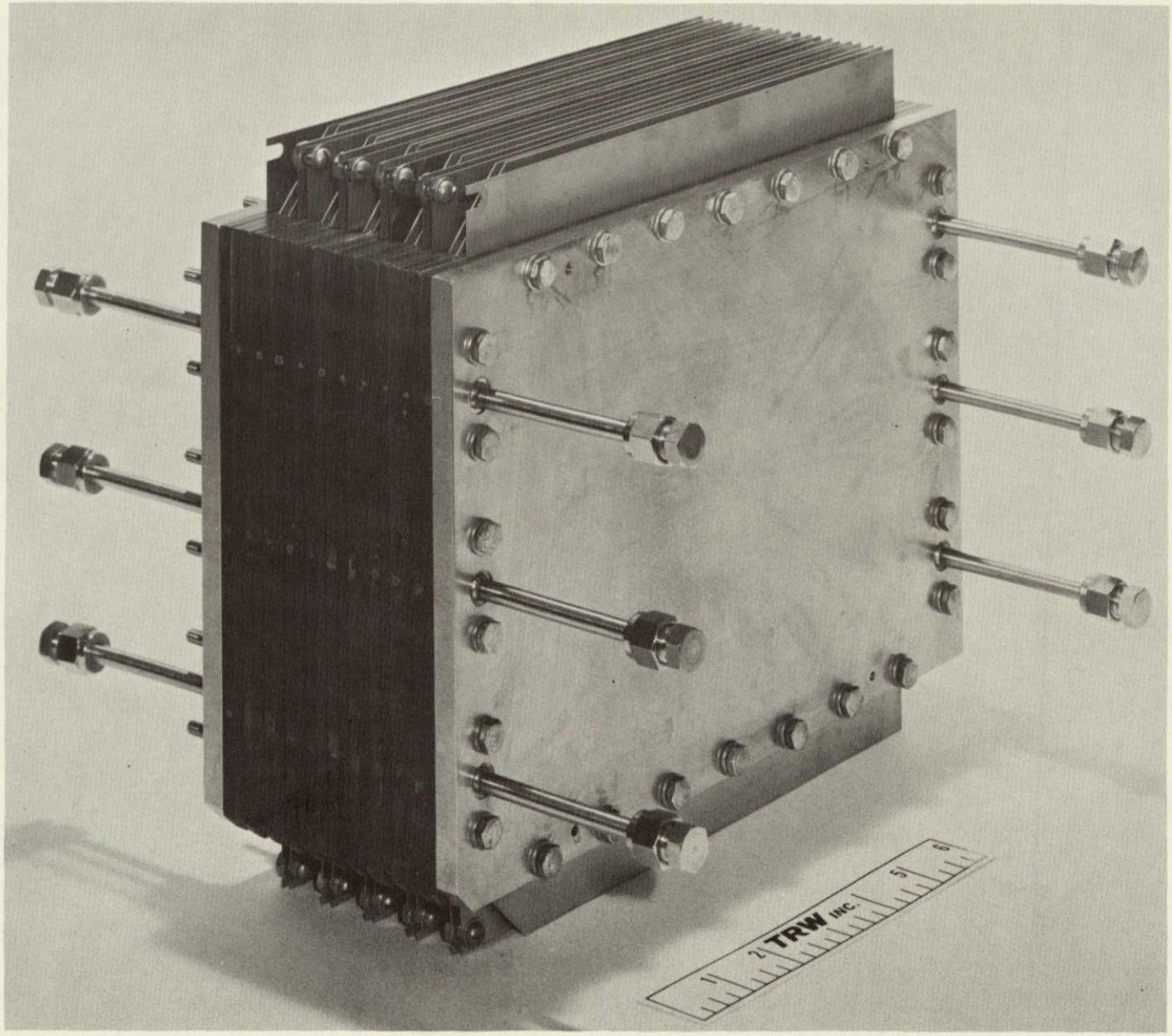

FIGURE 8 WATER ELECTROLYSIS MODULE - 10 CELL STACK

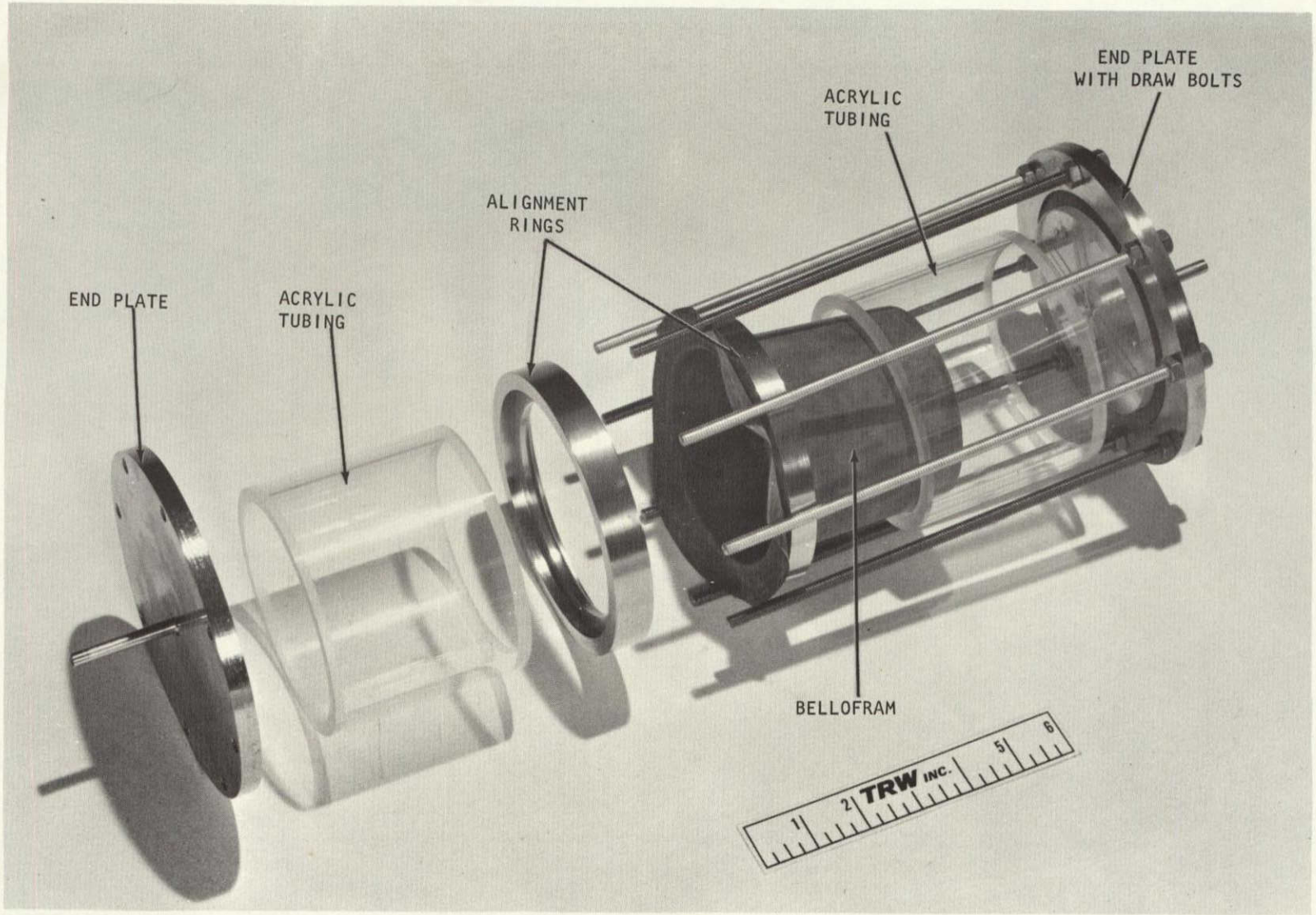

FIGURE 9 STATIC WATER FEED TANK

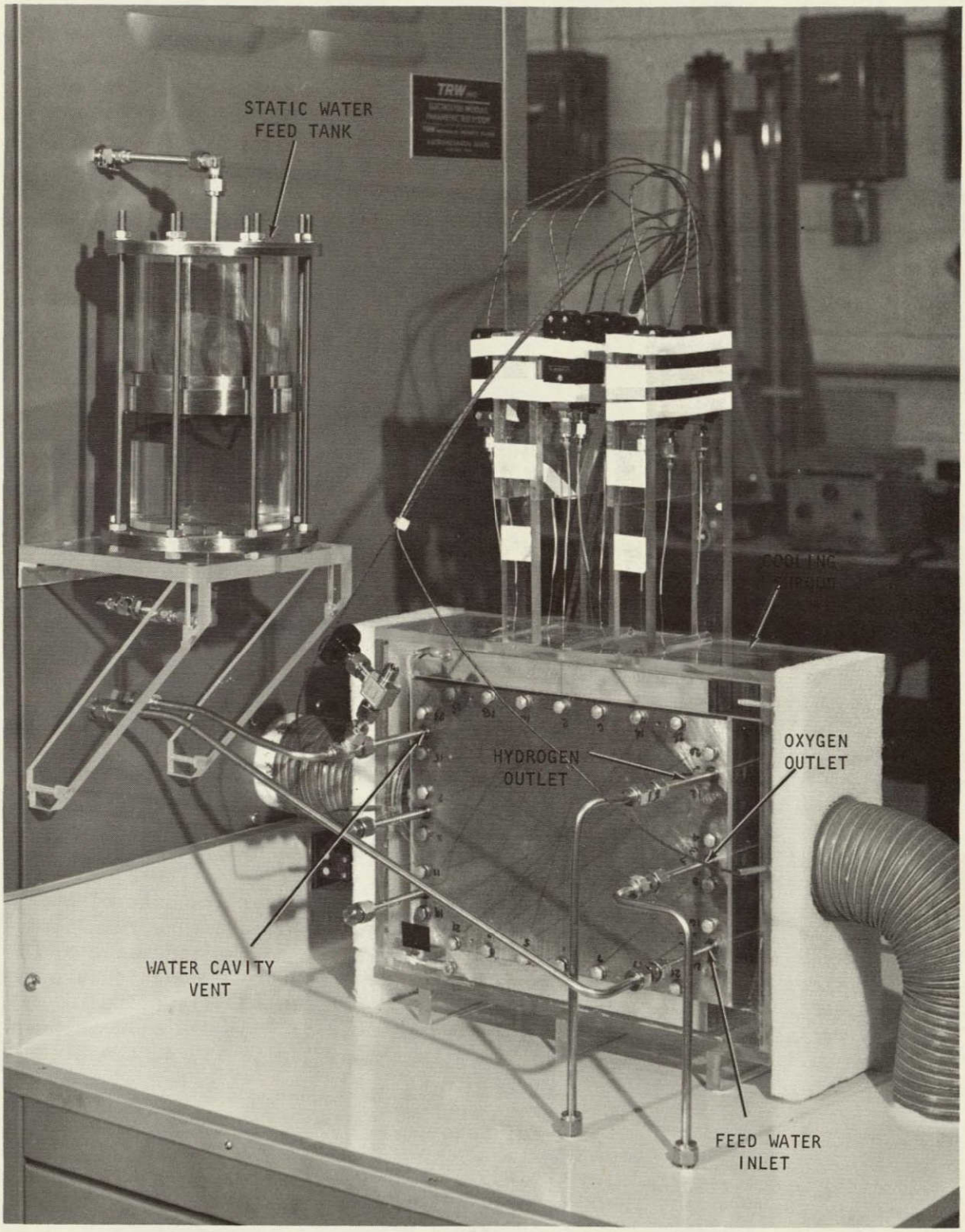

FIGURE 10 WATER ELECTROLYSIS MODULE AND FEED WATER TANK INSTALLED IN TEST RIG

2396D

ELECTROLYSIS MODULE TEST RIG

A complete schematic of the test system is shown in Figures 11, 12, 13, and 14. For maintenance, accessibility and construction purposes the system was divided into two distinct subsystems: the mechanical and the electrical. The interfaces are so defined to allow separate construction and a minimum integration time. This discussion will be divided along similar lines, i.e., mechanical and electrical subsystems with additional description of test rig revisions also given.

Mechanical Subsystem

The mechanical subsystem consists of a recirculating cooling loop, gas dehumidifiers and a control panel.

Electrolysis module temprature control is accomplished by using a recirculating air system. Minimum stack temperature is attained by applying no power to the air heater and flowing 100 CFM of room temperature air over the cell. Calculations have shown that at 100 CFM air flow a temperature difference between the cell and room temperature of approximately 5°F would exist. When higher temperature operation is required, the air heater temperature control and the damper are adjusted to provide the desired temperature. Since the temperature control and the blower are independent of the shutdown circuitry, preheating of the module may take place prior to startup. An interlock is provided to prevent operation of the air heaters without air flow from the blower.

To prevent condensation in the system instrumentation, gases produced by the electrolysis cell are dehumidified by water-cooled condensers soon after it leaves the module. Lines from the module to the condensers were initially trace-heated and taps were provided for shutdown valves and humidity measuring instrumentation. Humidity measurements were performed gravimetrically.

Electrolysis cell pressure is controlled by adjusting the needle valve on the oxygen rotameter. Changes in pressure produced by adjustment of this valve are reflected throughout the system by the differential pressure control which regulates module hydrogen pressure and by the differential pressure regulator which controls module oxygen pressure. Pressures shown on the schematic are the nominal expected operating pressures in the system, but components were selected to allow pressure excursions from atmospheric to 80 psia. The differential pressure control may be adjusted to provide from 0-5 psid between the hydrogen cavity and the oxygen cavity with the oxygen cavity at the higher pressure.

Electrical Subsystem

The electrical subsystem consists of the control circuitry, a safety shutdown system and the power circuitry. The control circuitry includes switches, circuit breakers and the temperature controller.

In order to prevent damage to the module or permit a possible safety hazard to exist, a shutdown system was included in this design. This feature is not only

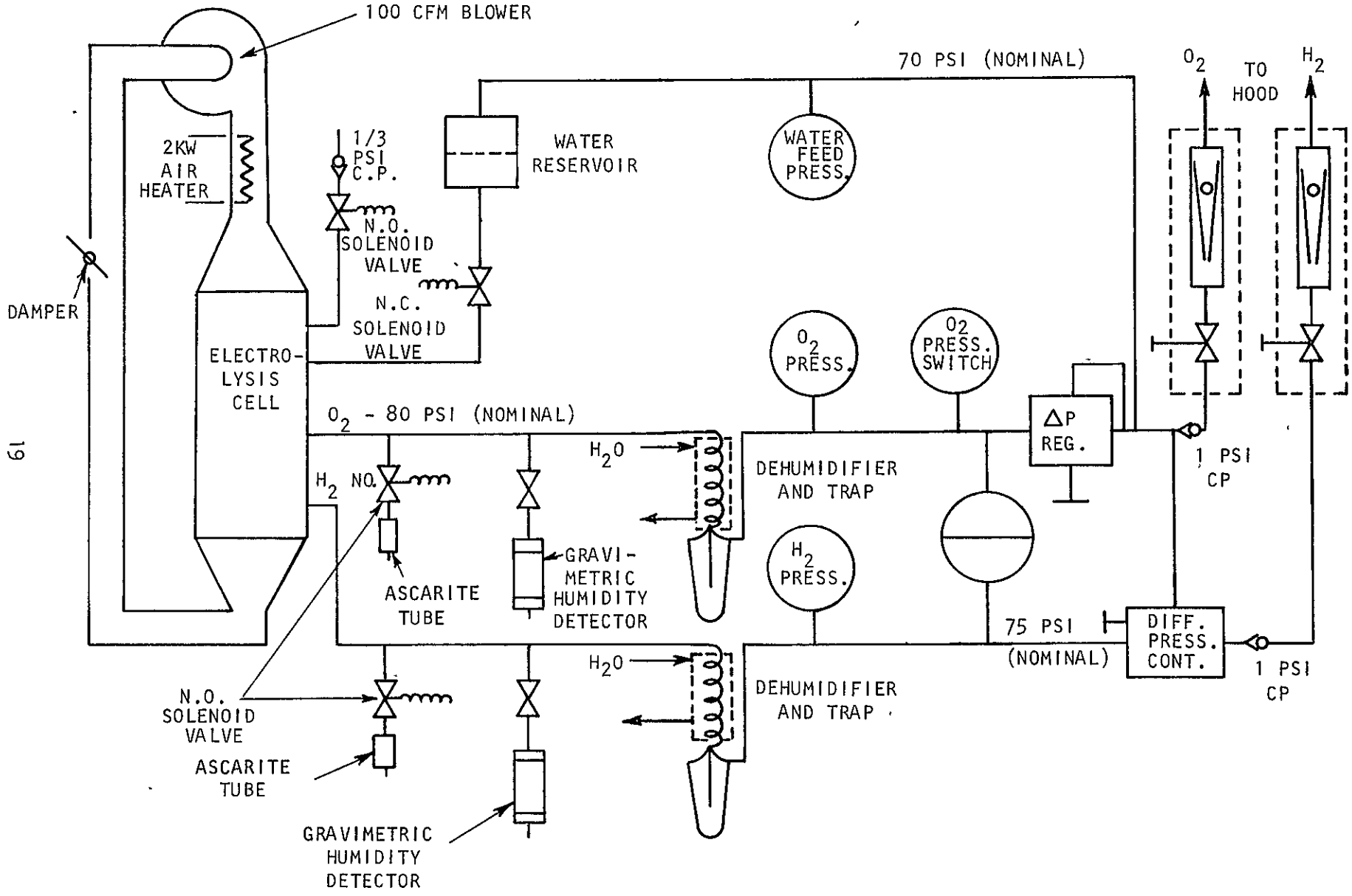

FIGURE 11 NAOS ELECTROLYSIS CELL TEST SYSTEM SCHEMATIC

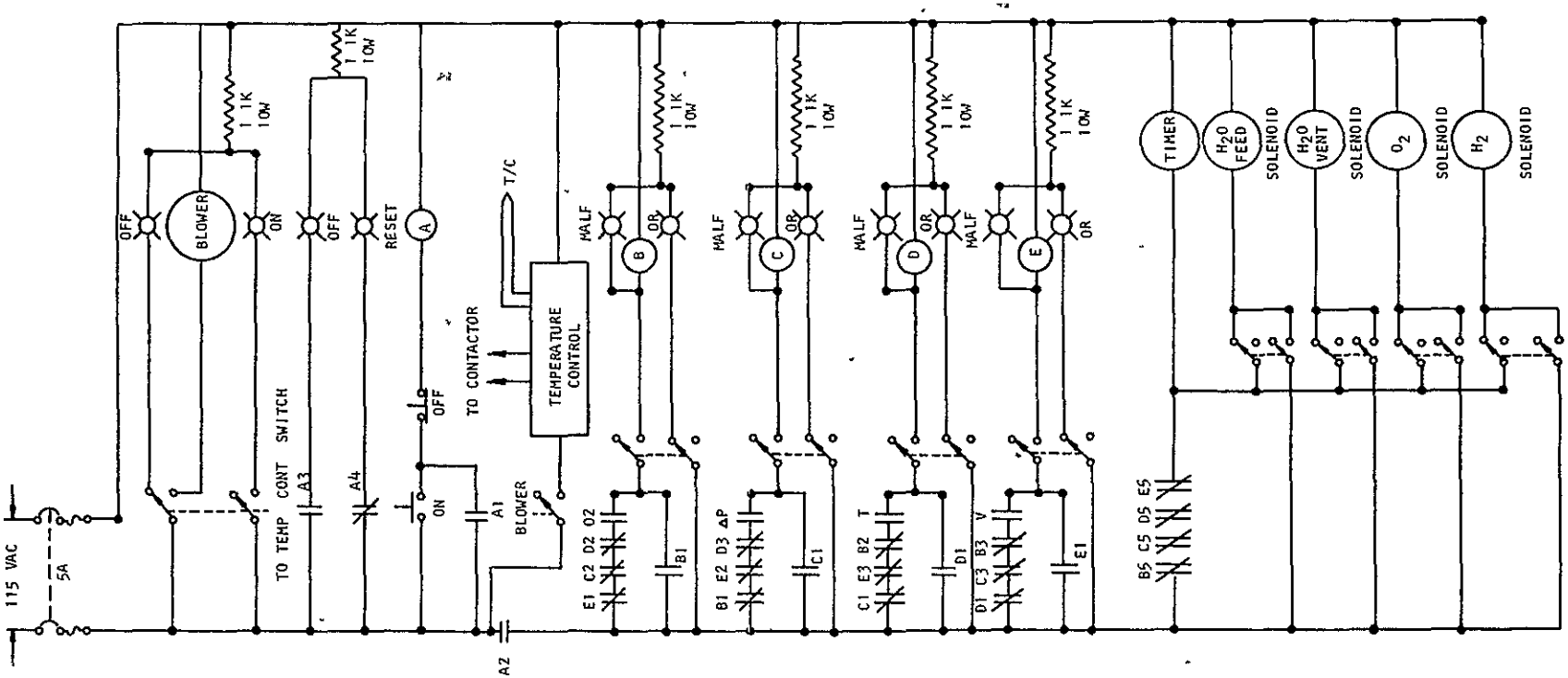

FIGURE 12 ELECTROLYSIS CELL TEST RIG CONTROL CIRCUIT

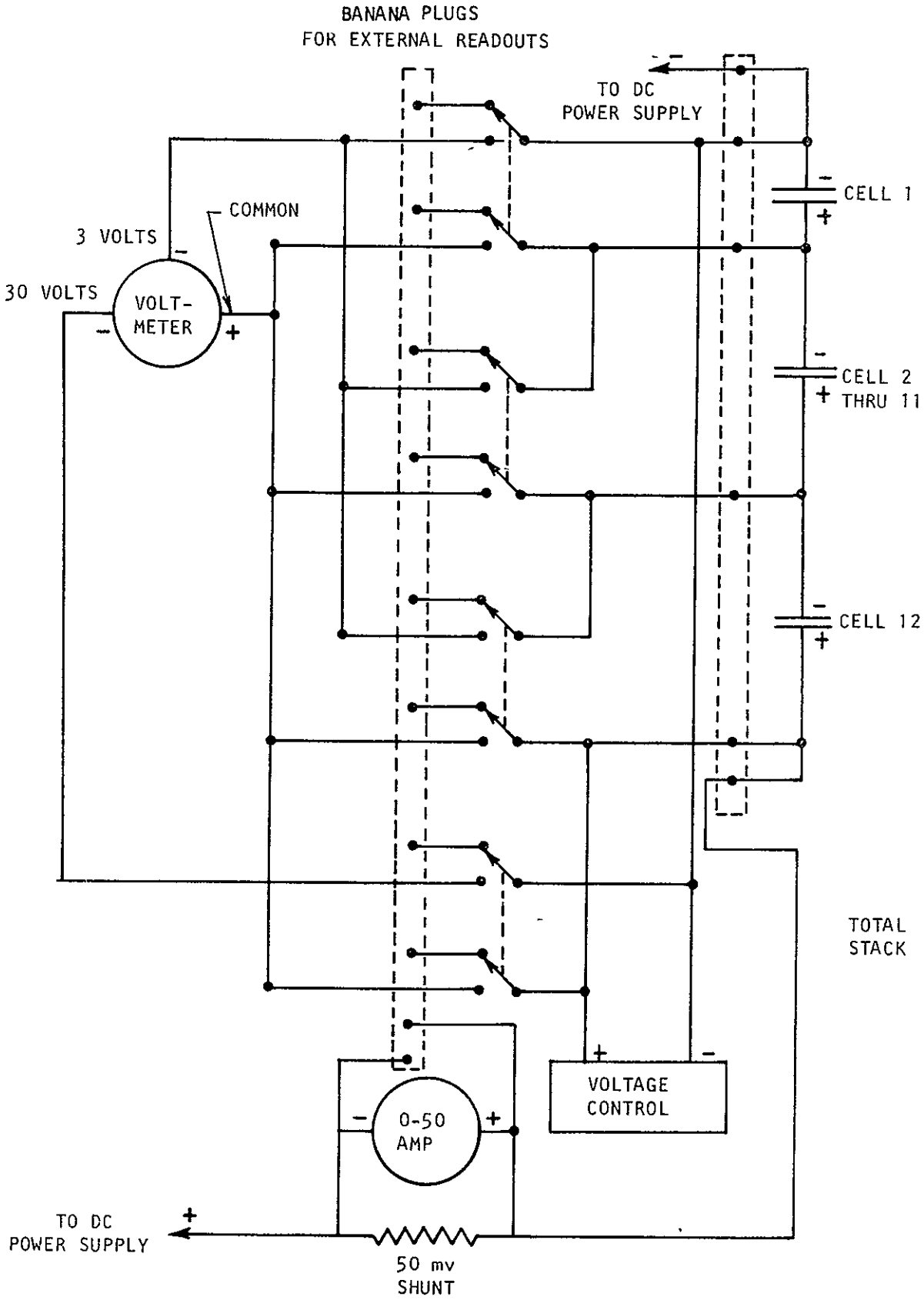

FIGURE 13 VOLTAGE SWITCHING NETWORK

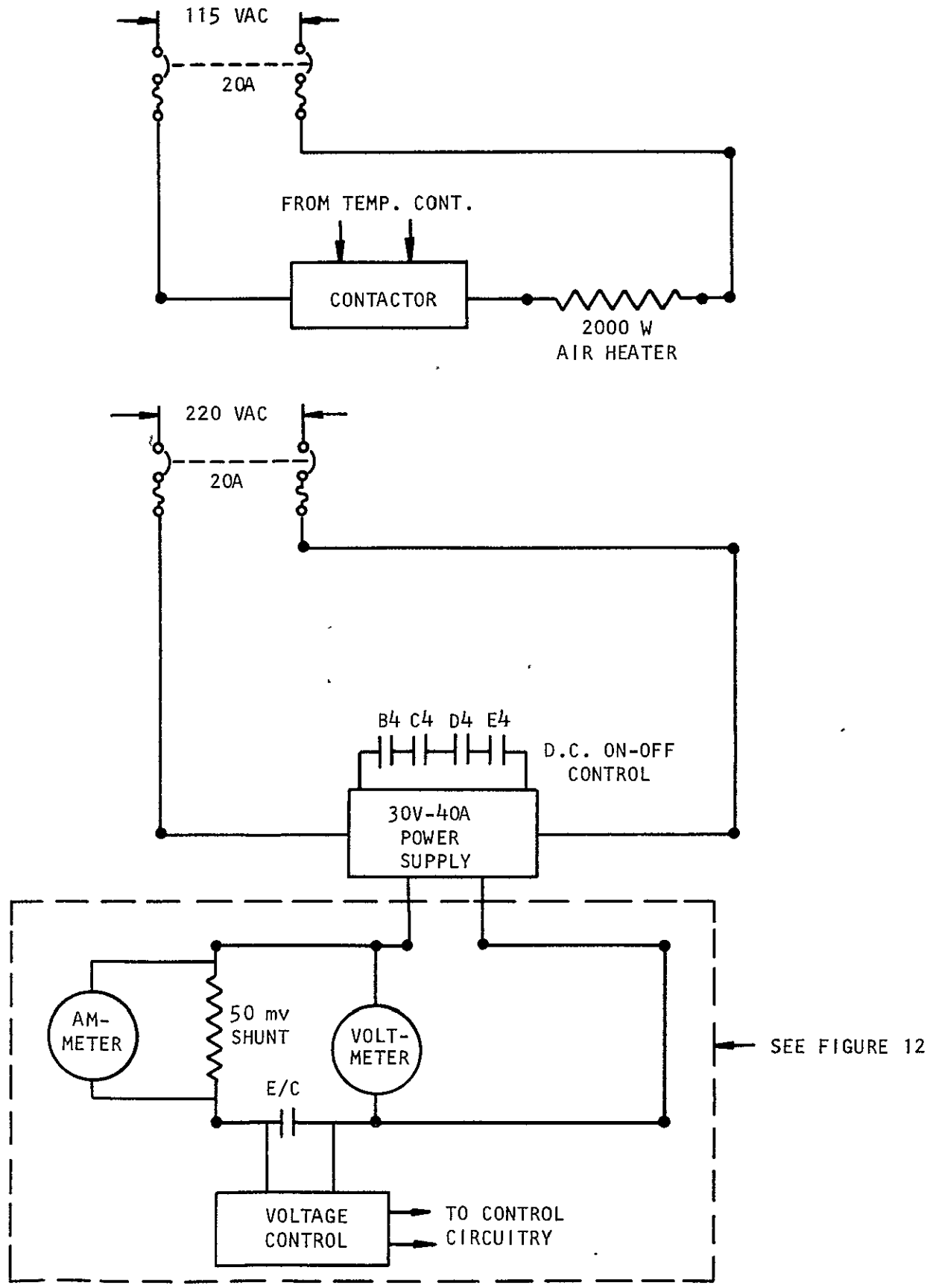

FIGURE 14 ELECTROLYSIS CELL TEST RIG POWER CIRCUITS

necessary for unattended operation but provides some measure of protection for personnel in the area. Parameters which can effect a shutdown include: oxygen pressure greater than 85 psia, pressure differentials greater than 5 psid or less than 0 psid between the oxygen and hydrogen cavities, module temperatures greater than 200°F and total stack voltage greater than 20 volts. All shutdown circuits are equipped with overrides in case the test plan calls for exceeding limits for a short time. When a malfunction occurs and a shutdown follows, an automatic lockout prevents other shutdown circuits from being triggered and therefore only the light indicating the parameter which caused the shutdown remains lighted. When an automatic shutdown occurs, all system solenoid valves which shut off the water flow and vent the module water, hydrogen and oxygen cavities are de-energized.

The voltage switching and monitoring network is shown on Figure 13. This circuit allows internal and external monitoring of individual cell voltages, total stack voltage and stack current.

Due to the high current output of the DC power supply (40V, 50A), it was necessary to use 220V AC for input power. When a shutdown occurs, the power is removed from the module. Rather than use a mechanical contactor, a power supply was chosen which is remotely programmable. This allows switching of low voltage to shut off the power supply. Internal construction of the power supply prevents reverse current flow, thus eliminating the possibility of the electrolysis cell becoming a fuel cell when the driving current is removed.

Test Rig Revisions

Post-Parametric Test - Figure 15 shows the revised Electrolysis Module Test System (EMTS) schematic. The water fill and water pressure vent valves were added while the EMTS was under construction. The vent valve controls the gas supply to the water reservoir. Using this valve the water reservoir may be vented or the pressurizing gas supply shut off. The water fill valve allows the water reservoir to be filled while the electrolysis cell is in operation.

The most significant change in the configuration of the system was the relocation of the differential pressure gage and switch. During preliminary electrolysis cell testing it was found that the differential between the hydrogen and water cavities was more critical than the differential between the hydrogen and oxygen cavities. It was also found that the water pressure gage was of little use after the differential pressure gage was relocated.

No changes of significance were incorporated in the electrical system as a result of preliminary testing.

The completed water electrolysis module parametric test system with module installed is shown in Figure 16.

Test Rig Modifications for Life Testing - The purpose of the modifications for the water electrolysis life test rig was to decrease the frequency and duration of service requirements and to eliminate or replace those components of the test rig that had caused frequent shutdowns. Two types of services were required to keep the water electrolysis module in operation. First, water had

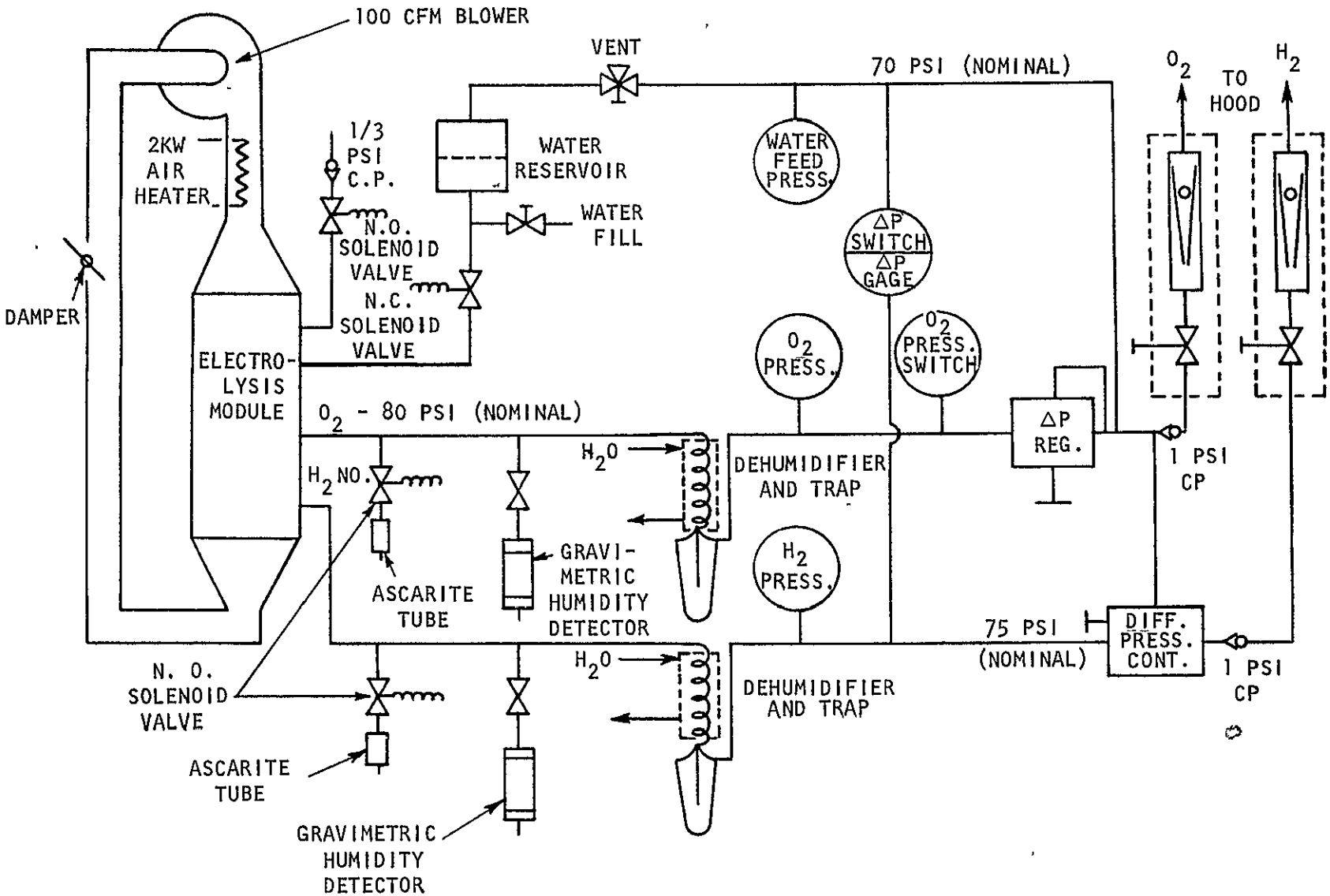

FIGURE 15 NAOS ELECTROLYSIS MODULE TEST SYSTEM SCHEMATIC (REVISED CONCEPT)

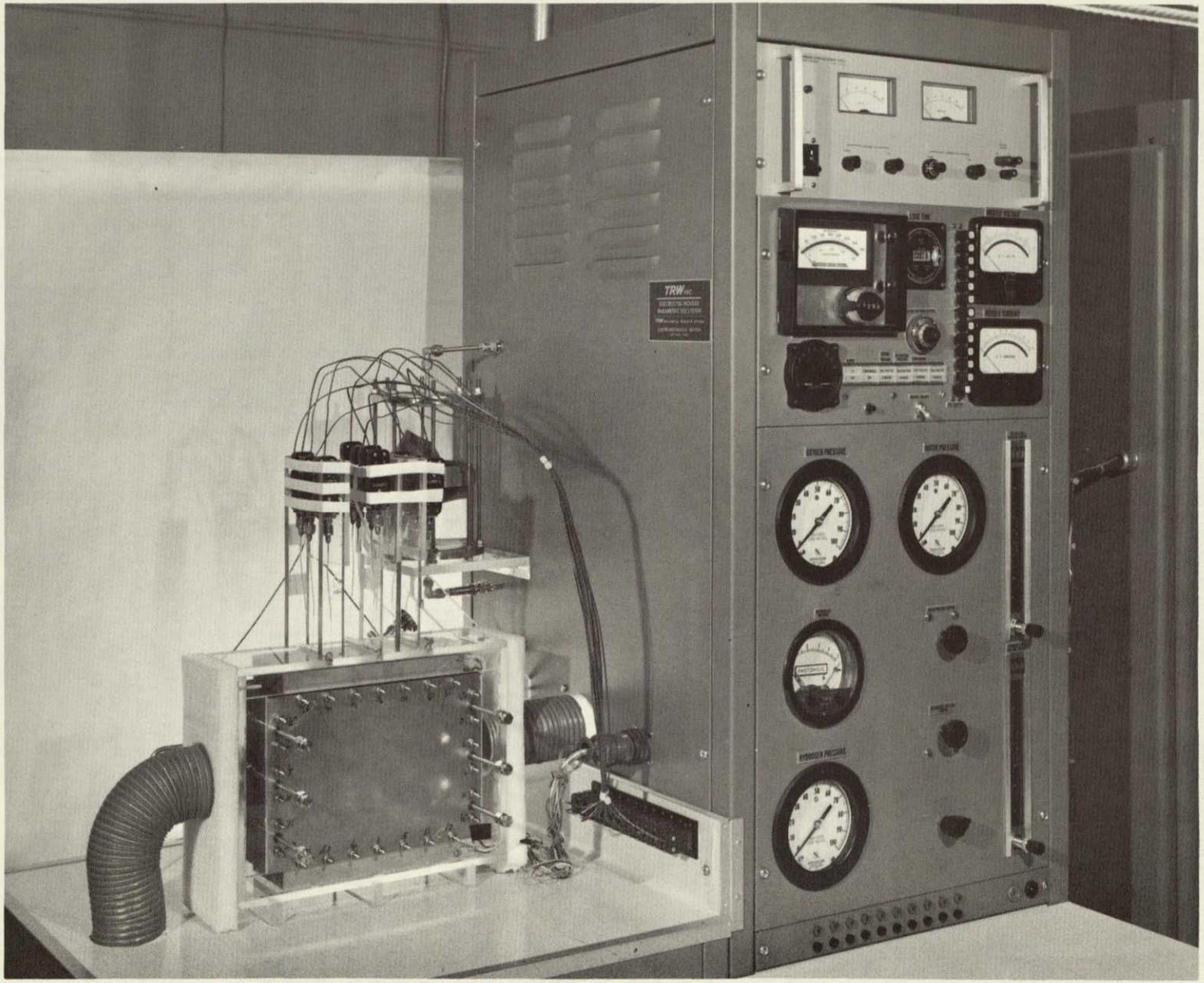

FIGURE 16 WATER ELECTROLYSIS MODULE PARAMETRIC TEST SYSTEM

to be added to the feed water tank and second, the accumulated condensate had to be drained from the traps in both the hydrogen and oxygen lines. Prior to the modifications, the water tank required refilling once every 17 hours with the water electrolysis module operating at life test conditions. Emptying of the condensate traps was required once every two days of operation. A large capacity water tank sized for a minimum of four days of operation (at life test conditions) was designed and fabricated. The useful volume of the new tank is approximately 600 cu. in. as compared to 89 cu. in. of the smaller water tank. The outside dimensions of the new tank are approximately 10" diameter by 15" long. The capacity of the condensate trap arrangement was increased by using two traps in series for each of the product gases.

The first trap in line from the cell contains no filter element and is strictly used as an accumulator for condensate. The second trap mounted vertically above the first trap contains a 100 micron filter element and is used to strip entrained liquids from the generated gases. This liquid can run back to the lower trap since a sufficiently large tube is provided to allow simultaneous liquid flow downward and gas flow upward. A sight gage was added to the lower condensate trap for ease in determining the liquid level in the trap. This trap arrangement also eliminated the problem that caused water to be pumped into the plumbing due to the ΔP generated by wet submerged filter elements. The capacity of the traps is sufficient to require emptying only once in a four-day period. The traps are constructed from stainless steel thus eliminating one of the early causes of test rig failure that had resulted from cracking of plastic condensate traps.

Another type of component in the WEM test rig that had caused frequent test shutdowns were the solenoid valves. These valves were used to vent the oxygen, hydrogen and water cavities to atmosphere and also to shut the water supply from the tank to the cell in case of an automatic shutdown. The modified test rig has no solenoid valves. Their functions were simulated by 1) mounting the water tank below the electrolysis module thus preventing flooding in case of an automatic shutdown, and 2) adding relief valves to the hydrogen and oxygen lines oriented in such a way that inflow into the system is permitted but no outflow is allowed. This function prevents water being sucked into the cell after shutdown due to possible recombination of the product gases. These check valves are required since backflow through the pressure regulating network (pressure regulators) is not possible. With the new plumbing arrangements the original check valves immediately before the flow meters were no longer required and were removed from the test rig.

At the time the modification of the test stand was in progress, it was suspected that stray electrolysis occurred between the endplates and the cathodes of the various cells via leakage paths generated by electrolyte bridging from the feed matrix to the hydrogen current collectors. This, of course, would cause gas generation to occur on any metallic part in the water feed system. To eliminate or greatly reduce this possibility the endplates of WEM #1 were electrically isolated from ground and hence allowed to electrically float about the cell potential. To accomplish this, high pressure plastic tubing was used in connecting the module to the test rig plumbing.

ELECTROLYSIS MODULE TESTING

After assembly and pressure check at 80 psig the module assemblies were vacuum charged with 25 wt% KOH solution. Prior to installation on the test stand, checks for intercavity cross-leaks were routinely made at a 5 psid pressure differential across both the cell and feed matrices.

Initial Shakedown Parametric Test Series

Initial tests were at low pressure (16 psig) due to use of slightly undersized O-rings used in the initial module assembly. The results of test at low pressure are summarized as follows:

Oxygen Purity Tests - Two oxygen purity tests were conducted with the Beckman E-2 analyzer (Model 118523). Both tests showed oxygen purity greater than 99.5% by volume. The first test was conducted at 26.8 hours total running time with oxygen cavity pressure at 16 psig and hydrogen cavity pressure at 14 psig, while the second test was conducted at 49.2 hours total running time with both oxygen and hydrogen cavity pressures at 16 psig.

Effect of Cell Temperature - Cell performances were obtained after 37 hours of total running time, for 25, 50, 75 and 100 ASF for each of the following average stack temperatures: 95°F, 125°F, 151°F and 182°F. The results are shown in Figure 17.

Moisture Balance - The moisture balance test was conducted over a period of 130 minutes at 100 ASF, 185°F and 20 psig. A gravimetric humidity detection method was used. The results showed that the change in feed water tank was 199 grams while 221 grams could be accounted for due to gases generated, including humidification of generated gases. This 10% difference is most likely due to the small range in tank weight change when compared to total tank weight (approximately 3%) and the inherent inaccuracy of gravimetric humidity detection.

Overcapacity - For the overcapacity test the module was operated at 150 ASF for 1.55 hours after a 3.2 hour run at 100 ASF. Figure 18 shows the stack voltage versus running time. As can be seen from the figure, the stack voltage started to level out at 19.1 VDC after 1.3 hours at 150 ASF.

Initial High Pressure Operation - While trying to verify module and test rig capability to operate at 80 psia (after accumulating 35.2 hours of operation) a sudden drop in voltage and rise in temperature of cell number 3 (cell number 1 next to most positive end of stack) occurred, indicating crossover. Since the voltage drop was sudden and not preceded by a gradual rise, matrix dry up was not suspected. Possible cause could have been a shift in internal cell components during pressurization resulting in matrix tear. After this crossover had occurred the module was still operable with low differential pressure levels in oxygen and hydrogen compartments. Figure 19 shows module operation after apparent crossover failure.

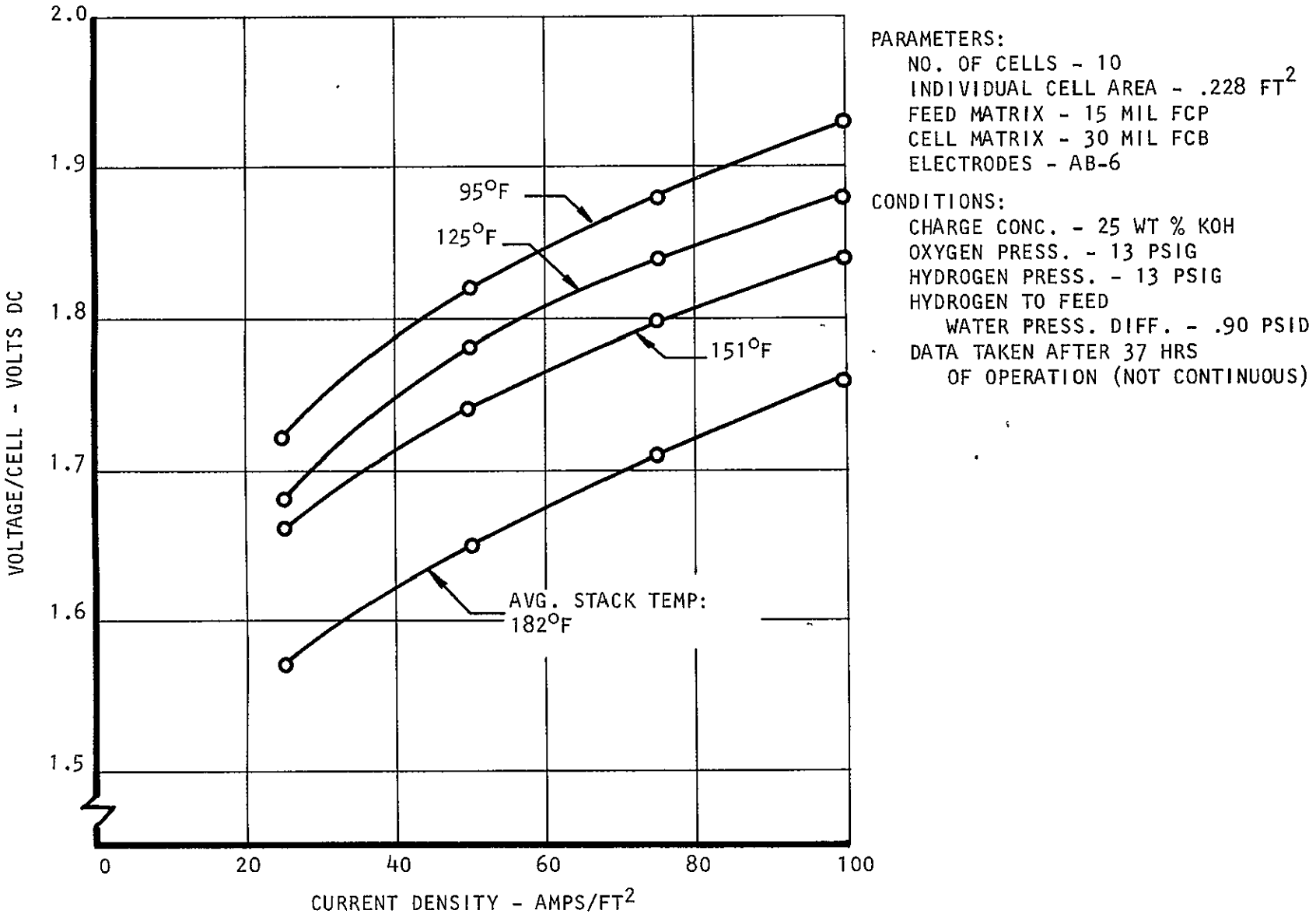

FIGURE 17 AVERAGE CELL VOLTAGE VS. CURRENT DENSITY AS A FUNCTION OF AVERAGE STACK TEMPERATURE

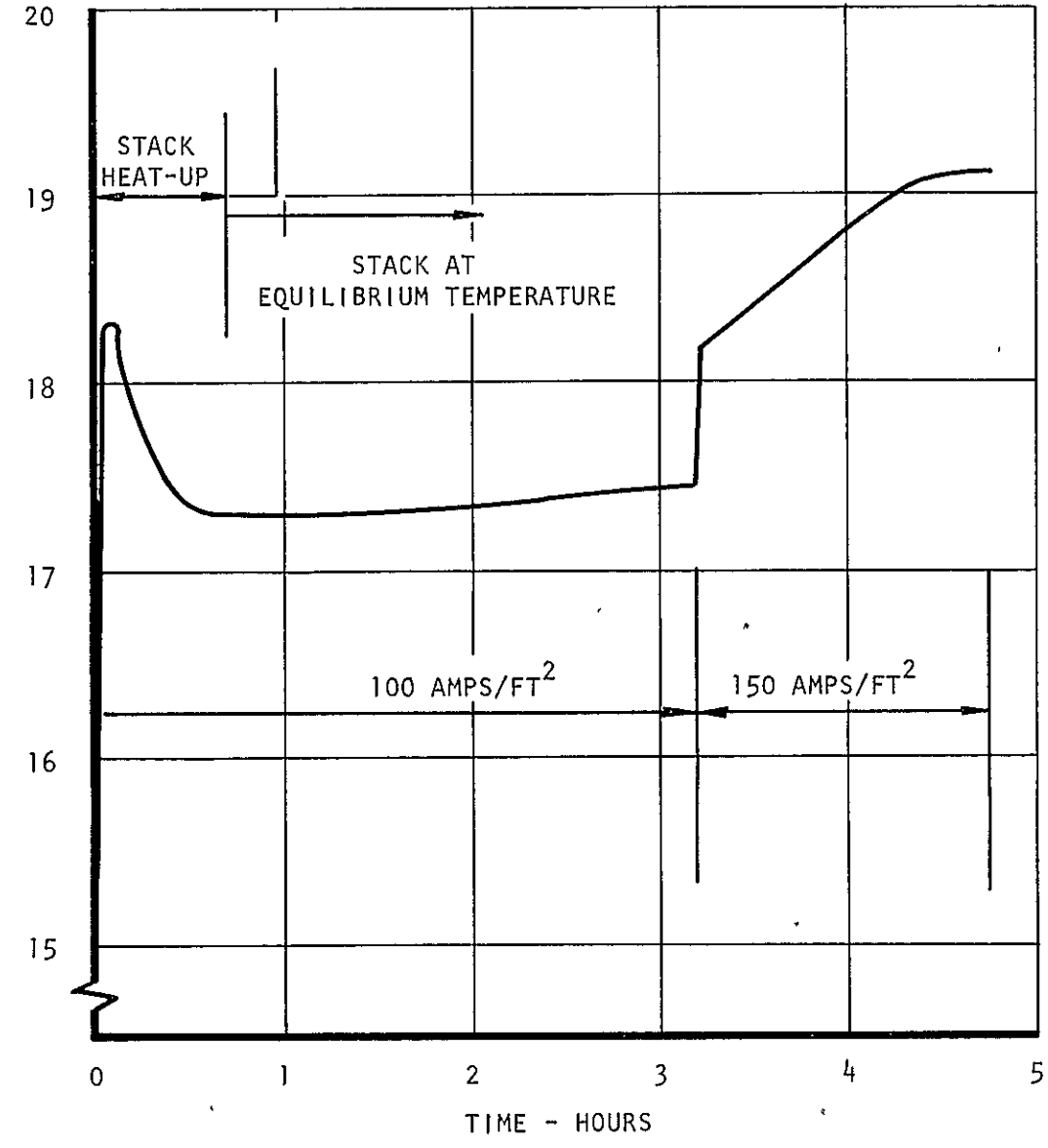

PARAMETERS:

NO. OF CELLS - 10
INDIVIDUAL CELL AREA - .228 FT^2
FEED MATRIX - 15 MIL FCP
CELL MATRIX - 30 MIL FCB

CONDITIONS:

AVG. STACK TEMPERATURE - 185°F
OXYGEN PRESSURE - 16 PSIG
HYDROGEN PRESSURE - 16 PSIG
HYDROGEN TO FEED
WATER PRESSURE DIFF. - ,85 PSID
CHARGE CONC. - 25 WT. % KOH

FIGURE 18 ELECTROLYSIS CELL STACK VOLTAGE VS. TIME (100 ASF AND 150 ASF)

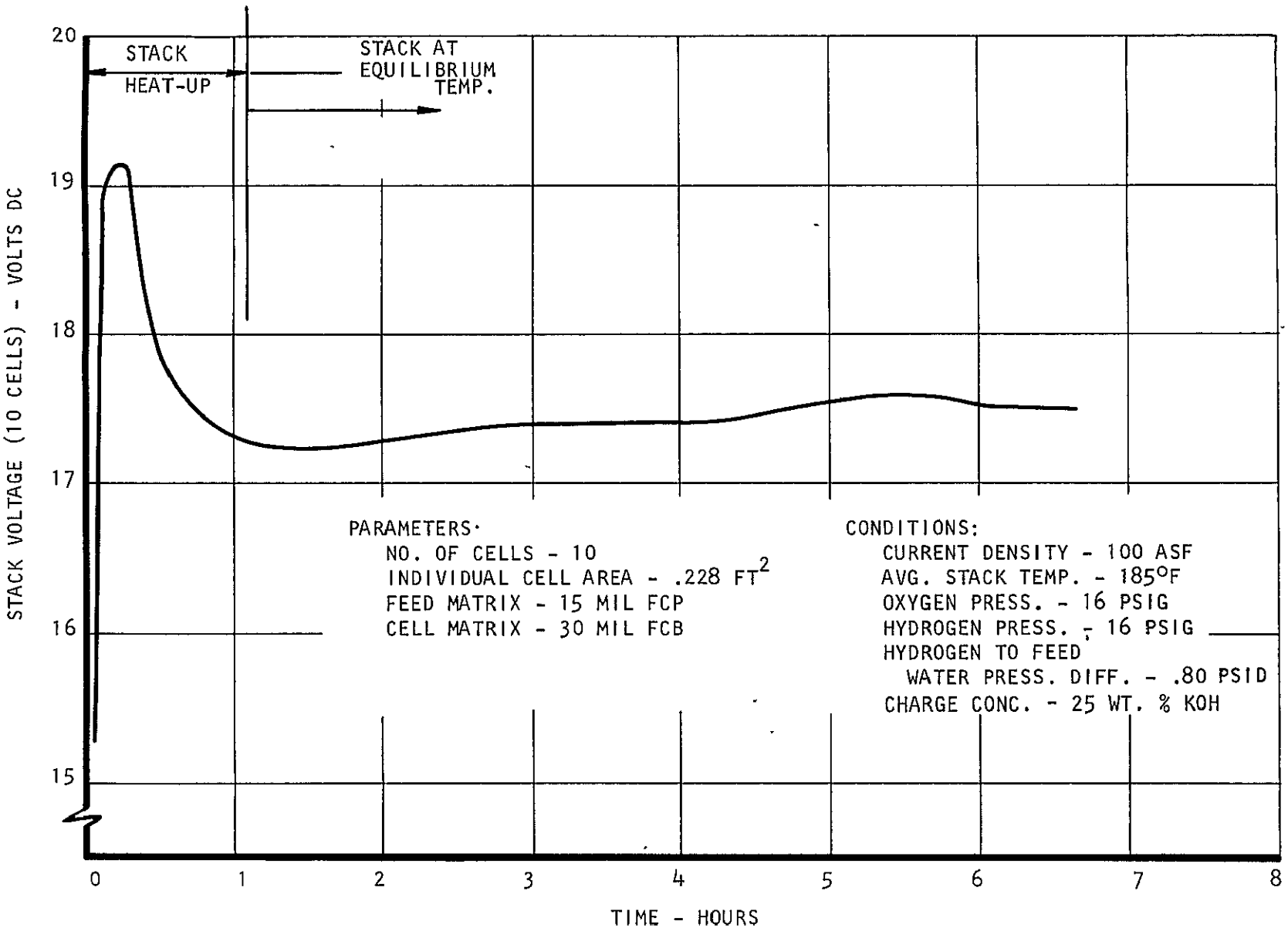

FIGURE 19 ELECTROLYSIS CELL STACK VOLTAGE VS. TIME (AT 100 AMPS/FT^2)

Disassembly of the module after 53.3 hours of total operation verified that crossover had occurred in cell number 3. A pin hole was found in the cell matrix. Close inspection of the matrix showed a circular crease, approximately one-quarter inch in diameter on the asbestos surface. Poor quality asbestos in that region could have been the cause of crossover.

Final Parametric Test Series

The final parametric test series were conducted using the module reassembled with the O-rings of proper dimensional tolerance. Prior to initiation of the final parametric test series, several test rig modifications were also completed based upon the results of the preliminary parametric tests. These modifications were discussed in a previous section. The final parametric test results are as follows:

Oxygen Purity Test - Two additional oxygen purity tests were conducted using the Beckman E-2 Analyzer (Model 118523). Both tests again showed the purity of the generated oxygen to be greater than the required 99.5% by volume. Total accumulated running times and oxygen to hydrogen pressure differentials were 90.7 hours and 0.8 psid for the first test and 312.5 hours and 1.4 psid for the second test.

Pressure Differential Tests - Numerous tests were conducted throughout the test period to verify the stability of the electrolysis cells to $\pm$ 5.0 psi pressure differentials between the oxygen and hydrogen compartments. No reduction in the structural integrity of an electrode-matrix combination was noted. During these tests it was observed that cell voltage would decrease appreciably as the oxygen to hydrogen pressure differential changed from positive to negative. This voltage change occurred with negligible time lag. The most probable factor causing this voltage-pressure differential relationship is the redistribution or shift of the electrolyte volume within the electrode-matrix sandwich. Figure 20 shows cell voltage as a function of oxygen to hydrogen pressure differential.

Moisture Balance Test - A long-term moisture balance test was conducted over a time period of 121 hours of continuous module operation. For this test the amount of water added to the feed water tank and the amount of water collected in each of the condenser traps was measured and recorded. The weight of the product gases was calculated based on the duration of the test and the current density. Throughout the test, current density and stack temperature were held constant at 100 ASF and 180°F, respectively. The moisture balance test results showed that during the 121 hours of operation 12.71 kg of water were added to the feed tank while 12.80 kg of product gases, including moisture removed due to humidification, could be accounted for. The resulting 0.71% error is well within acceptable limits.

For the first 73 hours of testing both the oxygen and hydrogen pressure levels were held constant at 17.5 psig. The remaining 48 hours of testing were conducted with an oxygen pressure level of 16.6 psig and a hydrogen pressure level of 14.3 psig. These pressure changes were made to study the effect of the oxygen to hydrogen pressure differential on effective electrolyte concentration levels with respect to product gas humidification.

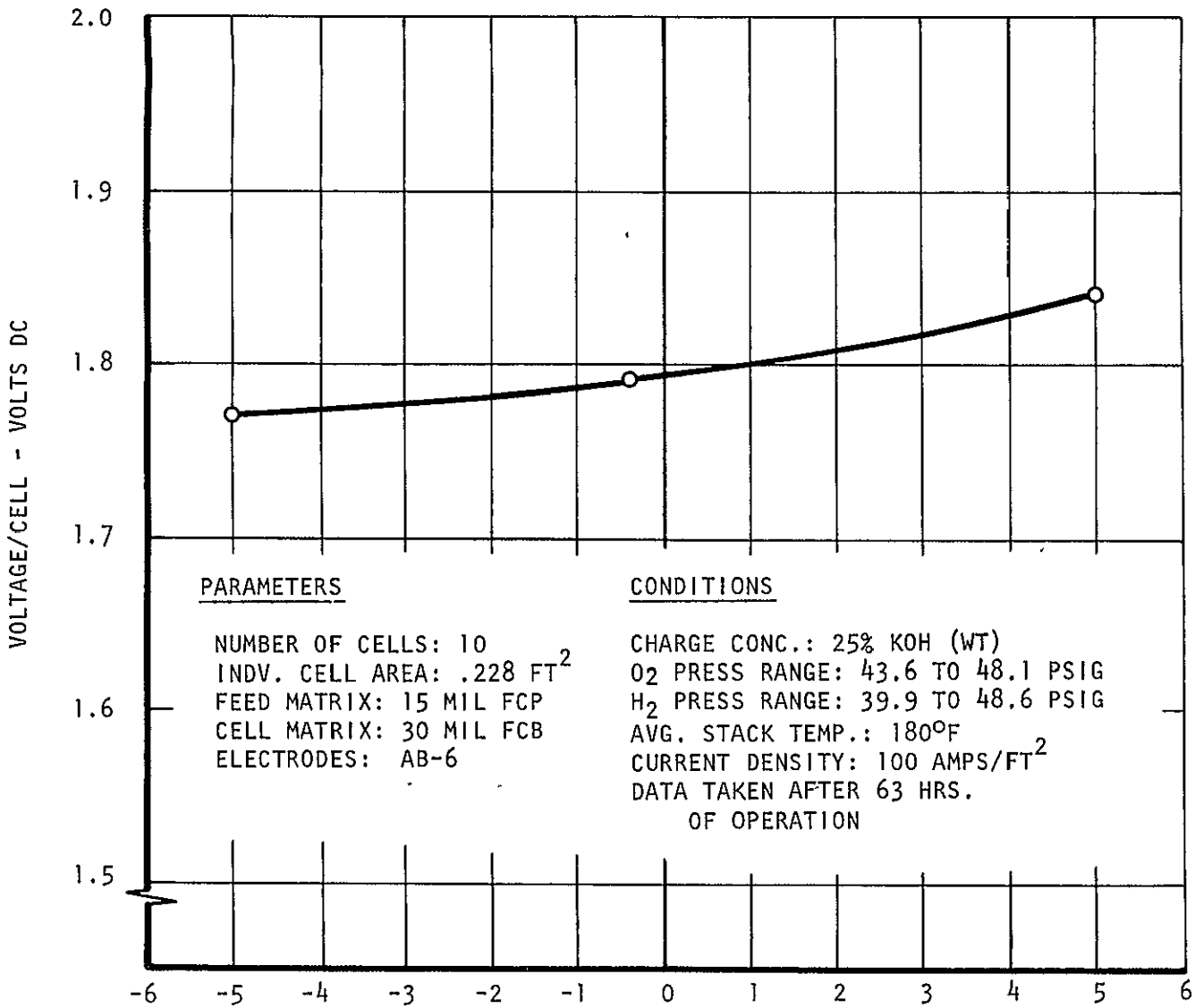

FIGURE 20 AVERAGE CELL VOLTAGE VS. OXYGEN TO HYDROGEN PRESSURE DIFFERENTIAL

With the oxygen and hydrogen pressure levels both at 17.5 psig, the specific humidities, based on the amount of liquid collected in the condenser traps, were calculated to be 0.193 lbs of water per pound of oxygen and 1.92 lbs of water per pound of hydrogen. Based on these values and on the average operating conditions the calculated effective electrolyte concentrations in the gas cavities (with respect to humidification) were that of pure water for the oxygen side and 22% KOH for the hydrogen side.

During the last 48 hours of the test period, with oxygen and hydrogen pressure levels at 16.6 psig and 14.3 psig, respectively, the following specific humidity values and effective electrolyte concentration levels were calculated: 0.15 lbs of water per pound of oxygen with a resulting concentration level of 13% KOH and 2.14 lbs of water per pound of hydrogen with a resulting concentration level of 22% KOH. Initial charge concentration of the module was 25% KOH.

Cell Performance Tests - Figures 21, 22, and 23 show average cell voltages versus current density as a function of average stack temperature for various oxygen and hydrogen pressure levels. Figure 24 shows the effect of temperature on cell voltage for various pressure levels at operating current density of 100 ASF. The random effect of pressure level on cell voltage at a constant temperature is due to the large time difference (including restarts and recharges) between performance tests and different values for the oxygen to hydrogen pressure differential. This was verified when cell performance was practically unaffected by a pressure level change from 17 psig to 67 psig within a time period of 0.7 hours. This test was conducted at a steady state temperature of 100°F. The result is shown in Figure 25.

Overcapacity Performance - Overcapacity (with respect to preliminary design current density of 100 ASF) performance of the electrolysis module, on a short time basis, is shown in the performance curves of Figures 21, 22 and 23. Figure 26 shows average cell voltage for the ten-cell module versus time at 150 ASF. Test duration was 8.6 hours.

Static Water Feed Evaluation - The pressure controlled, static water feed system for the aircraft oxygen water electrolysis module has performed satisfactorily for over 12,500 hours of module operation with a total water transfer of approximately 2500 pounds.

Initial water electrolysis module testing was performed using distilled feed water, pre-boiled to eliminate dissolved ambient gases (i.e., normal air constituents). To investigate the effect of feed water containing these dissolved gases on module operation unboiled distilled water was used after the first 240 hours of testing.

No change in electrolysis cell performance was apparent, nor was there an appreciable increase in gas quantities vented from the feed water cavities. All subsequent testing was performed with unboiled distilled water.

Module Life Testing

The module life test program included three separate test phases which were identified as cyclic, endurance and long-term life tests. The purpose of the first two phases was to evaluate module performance capability in varying

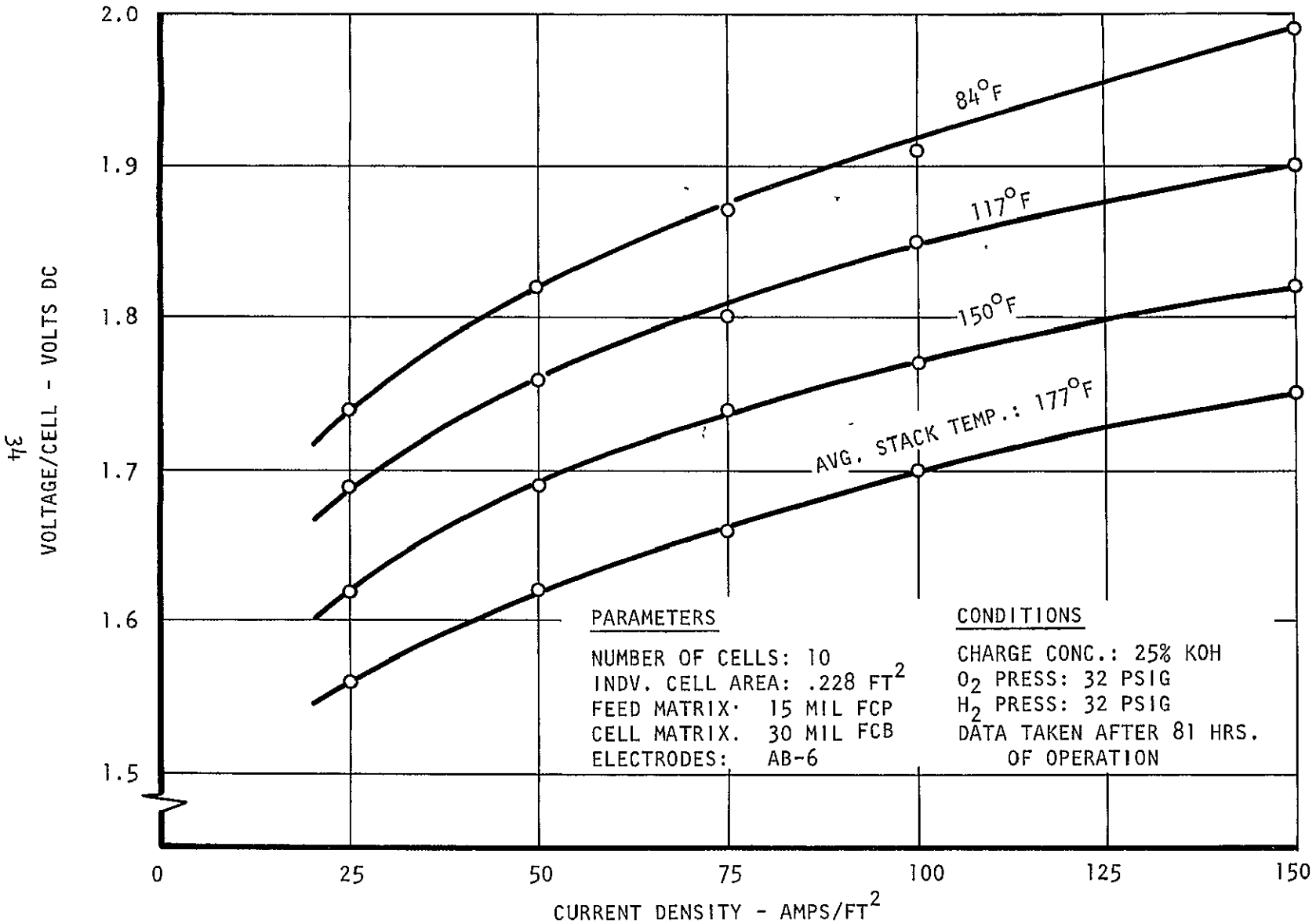

FIGURE 21 ELECTROLYSIS MODULE PERFORMANCE AT 32 PSIG

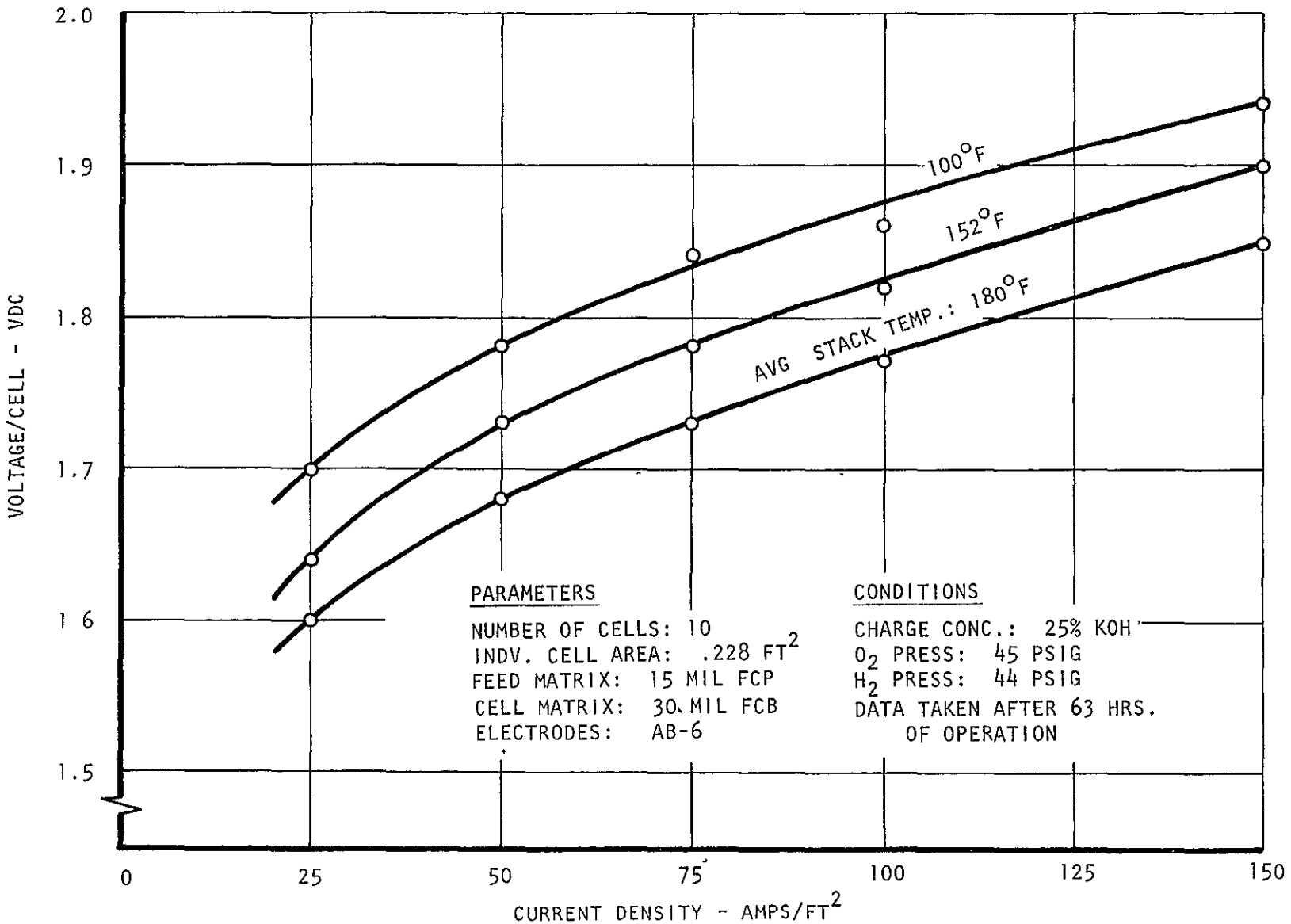

FIGURE 22 ELECTROLYSIS MODULE PERFORMANCE AT 45 PSIG

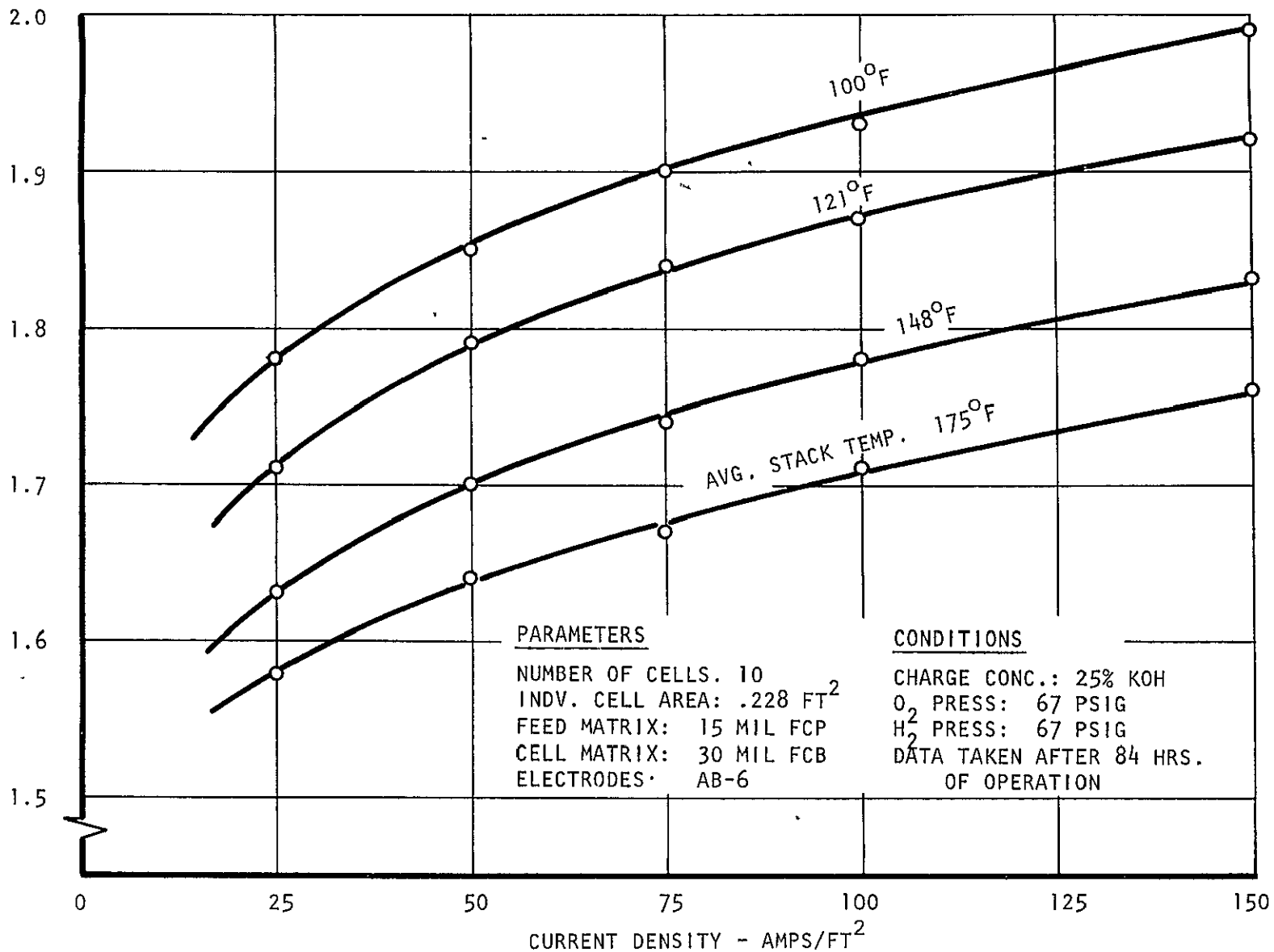

FIGURE 23 ELECTROLYSIS MODULE PERFORMANCE AT 67 PSIG

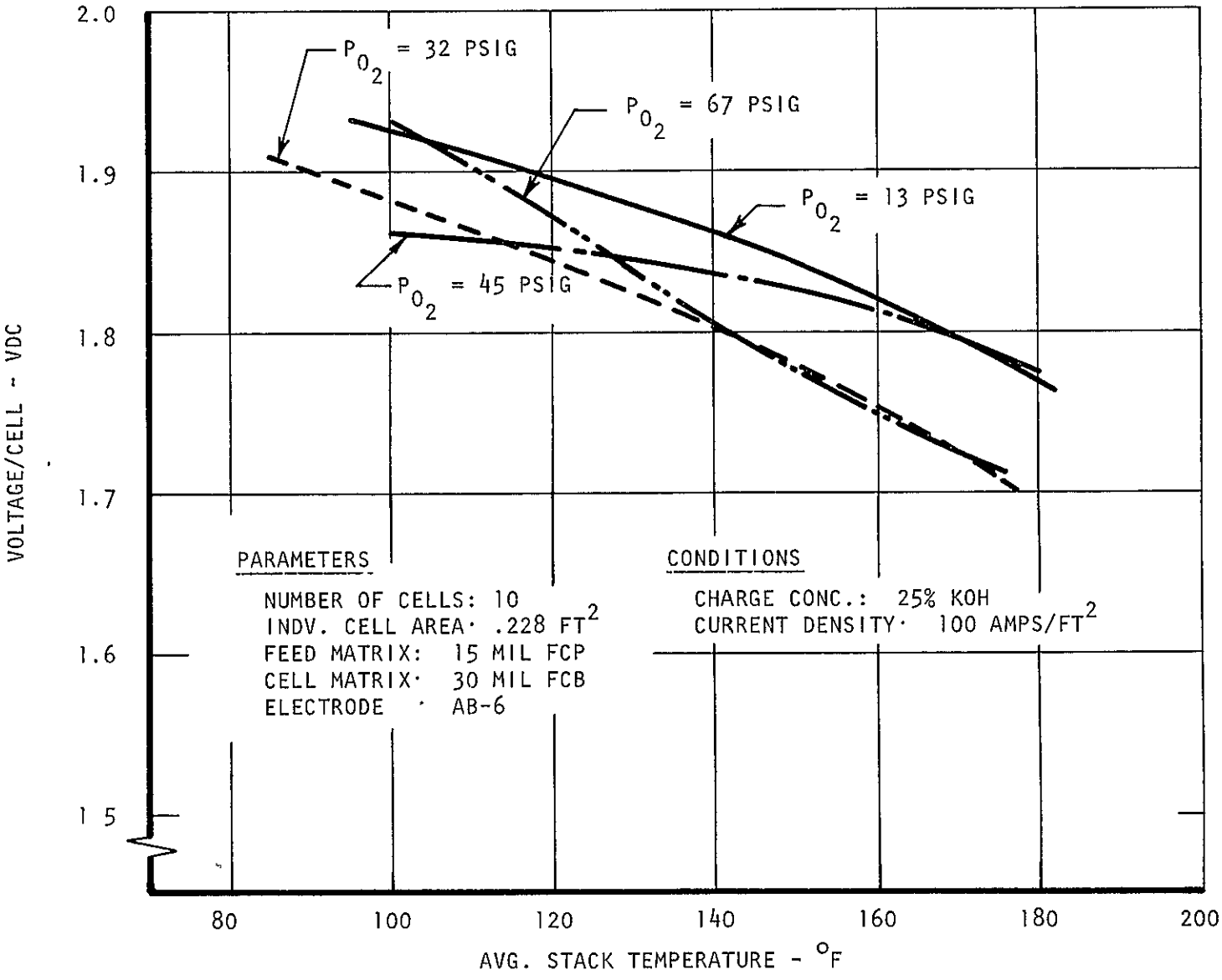

FIGURE 24 AVERAGE CELL VOLTAGE VS. STACK TEMPERATURE

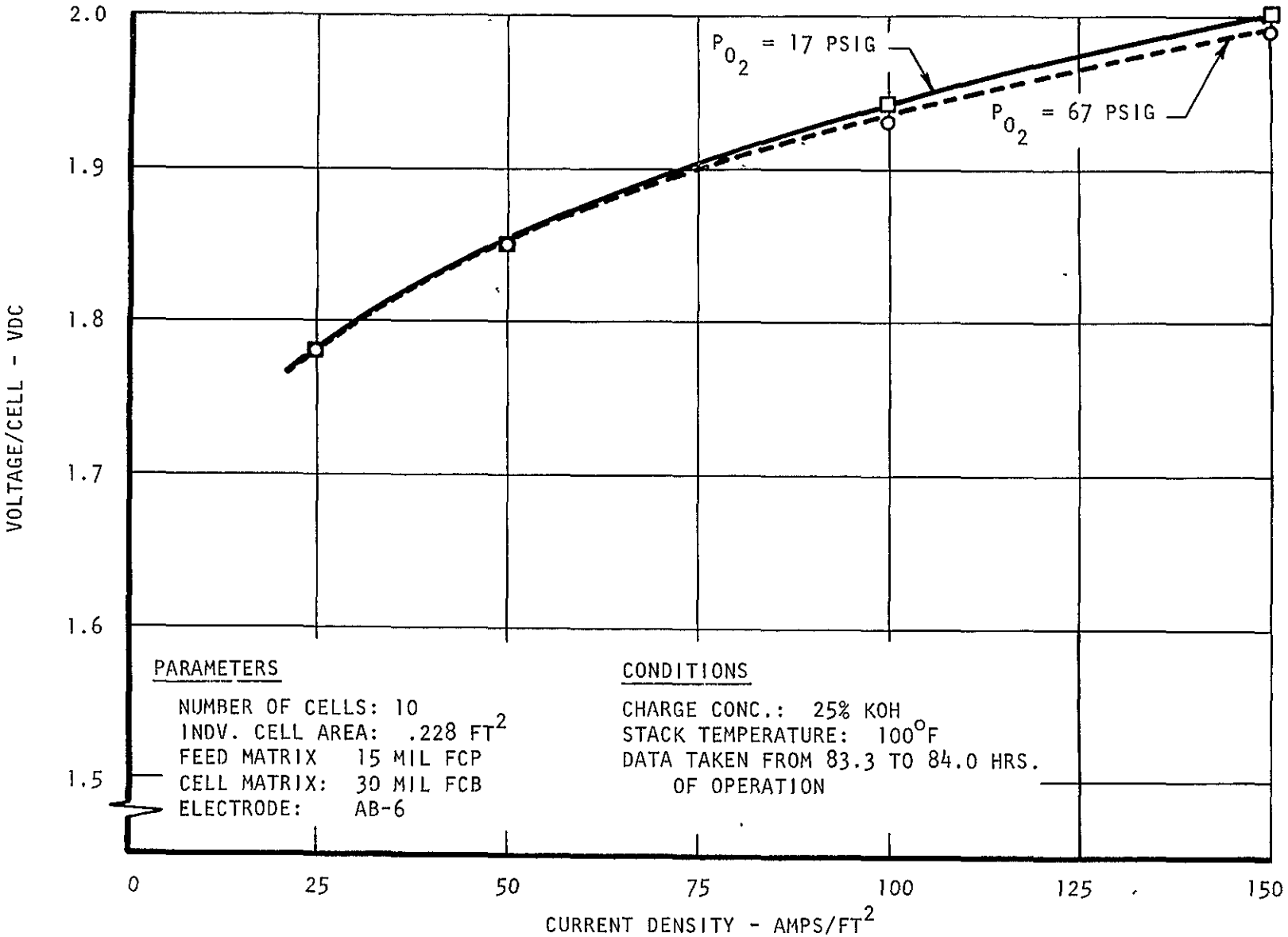

FIGURE 25 ELECTROLYSIS MODULE PERFORMANCE AT CONSTANT TEMPERATURE AND 17 PSIG TO 67 PSIG PRESSURE RANGE

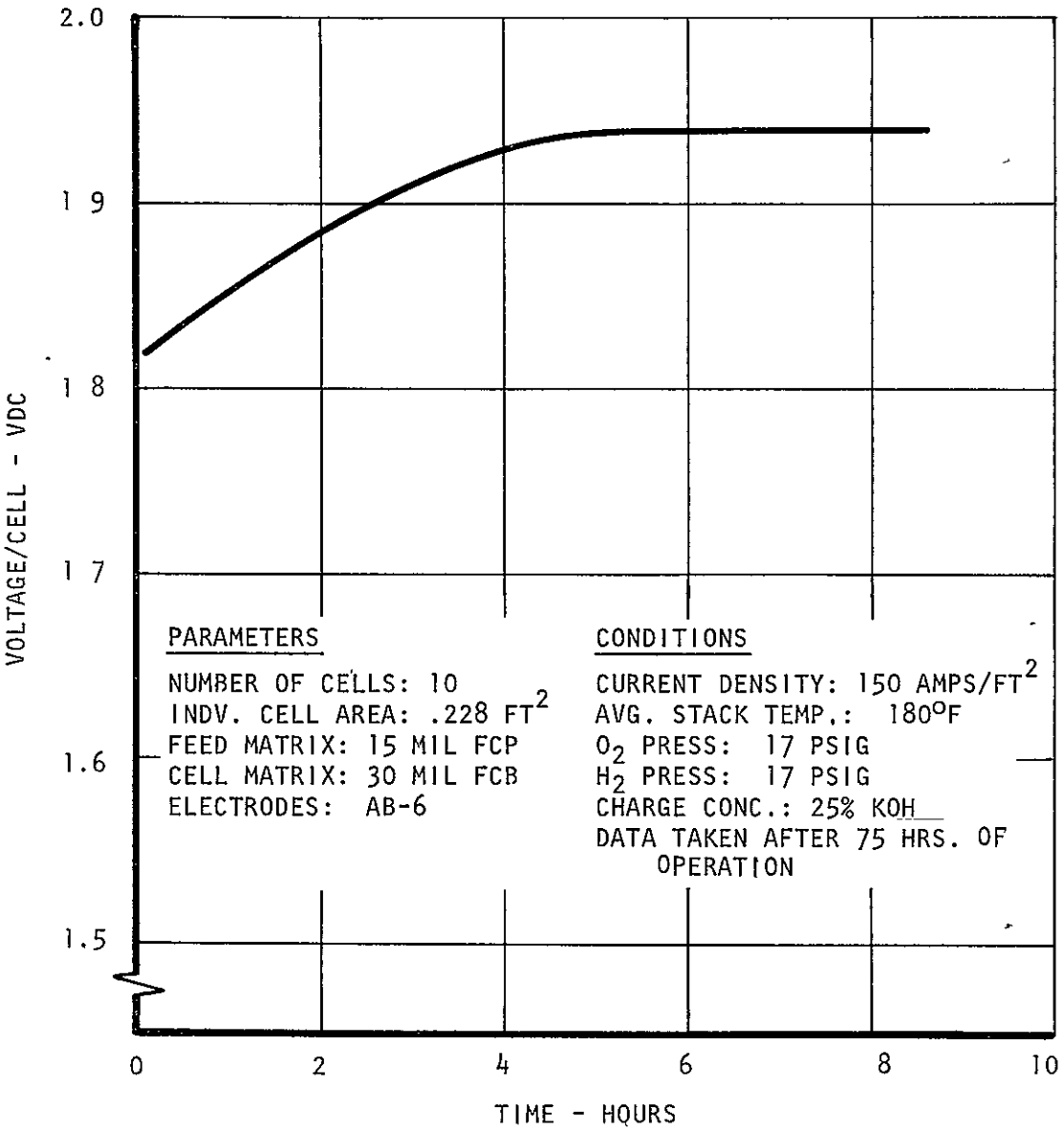

FIGURE 26 ELECTROLYSIS MODULE OVERCAPACITY PERFORMANCE

modes of operation. The objective of the third phase was the evaluation of module performance and construction materials during and after long-term exposure to the cell electrolyte and product gas flow.

Cyclic Testing - In this phase, the module assembly was subjected to a series of 19 simulated aircraft mission operating cycles. It was initially intended that each cycle should consist of a module startup, ten hours of continuous operation at module design conditions, and a module shutdown sequence. After the completion of one cycle, the module was allowed to return to room temperature and pressure conditions before initiating the next operating cycle. Module operating parameters during the nineteen operating cycles are summarized in Table III. Module assembly No. 1, which was employed in this test phase, had previously been subjected to parametric tests. At the completion of this phase, an additional 200 hours of operating time had been accumulated on this assembly, which increased the total module operating time to approximately 480 hours. This test phase successfully demonstrated module performance capability during intermittent duty cycle operations. The major problem encountered in this test phase was associated with the test rig facility. During module shutdown and servicing operations, faulty operation of the solenoid vent valves in the system occasionally resulted in a water flushing of the feed matrix. This intermittent flushing of the matrix eventually caused excessive electrolyte dilution. In order to restore module operating parameters to the desired levels, it was necessary to recharge the module assembly with electrolyte during this test phase.

Endurance Testing - During this test phase, module assembly No. 2 was subjected to continuous operation at design point oxygen generation rate conditions for a period of 1562 hours (65 days). This phase of testing was conducted in the laboratory breadboard system test rig facility. Consequently, the detailed results of this test phase will be found in the Laboratory Breadboard System Final Report (NASA CR-73396). However, a brief summary of module operating parameters and shutdown modes during the endurance test phase has been included (see Table IV) to permit a comparison with long-term life test results.

Long-Term Life Testing - As stated previously, the purpose of this test phase was to evaluate long-term module performance and the materials employed in the module construction. A total of 10,014 hours of life testing were accumulated over a period of 16 months extending from August, 1968 to December 1969. Total module operating time, including parametric and cyclic testing was 10,494 hours. Module assembly No. 1 was exposed to electrolyte for a total of 13,607 hours. Plots illustrating the module current density (amperes per square foot) and average cell voltage (volts D.C.) as a function of elapsed life test time (hours) are shown in Figure 27. Table V is a chronological listing of the various module shutdowns occurring during the test showing the elapsed time in life test, the cause of shutdown, and the corrective action taken to restore module operation. The summary in Table VI separates the module shutdowns into general categories and also illustrates the frequency of shutdowns during successive three-month intervals of testing. During the early phase of long-term testing, test rig component failures were responsible for a majority of the module shutdowns. For example, it was found that the five overvoltage shutdowns (over-voltage limit set at 22 volts for 10 cells) occurring during the first 2700 hours of life testing were caused by an increase in cell internal resistance which was due to loss of electrolyte. The loss of electrolyte, in turn, was the result of accidental flushing of module during automatic

TABLE III

ELECTROLYSIS MODULE, CYCLIC TEST SUMMARY

Run No.	Current Density, amps/ft^2	Stack Temp, °F	O_2 Press, psig	O_2 to H_2 P, psid	Stack Voltage,* VDC Initial	Stack Voltage,* VDC Final	Cycle Duration, hrs.
1	100	178	65	1.4	18.1	18.5	5.3
2	100	177	66	1.4	17.9	18.9	7.0
3	100	175	65	1.5	18.5	18.9	10.0
4	100	176	65	1.8	18.5	18.5	8.0
5	100	180	67	1.9	18.6	20.9	9.5
6	100	180	66	2.8	19.5	20.1	10.2
7	100	180	64	1.0	19.0	21.9	10.1
8	100	175	50	1.9	18.4	20.2	10.0
9	100	185	57	1.7	18.1	18.9	10.0
10	100	180	57	1.0	18.6	20.9	10.1
11	100	180	56	1.5	19.3	21.4	10.0
12	100	175	57	1.5	19.1	21.4	10.1
13	100	175	53	1.9	19.1	21.1	10.0
14	100	182	50	1.6	19.5	21.2	10.1
15	100	174	58	1.5	19.4	21.2	10.0
16	100	176	54	1.4	19.7	23.0	10.2
17	100	177	54	1.6	19.6	22.4	10.0
18	100	176	55	1.4	19.5	23.0	6.4
19	100	175	50	1.3	19.1	21.2	10.2

*For a ten-cell module

TABLE IV

WEM ENDURANCE TEST RESULTS

Total Elapsed Time - 1562 Hours (65 Days). Initial Plan - 1200 Hours (60 Days).

Current Density @ 100 ASF = 630 Hours (Voltage < 2.0 for 75% of Time)

@ 80 ASF - 880 Hours (Voltage < 2.0 for 88% of Time)

ENDURANCE TEST SHUTDOWN SUMMARY

Module Matrix Crossleak (O_2 - H_2)	1 at 700 Hours
Control System Malfunctions	
Differential Pressure (H_2 - H_2O)	3
Overvoltage	3
Solenoid Valve Malfunction (Module Flush)	4
Plant Power Shutdown	2
Voluntary Shutdown for Module Recharge	1
Short Time Power Failure	1
TOTAL:	15 Shutdowns

Module Recharges Required Six Times

Longest Operating Period Without Recharge - 453 Hours

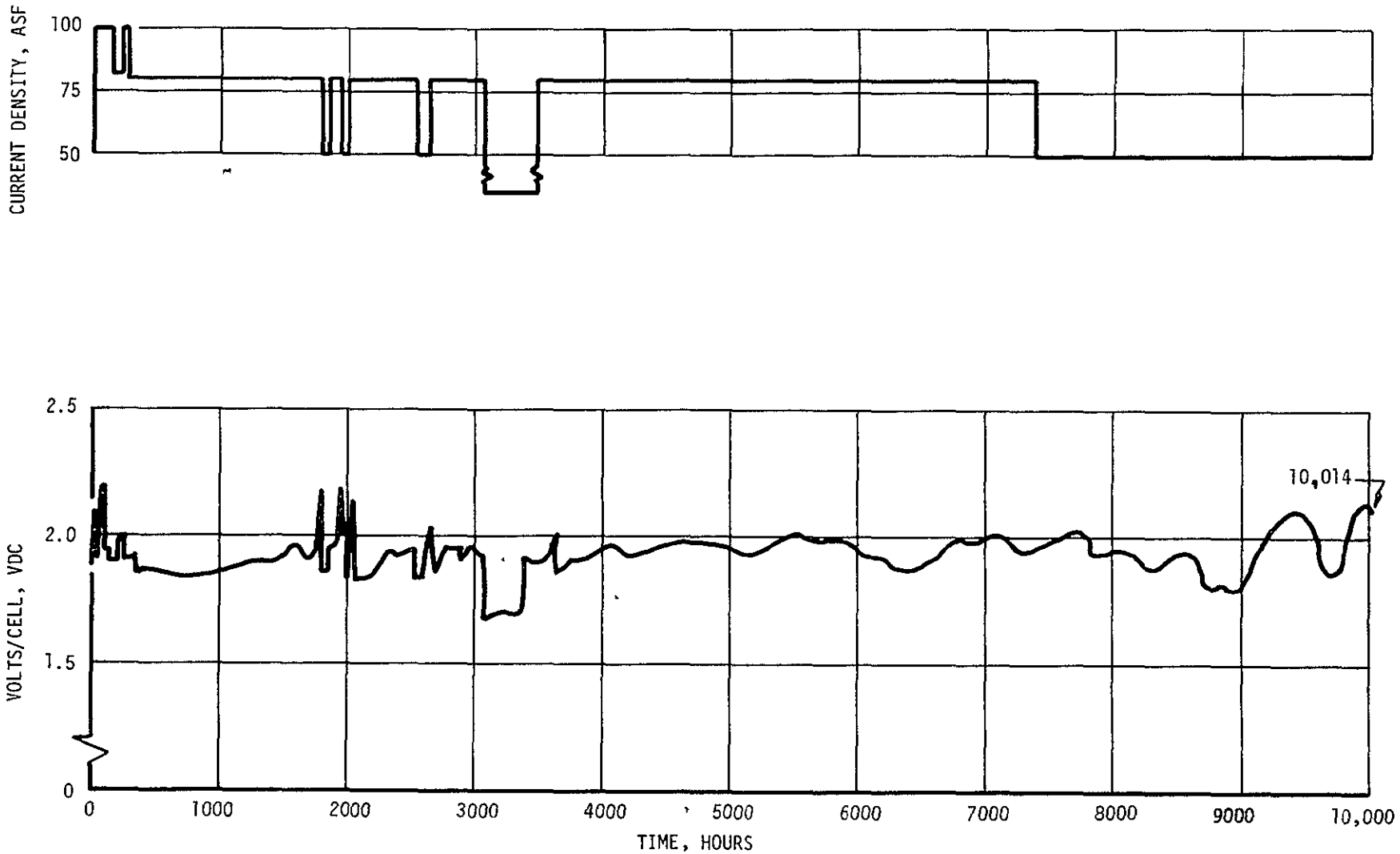

FIGURE 27 ELECTROLYSIS MODULE LIFE TEST

TABLE V

ELECTROLYSIS CELL LIFE TEST
SHUTDOWN SUMMARY

Elapsed Time (in life test) Hours	Cause of Shutdown	Corrective Action
45.8	Plant power shutdown	Restart
64.8	Overvoltage shutdown	Restart
82 to 98.2	Three overvoltage shutdowns; module flushing during automatic shutdowns	Module recharged
348.9	Operator error during rig service; 30 psid across all matrices with resulting module flush	Module recharged
352	Leak in condenser trap, H_2 line	Trap repaired, restart
900	Leak in condenser trap, H_2 line	Trap replaced, restart
1016	Pressure differential gage malfunction	Gage replaced, restart
1255	Split fitting on O_2 flowmeter	Fitting replaced, restart
1542	Leak in condenser trap, H_2 line	Trap repaired, restart
1756	Leak in condenser trap, O_2 line	Trap replaced, restart
1793	Differential pressure limit exceeded	Restart
1885	Differential pressure limit exceeded	Restart
1947	Overvoltage shutdown	Restart
2025	Differential pressure limit exceeded	Restart
2039	Differential pressure limit exceeded. Module accidentally flushed with 700 ml of water (water cavities through O_2 cavities)	Restart, addition of 180 ml of 25% KOH to cell matrix

Table V - continued

Elapsed Time (in life test) Hours	Cause of Shutdown	Corrective Action
2403	Operator error during rig service	Restart
2887	Differential pressure shutdown	Repair short in power supply
3503	Leaking condenser trap in H_2 line and O_2 line. Leaking solenoid valve in O_2 vent line	Replaced H_2 trap Replaced O_2 trap Replaced solenoid valve
3647	Operator error during rig service	Restart
4244	Building power service modification	Restart
4246	Overvoltage shutdown	Restart
5328	Differential pressure shutdown	Restart
5641	Differential pressure shutdown	Cleaned O_2 flowmeter valve and tube; restart
5936	Differential pressure shutdown	Restart
5938	Differential pressure shutdown	Restart
5962	Upper voltage limit (2.2 volts per cell) exceeded, overvoltage shutdown	Restart
6102	Upper voltage limit (2.2 volts per cell) exceeded due to temperature controller failure (module at $80^{o}F$), overvoltage shutdown	Temperature controller repaired; restart
6118	Voluntary shutdown for module recharge	Module recharged; O_2 flowmeter replaced; restart
6207	Operator error during rig service, voluntary shutdown	Replaced feed matrix assemblies in Cells #4 and #5; restart

Table V - continued

Elapsed Time (in life test) Hours	Cause of Shutdown	Corrective Action
6230	Differential pressure gage malfunction; feed water supply flushed through module; differential pressure shutdown	Module recharged; differential pressure gage replaced; restart
6277	Liquid in pressure control circuit; differential pressure shutdown	Replaced filter elements in condenser trap (100 rating instead of 5)
6435	Liquid in pressure control circuit caused by condenser water shutoff. Differential pressure shutdown	Cleaned O_2 flowmeter; restart
6469	Differential pressure shutdown	Pressure control system dried out; pressure regulators; O_2 check valve and H_2 solenoid valve replaced; restart
6517	Differential pressure gage malfunction, differential pressure shutdown	Restart in differential pressure override mode
6522	H_2 to H_2O crossleak	Test rig modifications; partial module disassembly; replaced water cavity subassembly of Cell #10; module charged; restart
6613	Building power failure	Restart
7143	Upper voltage limit (2.2 volts/cell) exceeded	H_2 to H_2O crossleak noted during recharge; partial module disassembly; water spacer screens, small support screens, and 15-mil feed matrices replaced in Cells 1,2,3,6,7,8 & 9; module charged; restart
7172	Upper voltage limit (2.2 volts/cell) exceeded	Soak at operating temp.; restart
7195	Leak around epoxied plug in H_2O plate	Re-epoxied in place; restart

Table V - continued

Elapsed Time (in life test) Hours	Cause of Shutdown	Corrective Action
7254	Plant power off	Restart
7282	Plant power off	Restart
7337	ΔP limit exceeded	Restart
7385	Leaks around two epoxied plugs in H_2O plates	Re-epoxied all plugs;
7493	ΔP limit exceeded	Restart
7767	ΔP limit exceeded	Restart
8296	Current fluctuations; high cell temp. (#9) = 225°F (max) large gas buildup in module	Restart at 25 ASF
8352	Plant power off	Restart at 50 ASF, reduced to 25 ASF
8488	ΔP limit exceeded	Restart
8806	ΔP limit exceeded	Restart
9293	ΔP limit exceeded	Restart
9444	ΔP limit exceeded	Restart
9641	Stack voltage limit exceeded	Restart
9647	Stack voltage limit exceeded	Restart and electrolyte injection
9661	ΔP limit exceeded	Restart
9808	ΔP limit exceeded	Restart
9815	ΔP limit exceeded	Restart
9830	Stack voltage limit exceeded	Restart
9845	ΔP limit exceeded	Restart
10014	Manual shutdown Low individual cell voltages High individual cell temps. Low hydrogen flowrate indication	Life testing termination due to Cell #1 matrix crossleak

control shutdowns or servicing procedures. However, module performance could be restored to original levels by restoring the electrolyte to its proper concentration by either injecting small amounts of electrolyte periodically or a complete module electrolyte recharge. A chronological summary of module recharges and electrolyte injections is found in Table VII showing elapsed life test intervals and the amount of electrolyte (25% KOH) added during module injections. The KOH injections were accomplished without shutting the module down by injecting the solution-into the oxygen manifold cavity of the module. The oxygen to hydrogen to water cavity pressure gradients caused the electrolyte to pass through all cell and feed matrix elements.

Two oxygen purity checks were performed using the Beckman E-2 Analyzer. The first test (after 1849 hours of life test) showed that oxygen purity exceeded the required value of 99.5% by volume. The hydrogen to oxygen pressure differential at the time of the purity test was 0.2 psid. The second oxygen purity check (after 6667 hours of life testing) showed an oxygen purity in excess of 99.7% by volume. The results of a module performance check after 2500 hours are shown in Figure 28. The results of a similar check after 6671 hours, of total test time are illustrated in Figure 29. The major module problems encountered in the course of life tests are summarized in Table VIII. The difficulties have been separated into two major categories. The first lists problems associated with module internal construction and materials, while the second is a summary of test rig oriented problems which contribute to erratic module operation and performance degradation.

The most significant module repair required in the life test program was the replacement of the water feed matrix support screens and water cavity spacer assemblies. These elements were replaced in Cell #4 and #5 after 6207 hours of life test, in #10 after 6522 hours, and in the remaining cells after 7143 hours as a result of reoccurring hydrogen to water cavity crossleaks during module operation. In reassembling the cells, it was found necessary to also replace the module assembly O-rings which had taken a severe permanent set. Dimensions of the O-ring, as taken from the module, measured 0.085" x 0.052" (in the direction of compression) as compared to their original diametral requirement of 0.070-0.073". The magnitude of this permanent set helped to explain the increasing seepage of electrolyte observed on the external surfaces of the module assembly as the life test progressed. Product gas leakage, however, appeared to be insignificant.

Leaks around the epoxied plug used to seal the hole employed in drilling the manifold-to-cavity ports were considered insignificant for over 7000 hours of life testing. One water plate leak was discovered after 7195 hours of life test and two additional water plate leaks occurred after 7385 hours of life test. At this time, the module was shutdown and all plugs on the module re-epoxied. As a result, it was estimated that the useful life of epoxy material (Minnesota Mining and Mfg. Co. Type EC-2216) employed in the module construction was approximately 11,000 hours at a temperature of 175°F when exposed to 25% KOH electrolyte solution.

TABLE VI

WEM LIFT TEST
SHUTDOWN SUMMARY

Reporting Date	9/68	12/68	3/69	6/69	9/69	12/69	3/70	TOTAL
Elapsed Time Life Test (Hours)	490	2700	4750	6500	7770	9660	10014	
1. Control System Malfunctions								
Differential Pressure (H_2-H_2O)	-	4	-	6	2	6	3	21
Overvoltage	4	1	1	2	2	2	1	13
Overtemperature	-	-	-	-	-	1	-	1
								35
2. Test Rig Problems								
Rig Component Failures	-	6	2	3	-	-	-	11
Operator Error	1	1	1	1	-	-	-	4
Plant Power Shutdown	1	-	1	-	3	1	-	6
								21
3. Module Problems								
Module Repair (Matrices)	-	-	-	1	1	-	1	3
Epoxy Leaks	-	-	-	-	2	-	-	2
Module Electrolyte Recharge	-	-	-	1	-	1	-	2
								7
					TOTAL SHUTDOWNS			63

TABLE VII

SUMMARY OF MODULE ELECTROLYTE RECHARGE
AND INJECTION SCHEDULE

Elapsed Life Test (Hours)	Action	Cause
98.2	Module recharge	Module flush
348.9	Module recharge	Module flush
1995	Injection (180 ml KOH)	
2039	Injection (180 ml)	
2046	Injection (180 ml)	
2711	Injection (120 ml)	
3386	Injection (120 ml)	
3667	Injection (120 ml)	
4249	Injection (120 ml)	
5642	Injection (120 ml)	
5964	Injection (100 ml)	
6064	Injection (100 ml)	
6118	Module recharge	Shutdown frequency
6230	Module recharge	Module flush
6522	Module recharge	Module repair
6980	Injection (120 ml)	
7143	Module recharge	Module repair
7283	Injection (100 ml)	
7383	Injection (120 ml)	
7770	Injection (100 ml)	
8087	Injection (120 ml)	
8320	Injection (120 ml)	
8449	Module recharge	Erratic cell performance
9003	Injection (120 ml)	
9647	Injection (80 ml)	

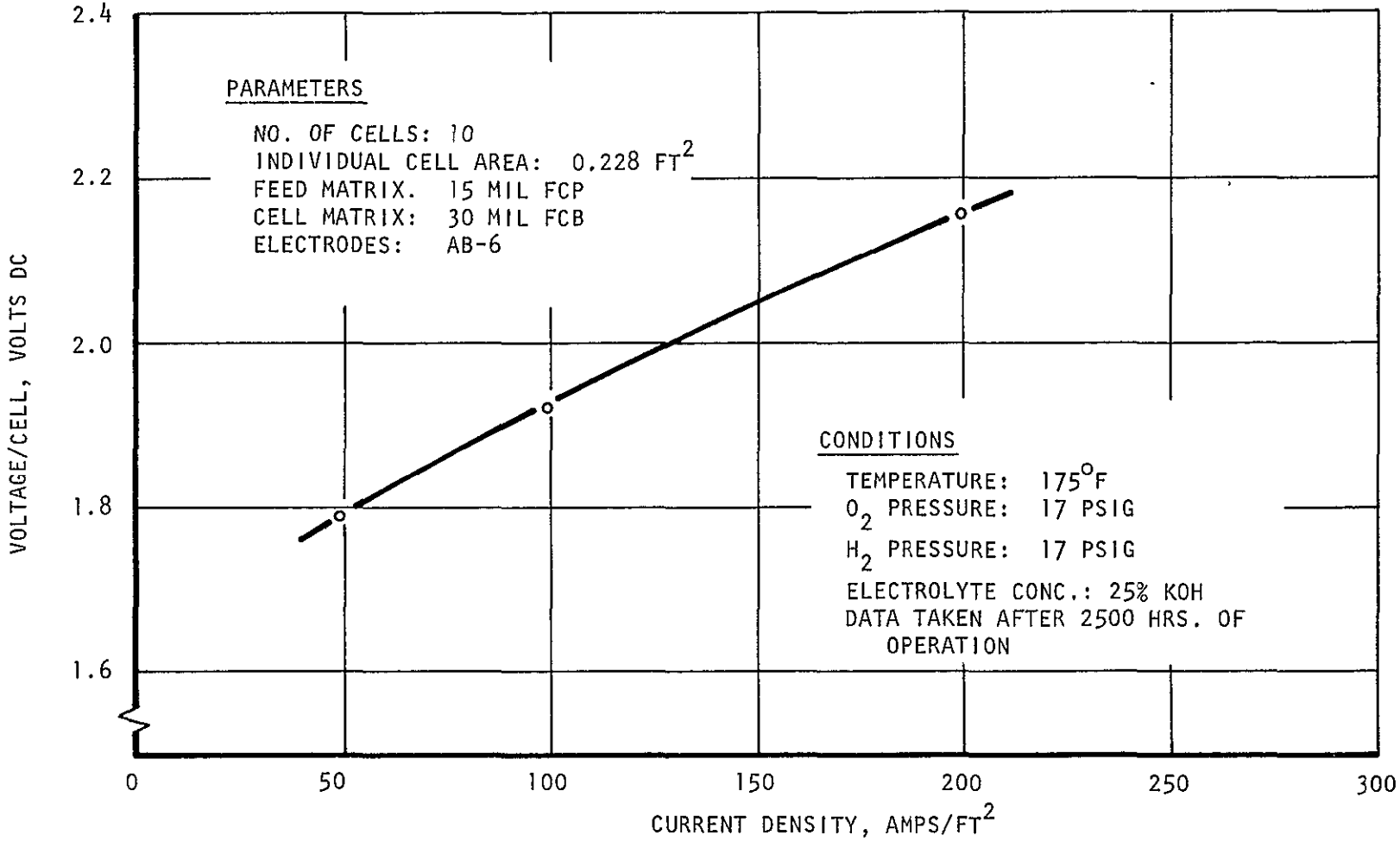

FIGURE 28 ELECTROLYSIS MODULE PERFORMANCE AFTER 2500 HRS. TOTAL OPERATING TIME

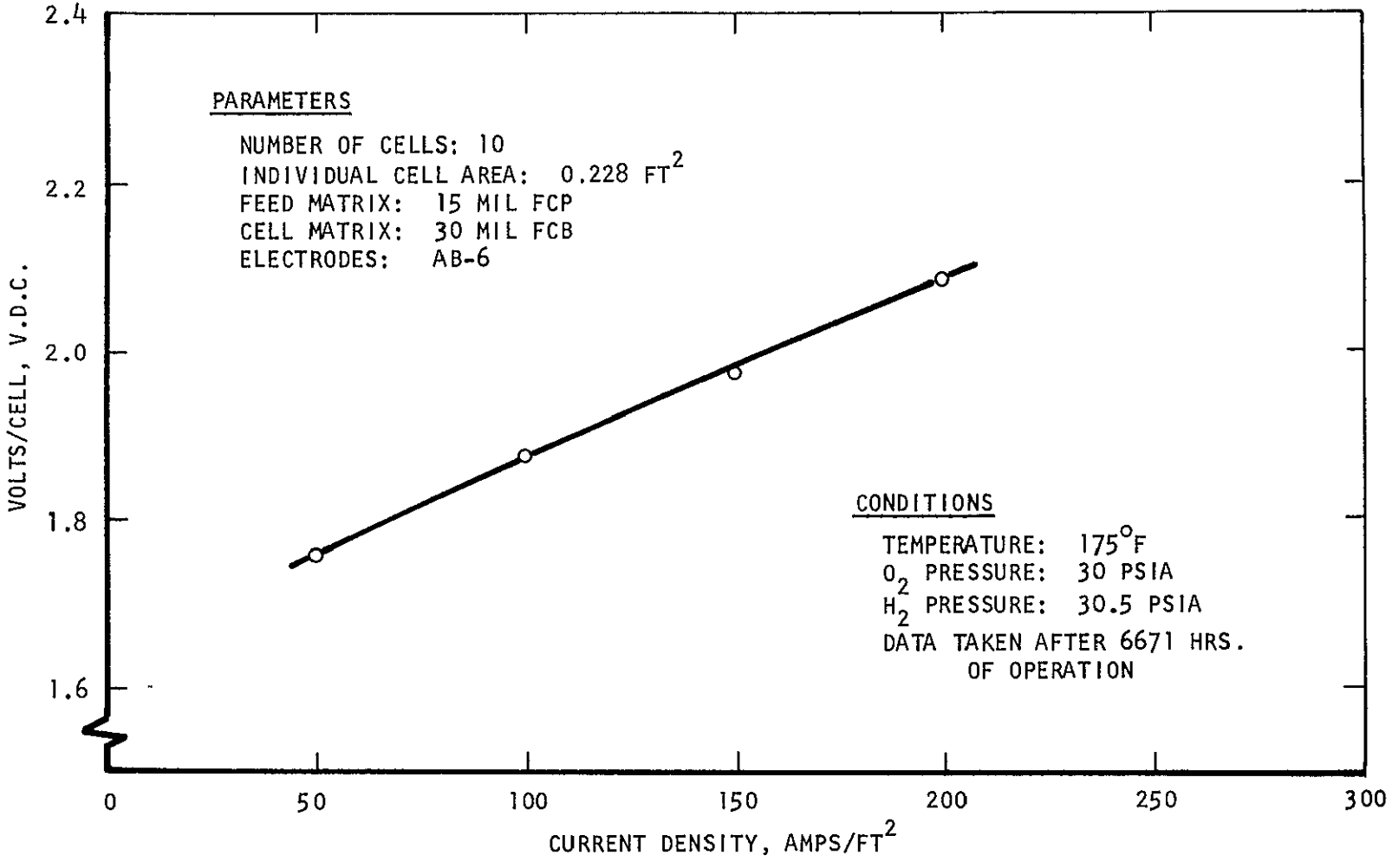

FIGURE 29 ELECTROLYSIS MODULE PERFORMANCE AFTER 6671 HOURS OF TOTAL OPERATING TIME

TABLE VIII

MODULE PROBLEMS DURING LIFE TESTING

A. Module Design and Materials

Component	Problem	Apparent Cause	Result
1. Water cavity spacer and matrix support screens	Material shrinkage and embrittlement (polypropylene)	Chemical action of electrolyte plus elevated temperature	Mesh deterioration and loss of matrix edge support
2. O-ring elements	Permanent deformation	Assembly compression load plus temperature	Loss of sealing capability and electrolyte leakage (external)
3. Water plate assemblies	Manifold plug epoxy joint failures	Plate expansion and contraction cycles due to temperature	External gas and electrolyte leakage
4. Cell matrices	Matrix rupture (crossover)	(a)matrix dryout due to excessive gas formation (b)excessive ΔP across matrix element (c)material flaws	Crossover $O_2 \rightarrow H_2$ cavity $H_2 \rightarrow H_2O$ cavity Loss of cell and module performance

B. Test Rig Oriented Problems

1. Module electrolyte dilution	Module flushing during control shutdowns and servicing (solenoid valves, condenser trap, operator error.
2. Overvoltage control shutdowns	Increased internal cell resistance due to electrolyte dilution
3. Pressure control circuitry	Water backflow into module, gages, and regulators due to condenser trap filter saturation
4. H_2-H_2O ΔP control shutdowns	O_2 flowmeter valve sticking - pressure shift. Regulators employed lack capability of ΔP adjustment during system pressure level shift
5. Servicing requirements for water tank and condensor traps	Frequency increased chances of electrolyte dilution due to operator error
6. Low module current input	Constant current control limitations (electrolyte dilution)

It should be emphasized that only one matrix element failure was experienced during more than 10,000 hours of module testing. This failure occurred just prior to the termination of the life test program. A rapid decrease in the damaged cell voltage and a significant drop in hydrogen product gas flowrate indicated an oxygen-hydrogen matrix failure. A manual shutdown sequence was employed to avoid further module damage. Following an unsuccessful attempt to recharge the module with electrolyte (because of the matrix crossleak), the module was disassembled in preparation for a post-life test inspection. The results of the module post-test inspection are described in detail in Appendix C. Photographs were taken to illustrate the condition of typical internal cell components and also document any isolated instances of extreme component damage observed during the inspection procedure.

CONCLUSIONS

The following conclusions relative to the water electrolysis module assembly were reached on the basis of information derived from the NAOS development program.

1. The long-term operational capability of the Water Electrolysis Module as designed was demonstrated in the life test in which WEM #1 was operated continuously for more than 10,000 hours. Required replacement of module components was minimal.

2. The ability to maintain design performance capability for extended periods of continuous operation was successfully demonstrated.

3. The module proved capable of immediate full operation after long storage periods in the charged (electrolyte) condition.

4. Additional study is required to establish more suitable materials for use in supporting the water feed matrix.

5. For operation of water electrolysis modules for durations exceeding 10,000 hours, elimination of epoxy sealed ports will be required.

6. Gas analyses results reveal gas purities within expected ranges.

7. The water feed cavity and water feed lines must be electrically isolated to prevent stray electrical currents which may cause electrolysis to occur in the water feed lines.

8. Evaporative cooling of the electrolysis module does not appear practical for aircraft application.

9. The Water Electrolysis Module meets the system design specifications for oxygen generation using the static water feed principle. Degassing of the feed water prior to use is not required.

10. An electrolysis cell using static water feed could be operated using tap water for at least several hundred hours, if distilled water were not available. In an emergency, water-glycol mixtures could be used for short-duration runs.

RECOMMENDATIONS

Based on NAOS program experience, the following recommendations are made with regard to module design modifications and the selection of materials employed in the cell construction:

1. A materials investigation should be conducted to improve material compatibility in the water feed matrix support screen and water cavity spacer components. This investigation should include the possibility of improving the present plastic material (propylene) employed through improved heat stabilization techniques as well as uncover more suitable material alternatives.

2. The fabrication technique employed in providing product gas porting (cell to manifold connection) in the water plate subassembly should be modified to eliminate the need for external epoxied plug installations in the plate construction.

3. Because of the excessive permanent setting of O-rings experienced in the module testing, the following possibilities should be explored:

   - Reduction of the number of O-rings installations in the assembly
   - More compatible O-ring materials
   - Modify O-ring groove dimensions to establish minimum section squeeze required to insure positive sealing in application
   - Examine alternate seal types with equivalent groove geometry

4. A Water Electrolysis Module Development Program should be continued incorporating the following:

   - Provision of a liquid-gas separator for degassing feed water cavity
   - Improved water feed matrix support
   - Decrease number of cell components and number of seals per cell.
   - Provide more integral structure for metal components to reduce electrical losses due to formation of oxides.
   - Improve sealing design
   - Elimination of epoxied access ports
   - More optimum selection of cell electrolyte concentrations

- Selection of oxygen electrode more specifically designed for application
- Incorporation of internal liquid cooling passages
- Submodule construction to improve ease of assembly, check-out and repair.

APPENDIX A-1

TABLE OF CONTENTS

APPENDIX A

EFFECTS OF WATER FEED QUALITY ON PERFORMANCE OF A STATIC FEED WATER ELECTROLYSIS CELL

INTRODUCTION AND SUMMARY

An on-board aircraft oxygen generating system, which uses water electrolysis as the source of oxygen, would have a decreased maintenance requirement if the source of water for electrolysis could be obtained from an existing source, e.g. water used for the aircraft cooling system. These water stores generally have other constituents such as methanol or ethylene glycol. These water sources could be considered for use in the electrolysis cells, if the cells could tolerate water of that quality. A testing program was conducted to establish whether or not an electrolysis cell can efficiently be operated using water feeds of non-distilled quality.

The objective of this program is establishing the degree of effectiveness of aqueous glycol, aqueous methanol and tap water feed systems in a static water feed electrolysis system.

The results indicate that an aqueous feed with an impurity level of approximately 10% of the total feed can be effectively used and can be expected to function within operating limits for specified durations of time. In the case of low vapor pressure of contaminant the outlook is particularly attractive whereas for impurities with a high vapor pressure, added components would be required to reduce possible contamination in an effluent oxygen stream.

THEORETICAL ANALYSES

In order to properly evaluate this program, it is necessary to undertake a thorough analysis of the vapor feed electrolysis cell.

The vapor feed electrolysis unit operates as a function of the concentration difference between the feed matrix and the electrolyte matrix. Flow of water vapor is directly proportional to the vapor pressure difference. The problems encountered in the non-pure water feed systems are principally a function of increased impurity build-up in the feed cavity with a corresponding decrease in the vapor pressure of the water.

Electrolysis of Water

Electrolysis is divided into the anodic and cathodic electrode processes.

Cathode: $2H_2O + 2e^- \longrightarrow 2OH^- + H_2$ (1)

Anode: $2OH^- \longrightarrow 2e^- + 1/2\ O_2 + H_2O$ (2)

Overall Process: $H_2O \longrightarrow H_2 + 1/2\ O_2$ (3)

Utilization of water is divided into the electrolysis of the water; the humidification of the hydrogen gas produced and the humidification of the oxygen gas produced.

According to Faraday's Laws of Electrolysis, the summarizing equation is:

$$\frac{m}{M.W.} = \frac{It}{/z/F} \qquad (4)$$

m = mass of water electrolyzed; grams

MW = gram molecular weight; grams of water

I = current; amps

t = time; seconds

/z/ = equivalent charge for the process, absolute value

F = Faraday's constant 96,479 coulombs (amp-seconds)

From equations (1) and (2) the equivalent charge for the process is 2. The molecular weight of water is 18.016 grams. Figure A-1 gives the mass of water electrolyzed as a function of current for 1 minute.

From equation (2) it must be noted that 1 molecule of water is produced at the anode. For an electrolysis system employing an electrolyte matrix instead of a free electrolyte subsystem it must be realized that there are diffusion

considerations resulting in a concentration gradient that will be set up in the electrolyte matrix. Therefore, the number of molecules of water, on the average, to produce one molecule of oxygen is slightly greater than two.

Generation And Humidification Of Hydrogen And Oxygen

According to equation (4) the mass of hydrogen and oxygen gas is generated as a function of current. Figures A-2 and A-4 show the mass flow per minute versus current. The humidification of evolving gas is a function of temperature, electrolyte concentration, feed matrix concentration and current at a total pressure of 1 atmosphere. Consider the following:

$$\frac{E}{D} = \frac{\text{water required for humidification of hydrogen and oxygen}}{\text{water electrolyzed}} \tag{5}$$

$$\frac{E}{D} = \frac{P_{H_2O(H_2)}}{p_T - p\ H_2O(H_2)} + 1/2\ \frac{P_{H_2O(O_2)}}{p_T - p\ H_2O(O_2)} \tag{6}$$

where $P_{H_2O(H_2)}$ = partial pressure of water vapor in H_2 effluent and $P_{H_2O(O_2)}$ is the partial presure of water vapor in oxygen effluent and P_T is total pressure of gases. If

$$P_{H_2O(H_2)} = P_{H_2O(O_2)} = P_{(H_2O)}$$

p_T is constant but p_{H_2O} varies as the temperature and electrolyte concentration change, as shown in Table A-1.

TABLE A-1

WATER VAPOR PRESSURE FOR AQUEOUS KOH SOLUTIONS

Water Vapor Pressure, pounds per square inch

	Temperature, °F		
Per Cent KOH	150	160	170
40	1.45	1.90	2.40
32	2.10	2.70	3.40
20	2.95	3.75	4.75
0	7.70	4.75	6.00

Since oxygen is humidified on the anode side the partial pressure of water will be that of the charging concentration of electrolyte. Therefore,

$$\frac{E}{D} = \frac{P_{H_2O(O_2)}}{P_T - P_{H_2O(O_2)}} \tag{7}$$

$$= 1/2\ \frac{3.4}{14.7 - 3.4} = 1/2\ \frac{3.4}{11.3} = 0.15 \quad \text{at } 170^{\circ}F$$

$$= 1/2\ \frac{2.7}{14.7 - 2.7} = 1/2\ \frac{2.7}{12} = 0.11 \quad \text{at } 160^{\circ}F$$

$$= 1/2\ \frac{2.1}{14.7 - 2.1} = 1/2\ \frac{2.1}{12.6} = 0.08 \quad \text{at } 150^{\circ}F$$

The situation on the hydrogen side is altered because of the water vapor present from the water feed cavity and this will be a function of concentration of water in the feed cavity. The electrolyte concentration may be omitted because the cathode is a water utilizing electrode. Assume 20% concentration in the water feed cavity.

$$\frac{E}{D} = \frac{P_{H_2O(H_2)}}{P_T - P_{H_2O(H_2)}} \tag{8}$$

$$= \frac{4.75}{14.7 - 4.75} = \frac{4.75}{9.95} = 0.48, \quad \text{at } 170^{\circ}$$

$$\frac{3.75}{14.7 - 3.75} = \frac{3.75}{10.95} = 0.34, \quad \text{at } 160^{\circ}$$

$$\frac{2.95}{14.7 - 2.95} = \frac{2.95}{11.75} = 0.30, \quad \text{at } 150^{\circ}$$

Figures A-3 and A-5 give rate of water loss on humidification of gas.

Criteria Of Operation

Nominal design operating point for the water electrolysis cell is at a current density of 100 ASF with a terminal voltage no greater than 2.0 volts. Normal mission time will be ten hours. In the experimental analysis, 100 ASF corresponds to 6.25 amps with an electrode area of 0.0625 ft^2. The electrolyte in the system is 32 weight %KOH. This concentration gives a near maximum specific conductivity. High operating temperature (e.g., 160°F) compromises the effect of increased diffusion of water vapor against humidification of evolving gases.

Diffusion of Water Vapor Across Hydrogen Cavity

The amount of water vapor transported from feed matrix to electrolyte matrix is a function of vapor pressure differential between the two matrices. Consider the equation for equimolar counter diffusion:

$$N_A = \frac{D_V}{RTB} (p_1 - p_2) \tag{9}$$

which describes the mass of water transported across the hydrogen cavity.

At this point the assumption is made that the water vapor diffuses through an atmosphere of hydrogen and saturates it. Water loss, because of humidification of hydrogen gas, is treated in an above section. Also, it is assumed there is no aerosol formation.

In equation (9);

N_A = net rate of diffusion of water vapor, g-moles/sec cm^2

D_V = diffusivity of water vapor, cm^2/sec

R = universal gas constant, 82.06 cc atm/g-mole ^oK

p_1 = vapor pressure of water in feed matrix, atm.

p_2 = vapor pressure of water in electrolyte matrix, atm.

T = temperature, ^{o}Kelvin

B = thickness of gas between two matrices, cm

The temperature and pressure dependence of the diffusivity is described in the following equation:

$$D_V = D_o \left(\frac{T}{T_o}\right)^m \frac{P_o}{P} \tag{10}$$

where

$T_o = 273^o$ Kelvin

P_o = 1 atm

D_o = diffusivity at 273^oK and 1 atm

m = empirical constant, dependent on size of molecules

Hence, for hydrogen in water vapor:

$m = 1.75$

$D_o = 0.7516\ cm^2/sec$

$P = 1\ atm$

$T = 160^oF\ (343^oK)$

Therefore, $D_V = 1.12\ cm^2/sec$

Since $T \doteq 343^oK$ and $B = 0.318$ cm

$N_A = 1.25 \times 10^{-4}\ (p_1 - p_2)\ mole/cm^2\ sec$

For a 3" x 3" area

$N = 0.7840\ (p_1 - p_2)\ gm/min$

This data is plotted in Figure A-6 at different temperatures.

Note: Some data has been generated for feed matrices of different thickness and it has been shown that the rate controlling step of the water vapor across the cell may actually be dependent upon diffusion of water through the asbestos matrix.

Ethylene Glycol - Water Feed System

In this section the feasibility of this type of feed system will be demonstrated for a range of concentrations. The vapor pressure for 32% KOH ranges from 50mm Hg at 120^oF to 218mm Hg at 180^oF with a vapor pressure of 126mm Hg at 160^oF. This data is plotted in Figure A-7.

Vapor pressure of Ethylene Glycol-Water solutions as a function of concentration for different temperatures is presented in Figure A-8. The expected operating time of each feed system under the conditions already specified is presented in Table A-2. This table is generated by computing the rate of impurity buildup in the feed cavity and by equating at which time the vapor pressure of the water component in the feed cavity is equivalent to the vapor pressure of the water in the charging solution.

Figure A-9 presents the water loss from the feed cavity as a function of current and temperature and knowing the vapor pressure of water in the electrolyte cavity it is possible to generate Table A-2.

It is realized that as electrolysis proceeds, electrolyte concentration in the matrix will increase thereby increasing the flow of water vapor across the hydrogen gas cavity. However, it is difficult to calculate the electrolyte concentration and the concentration gradient that is established in the system once electrolysis begins. Therefore, neglecting power requirements, Table A-2 presents the minimum amount of time that the unit will function.

TABLE A-2

EXPECTED CELL OPERATING TIME WITH WATER-GLYCOL FEED SYSTEM

Concentration	Expected Operating Time
90% Water 10% Glycol	30 Hours
80% Water 20% Glycol	15 Hours
70% Water 30% Glycol	7 Hours
50% Water 50% Glycol	2 Hours

Note: Ethylene Glycol is infinitely soluble in water. Vapor pressure of glycol at 160°F is 5 mm Hg. Glycol compatibility with KOH is substantiated by the process of glycol production from permanganate oxidation of the alkene with KOH as a by-product. This is a relatively low temperature process (less than 200°C; boiling point of glycol is 197.2°C).

Methanol-Water Feed System

In Table A-3 the expected operating time of a methanol-water feed system of varying concentrations is presented.

Table A-3 is based on Figure A-10 for water loss from feed cavity data. The chemical properties of methanol are similar and interaction with KOH is not expected. However, unlike glycol, methanol has a very high vapor pressure and will tend to concentrate in the electrolyte cavity replacing the water vapor and possibly accelerating the degradation of the electrolysis cell.

TABLE A-3

EXPECTED CELL OPERATING TIME WITH WATER-METHANOL FEED SYSTEM

Concentration	Expected Operating Time
90% Water 10% Methanol	20 Hours

Concentration	Expected Operating Time
80% Water 20% Methanol	8 Hours
70% Water 30% Methanol	4 Hours
50% Water 50% Methanol	0.5 Hours 0.5 Hours

Tap Water Feed System

Tap water has the usual impurities which are listed in Table A-4, with their normal and maximum concentrations.

Table A-5 lists solubility data at 160°F. Table A-5 notes that of all the possible chemical interactions only the $Mg(OH)_2$ is expected to be somewhat insoluble. The Mg has a maximum concentration of 20 ppm. Therefore 17 ppm of $Mg(OH)_2$ will precipitate out of solution. Compared to the total amount of solids in the water this is rather insignificant.

Figure A-11 presents the rate of impurity build-up in the feed cavity and shows that systems with an initial 300 ppm impurity level could have expected operating time of over ten thousand hours whereas a system with an initial impurity of 400 ppm has an expected operating time of well over 5000 hours.

TABLE A-4

NORMAL IMPURITIES IN TAP WATER*

Impurity	Normal Concentration	Maximum Concentration
CO_2 (free)	7 ppm	20 ppm
Ca	36.1 ppm	50 ppm
Mg	8.7 ppm	20 ppm
SO_4	26.7 ppm	40 ppm
Cl	27.0 ppm	40 ppm
Total Solid	300 ppm	400 ppm

*Water Department, Cleveland, Ohio

TABLE A-5

WATER SOLUBILITY DATA*

Compound	Solubility gms/100 gms H_2O at 160°F
$CaCl_2$	141.7
$CaSO_4$	1.97×10^{-1}
$Ca(OH)_2$	1.06×10^{-1}
$Mg(OH)_2$	10^{-4}
$Mg(Cl_2)$	66.0
$Mg(SO)_4$	37.3
KCl	45.5
KOH	178.0
K_2SO_4	19.75

*Handbook of Chemistry & Physics 41st Edition

Calculation Of Ohmic Polarization

From Figure A-12 it is evident that the maximum specific conductivity of KOH occurs in the region of 32 weight percent.

The cell resistance may be calculated from the equation:

$$R = \frac{L}{A\ K_c} \tag{11}$$

where

R = cell resistance; ohms

L = distance between electrodes; cm

A = area of electrode, cm^2

K = specific conductivity, ohm^{-1}, cm^{-1}

From this equation it is readily evident that as the specific conductivity decreases the cell resistance will rise but it is also necessary to examine the A term.

Separating the electrodes is an asbestos matrix which contains the electrolyte. Electrolyte concentration increases as the aqueous constituent is electrolyzed. The resistance is increased in these ways:

1) drop of conductance because electrolyte concentration increased

2) dissipation of solution volume allowing produced gases to fill

Therefore, the true or effective area should be cited rather than the geometrical area.

$$R = \frac{L}{A\ K_c} = \frac{0.0635}{40.7 \times 1.250} = 1.25 \times 10^{-3} \text{ ohms}$$

Where A is the effective area of the matrix between electrodes with a porosity of 70% and an area of 58.4 cm^2.

Since

$I = 6.25$ amps and $R = 1.25 \times 10^{-3}$ ohms

V = amps x ohms = 8 millivolts

Note: From experience it has been noted that iR drops as high as 340 MV have been recorded when the current is 6.25 amps and initial charge concentration is 32% KOH. In this case the resistance is 54.5×10^{-3} ohm. The geometrical area of the electrode is over 50 cm^2 but the "true" area is approximately 1 cm^2.

EXPERIMENTAL

A single cell system was constructed with appropriate thermal control, pressure regulation, external feed supply and D.C. power source to test the different feed systems. Figure A-13 presents a schematic diagram of the test system.

Chemicals

Pure Water - Singly distilled Stokes water.

Tap Water - City of Cleveland water containing a total solid impurity level of approximately 300 ppm.

Methanol - Mallinchrodt, 99.5% pure; 0.10% water; used as is.

Ethylene Glycol - Union Carbide, "Prestone"; Ethylene Glycol - 93% Soluble Inorganic Inhibitors - 2%; Insoluble Polar Film - 1%, Water - 3.6%; Dye - Trace, used as is.

Potassium Hydroxide - Fisher Scientific, 45.1% w/w - diluted to 32%; used to charge electrolysis cell.

Equipment

Electrolysis Cell - The cell (Figure A-14 shows a cross-section of the cell) consists of three plates, two endplates and a midplate. One endplate served as the current collector for the anode and was constructed of brass base with an electroplate of nickel and a flash of gold. The midplate serving as the cathode was of the same material composition. The other endplate was made of plexiglass and within it was the static feed cavity. The clear plexiglass afforded an excellent opportunity to monitor the liquid level.

The electrodes used were American Cyanamid AB-6, a gold-plated nickel screen with a platinum black-teflon mixture impregnated into the screen. Johns Manville fuel cell asbestos, 0.030" thick, was used as the electrolyte matrix between the two electrodes. A 0.015" asbestos matrix was used to separate the feed cavity from the cathode compartment and allowed feed to diffuse through the cathode. Appropriate neoprene gasketing separated the plates and insulated them from each other as well as sealing the cavities. Attached to the anode endplate are two Dale RH-50 heaters with a 50 watt capacity.

Temperature Control - Cell temperature was controlled by a Fenwall Temperature Controller which is capable of holding the temperature in a properly insulated cell $\pm 1^{o}F$. Controller readout was a Sim-ply-trol pyrometer with an iron constantan thermocouple calibrated with an external resistance of 10 ohm.

Pressure - Back pressure was applied to the individual gas cavities by venting the exhausted gases into individual bubblers of water. For both exhausts, the back pressure varied from four (4) to six (6) inches of water. An applied pressure differential from anode to cathode of two inches of water to force the water being produced at the anode into the electrolyte matrix is an

attempt to aid in the reduction of the concentration differential established as a result of the electrolysis.

External Feed Reservoir - This reservoir had a capacity that would feed the cell for three (3) days without replenishing under the condition stated in the following section. All the solutions used as feed, except Methanol solutions, were boiled in the reservoir and recondensed by an air-cooled condenser in order to evolve as much trapped gas from the solution as possible.

Purge Unit - In order to remove collected gases from the feed cavity and to flush the feed cavity a purge bottle with a rubber bulb was used to evacuate the chamber. These dissolved gases, when liberated, affect the amount of water transported to the cathode and decrease cell efficiency.

Electrical Instrumentation - A Kordesch Marko bridge of the 60 cps sine wave variety was used in obtaining all current and voltage information. This instrument has a capability of providing both terminal and iR-free voltage information for both the half cell and the total cell. The voltage scale can be read $\pm$ 0.001V for iR drop scale. Current scale can be read $\pm$ 0.02 amp. The bridge also serves as a power supply for cell operation.

Wet Testmeter - A wet testmeter (Precision Scientific) with a Drierite tube at its inlet was used to make spot checks to monitor stoichiometry of the system with respect to current. This unit has an accuracy of $\pm$ 0.002 CF.

Operating Conditions

The following operating conditions have been designed to give a high performance level. These conditions are based in part on the results obtained in the theoretical section of this report.

Current Density	100 ASF
Active Electrode Area	0.0625 ft^2
Current	6.25 amps
Temperature	160°F
Pressure O_2	6" H_2O
Pressure H_2	4" H_2O
Electrolyte Concentration	32% KOH (by weight)
Feed	Variable

Results

Pure Water - The experimental results for each of the eight experiments are presented in Table A-6. The pure water system underwent continuous operation for 140 hours, demonstrating a performance level of 1.73v at 100 ASF. Figure A-15 shows a period of stability covering the last 70 hours where increase in voltage rates for terminal voltage, iR-free voltage and iR drop voltage is zero, within the measuring capability of the meters. The iR drop voltage reached a peak of 70mv with a final iR-free voltage of 1.66v.

Tap Water - A tap water feed system (99.97%) with a 300 ppm total solid impurity level reached a terminal voltage of 2.00v after 122 hours of continuous operation. At the end of the run (145 hours) a total cell voltage of 2.07v was reached. Corresponding iR drop voltages for both points are 200mv and 225mv, respectively.

The values cited for the tap water experiment may be readily gleaned from Figure A-16 which shows a relatively stable state developed in the iR-free voltage over the duration of the run compared to an excessive ohmic polarization manifested by a 2.3mv/hr increase at the time the run was terminated.

Ethylene Glycol-Water - The results of the 85-15 test shown in Figure A-17 indicate that the system seems to be tending toward stability after 18 hours of testing. At the end of the run, the rate of increase of ohmic polarization accounts completely for increasing cell potential whereas at the 2.0v mark, the iR-free voltage was increasing at the rate of 6mv/hr and the iR drop was increasing at the rate of 13mv/hr. The 2.0v mark corresponds to 10.5 hours of continuous testing.

A rapidly rising terminal voltage for the 70-30 glycol feed started to stabilize at 2.05v after 4 hours of continuous operation. As Figure A-18 shows, this was short-lived for as the fifth hour the ohmic potential (iR drop voltage) started increasing at a rate of 40mv/hr. However, the iR-free voltage was increasing at this point at a rate of 27mv/hr and both rates maintained themselves until the end of the run at 7.5 hours. The 2.0v mark was reached at 3 hours of operation.

The most characteristic aspect of the 50-50 feed is an ohmic polarization rate of 167mv/hr at the 2.35v mark of total cell performance. This occurred after 6.2 hours of continuous performance. Figure A-19 demonstrates that a relatively stable iR-free region seems to be starting at the 6 hour mark. The 2.0v mark was reached at 3.8 hours of operation.

Methanol-Water - The 90-10 methanol system stabilized after 7 hours of continuous operation and terminal voltage increased from 1.95v to 1.97v for the remaining 24.5 hours of operation for a total run time of 31.5 hours. Over the last 24 hours the ohmic polarization steadily increased from 80mv to 100mv and the iR-free voltage remained at a constant 188v. Figure A-20 demonstrates the stability of the system.

TABLE A-6

PERFORMANCE DATA FROM FEED QUALITY TESTING PROGRAM

Feed Composition	Pure Water (Reference)	Tap Water (99.97% Pure)	15% Glycol - 85% Pure Water	30% Glycol - 70% Pure Water	50% Glycol - 50% Pure Water	10% Methanol - 90% Pure Water	15% Methanol - 85% Pure Water	30% Methanol - 70% Pure Water
Degassed	Yes	Yes	Yes	Yes	Yes	No	No	No
Theoretical Running Time (Hours)	--	10,000	22	7	2	20	12	4
Experimental Running Time (Hours)	140	145	18	7.5	6	31.5	30	3
Initial Terminal Voltage (VDC)	1.48	1.65	1.50	1.51	1.51	1.52	1.50	1.53
Initial iR Drop Voltage (millivolts)	40	45	40	30	30	30	30	35
Initial iR Free Voltage (VDC)	1.44	1.61	1.46*	1.48*	1.48*	1.49	1.47*	1.50
Final Terminal Voltage (VDC)	1.73	2.07	2.08	2.20	2.35	1.97	2.09	2.24
Final iR Drop Voltage (millivolts)	70	255	242	200	360	100	120	320
Final iR Free Voltage (VDC)	1.66	1.80	1.84	2.0	1.99	1.88	1.97	1.91
Total Run Time @ 20 Volts (Hrs)	--	122	10.5	3	4	--	13	2
Voltage Increase Rates (millivolts/hr)								
Terminal Voltage @ 2.0 Volts	--	3	19	72	133	--	8	75
iR Drop Voltage @ 2.0 Volts	--	2.3	13	15	72	--	3	67
iR Free Voltage @ 2.0 Volts	--	0.4	6	57	70	--	5	10
Terminal Voltage @ End of Run	0	3	4	67	167	0	5	240
iR Drop Voltage @ End of Run	0	2.3	4	40	167	0	0	220
iR Free Voltage @ End of Run	0	0.7	0	27	0	0	5	20

*iR Free Data not taken during these runs

Figure A-21 gives the graphical data for the 85-15 system. The 2.0v mark was reached after 13 hours of continuous operation and after 30 hours of operation the terminal voltage was 2.09v with a 120mv iR drop voltage. However, this ohmic polarization had been constant for the preceding 7 hours prior to that and it was increasing at a rate of 3 mv/hr. The iR-free voltage was increasing at a constant rate of 5mv/hr during the course of the run.

A 70-30 system demonstrated that within 3 hours from startup, a terminal voltage of 2.24v was reached. At the end of the run the iR drop voltage was 320mv with a rate of increase of 220mv/hr. Figure A-22 shows the iR drop voltage at the 2.0v mark to 100mv with a rate of increase of 67mv/hr and an iR-free voltage of 10mv/hr at 2.0v and 20mv/hr at the end of the run.

DISCUSSION

In order to properly evaluate the data accumulated for the different feed systems and to properly correlate this experimental data with that generated in the theory section it is necessary to weight all the parameters together rather than make conclusions on only one of them.

The ohmic polarization (iR drop voltage) indicates to what extent the cell is drying out as a function of the inability of the feed cavity to supply sufficient water to the cathode resulting in a voltage increase. In examining the pure water system there are evident some aspects which are very favorable other than duration of operation. For instance, complete voltage stabilization over the final hours. The rate of voltage increase at the end of the operation was approximately zero. A final iR drop of 70mv is very low compared to the ohmic polarization developed by the other experimental feeds.

The high iR drop exhibited by the tap water feed system is puzzling despite the fact the unit performed so long. At the time the run was terminated the unit demonstrated that to operate further would not be to do so efficiently. To proceed at this rate for an additional 1000 hours would result in an additional 3 volts total cell potential with an increased iR drop of 700mv possibly resulting in a cross over and total failure of the unit.

Possibly the initial impurity level is higher than is realized. For instance, the amount of KOH left in the feed matrix after charging and flush-equilibration is sufficient to raise the impurity concentration by an order of magnitude or more. In a more concentrated system this additional amount would be negligible. However, the system does exhibit a strong capability of being able to replace a pure water feed for extended periods of time.

The ethylene glycol-water feed systems with their degassed feed show definite promise for feeds with a low glycol concentration as exemplified by the 85-15 glycol feed system. This unit operated 18 hours with a total cell voltage of 2.08v and a rate increase of 4 mv/hr demonstrating that once the unit reaches "stability" it can operate for a long period of time. This system could operate for another 50 hours within reasonable power requirements. All the voltage increase seems to be due to the impurity buildup in the feed cavity as is evidenced by the stable iR free voltage at the end of the run. Therefore, if the impurity level can be kept low the system will demonstrate a high performance level.

The 70-30 and 50-50 systems do not show this same promise. After 7.5 and 6 hours respectively the systems demonstrate terminal voltage rate increase of 67 mv/hr and 167 mv/hr. Coupled with the high iR drops already evident gives limited operating time to both these types of feed because of matrix dryout resulting in crossover and total failure.

Comparing the observed results with the predicted values shows relatively good correlation for the 85-15 and 70-30 systems whereas the 50-50 system was predicted to run 2 hours and actually ran for 6 hours. The question may be posed

how long would a unit run if no feed cavity was present. Reasonable estimates predict less than a couple of hours. Therefore, the 50-50 system surpasses the theoretical estimate but at a terminal voltage of 2.35 volts and a rate increase of 167 mv/hr.

The 90-10 and 85-15 Methanol systems demonstrate final iR drop voltage rates of approximately zero mv/hr with running time 60% to 250% greater than anticipated. Since Methanol has such a high vapor pressure it does not collect as an impurity in the feed cavity but crosses over with the water vapor resulting in a minor impurity buildup hence a low practically non-increasing iR drop voltage at the end of the run. However, despite a relatively high concentration of Methanol passing through the system the rate of increase of the iR free voltage at the end of the run is 0 mv/hr, 5 mv/hr, 20 mv/hr for the 90-10, 85-15, and 70-30 feed respectively. This does not indicate that it is affecting the performance of the cell by poisoning the electrodes. The 70-30 system does show rapid degradation of performance (3 hrs running - 2.24 volt terminal with a rate of 240 mv/hr) and while the 85-15 system showed no increase in rate of iR free voltage between the 13th hour (at 2.0 volt) and at the end of the run (30th hour) the 70-30 run shows a 10 mv/hr rate of increase from the 2nd hour (2.0 volts) and end of the run (3rd hour) which may be indicative to poisoning of the system or just a reduction in the partial pressure of hydrogen and oxygen increasing the thermodynamic potential of the system.

In order to ascertain whether or not Methanol was in the system the oxygen side of the system was thoroughly cleaned and a small quantity of pure water was placed in a bubbler. This experiment was attempted after the end of the 90-10 run. After a short period of testing, Methanol, was conclusively identified as being present in the oxygen bubbler.

CONCLUSIONS

The following conclusions should be considered:

1. Impure water feed system with an impurity level of 300 ppm or less shows definite promise of continued performance for well over 100 hours.

2. Low concentration aqueous glycol system with 15%, by weight, or less, glycol show promise for short duration ($<$ 10 hours) operation.

3. Aqueous Methanol systems 10% and 15% Methanol, by weight, show considerable promise. However, the oxygen product gas must be scrubbed to remove all Methanol vapor.

4. Static feed systems allow for accumulation of impurities-periodic flushing of the cavity will reduce impurity level and improve performance.

5. Static feed systems allow for dissolved gas accumulation and this can be solved by adequate pretreating and venting during operation.

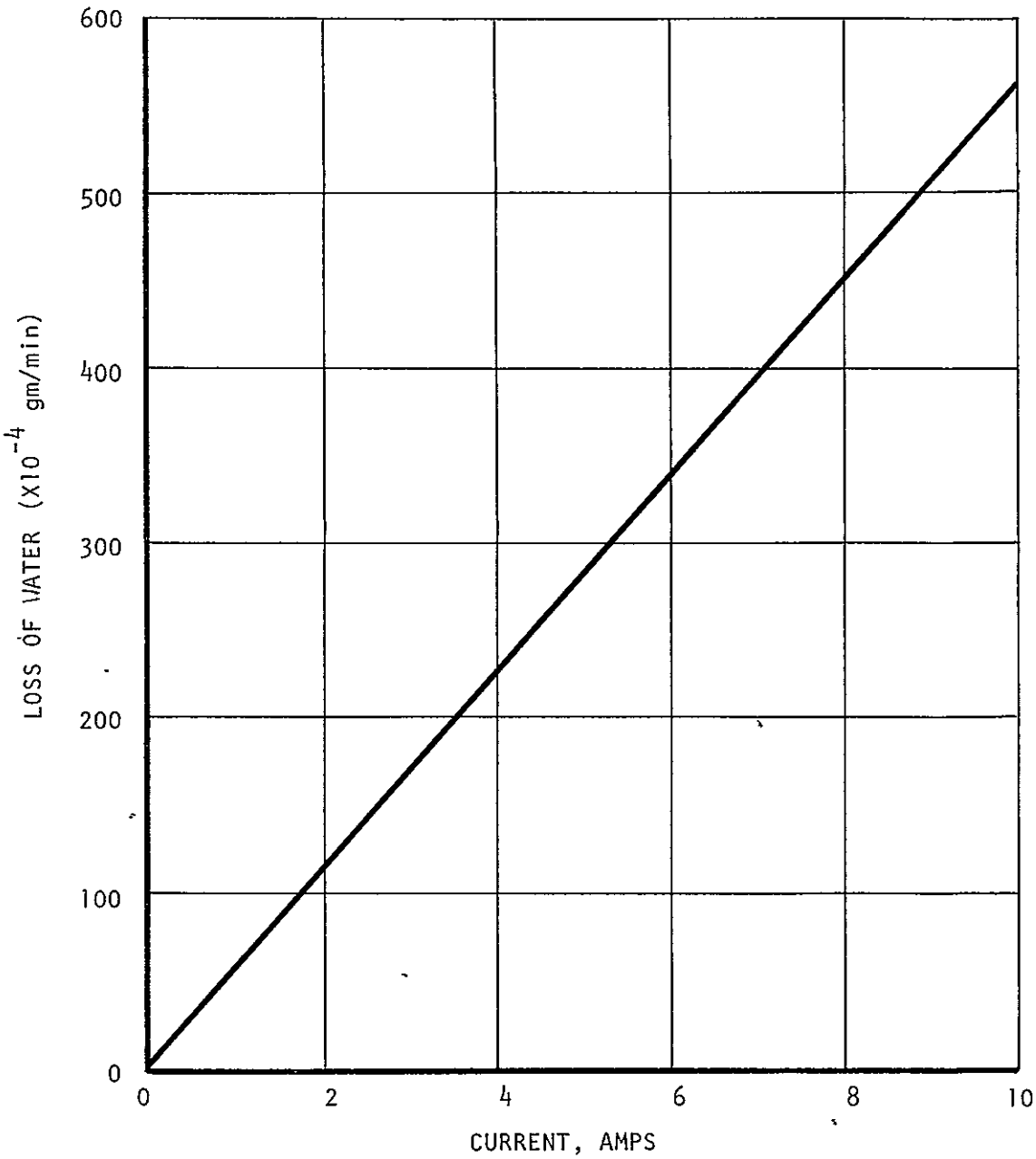

FIGURE A-1 WATER ELECTROLYSIS DECOMPOSITION RATE

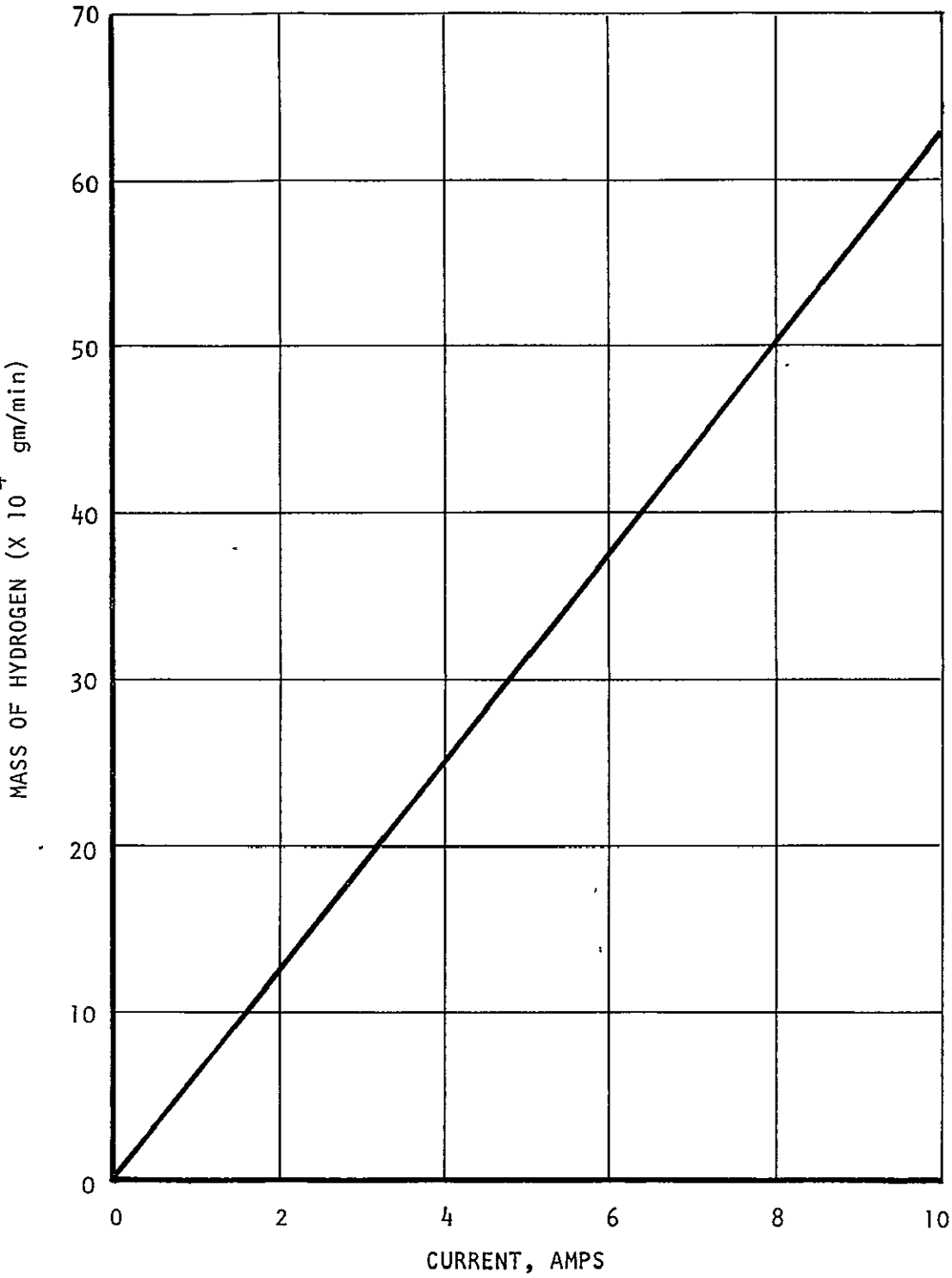

FIGURE A-2 MASS OF HYDROGEN GENERATED AS A FUNCTION OF CURRENT

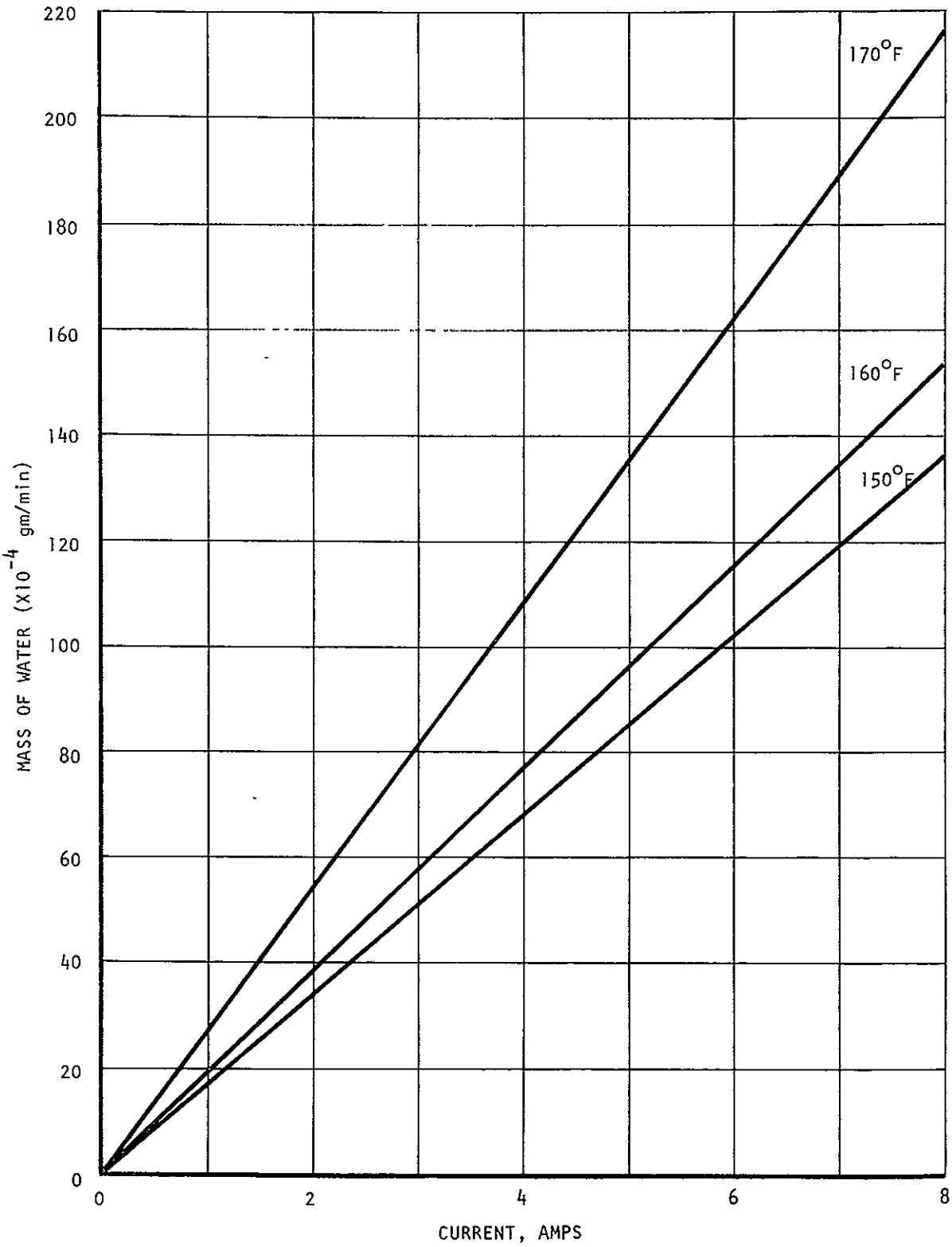

FIGURE A-3 HUMIDIFICATION OF HYDROGEN AS A FUNCTION OF CURRENT FOR DIFFERENT TEMPERATURES AT A CONSTANT KOH CONCENTRATION OF 20% AND TOTAL PRESSURE OF 1 ATMOSPHERE

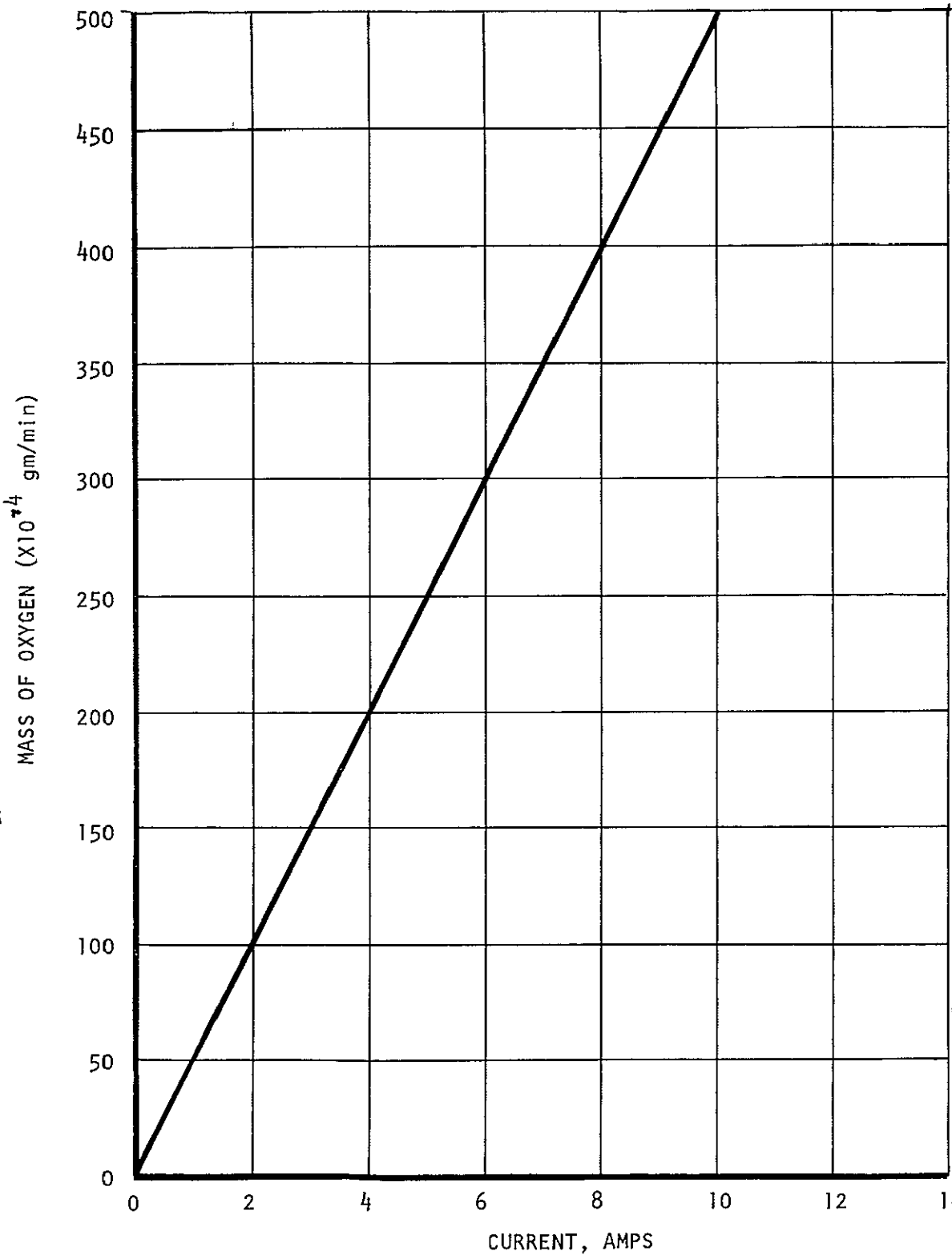

FIGURE A-4 MASS OF OXYGEN EVOLVED AS A FUNCTION OF CURRENT

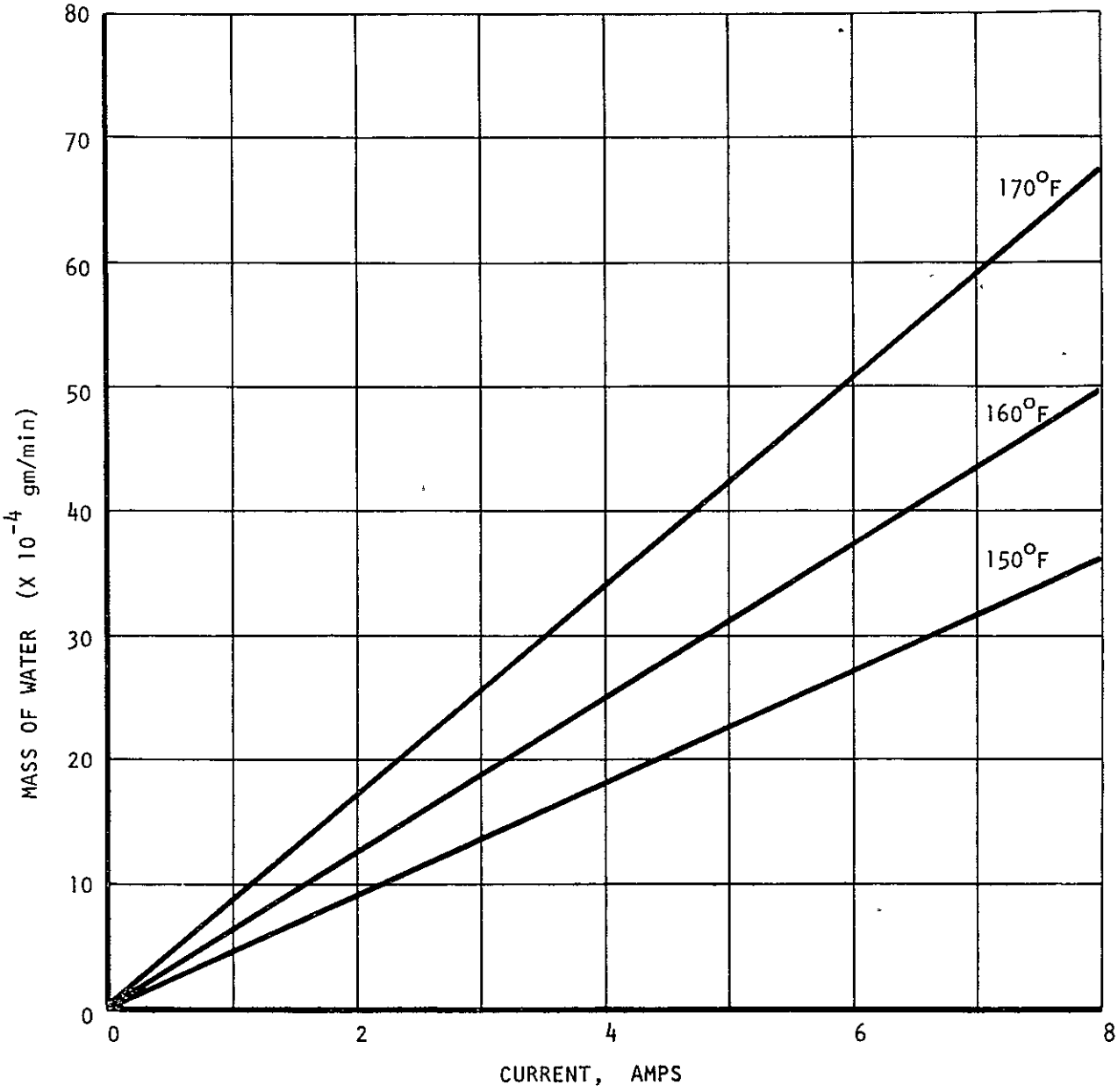

FIGURE A-5 HUMIDIFICATION OF OXYGEN AS A FUNCTION OF CURRENT FOR DIFFERENT TEMPERATURES AT A CONSTANT KOH CONCENTRATION OF 32% AND A TOTAL PRESSURE OF 1 ATMOSPHERE

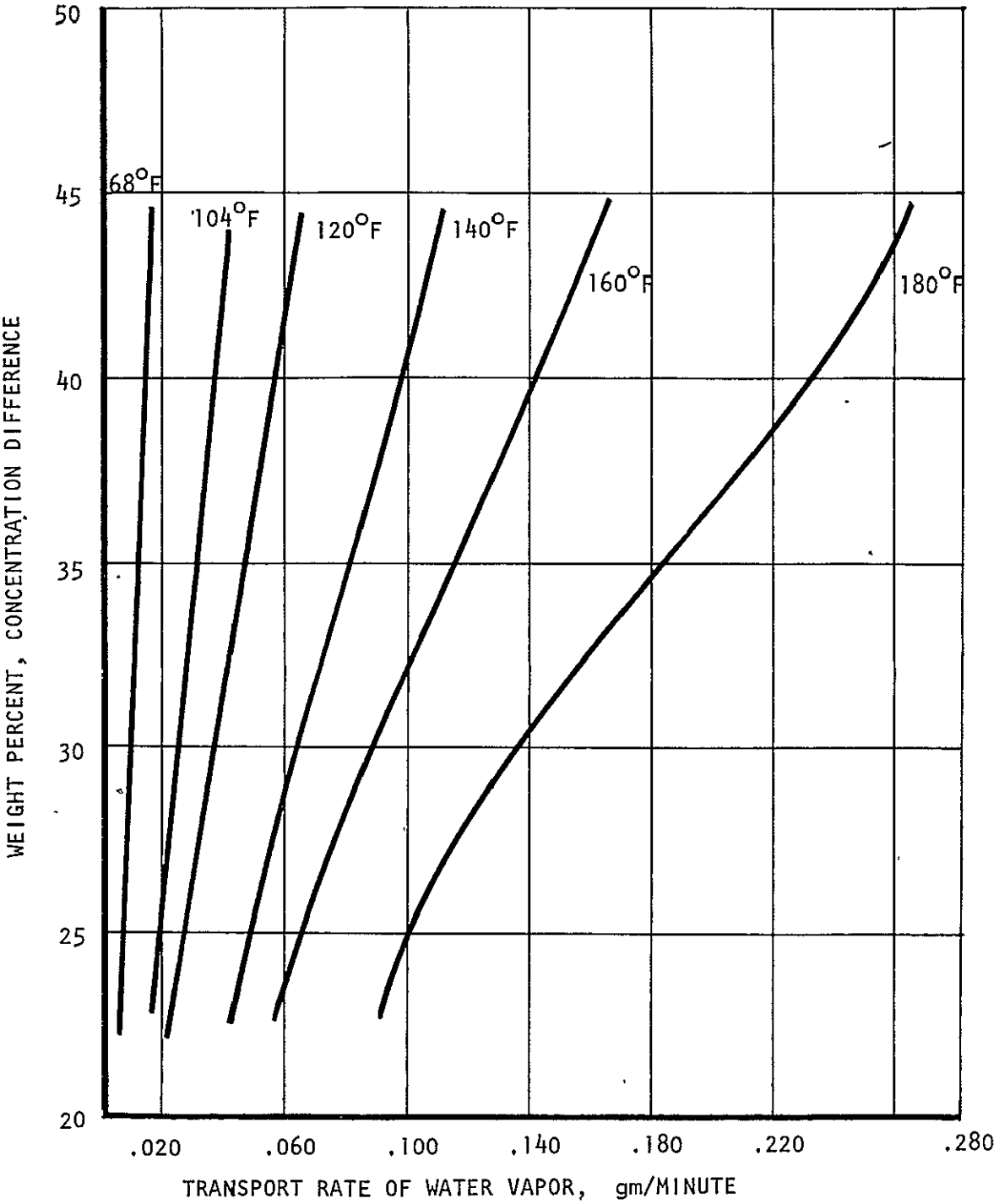

FIGURE A-6 MASS OF WATER TRANSPORTED ACROSS CELL AT DIFFERENT TEMPERATURES AS A FUNCTION OF CONCENTRATION DIFFERENCE AGAINST A REFERENCE OF 100% WATER

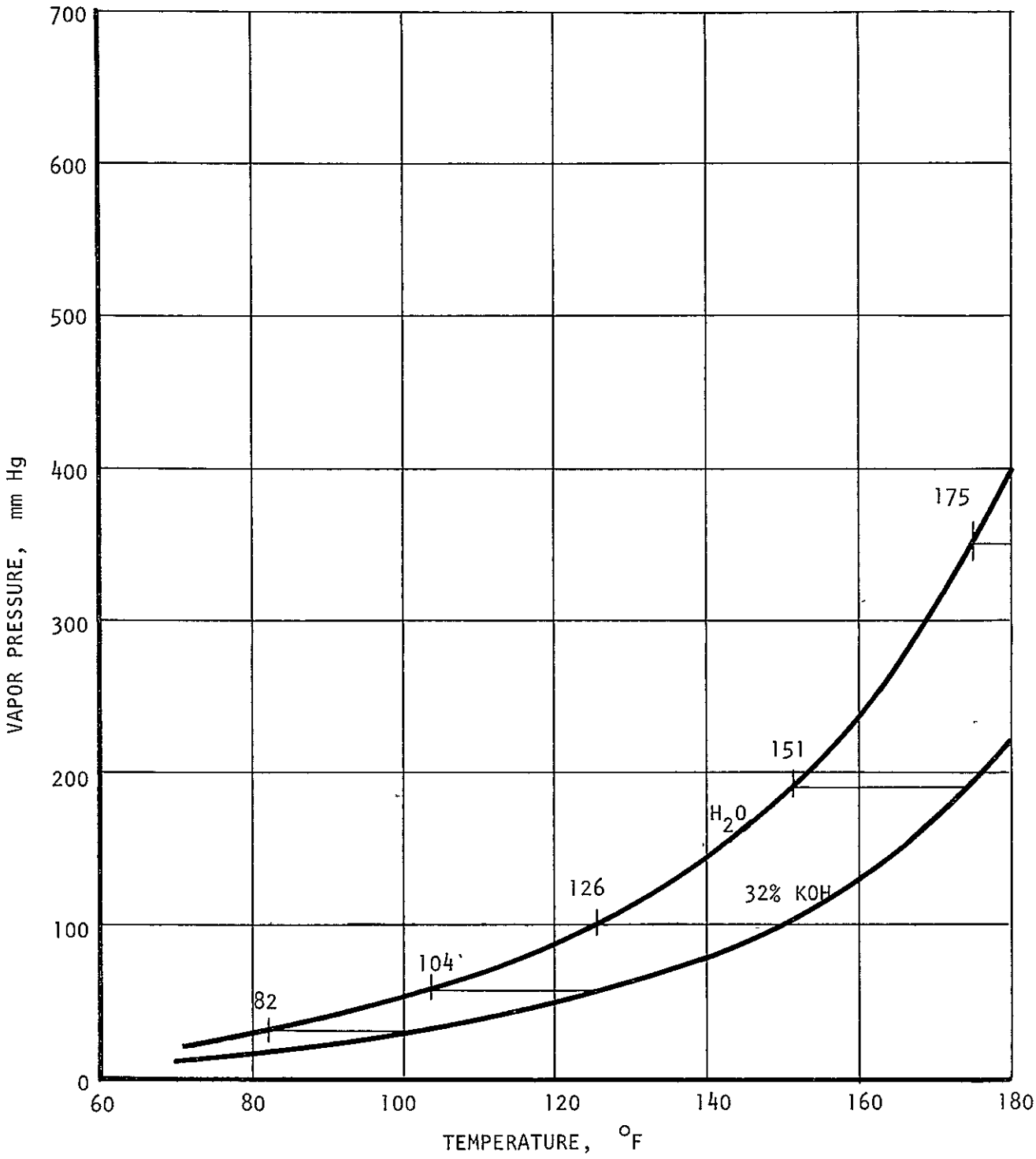

FIGURE A-7 VAPOR PRESSURE VS. TEMPERATURE FOR PURE WATER AND 32% KOH AT A TOTAL PRESSURE OF 1 ATMOSPHERE

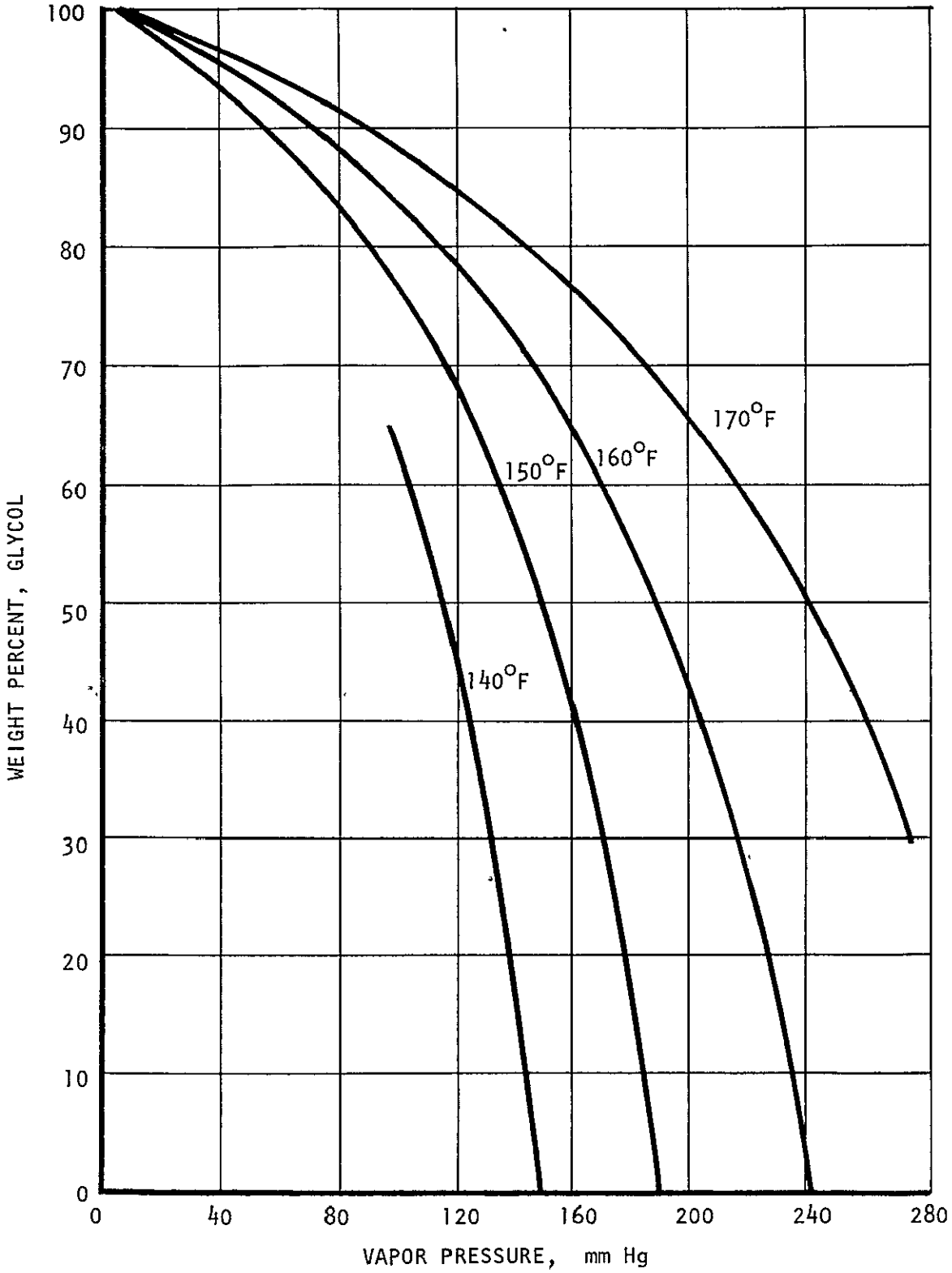

FIGURE A-8 VAPOR PRESSURE OF GLYCOL-WATER SOLUTION VS. CONCENTRATION AT DIFFERENT TEMPERATURES AND A TOTAL PRESSURE OF 1 ATMOSPHERE

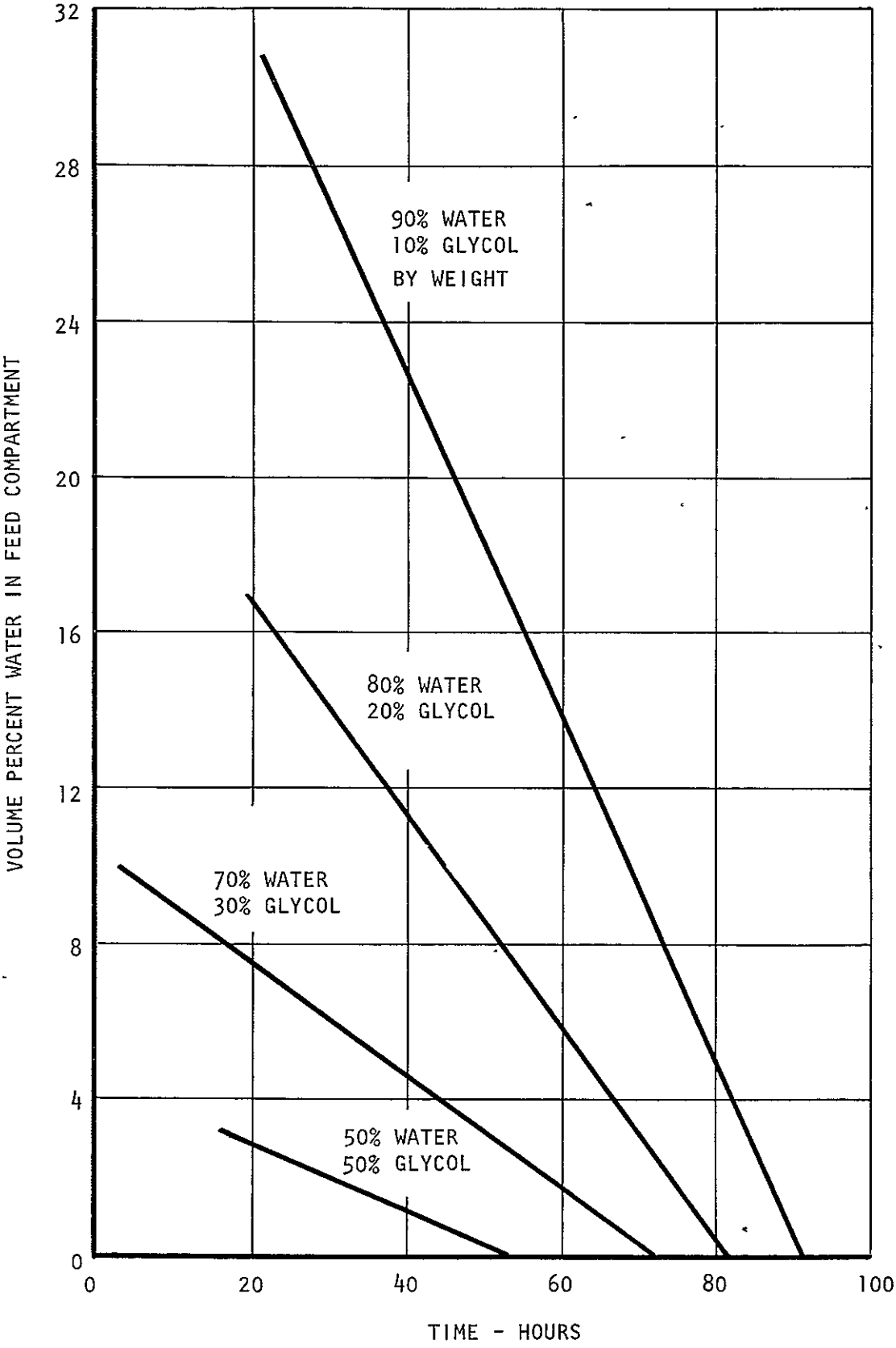

FIGURE A-9 WATER LOSS FROM FEED COMPARTMENT AS A FUNCTION OF TIME FOR CURRENT DENSITY OF 100 ASF AT 160°F

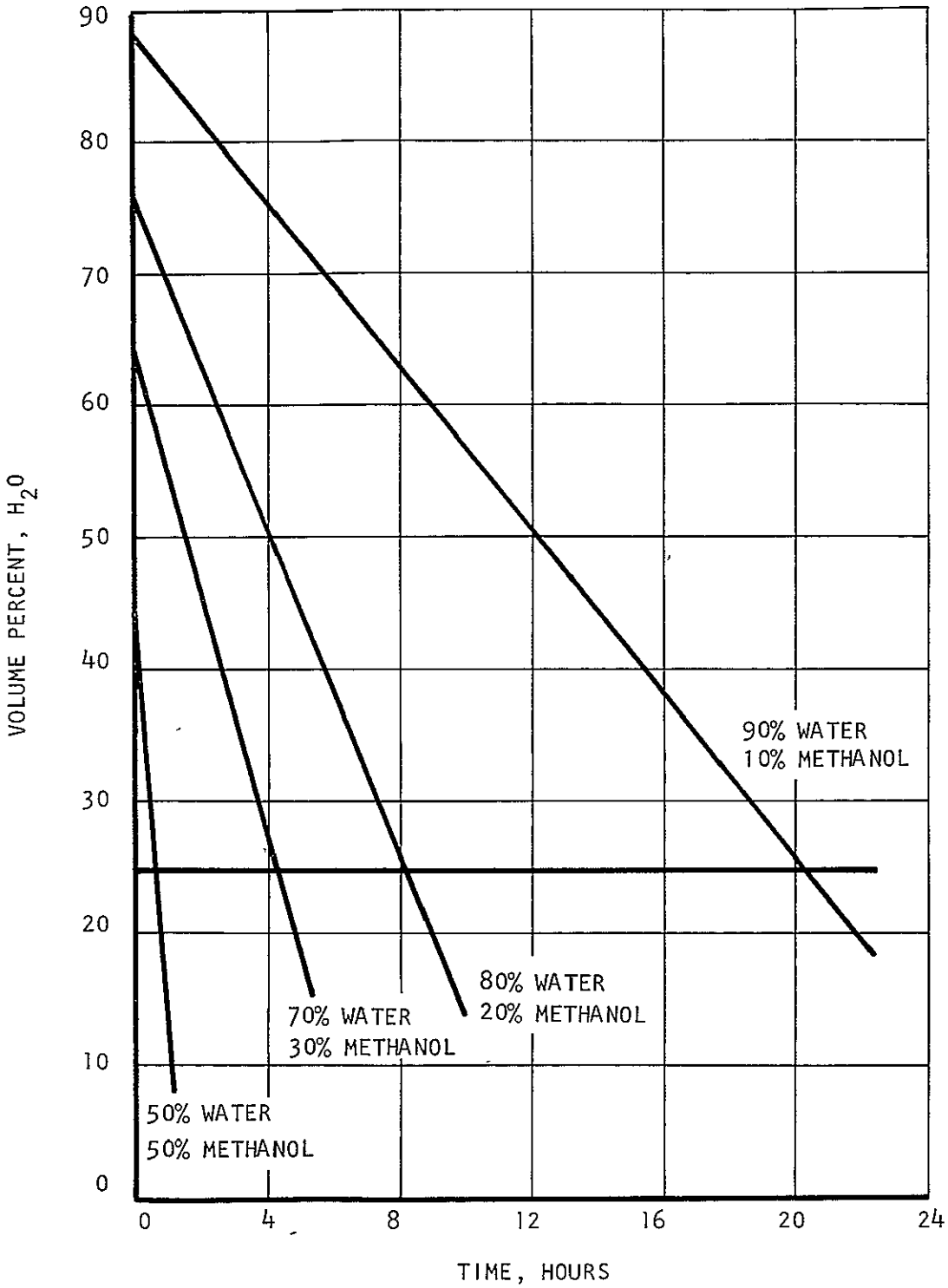

FIGURE A-10 WATER LOSS FROM METHANOL-WATER FEED CAVITY AT CURRENT DENSITY OF 100 ASF AND 160°F

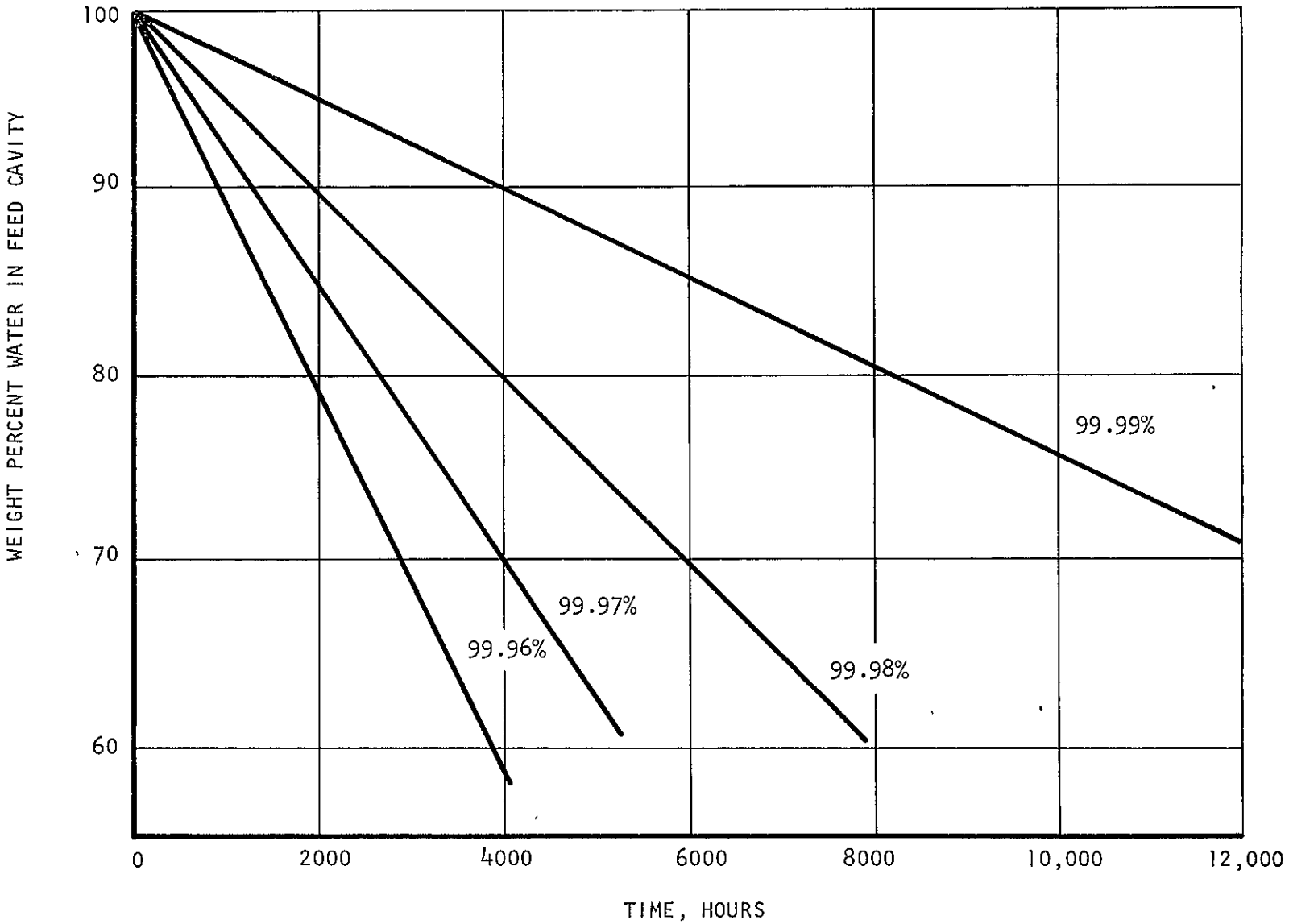

FIGURE A-11 WATER LOST FROM TAP WATER FEED SYSTEM AT 160°F AND A CURRENT DENSITY OF 100 ASF

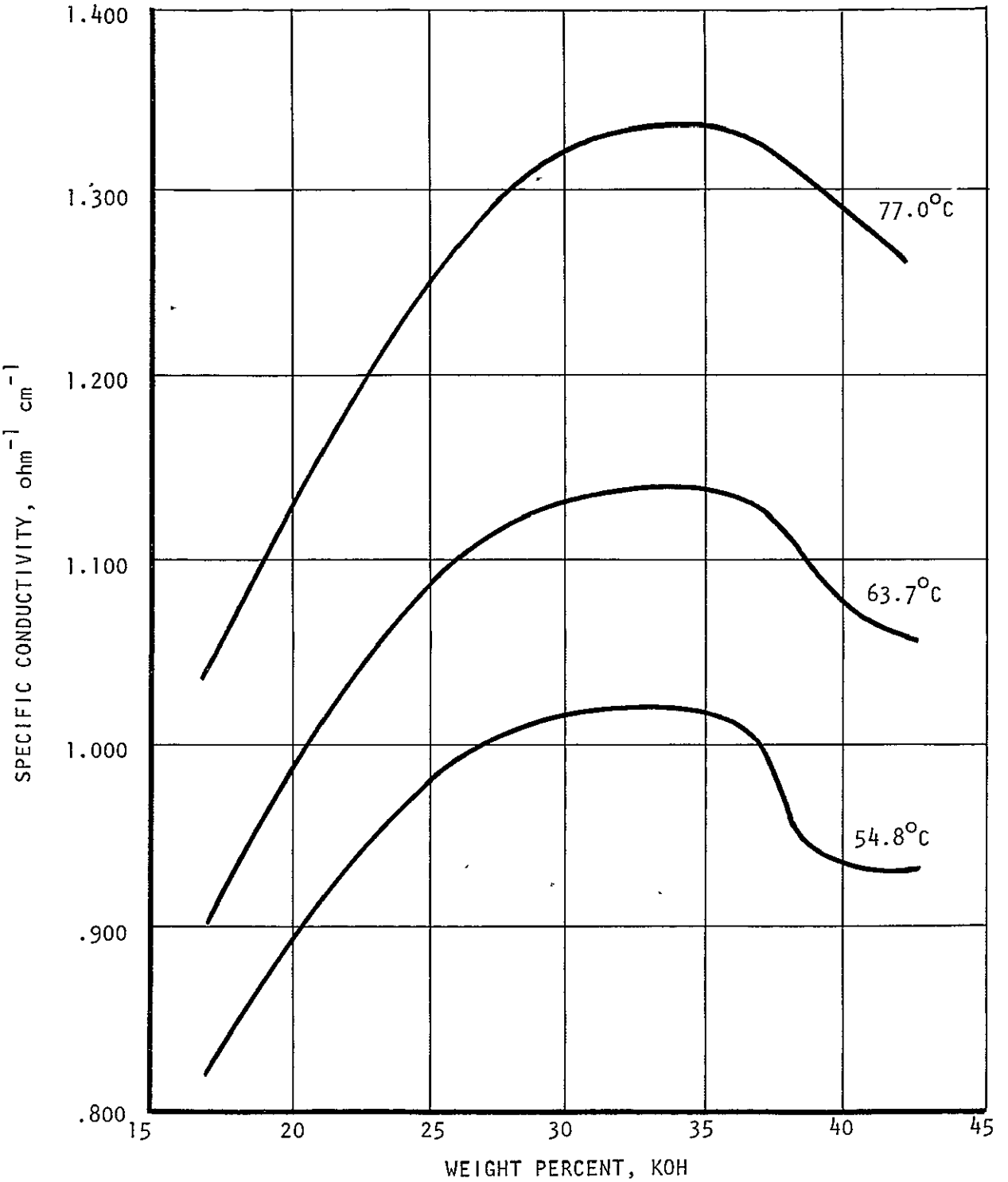

FIGURE A-12 SPECIFIC CONDUCTANCE OF KOH SOLUTION VS. WEIGHT PERCENT KOH AT DIFFERENT TEMPERATURES

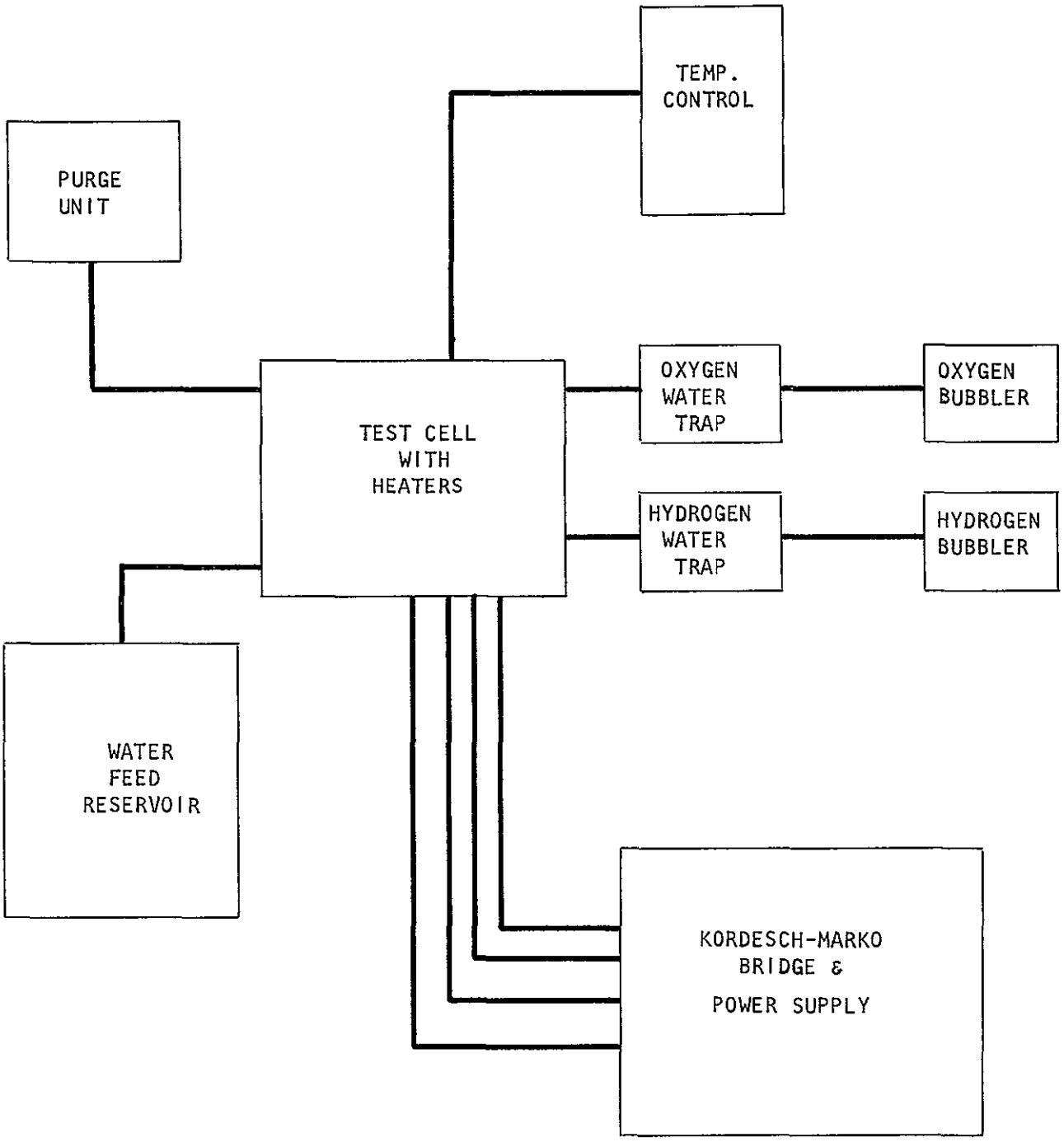

FIGURE A-13 TEST RIG SCHEMATIC FOR EVALUATION OF STATIC FEED, 3" X 3" WATER ELECTROLYSIS CELL

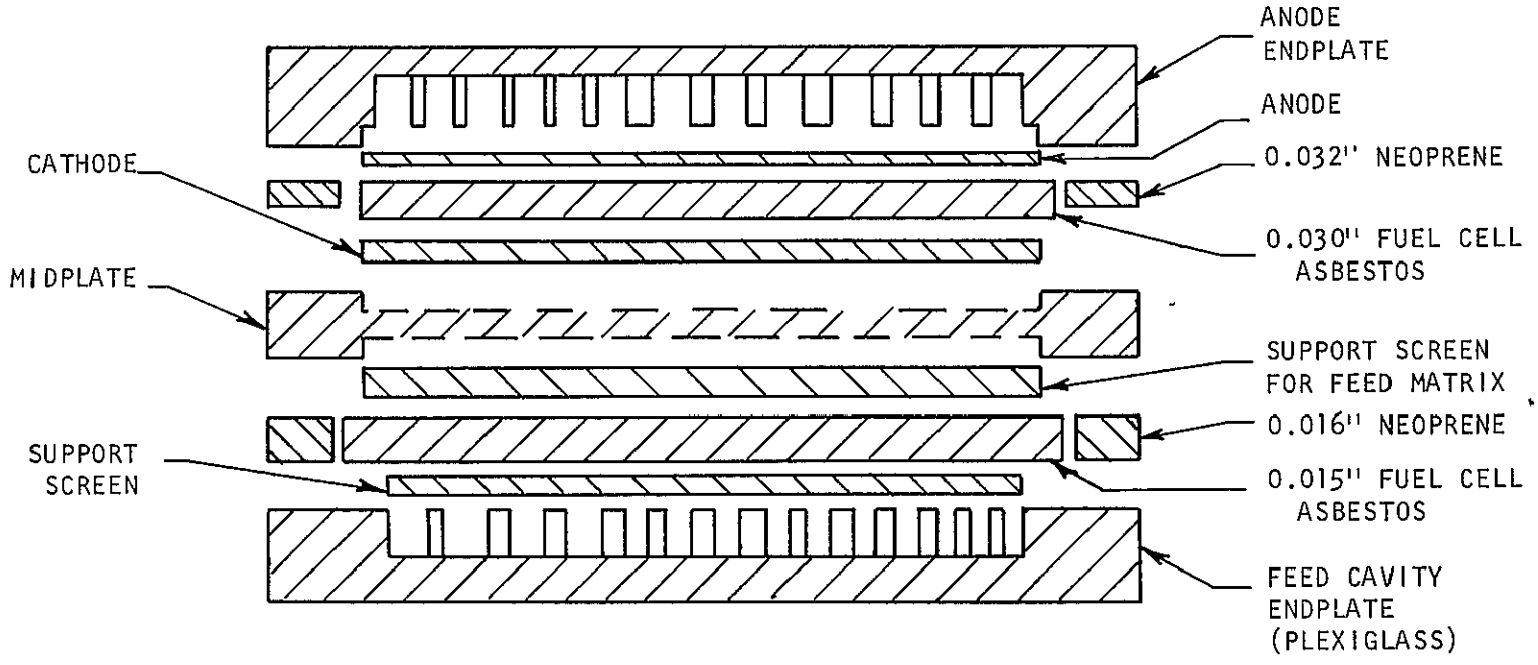

FIGURE A-14 CROSS-SECTION OF ELECTROLYSIS CELL

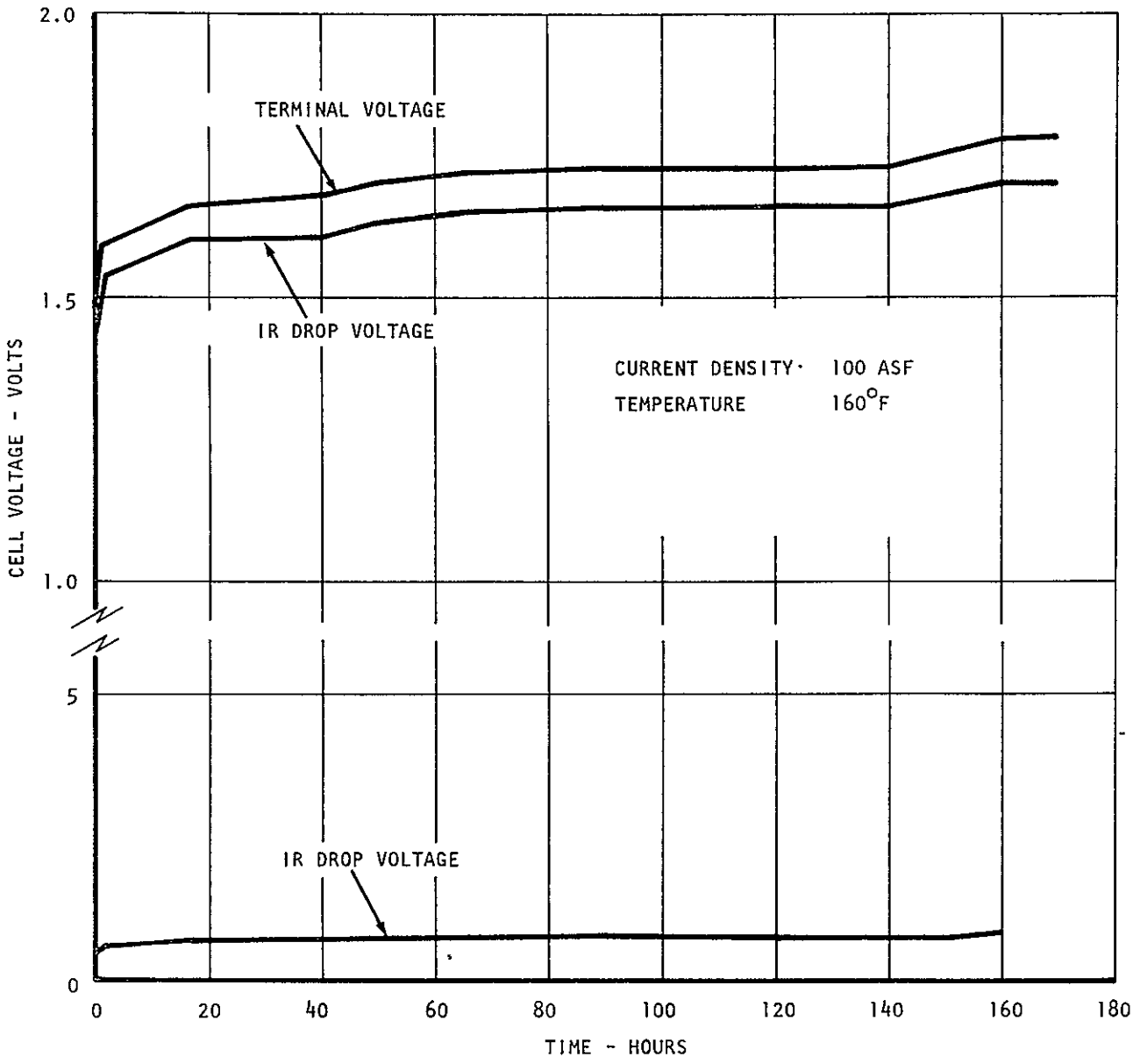

FIGURE A-15 CELL VOLTAGE VS. TIME FOR A PURE WATER FEED

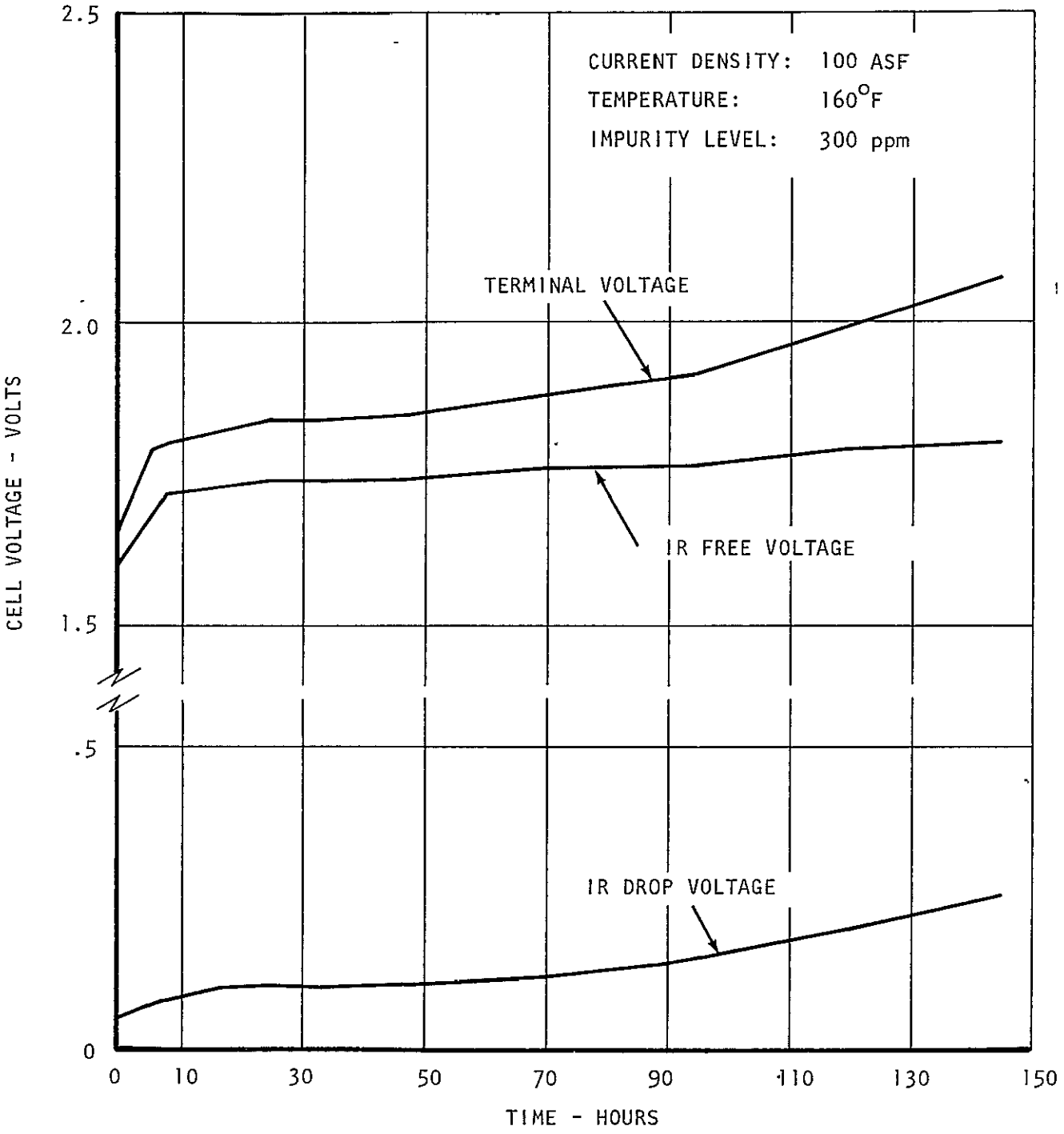

FIGURE A-16 CELL VOLTAGE VS. TIME FOR A TAP WATER FEED

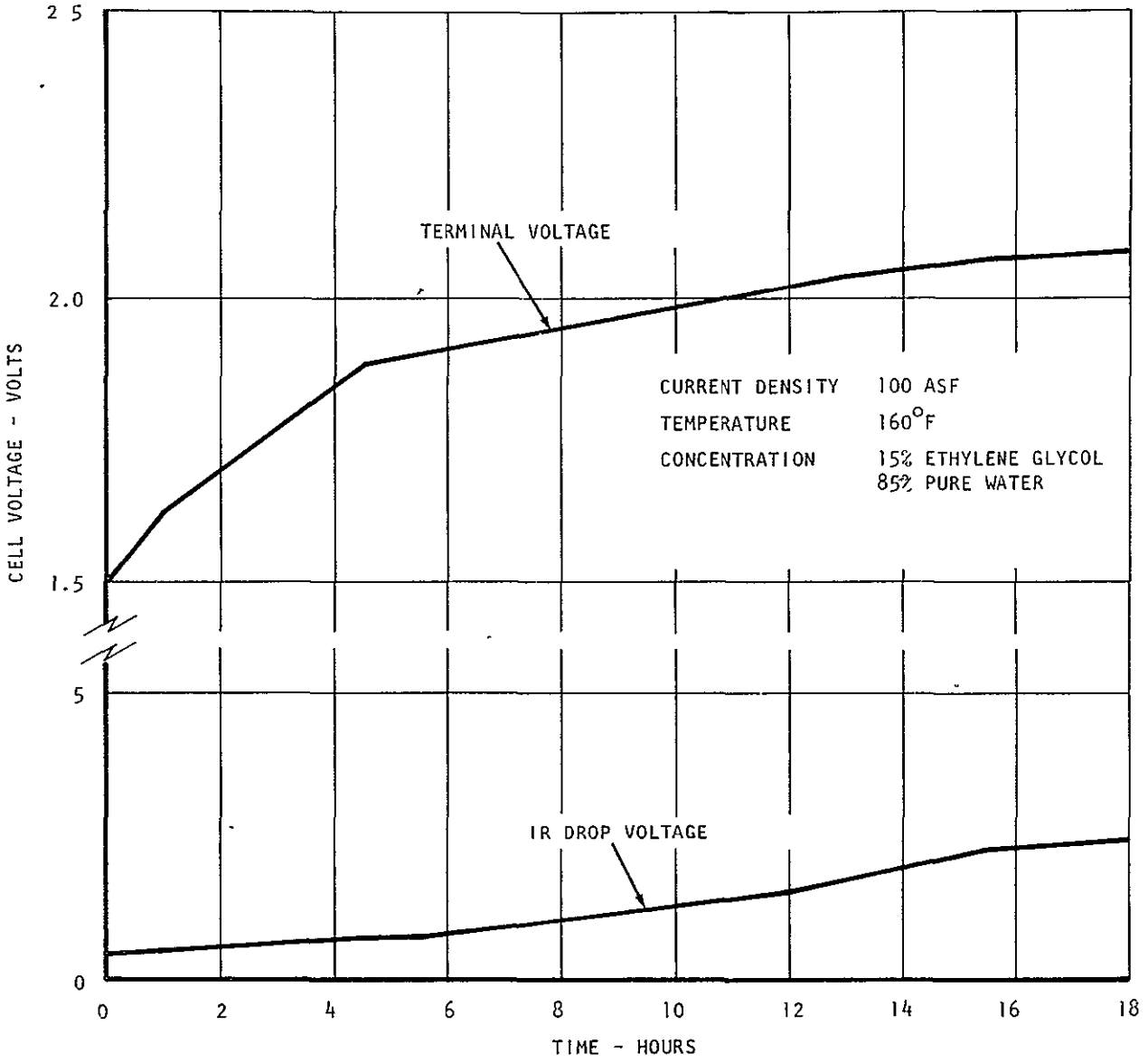

FIGURE A-17 CELL VOLTAGE VS. TIME FOR A 85-15 WATER-GLYCOL FEED

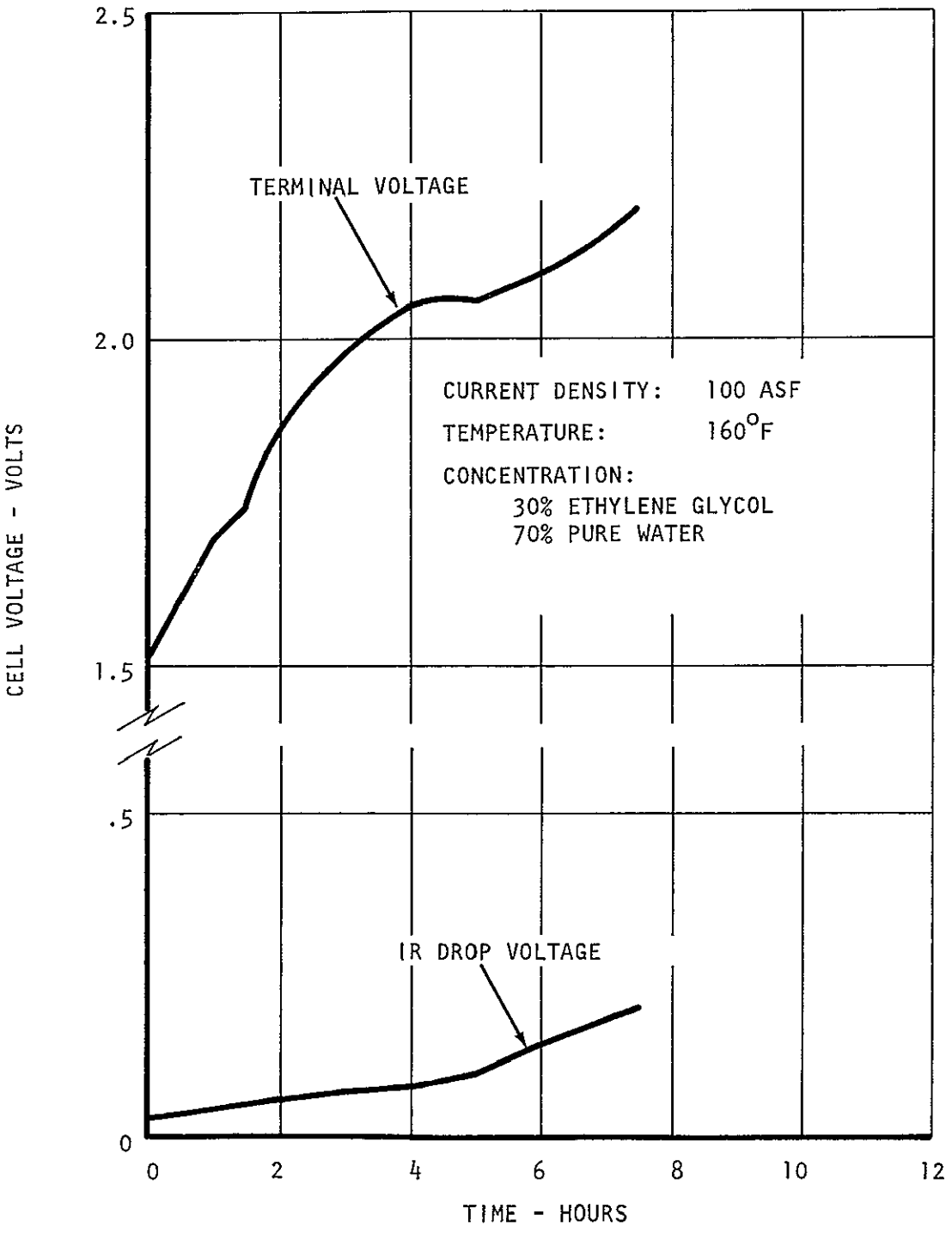

FIGURE A-18 CELL VOLTAGE VS. TIME FOR A 70-30 GLYCOL FEED

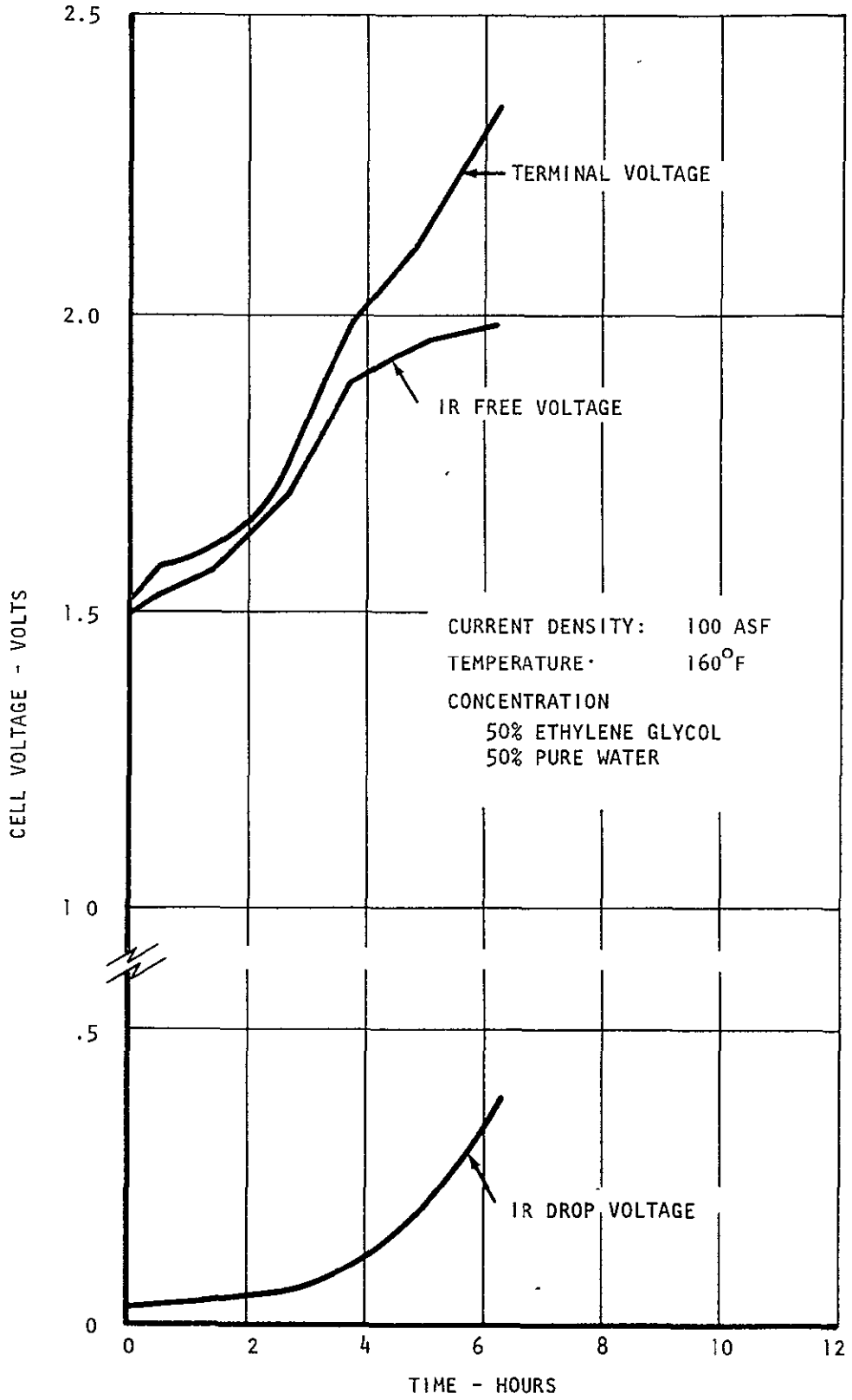

FIGURE A-19 CELL VOLTAGE VS. FEED FOR A 50-50 GLYCOL FEED

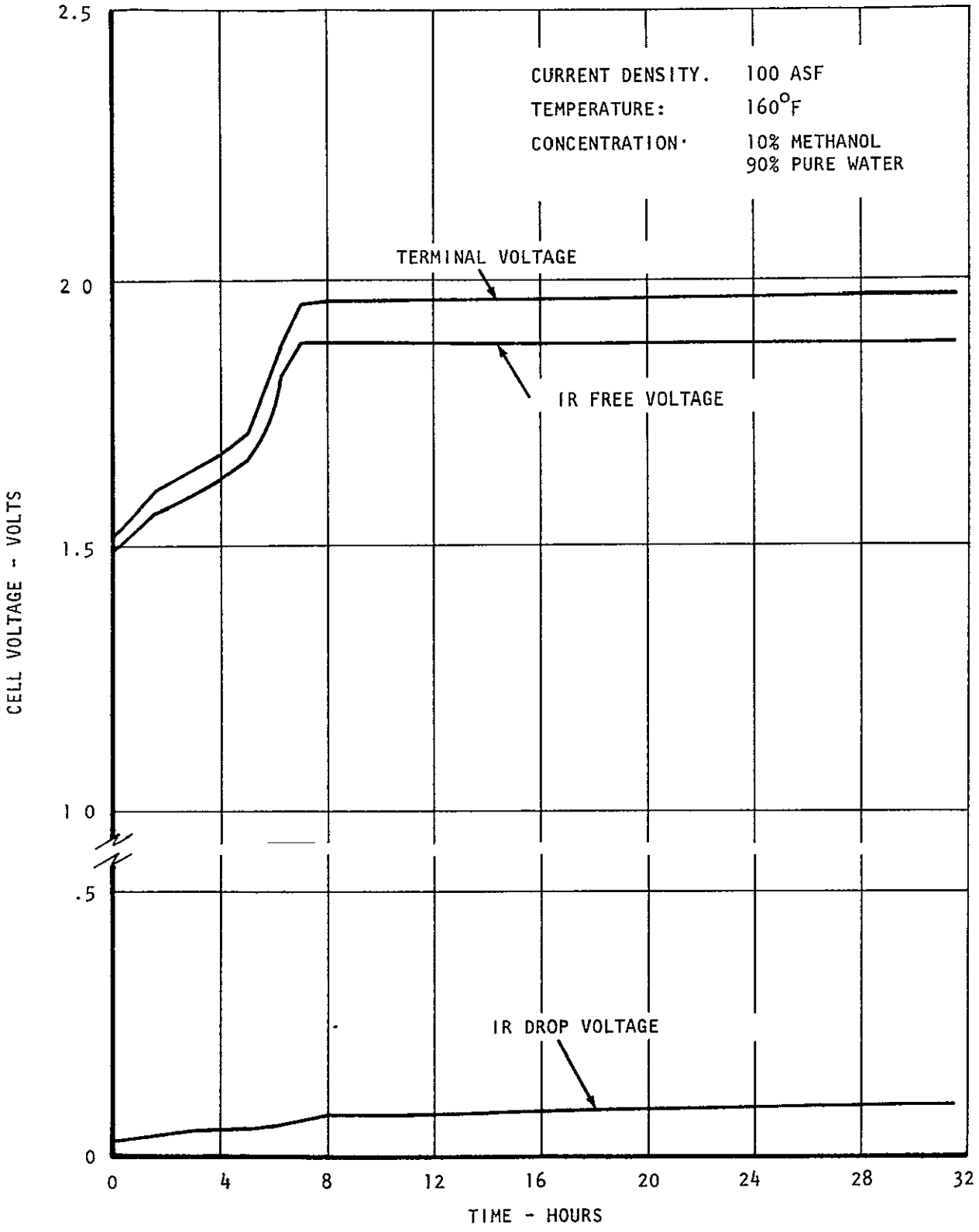

FIGURE A-20 CELL VOLTAGE VS. TIME FOR A 90-10 METHANOL FEED

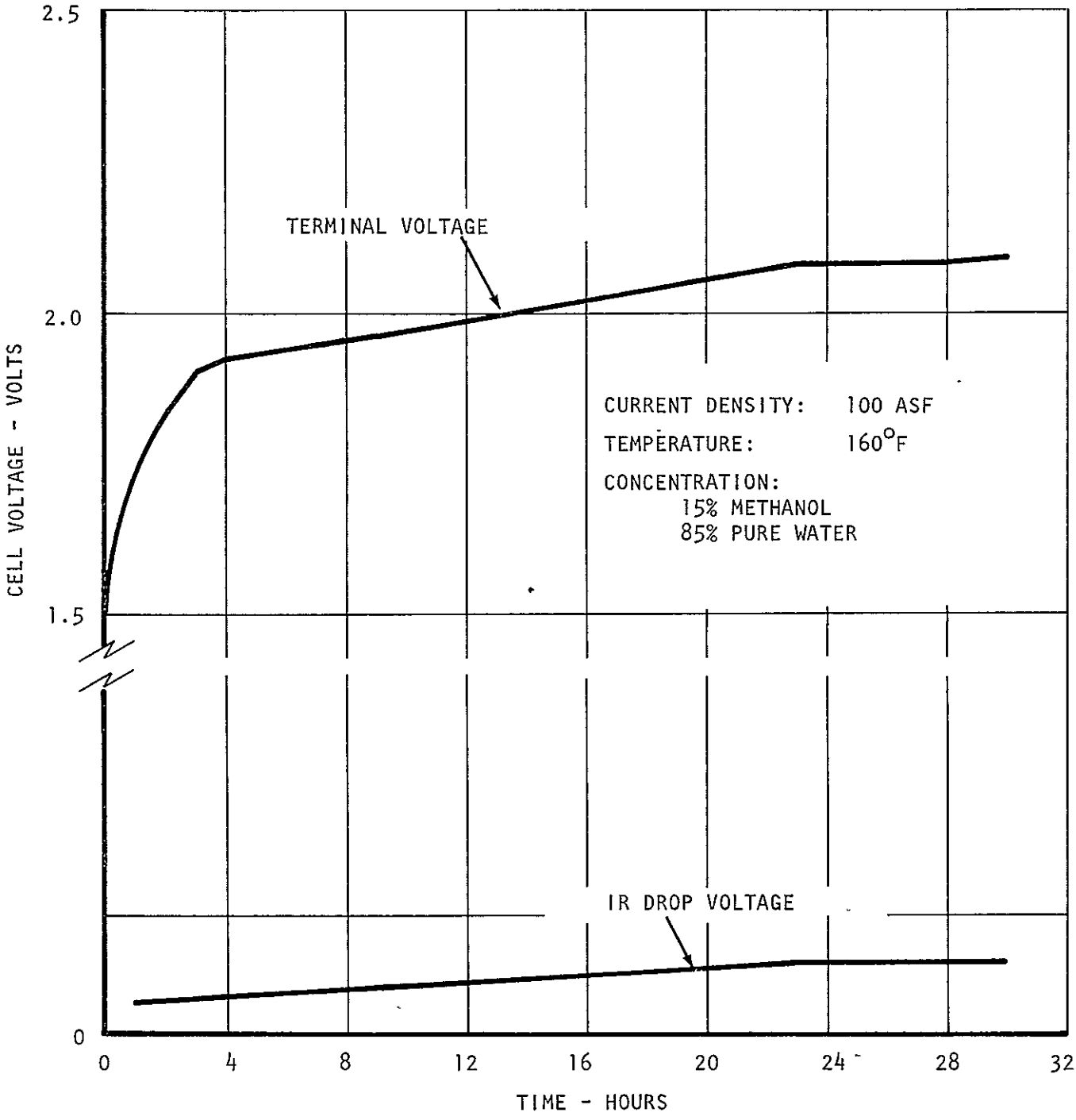

FIGURE A-21 CELL VOLTAGE VS. TIME FOR 85-15 METHANOL FEED

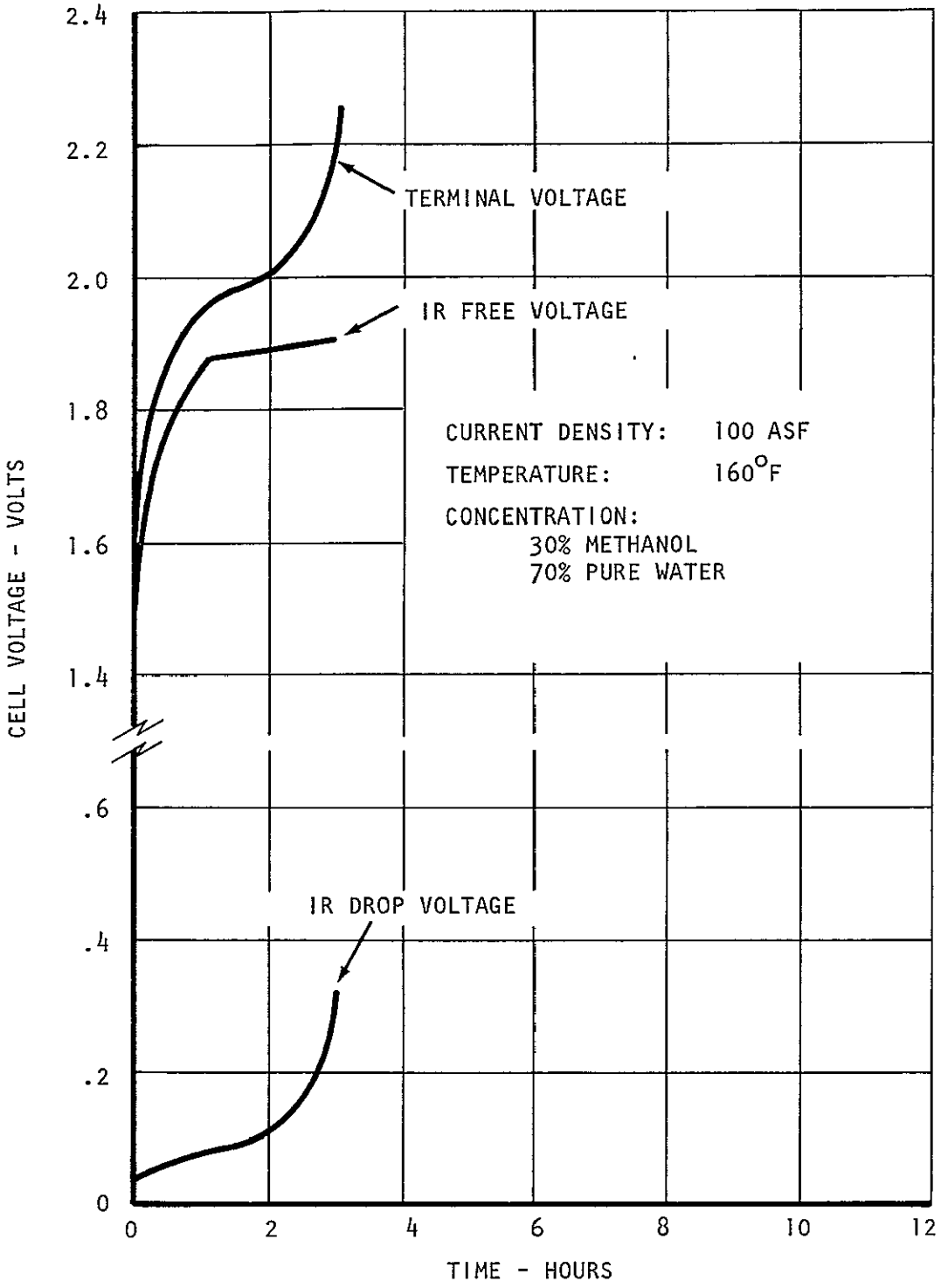

FIGURE A-22 CELL VOLTAGE VS. TIME FOR 70-30 METHANOL FEED

APPENDIX B

WATER ELECTROLYSIS SUBSYSTEM - THERMAL ANALYSIS

TABLE OF CONTENTS

SUMMARY

The NAOS System, designed for ultimate use on board the F-111 weapon system, uses a water electrolysis module to generate 0.15 pounds of O_2/hr. Provisions must be made to remove the heat generated within the water electrolysis module due to cell inefficiencies.

Four heat removal methods were considered applicable for aircraft use. They are: 1) evaporative cooling (heat removal due to product gas humidification), 2) air cooling of external fins, 3) liquid cooling through internal passages, and 4) cooling achieved through circulating electrolyte through the water cavities.

The electrolysis module would not require external cooling provisions if evaporative cooling was selected; however, due to the required operating pressure level and the state-of-the-art electrolysis module cell voltage performance, evaporative cooling cannot be achieved.

The F-111 aircraft does not have suitable liquid cooling aboard; however, cooling air in ranges from -65°F to 390°F is available within its environmental control system. This cooling air could be used directly for the air-cooled fin method. In the circulating coolant and circulating electrolyte methods, liquid-to-air heat exchangers are required to reject the heat to the aircraft's cooling media. It is anticipated, at this time, that a single liquid cooling loop common to the NAOS subsystems will be chosen.

Based on this assumption and on the potential weight and volune savings, the circulating cooling method was selected for the water electrolysis subsystem.

INTRODUCTION

The generation of oxygen and hydrogen in the NASA Aircrew Oxygen System is accomplished by the electrolysis of water. A ten-cell water electrolysis module employing a static water feed method generates 0.15 pound of O_2/hr and 0.0188 pound of H_2/hr at a current density of 100 ASF (ten cells, each 0.228 sq. ft. in area, electrically connected in series at a current of 22.8 amps).

In practical applications of present-day low temperature water electrolysis cells, the formation of gaseous oxygen and hydrogen from water is accompanied by the release of heat energy. A means to remove this heat must be provided to limit module operating temperature to desired levels.

The NAOS system presently uses the requirements of the F-111 weapons system as its design criteria. The selection of a cooling method for the water electrolysis subsystem will, therefore, be greatly influenced by the heat removal optimization study at the NAOS system level. It is therefore, a primary aim of this analysis to establish ranges in interface requirements with respect to water electrolysis subsystem heat removal as a function of module operating parameters and to define general module configurations including weight and volume variations and additional hardware requirements for various cooling modes considered. This information, together with similar analyses for the other NAOS subsystems and trade-off data for the F-111 weapon systems, will enable the designer to perform a NAOS system heat removal optimization study.

The practical heat removal methods applicable to aircraft use and selected for consideration are: 1) evaporative cooling, 2) forced convective cooling (air over external fins or liquid through internal passages, and 3) circulating electrolyte through the feed water cavities.

ELECTROLYSIS CELL HEAT LOAD THEORY

The electrolysis of water can be an exothermic or endothermic reaction depending on the terminal cell voltage for a given set of operating conditions. The net heat generation by these reactions within the system can be predicted theoretically and expressed in terms of cell potential and reaction entropy. According to the first law of thermodynamics for a system at constant pressure,

$$Q = \Delta H + W_e \qquad (1)$$

where,

Q = the heat flowing into the system

ΔH = the change in enthalpy of the system

W_e = the electrical work done by the system on the environment

Also,

$$W_e = nF(-V_c) \tag{2}$$

and ΔH can be expressed as:

$$\Delta H = nF\ V_a \tag{3}$$

where,

n = number of equivalents per mole of decomposed water

F = Faraday's constant

V_c = terminal cell voltage

V_a = adiabatic cell voltage

Combining equations 1, 2 and 3, results in:

$$Q = nF\ (V_a - V_c) \tag{4}$$

Equation 4 shows that when $V_a = V_c$ the net heat release by the reaction equals zero (resistance heating due to electrolyte is not included).

V_a can be determined using the second law of thermodynamics:

$$\Delta H = \Delta F + T\Delta S \tag{5}$$

F = free energy change of the system

T = temperature

ΔS = change in entropy of the system

but the free energy can also be expressed as:

$$\Delta F = nFV^o \tag{6}$$

V^o = decomposition voltage

Combining equations 3, 5 and 6 results in the following expression for the adiabatic cell voltage:

$$V_a = V^o + \frac{T\Delta S}{nF} \tag{7}$$

In the NAOS electrolysis module, pure sub-cooled water is fed into an electrolyte feed cavity. The water is then evaporated from a feed matrix and is transported by diffusion to the cell matrix where it is condensed and

decomposed. Depending on operating conditions, some of the water evaporates from both feed and cell matrices and serves to humidify the product gases.

It can be shown that the net change in enthalpy of the above system, based on the amount of water electrolyzed (excluding that required for humidification), consists basically of the sensible heating of the sub-cooled water and the enthalpy change associated with electrolysis, as discussed above. This is true since the heat of solution in the cell matrix and feed cavity are cancelled by the heat of dissolution and the latent heat of evaporation required at the feed matrix is regained during condensation at the cell matrix.

Figure B-1 shows the adiabatic cell voltage, V_a (system) and the net change in enthalpy, ΔH (system) per pound of water electrolyzed versus the electrolysis cell temperature.

The net enthalpy and adiabatic voltage are based on supplying the electrolysis module with sub-cooled water at a temperature of 75°F ($\pm$25°F change results in less than 0.4% error) and the product gases are considered to be within the 14.7 to 250 psia pressure range indicated and at a temperature level equal to the electrolysis cell temperature.

Since ΔH (system) is based only on the water electrolyzed, the net heat loss due to product gas humidification is not included. This heat loss, however, is discussed in a subsequent section. As can be seen from the adiabatic cell voltage ranges of 1.48 to 1.51 volts, the reactions within practical, low temperature electrolysis cells will be of exothermic nature, i.e., net heat will be released.

Figure B-2 is based on Figure B-1 and shows specific cooling load in BTU/lb of oxygen generated and the cooling rate in BTU/hr for a 0.15 pound of O_2/hr generation rate versus cell voltage for cell temperatures of 100°F and 200°F. As can be seen, the cell temperature effect is small; approximately a difference of 60 BTU/lb of oxygen for 100°F-200°F range.

Water Electrolysis Subsystem Design Point

The design operating point selected for the NAOS Water Electrolysis Subsystem is as follows:

Oxygen Generation Rate	0.15 lb/hr
Hydrogen Generation Rate	0.0188 lb/hr
Stack Temperature	150°F
Oxygen Pressure	75 psia
Hydrogen Pressure	73 psia

The nominal design cell voltage, at a current density of 100 ASF (equivalent to the 0.15 lb/hr generation rate), is 2.0 volts per individual cell. Test results, however, have shown that this voltage level is conservative. It is also possible that the NAOS system heat removal optimization study will result in a change in the water electrolysis subsystem operating temperature level.

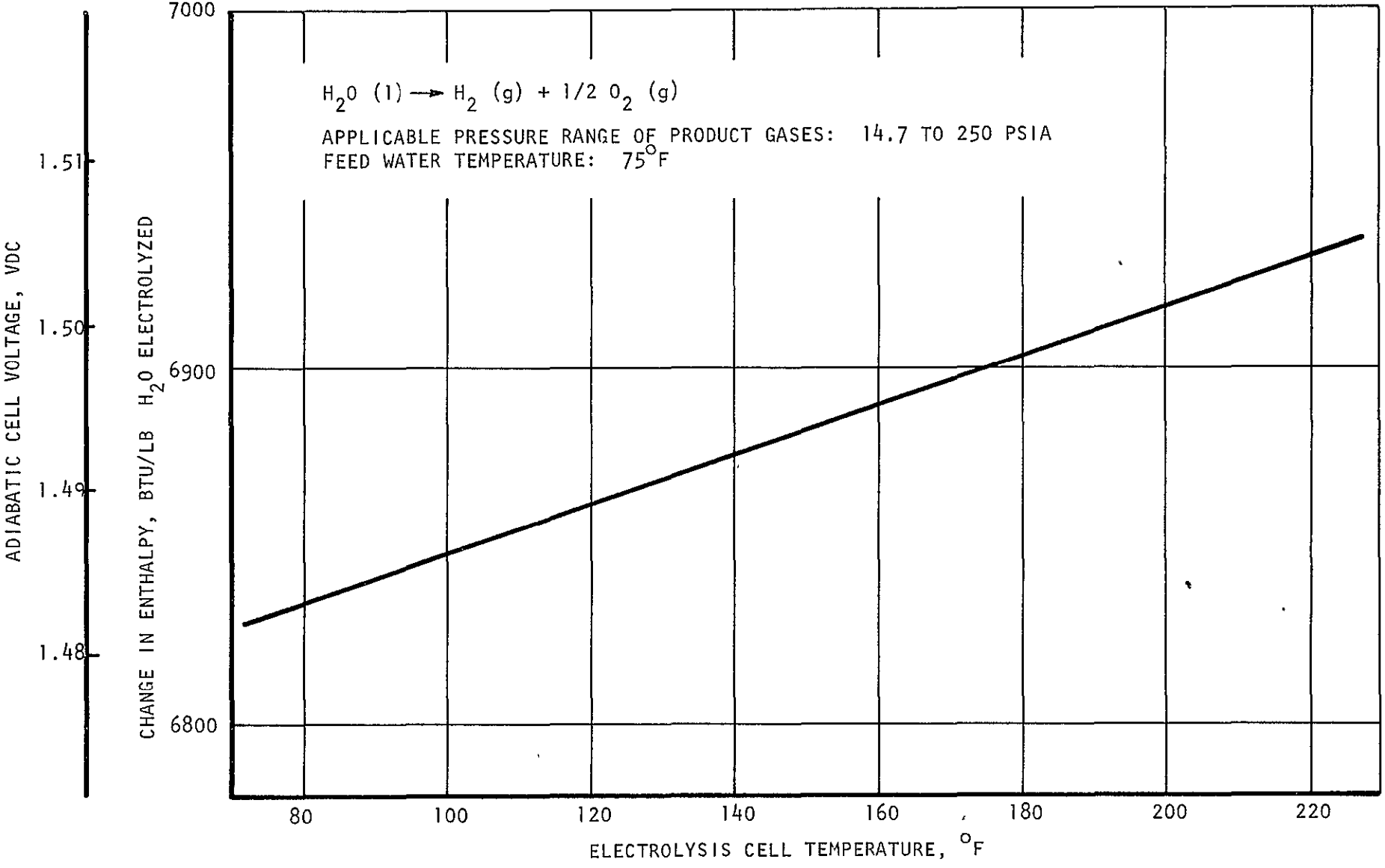

FIGURE B-1 WATER ELECTROLYSIS, ENTHALPY OF REACTION

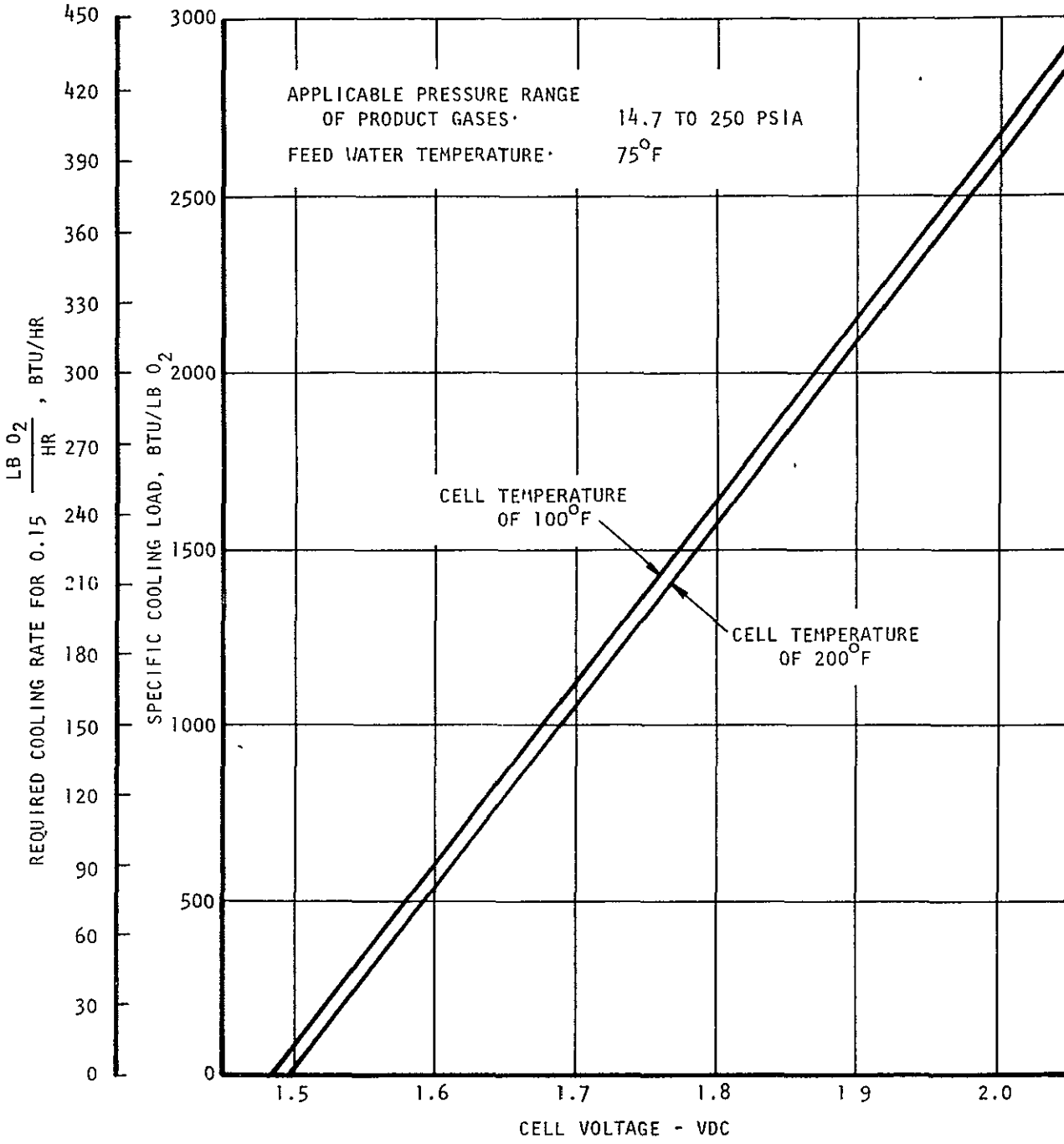

FIGURE B-2 SPECIFIC COOLING LOAD

Since the heat load is directly dependent on cell voltage, and cell voltage is a strong function of stack temperature, the relationship between these parameters is required. Figure B-3 shows cell voltage versus stack temperature for a current density of 100 ASF. The range shown was obtained experimentally during parametric testing of the NAOS Water Electrolysis Subsystem. Applicable pressure range is 15 to 82 psia. The average slope is approximately 2 MV/F^{o}.

F-111 Environmental System

The F-111 weapons system utilizes both air and a liquid coolant (10% ethylene glycol) in its environmental control system. The liquid coolant, however, is used in an evaporative cooling mode and will, therefore, reach temperatures in excess of those required for the electrolysis module.

The aircraft air conditioning system basically uses air at -65^{o}F and mixes it with 390^{o}F air to obtain desired temperature levels for cabin cooling, pressure suit cooling, and electronic equipment cooling. Various types of modulating valves and temperature sensors are used to perform these functions. A similar system could be utilized to supply cooling air at a desired temperature level to NAOS system components or their secondary cooling loops.

HEAT REMOVAL METHODS

Evaporative Cooling

Water electrolysis modules can be operated without provisions for external cooling. This is possible when the waste heat generated within the electrolysis cells is equal to the heat required to evaporate the water necessary for the humidification of the product gases. The terminal cell voltage must, of course, be higher than the adiabatic voltage (see Section on Heat Load Theory).

The above implies that the heat loss from the module to the environment is negligible. If this cannot be assumed, the evaporative cooling load will be reduced by an amount equal to this heat loss. A specific example is discussed in detail below.

The heat removed by the humidification process is dissipated in one or more of the following ways: 1) condensation within the plumbing, 2) overboard venting of gas and vapor, or 3) in special dehumidification heat exchangers. When using evaporative cooling and when it is undesirable to have condensation inside these gas passages, the dewpoint throughout these passages must be kept below ambient temperature levels or trace heating must be employed. Figure B-4 shows the dewpoint for both the oxygen and hydrogen streams after expansion to the breathing loop pressure level versus electrolysis module temperature as a function of gas generation pressures.

The humidification rate per pound of water decomposed is a function of temperature, pressure and effective electrolyte concentration of each of the product

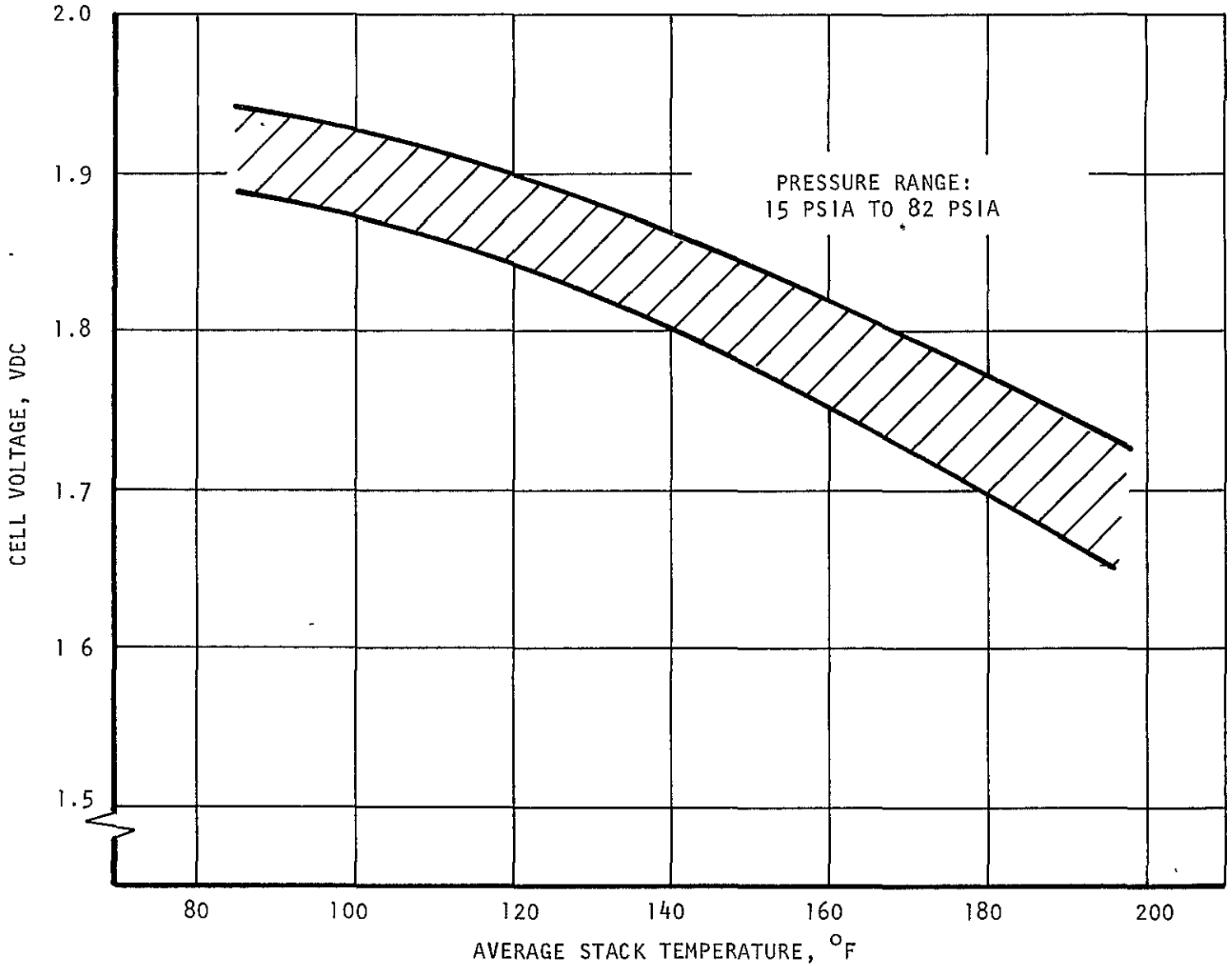

FIGURE B-3 PERFORMANCE BAND FOR WATER ELECTROLYSIS MODULE AT 100 ASF

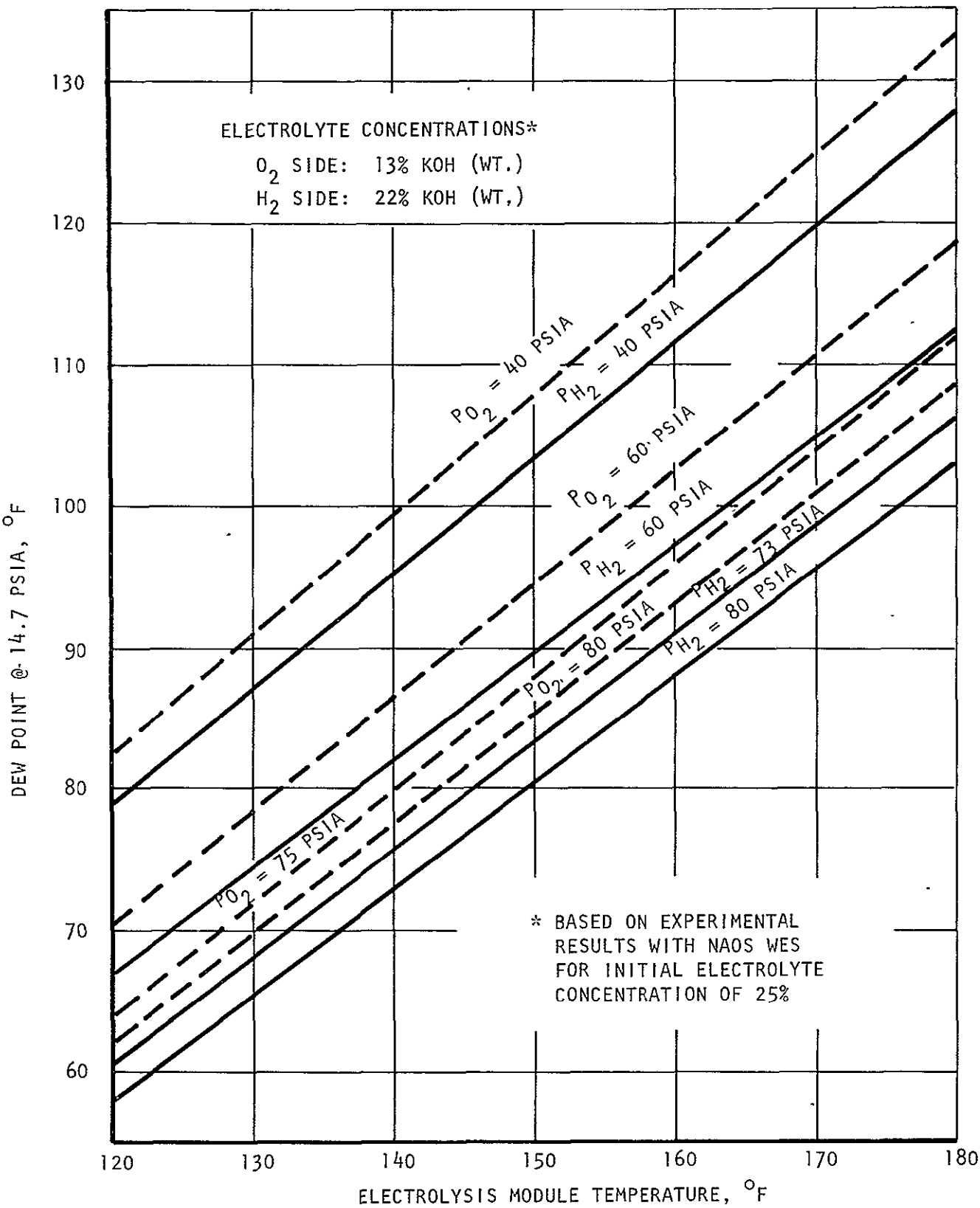

FIGURE B-4 DEW POINT IN PRODUCT GASES

gas environments. Based on the data collected during the long-term moisture balance tests, it will be assumed for the purpose of the NAOS module calculations that the effective electrolyte concentrations are equal to 13% KOH and 22% KOH for the oxygen and hydrogen cavities, respectively. It will also be assumed that these levels remain constant throughout the anticipated pressure and temperature ranges of operation (based upon the initial electrolyte concentration of 25% KOH and an oxygen-to-hydrogen pressure differential of 2 psi).

Figure B-5 shows the temperature level necessary to achieve evaporative cooling for a range of cell operating voltages as a function of oxygen pressure level. The above stated assumptions apply. Figure B-5 shows, for example, that an electrolysis module operating at a terminal voltage of 1.7 volts per cell and at 20 psia will reach 190°F if the heat loss due to the environment is negligible. If, however, this heat loss to the environment is appreciable, the following example would demonstrate the use of Figure B-5.

Assuming a module skin temperature of 120°F, ambient temperature of 80°F, and a surface area of 2 sq. ft., the loss for this condition would equal approximately 60 BTU/hr due to free convection. Converting this loss into an equivalent voltage for a module electrolyzing 0.1688 pounds of H_2O/hr gives:

$$\frac{60 \text{ BTU/hr}}{0.1688 \text{ lb } H_2O/\text{hr}} \times 0.000217 \text{ volts/BTU/lb of } H_2O \text{ decomposed} = 0.077 \text{ volts.}$$

Applying the heat loss to the original example above, results in 1.70-.077 = 1.623 volts for which, according to Figure B-5, the module temperature would have to reach 174°F. By establishing allowable operating temperature limits, an equivalent change in voltage, i.e., in heat loss to environment can be established and thus insulation for the module can be sized.

It can be seen from Figure B-5, however, that selection of the evaporative cooling method for a NAOS water electrolysis module operating at the required 75 psia pressure level is highly unlikely. This conclusion is based on the fact that for the designs with negligible heat loss to the environment, state-of-the-art electrolysis module performances do not match the required voltages of less than 1.53 volts for 75 psia operating pressure. It is also undesirable to design for a major portion of the heat load to be rejected directly to the environment since module temperature limits would be highly unpredictable and could easily reach catastrophic levels.

Air Cooling

In an air-cooled electrolysis module, the waste heat generated within the module is conducted to external fins and air is forced over the fins to remove this heat. This method of heat removal strongly influences module configuration since high conductance, electrically insulated, heat paths must be provided from the cell interiors to the external fins. The product of thermal conductivity and heat path thickness must be sufficiently high to limit the temperature gradients within the cell to safe levels.

For similar reasons, minimum air flow rates can be determined based on maximum allowable air temperature rise, i.e., longitudinal fin temperature gradients.

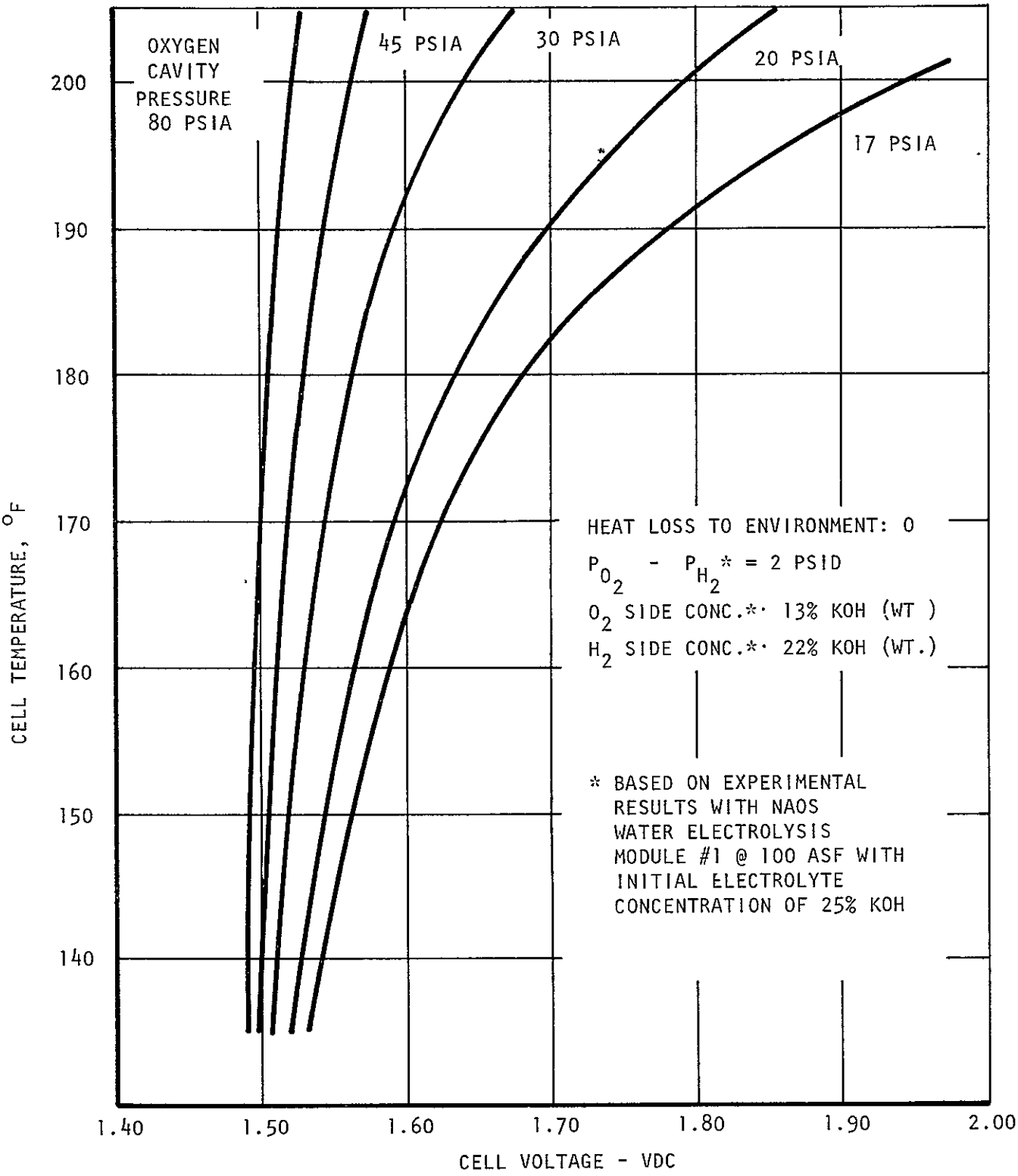

FIGURE B-5 ELECTROLYSIS CELL PARAMETRIC RELATIONSHIPS FOR EVAPORATIVE COOLING

The water electrolysis modules constructed for the NAOS program utilize this method of heat removal. The maximum internal temperature gradient and maximum air temperature rise allowed in the present NAOS module design is $6^{o}F$ and $20^{o}F$, respectively. These values are also used for this analysis since module performance has been satisfactory under these conditions. The $6^{o}F$ allowable temperature gradient results in a required thermal conductivity times thickness value of 0.367 BTU/hr/^{o}F for a copper plate of 0.025 inch thickness. The $20^{o}F$ allowable temperature rise results in an 83.4 lb/hr (20.4 cfm at $120^{o}F$, 14.7 psia) air flow for a module producing 0.15 pounds of O_2/hr at an average cell voltage of 2.0 volts.

The above values are based on active cell area dimensions of 4.75 inches by 7.0 inches. Figure B-6 shows maximum electrolysis module temperature versus cooling air inlet temperature as a function of average cell voltage. Curves for both 1 inch fin lengths and 0.25 inch fin lengths are shown.

In using Figure B-6, the cell voltage must first be corrected by the equivalent voltages for evaporative cooling and heat loss to the environment. For example, a module with an actual cell voltage of 2.0 volts operating at $150^{o}F$ and 75 psia and a heat loss of 60 BTU/hr would have the following voltage corrections.

From Figure B-1, V_a = 1.493 volts and, from Figure B-5, the cell voltage = 1.495 volts for the above conditions. The evaporative heat-loss-voltage-equivalent is therefore, 1.495 - 1.493 or .002 volts. The 60 BTU/hr heat loss equivalent is 0.077 volts (see section on Evaporative Cooling). To find the maximum module temperature for a given air inlet temperature from Figure B-6 therefore, 0.079 volts (.002 + .077 volts) must be subtracted from the actual cell voltage of 2.0 volts.

Figure B-7 shows volumetric air flow rates and static pressure loss versus average temperature of cooling air for a constant mass flowrate of 83.4 lb/hr. Data for 5.0, 14.7 and 45 psia for the 1 inch fin and 0.25 inch fin is presented in the figure.

The cooling air could be supplied either from the F-111 air conditioning system by proper mixing of $-65^{o}F$ and $390^{o}F$ air or by a fan blowing ambient air over the fins. The first method is quite feasible and would utilize temperature sensors and modulating valves similar to those utilized elsewhere on the aircraft. A basic schematic of the system would look as follows:

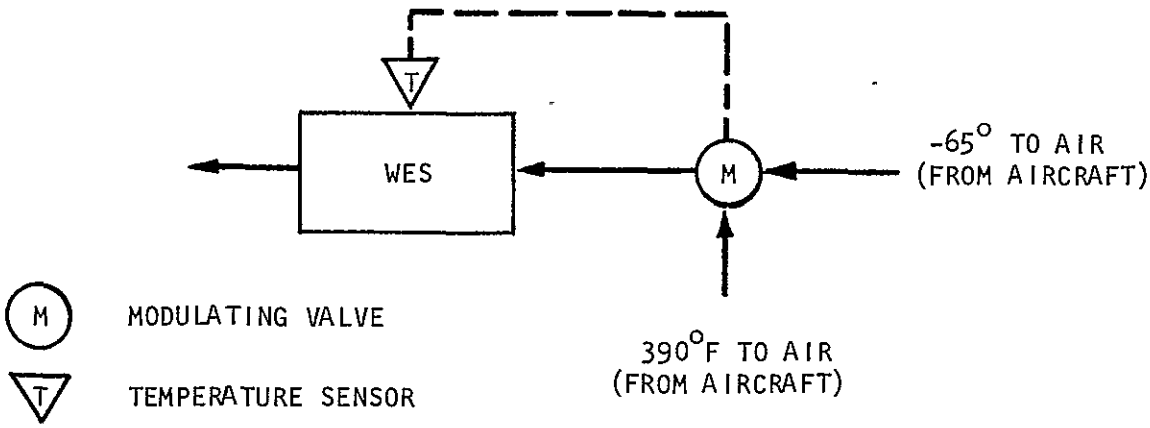

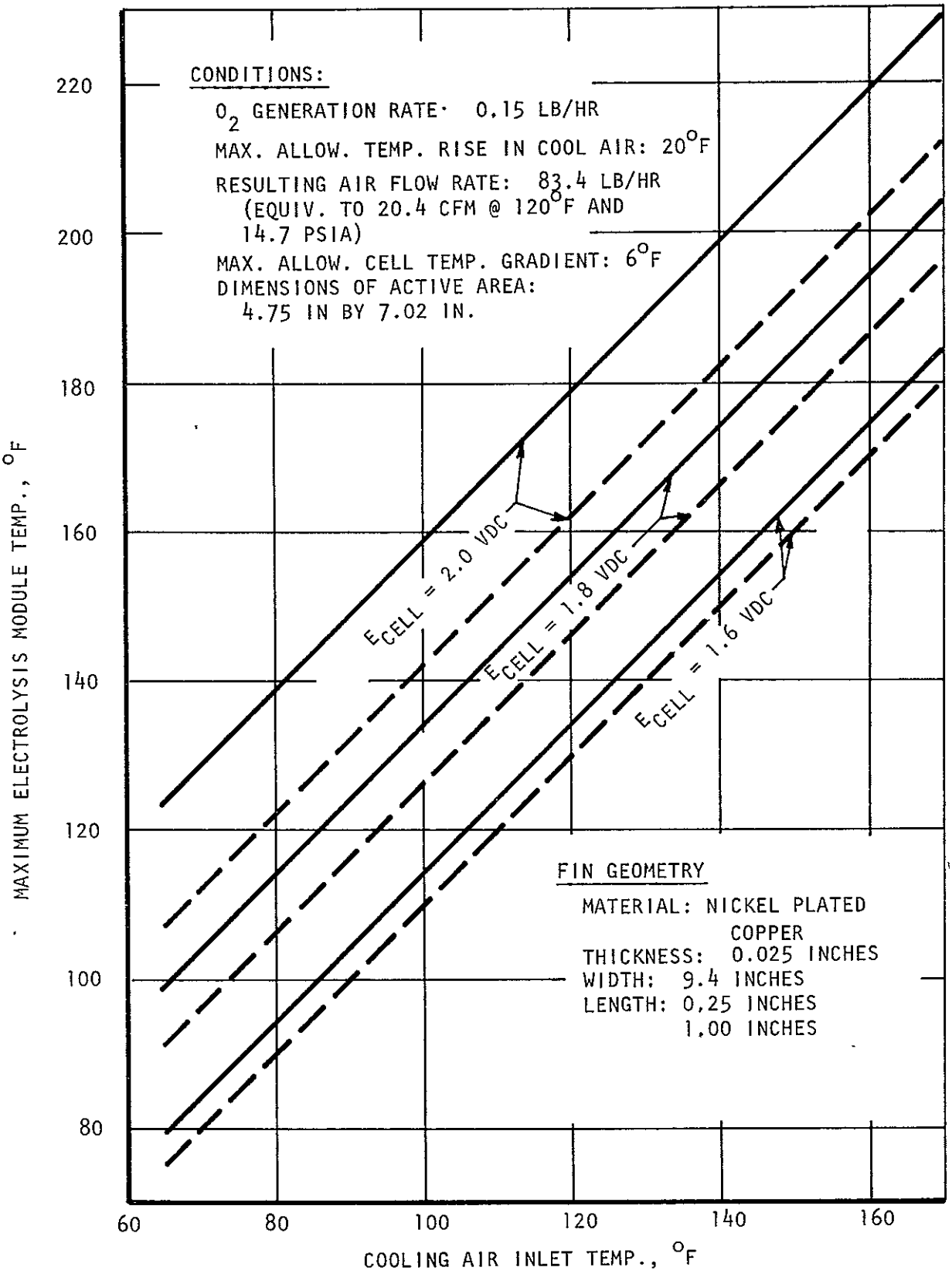

FIGURE B-6 ELECTROLYSIS MODULE TEMPERATURE VS. COOLING AIR INLET TEMPERATURE

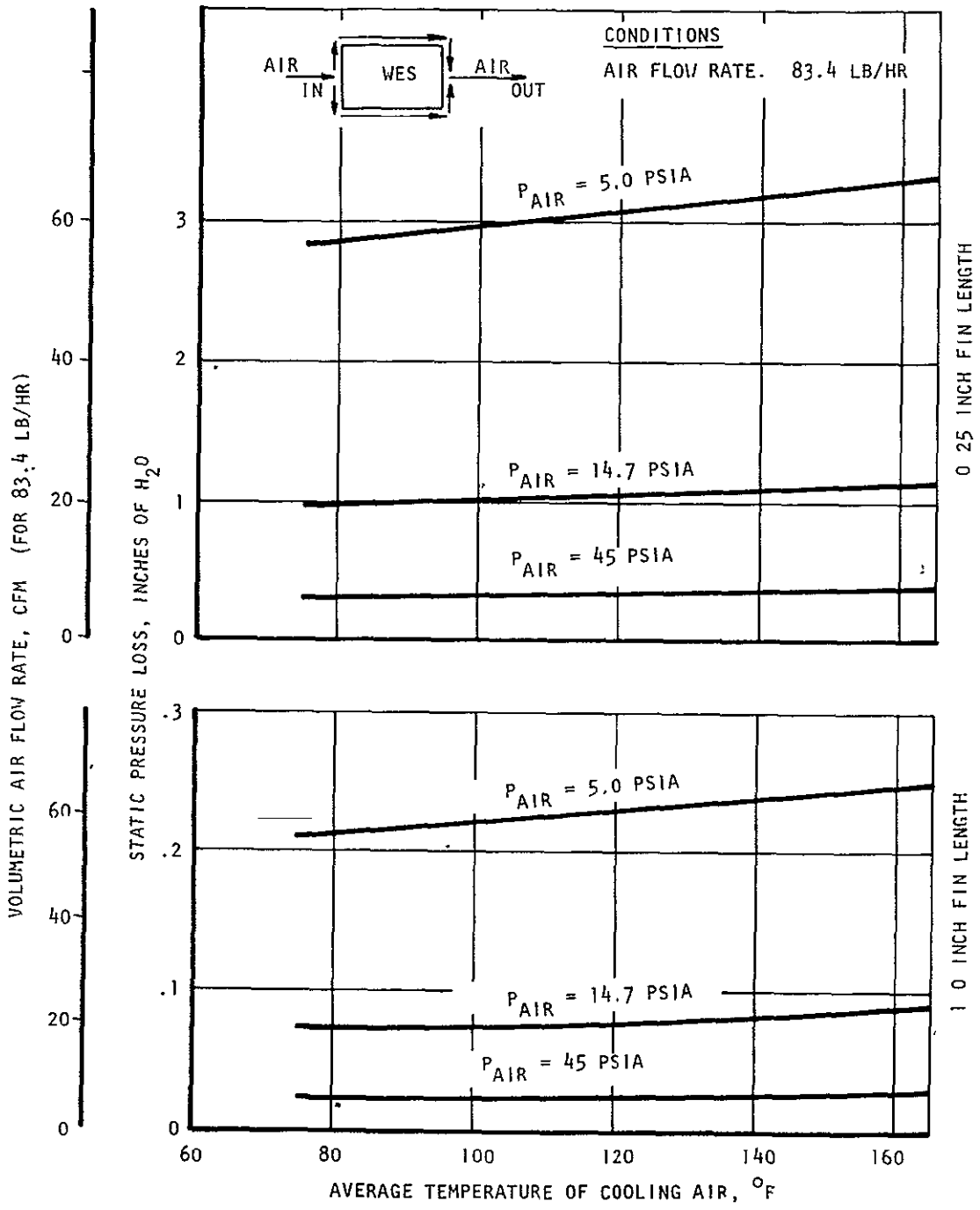

FIGURE A-7 STATIC PRESSURE LOSS ACROSS AIR COOLED ELECTROLYSIS MODULE

A fan supplying sufficient amounts of ambient air at high altitudes would be of relatively large size and this method of air supply is not considered practical for aircraft application.

Liquid Cooling

Liquid-cooled water electrolysis modules utilize internal cooling passages. Normally each individual cell has such a passage. Either parallel or series flow may be used. In series flow, however, undesirable temperature gradients may exist across the electrolysis stack. This can be lessened by increasing flowrates, however, this results in an increase in the pressure drop penalty. To minimize pressure loss and stack temperature gradients, a parallel flow configuration was selected and analyzed. Again, a cell of NAOS-type dimensions was used. Each water cavity plate has a three-pass cooling groove approximately 20 inches long with a 0.5 x 0.032 inch cross section, see Figure B-8.

The coolant selected was a 10% solution of ethylene glycol. Flowrates of 2.5 lbs/hr per cell, 5.0 lb/hr per cell, and 7.5 lb/hr per cell were investigated for a module producing 0.15 pounds of O_2/hr. Figure B-8 shows maximum electrolysis module temperature versus coolant inlet temperature as a function of cell voltage for the above coolant flows. Figure B-9 shows the temperature rise in coolant versus coolant flow rate as a function of cell voltage. This temperature rise will also approximate cell temperature gradients.

Again, voltage equivalents for evaporative and environmental heat losses must first be calculated before using Figures B-8 and B-9 (see section on Air Cooling for sample calculations).

Figure B-10 shows pressure drop in inches of water versus liquid coolant flowrate in lbs/hr per cell. The configuration of a liquid-cooled module compared to that of an air-cooled module is much simpler and the absence of fins and conductance paths results in a lighter and smaller module for a given capacity. Total weight savings are approximately 1.1 pounds per individual cell. Volume reduction is approximately 5 cubic inches per cell.

Since the F-111 has no suitable liquid coolant on board, the water electrolysis subsystem would have to be equipped with its own liquid coolant loop or share, for example, a liquid coolant loop with other NAOS subsystems. The primary additional components needed for such a loop would be a circulating pump, an expansion tank, and a liquid-to-air heat exchanger to reject the heat to the aircraft's air cooling system. A basic schematic of such a system is shown on page B-23.

Circulating Electrolyte

The waste heat generated within the electrolysis module can also be removed by circulating the electrolyte through a feed water cavity. This approach is quite similar to that of the liquid cooling method. Again, parallel flow is recommended. The module construction, however, is simpler compared to the one having the separate cooling loop. This is true since no cooling passages and no additional manifolds and porting are required. The module configuration for a given capacity would be identical to one using evaporative cooling.

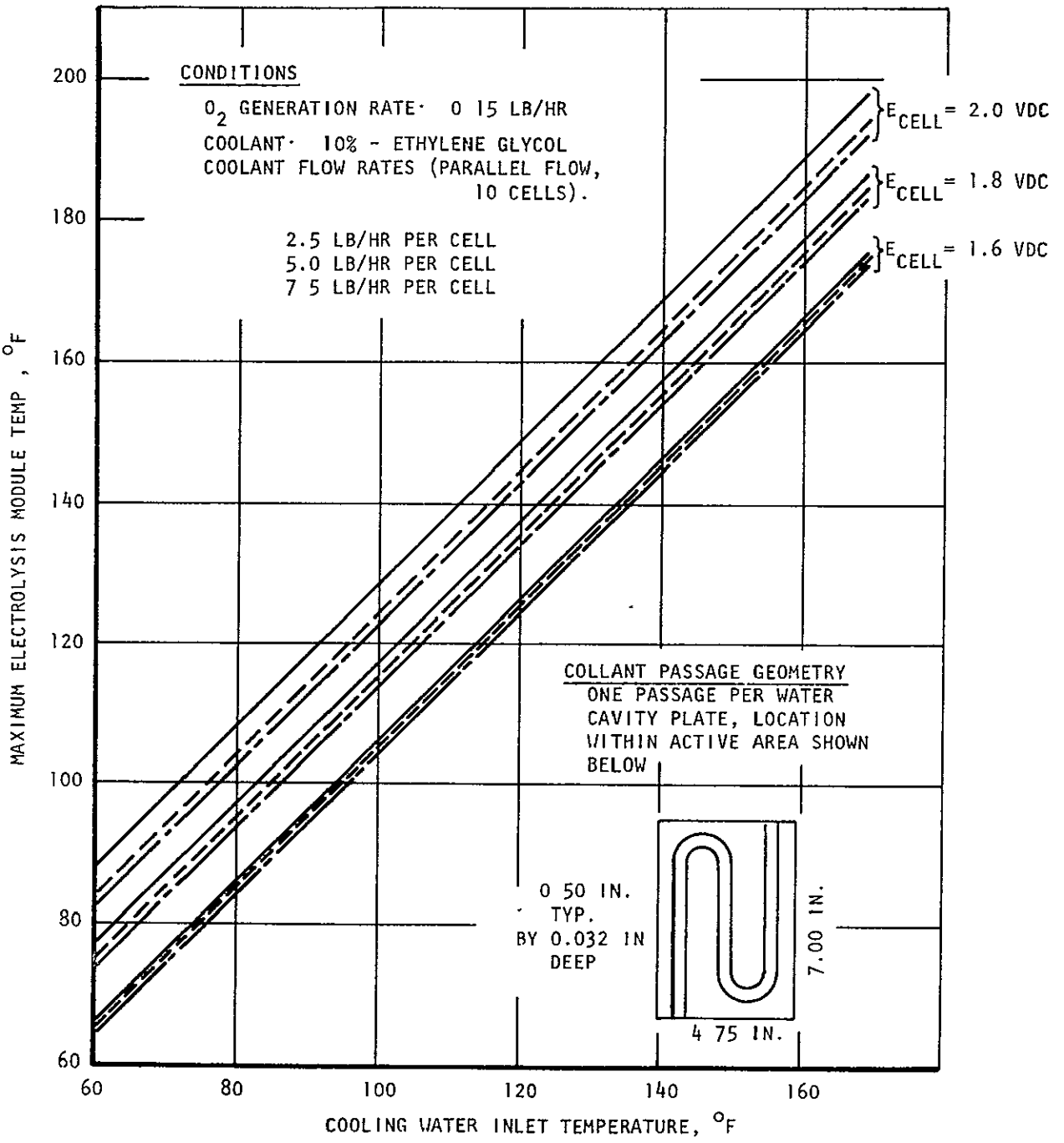

FIGURE B-8 ELECTROLYSIS MODULE TEMPERATURE VS. COOLING WATER INLET TEMPERATURE

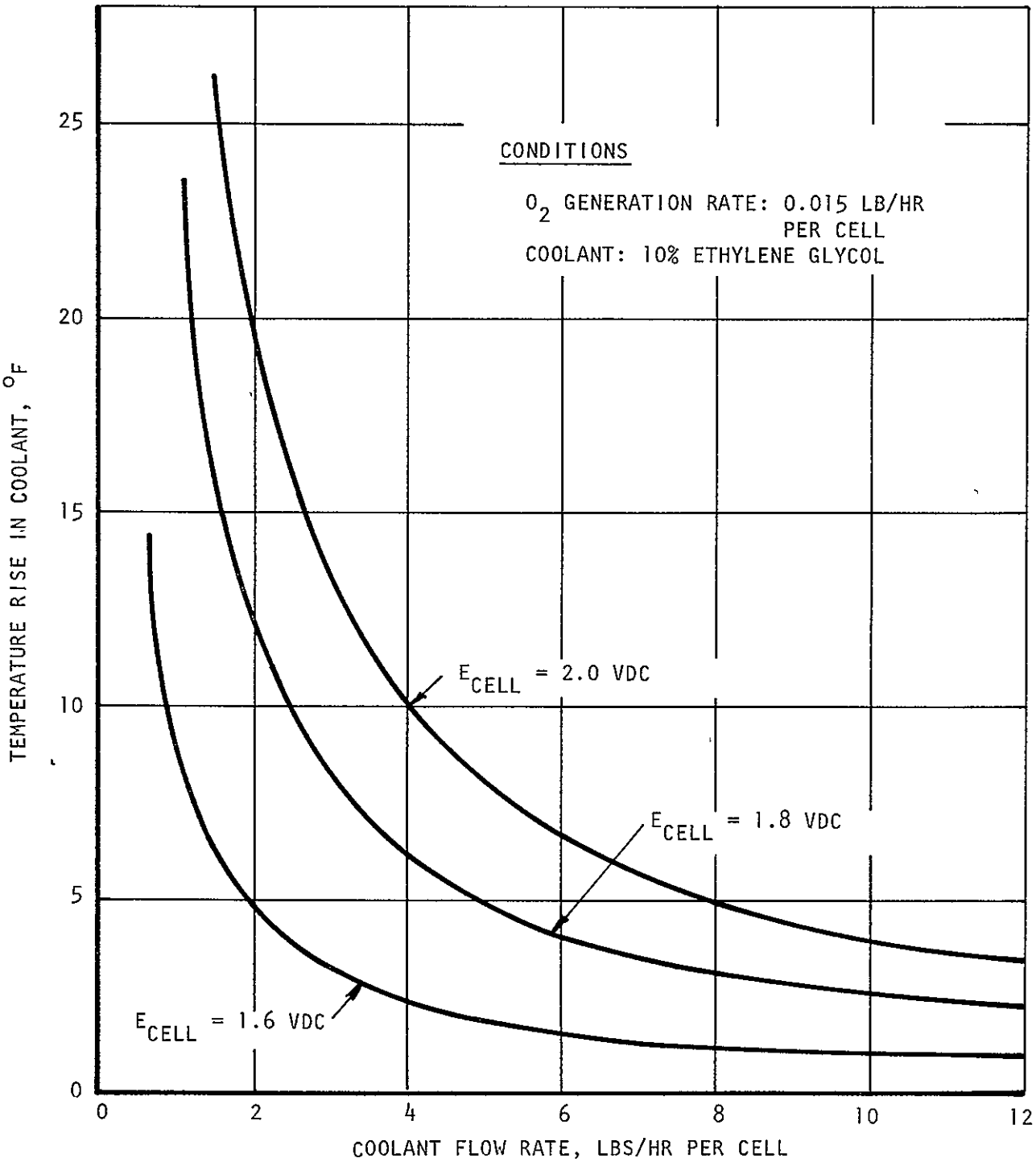

FIGURE B-9 TEMPERATURE RISE IN LIQUID COOLANT

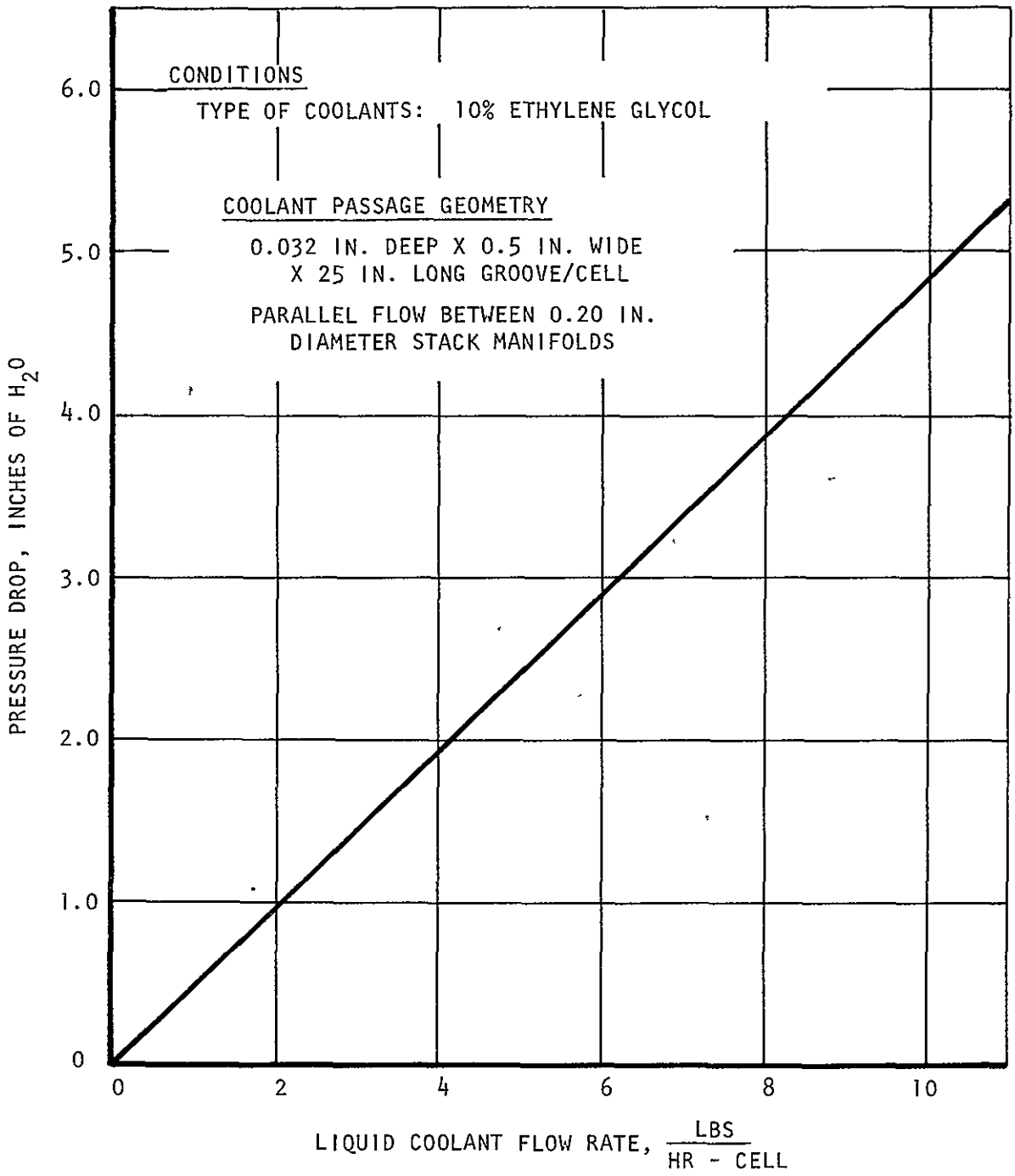

FIGURE B-10 LIQUID COOLANT PRESSURE LOSS THROUGH ELECTROLYSIS MODULE

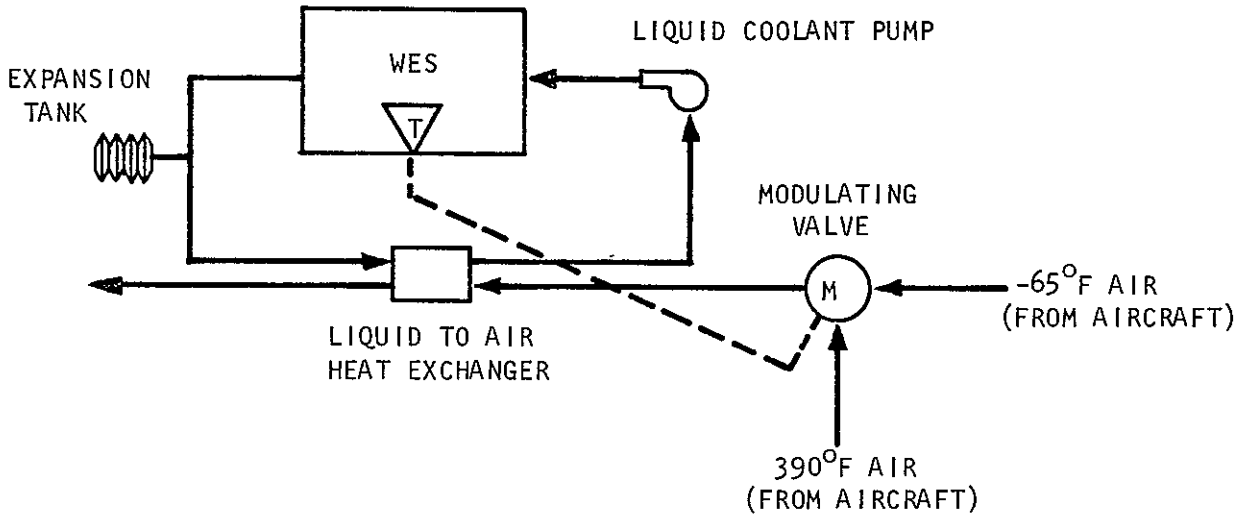

Circulating Electrolyte - continued

The additional components required for a water electrolysis subsystem using the circulating electrolyte method are a circulating pump, an electrolyte reservoir and a liquid-to-air heat exchanger. The feed water tank connects to the electrolyte reservoir and would serve as the expansion tank. An additional benefit would also be derived from the circulating electrolyte method. The dissolved gases in the feed water which accumulate within the water cavities would be carried out of the cavities and into the electrolyte reservoir. Pre-degassing of the feed water or similar methods would therefore be eliminated. Intervals between venting times of the reservoir tank would depend on the tank size. The corrosive nature, however, of the circulating loop coolant will complicate coolant loop components selection.

Pressure drop data was experimentally determined using a NAOS type water cavity. This cavity is 4.75 inches by 7.0 inches by 0.04 inches deep containing a 13-mesh polypropylene screen. Diagonally opposite, ports 0.042 inches in diameter by 1.5 inches long lead into and out of the cavity.

The experiment was conducted with 66°F water. The data was analytically corrected for 25% KOH at 150°F. Figure B-11 shows the pressure drop versus flowrate for the above conditions. Figure B-12 shows the temperature rise for the electrolyte flowrate as a function of cell voltage. This voltage must also be corrected for evaporation and environmental heat losses (see section on Air Cooling).

Comparing the pressure drop data of Figures B-10 for liquid cooland and B-11 for circulating electrolyte, shows that module pressure drop in the latter is

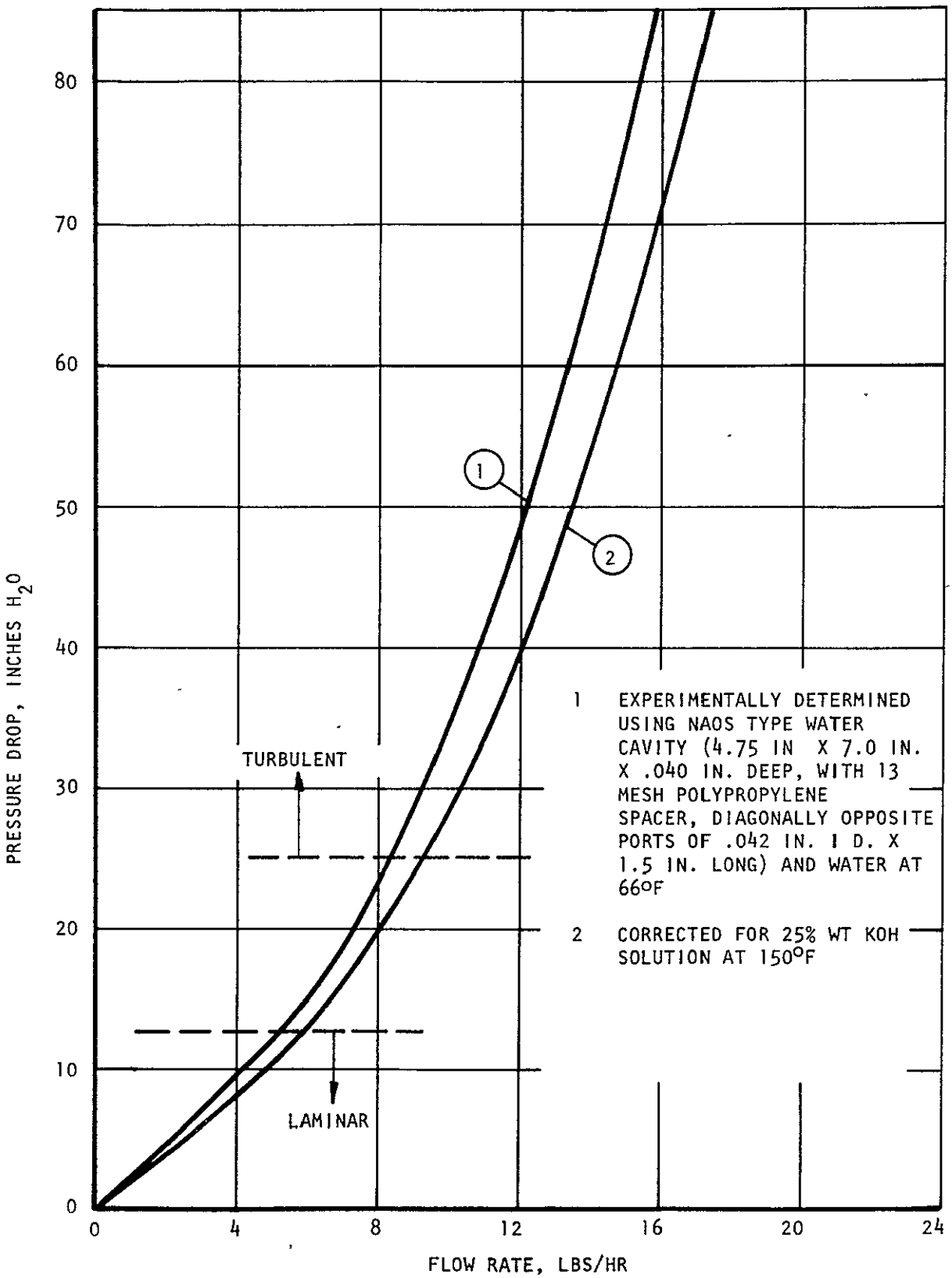

FIGURE B-11 PRESSURE DROP THROUGH ELECTROLYSIS CELL WATER CAVITY

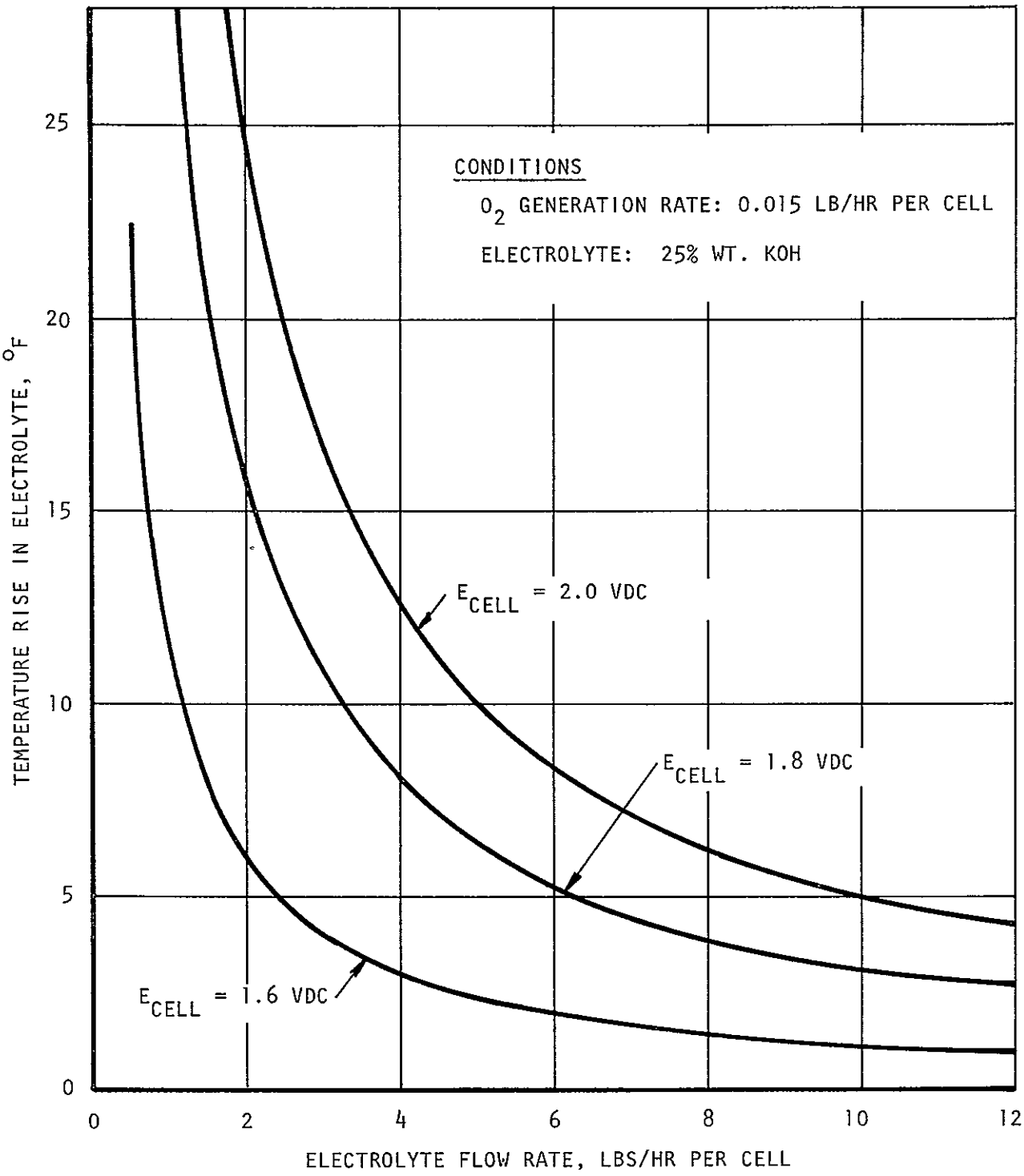

FIGURE B-12 TEMPERATURE RISE IN CIRCULATING ELECTROLYTE

four times higher. This is true in the laminar region only. In the turbulent region, this ratio continually increases. A basic schematic of a water electrolysis subsystem using the circulating electrolyte cooling method is shown below.

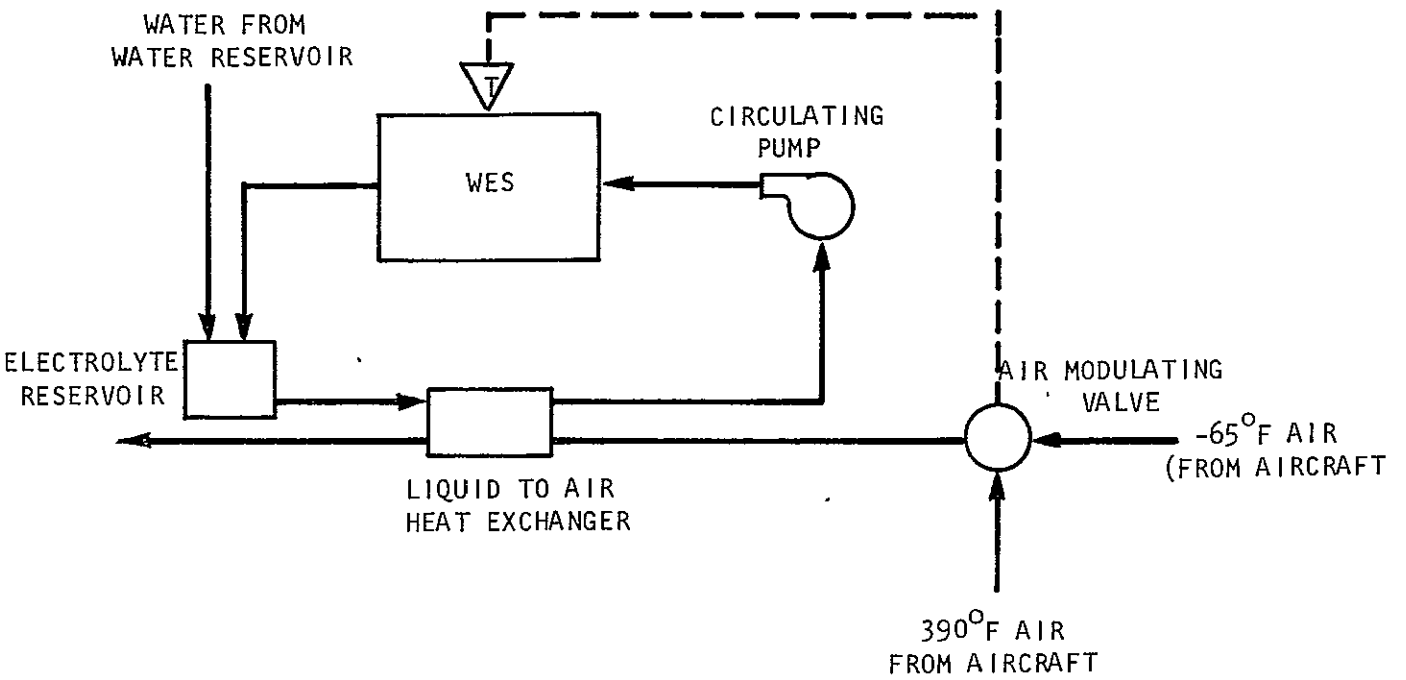

HEAT REMOVAL METHOD RATING

Table B-1 lists the four heat removal methods considered in this analysis and indicates weight and volumes on an individual cell basis. These weights and volumes are based on construction methods and materials used in the present NAOS electrolysis modules. Also listed in the table are the coolant loop components required by each method. A relative rating with respect to the reliability, power requirements, and cost for the water electrolysis subsystem is presented.

CONCLUSION AND RECOMMENDATIONS

Four heat removal methods were considered applicable for aircraft use for the water electrolysis subsystem of the NAOS system. They are: 1) evaporative cooling, 2) forced convection air cooling, 3) forced convection liquid cooling, and 4) circulating electrolyte cooling.

TABLE B-1

COMPARISON RATING OF WES HEAT REMOVAL METHODS

Heat Removal Method	Unit Cell (.228 ft^2 Active Area)*		Coolant Loop Components	Relative Ratings			Remarks
	Weight, lbs	Volume, in^3		Reliability**	Power Req.	Cost	
Evaporative	1.5	30	Condensers in product gas lines, depending on operating conditions	4	1	1	Cannot be achieved at 75 psia with state-of-the-art module performance
Air Cooling	2.6	35	Temp. sensor w/control circuit and air modulating valve, cooling air shroud and ducting	1	2	2	
Liquid Coolant	1.5	30	Temp sensor w/control circuit and air modulating valve; liquid coolant pump, expansion tank; liquid to air heat exchanger; coolant lines	2	3	3	
Circulating Electrolyte	1.5	30	Temp. sensor w/control circuit and air modulating valve; electrolyte circulating pump; electrolyte reservoir; liquid to air heat exchanger; circulating lines	3	4	4	Lessens problem of dissolved gas in feed water. Continuous mixing of electrolyte in feed cavity may improve cell performance. Corrosive fluid in coolant loop

*Using present NAOS module properties as guidelines.
**Rating of 1 is optimum.

The analyses showed that the evaporative cooling method, although highly attractive from a weight and component requirement viewpoint, is not a probable candidate due to the low cell voltage requirements at the 75 psia module operating pressure.

The method using modulated aircraft air directly as a cooling media is simple and reliable. Module size and weight are disadvantages. The selection of this method is not recommended if the water electrolysis subsystem is installed as an integral part of the NAOS system. This conclusion is based on the rate and volume figure and on the air ducting and routing requirements. This method may, however, become more attractive if the water electrolysis subsystem is installed separately on the aircraft.

It is anticipated at this time that the NAOS system will use a liquid coolant loop common to its subsystems. This loop would use one circulating pump and one liquid-to-air heat exchanger, but separate temperature sensors and modulating valves for each subsystem.

Based on this assumption and on the result of this analysis, a circulating liquid cooling method is selected. The advantages of the circulating electrolyte, i.e., no de-gassing of feed water and simplicity of module construction are not considered sufficient to warrant a second pump and a liquid-to-liquid heat exchanger.

It is recommended that a heat removal optimization study be conducted at the NAOS system level. For this reason the data was presented for ranges of parameters rather for one specific operating point. This system analysis may result, of course, in changes in operating points and in the cooling method recommended herein.

APPENDIX C

POST-TEST INSPECTION OF

WATER ELECTROLYSIS MODULE (WEM #1)

APPENDIX C

POST-TEST INSPECTION OF
WATER ELECTROLYSIS MODULE (WEM #1)

1. When the plastic frame of the module was removed, appreciable salt deposits were observed on the outer surface of the module plate construction. This indicates seepage of electrolyte past the O-ring seals in the module construction. The heaviest deposits were found on the bottom surfaces of the overall module construction. Several photographs were taken to illustrate the general characteristics of the leakage deposits (Figure C-1).

2. The module was initially disassembled so that general observations relative to the condition of the overall assembly components and individual cell unit construction could be made. The following observations appeared significant:

   a. All of the O-ring elements appear to be flattened and permanently distorted. However, they still retain some elasticity (not brittle).

   b. In general, metal components in the hydrogen side cavities of cell units show no significant corrosion effects.

   c. In general, metal components in the oxygen side cavities of cell units are badly corroded in every individual cell. Surfaces on exmet spacer and current collector elements are coated with a black oxide deposit. There is a small amount of green oxide deposits on several of the solid collector plates (Cell #4 through #10). The heaviest deposits are found on the Cell #9 collector.

   d. Except for a slight discoloration, the polysulfone hydrogen-oxygen and water cavity plates appear to be in excellent condition. The polypropylene plastic spacer and matrix support screen elements also appear to have been unaffected and are in excellent condition.

   e. The internal surfaces of both endplate assemblies shows surface corrosion (oxidation) effects. The discoloration appears to be some form of iron oxide (reddish brown).

Following is a partial breakdown of the overall module assembly. The individual cell units consisted of four basic packages:

1. Water plate subassembly

   a. Plate element proper (water cavity plate)
   b. Spacer (heavy mesh plastic screen)
   c. Matrix support (fine mesh plastic) at spacer-matrix interface
   d. Matrix (asbestos)
   e. Matrix support (fine mesh plastic)

2. Slotted current collector subassembly

   a. Slotted spacer (plastic sheet)
   b. Plate proper

3. Hydrogen-oxygen plate subassembly

   a. Hydrogen cavity spacer (exmet)
   b. Hydrogen cavity compression ring
   c. Hydrogen cavity electrode
   d. Matrix (asbestos)
   e. Oxygen cavity electrode
   f. Oxygen cavity compression ring
   g. Oxygen cavity spacer
   h. Hydrogen-oxygen plate proper

4. Plain collector plate element

Components from Cell #5 were photographed in order to illustrate the physical appearance (typical of all cells) of cell components after being subjected to module operating and electrolyte immersion during life test. Photographs were taken of the following areas:

Figure C-2 Oxygen cavity corrosion showing electrode-cavity spacer interface. Note black deposits on electrode, spacer, and electrode surfaces.

Figure C-3 Comparison of new versus life test components at oxygen cavity electrode-cavity spacer interface.

Figure C-4 Oxygen cavity corrosion at cavity spacer-collector interface showing black deposits on plain collector surface.

Figure C-5 Hydrogen cavity corrosion at electrode-cavity spacer interface. Comparison of Figures C-2 and C-5 illustrates minimum corrosion conditions in hydrogen cavity.

Figure C-6 Comparison of new versus life test components at hydrogen cavity electrode-cavity spacer interface.

Figure C-7 Smearing on water plate element face external to water cavity. Comparison with a new component illustrates the smearing which appears on several other water plate elements.

Figure C-8 Comparison of new versus life test water plate elements showing water cavity face views. This comparison illustrates the excellent condition of the used plate element.

Figure C-9 Water plate subassembly teardown. Note the tear in the matrix support screen located between the matrix and cavity spacer elements at the bottom edge of the assembly. This cavity spacer element did not appear to reinforce the matrix support element along this edge due to either shrinkage or insufficient size

initially. The pressure differential across the matrix apparently caused a matrix support element failure. Smearing on the reverse face of the plate assembly can also be seen.

Figure C-10 Hydrogen cavity electrode-matrix interface. Note the excellent condition of the electrode and matrix elements which showed no tendency to adhere to one another in the disassembly process.

Figure C-11 Oxygen cavity electrode-matrix interface. Note the heavy black corrosion deposits on the electrode and matrix surfaces. The pattern of deposits on the matrix surface varies from almost full coverage on some cell units to local spots on others. The local tearing of the matrix due to adherence of the electrode and matrix surfaces was a common occurrence in the teardown of individual cell hydrogen-oxygen plate subassemblies.

Figure C-12 Oxygen cavity spacer - comparison of new versus life test components illustrates effects of corrosion, including material breakdown and deposits. Note piece broken out of life test element which was found to be extremely brittle as compared to the initial ductility of the mesh structure.

Figure C-13 Cleaned plain current collector plate (Cell #5). Most of the surface corrosion and black deposits on the collector surface were removed by cleaning the surface with detergent, scouring powder, and steel wool. However, severe local corrosion of the nickel plate is indicated by the deep pitting of the collector surface. It appears that the nickel plate has been completely removed in some spots.

Except for Figure C-17, the remaining photographs taken of disassembled components were devoted to the documentation of isolated cell unit problems rather than problems common to all cell units.

Figure C-14 Structural endplate surface corrosion. The surface shown in this photograph was exposed to electrolyte and gas flow leakages. Corrosion of the surface appears to be restricted to surface oxidation. Reddish-brown color indicates presence of iron oxides.

Figure C-15 Exploded view of matrix crossover failure (Cell #1).

Figure C-16 Hydrogen-oxygen matrix crossover failure (Cell #1). This photograph shows the location of the matrix puncture responsible for test rig shutdown in life test operations. The puncture is adjacent to the hydrogen port in the hydrogen-oxygen plate assembly as shown in the photo.

Figure C-17 Comparison of new and used O-ring components. The purpose of this photo was to illustrate the characteristic condition of O-ring components removed from the module assembly. A permanent set or flattening of the circular cross-section has occurred in all the O-ring assemblies. Measurements indicate that the

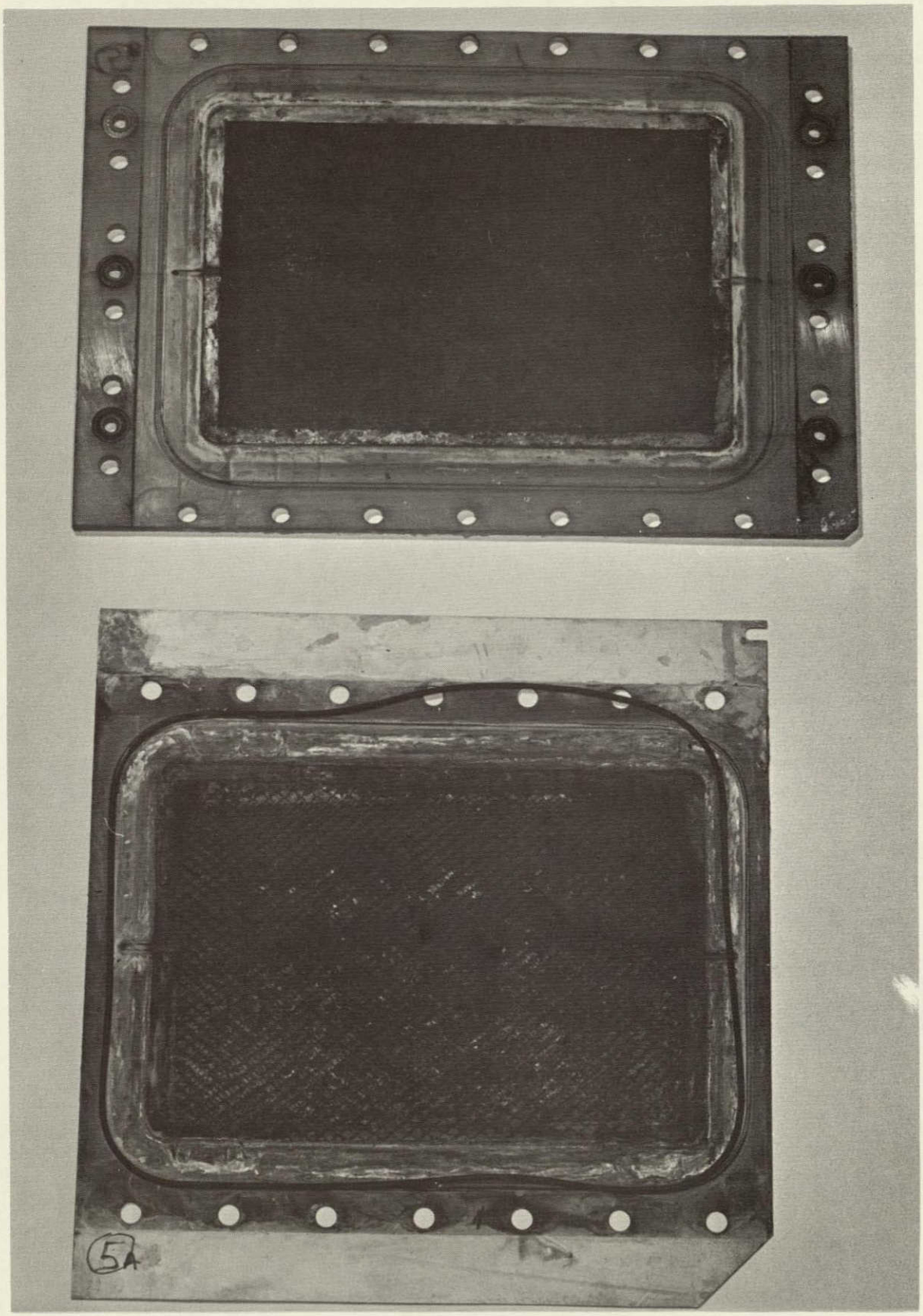

FIGURE C-2 WEM #1 OXYGEN CAVITY COMPONENTS - TYPICAL POST-LIFE TEST CONDITION

23180

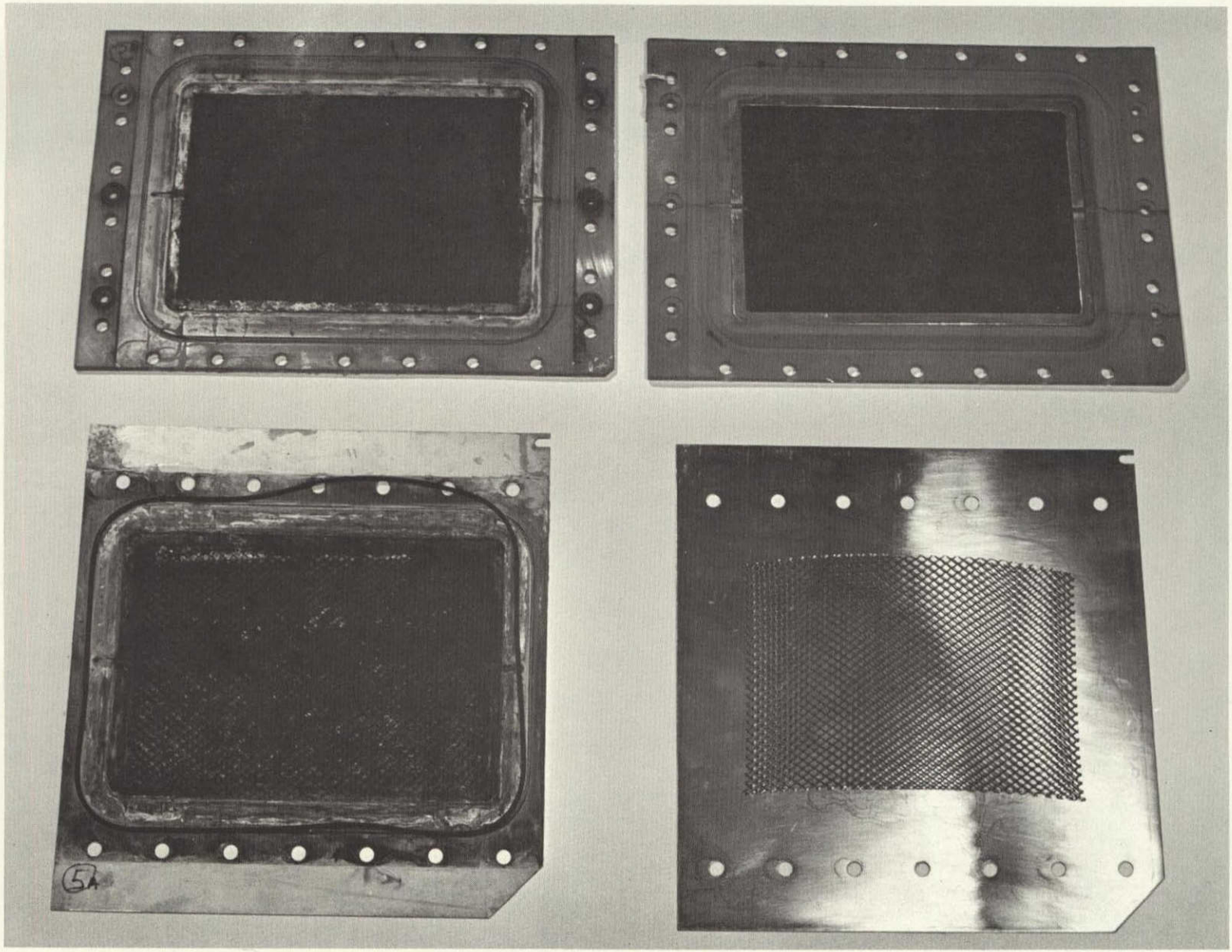

FIGURE C-3 COMPARISON OF NEW VERSUS WEM #1 POST-LIFE TEST OXYGEN CAVITY COMPONENTS

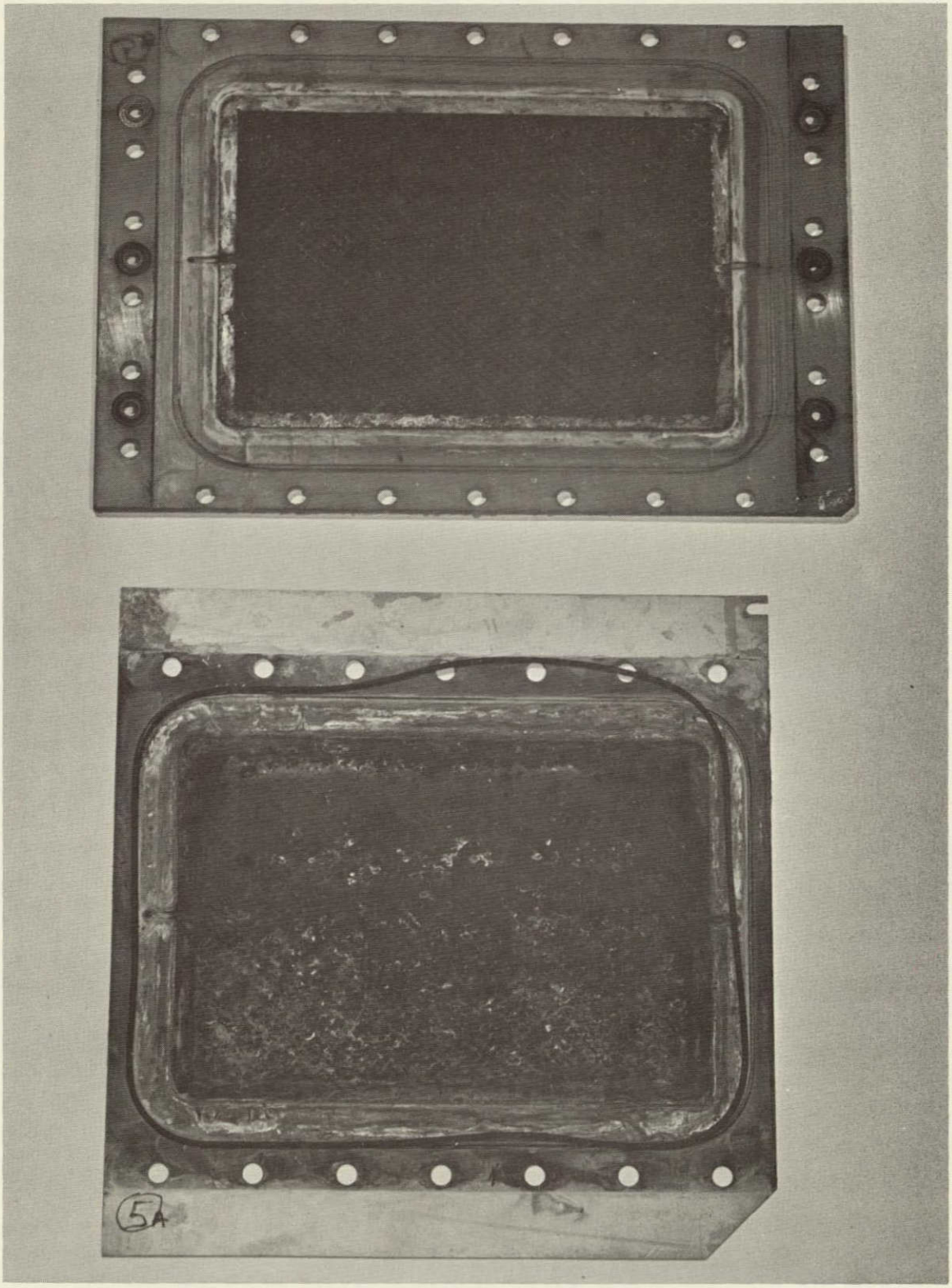

FIGURE C-4 WEM #1 OXYGEN CAVITY COMPONENTS - POST-LIFE TEST COLLECTOR PLATE DEPOSITS

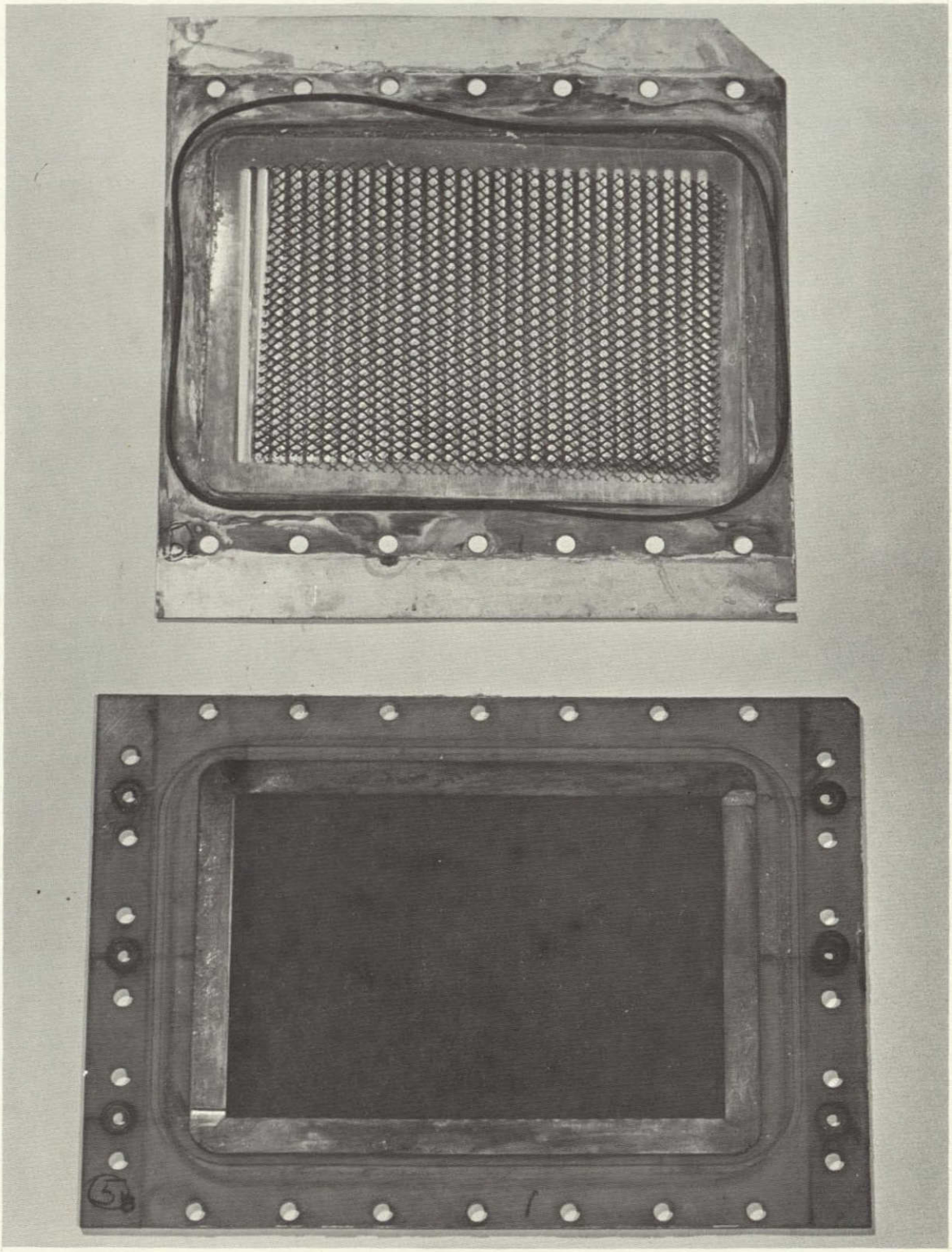

FIGURE C-5 A-5 WEM #1 HYDROGEN CAVITY COMPONENTS - TYPICAL POST-LIFE TEST CONDITION

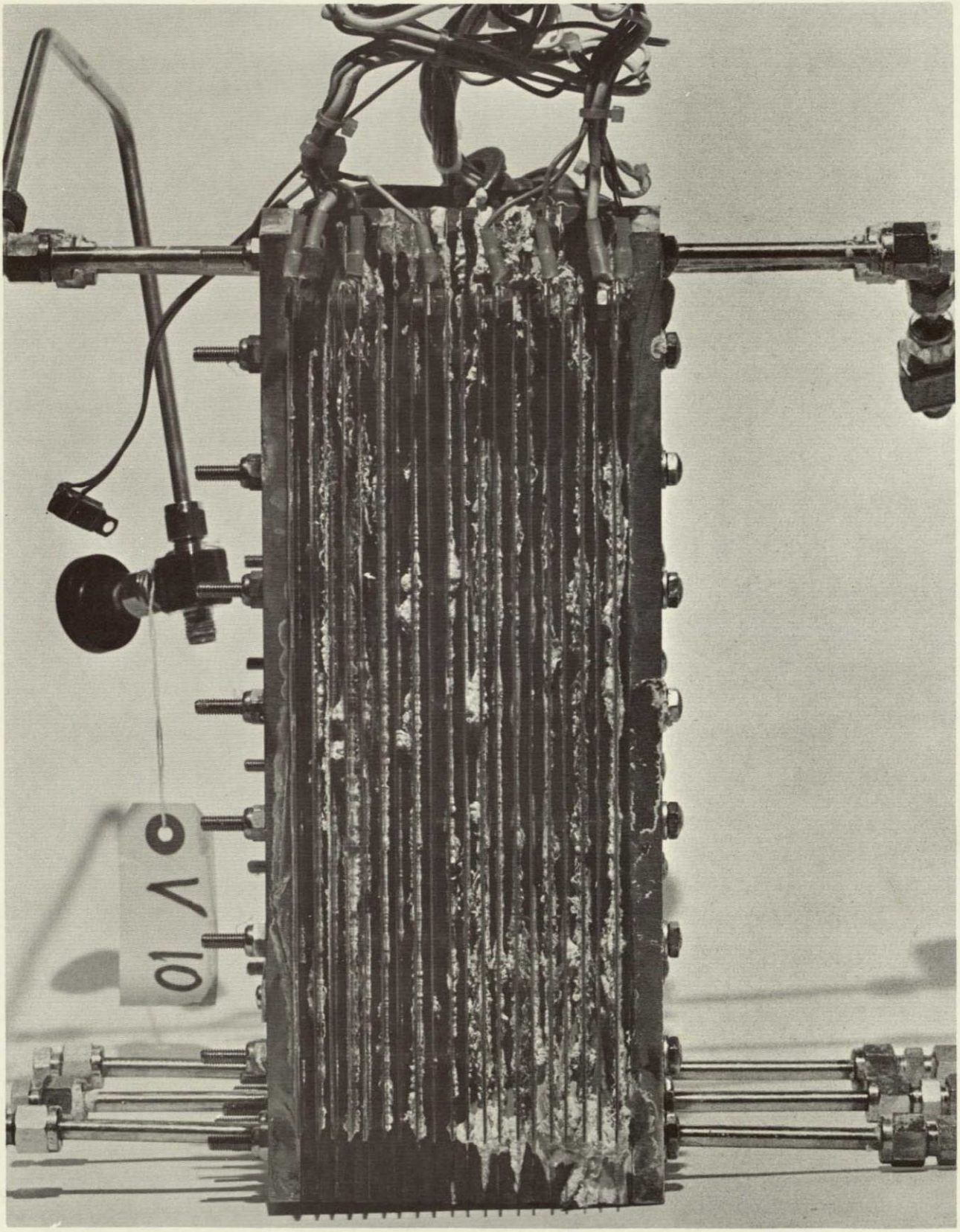

FIGURE C-1 WEM #1 MODULE ASSEMBLY - POST-LIFE TEST CONDITION

5. The hydrogen cavity compression rings were in excellent condition except for minor surface oxidation.

6. The oxygen cavity compression rings had fairly heavy surface corrosion and, as cited previously, had some galvanic interaction with the oxygen electrode elements. The ring corrosion appeared to be restricted to a surface condition, in that no noticeable pitting occurred.

7. Inspected water ports in water plate assemblies for possibility of plugging. Very slight deposits were found in cell units 1, 2, 3 and 8; all other units were relatively free of deposits. It appears doubtful that any of the passages were blocked to the extent that water feed to the cell would be decreased or shut off completely.

original cross-section diameter (nominal dimension 0.070 ± 0.003") has been decreased to a dimension of 0.058 to 0.060" in height measured in the direction of installation compression. This condition could be the result of overcompression in assembly and compression setting of the O-ring material under load for extended time periods at elevated temperature (170°F nominal). Lesser possibilities include chemical interaction with cell electrolyte and plastic materials employed in the module construction. The loss of O-ring sealing capability with time as evidenced by module electrolyte leakage is a design problem which must be given additional consideration in future module designs.

Figure C-18 Water plate assembly matrix support damage (Cell #4). This photo shows a breakdown of the matrix support fabric along the plate support edge. This condition appears to be the result of insufficient reinforcement by the water plate spacer element. When the matrix support is required to bridge too large a gap between the spacer and plate cavity edges, the matrix pressure differential loading apparently stresses the matrix support element to a failure condition.

Figure C-19 Water plate assembly matrix support and spacer damage (Cell #10). The extensive matrix support fabric damage and the evident change in appearances of water spacer material (transparent to opaque) can be seen. The most plausible reason for this condition is the proximity of Cell #10 to the water inlet and gas exhaust manifold ports. This cell would appear to be most vulnerable to pressure fluctuations produced by gas flow and water flowrate variations, water supply pressure variations, and module gas cavity venting operations. Such pressure fluctuations could produce the matrix support damage which occurred. The apparent change in the water spacer material could be due to locally high gas evolution rates or electrolyte flow conditions during gas cavity venting operations which were conducted frequently during life tests.

Figure C-20 Hydrogen cavity matrix and electrode damage (Cell #10). The corresponding patterns of electrode material removal and matrix deposits in localized spots is illustrated in this photo. Locally excessive gas evolution rates could explain the random pattern of the spots with the electrode material being blown off the electrode mesh to the matrix surface.

Figure C-21 Oxygen cavity matrix and electrode corrosion (Cell #10). The black deposits on the lower half of the matrix area and local spots on the upper half of the matrix are characteristic cell corrosion results, i.e., the local adherence of the matrix material to the electrode surface. The deep brownish color in the central area of the matrix surface is peculiar to this cell unit. Because of its proximity to the gas venting port, it appears conceivable that this cell would be most prone to the backflow of corrosion products from the stainless steel vent line installation in the test rig (iron oxide particles).

Figure C-22 Oxygen cavity gas port deposits (H_2-O_2 plate assembly - Cell #8). The gas ports in the plate assembly appear to be completely blocked off by deposits in this cell unit. This condition could account for some of the erratic module operations occurring during the latter phase of life tests. A complete blockage of oxygen flow from one cell would produce a maldistribution of cell gas flows, voltages and pressures. The port blockage condition in this cell is considerably worse than any of the other units.

General Observations in Water Plate Subassembly Teardowns:

1. Matrix support on hydrogen cavity side of matrix was in excellent condition.

2. Matrix in excellent condition except for slight discolorations in area of gas ports (Cells #3, 4, 7, 8 and 9). Discoloration along one long plate edge in Cell #10 where plate side matrix support was badly damaged.

3. Matrix support on plate side of matrix in excellent condition in Cells #1, 2, 3, 6, 7, 8 and 9 except for discoloration adjacent to gas port outlets. In Cell #4, the matrix support fabric was split locally at a corner adjacent to the gas port outlet. Matrix support element damage in Cells #4, 5 and 10 is documented in photographs.

4. Water cavity spacer elements were in excellent condition except for discoloration adjacent to gas port in Cell #4 and extensive material appearance change in Cell #10 which is shown in Figure C-19.

General Observations in Hydrogen-Oxygen Plate Subassembly Teardowns:

1. The hydrogen electrode element in each cell appeared to be in excellent condition except for local spot removal of electrode coating in Cell #10.

2. Except for the crossover puncture in Cell #1, the condition of hydrogen side of the matrix element was good with surface slightly gray in color.

3. The oxygen cavity side matrix surface was covered with a black deposit to some degree on all elements varying from full area coverage to lower half coverage, with local spotting of upper half. In disassembly, the matrix adhered to the electrode surface in the areas of heavy deposits. The matrix material, in a few instances, was slightly discolored at gas port locations.

4. The oxygen electrode element surfaces on the oxygen cavity side were entirely covered with a heavy black deposit. Deposits were exceptionally heavy along the bottom edge of the oxygen compression ring. Galvanic action between compression ring and electrode resulted in local welding of the components in many of the cell units. As a consequence, the edge of the electrode was torn or damaged during disassembly. Except for heavy deposits and disassembly damage, the electrodes appeared to still be in fairly good condition. There appeared to be some slight tendency to remove electrode deposits in the gas port areas, with a slight puncture noted in this area at Cell #4. The galvanic action between the compression ring and electrode had a tendency to embrittle the electrode element along its edges.

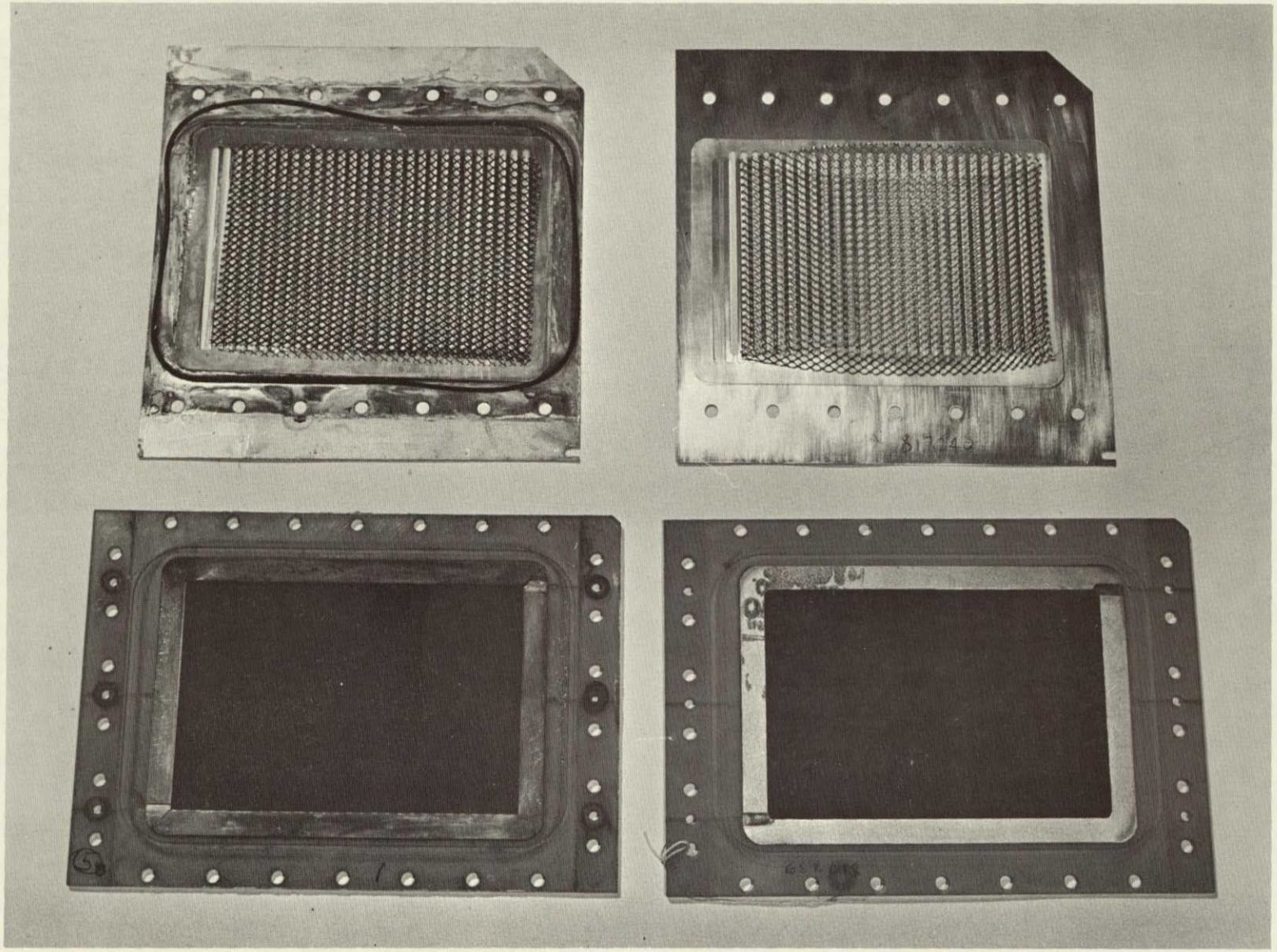

FIGURE C-6 COMPARISON OF NEW VERSUS WEM #1 POST-LIFE TEST HYDROGEN CAVITY COMPONENTS

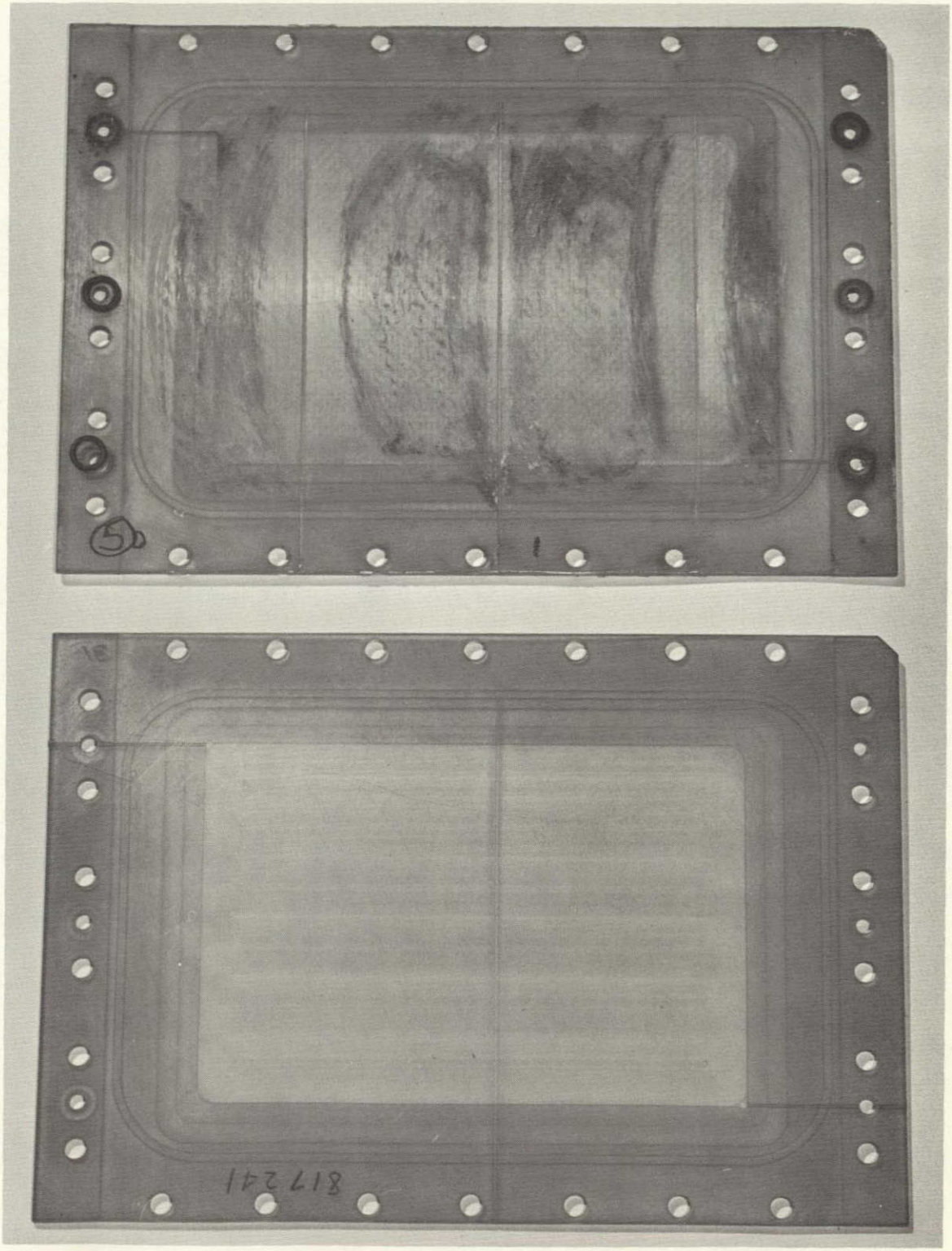

FIGURE C-7 WEM #1 H_2O PLATE - TYPICAL POST-LIFE TEST CONDITION VERSUS NEW

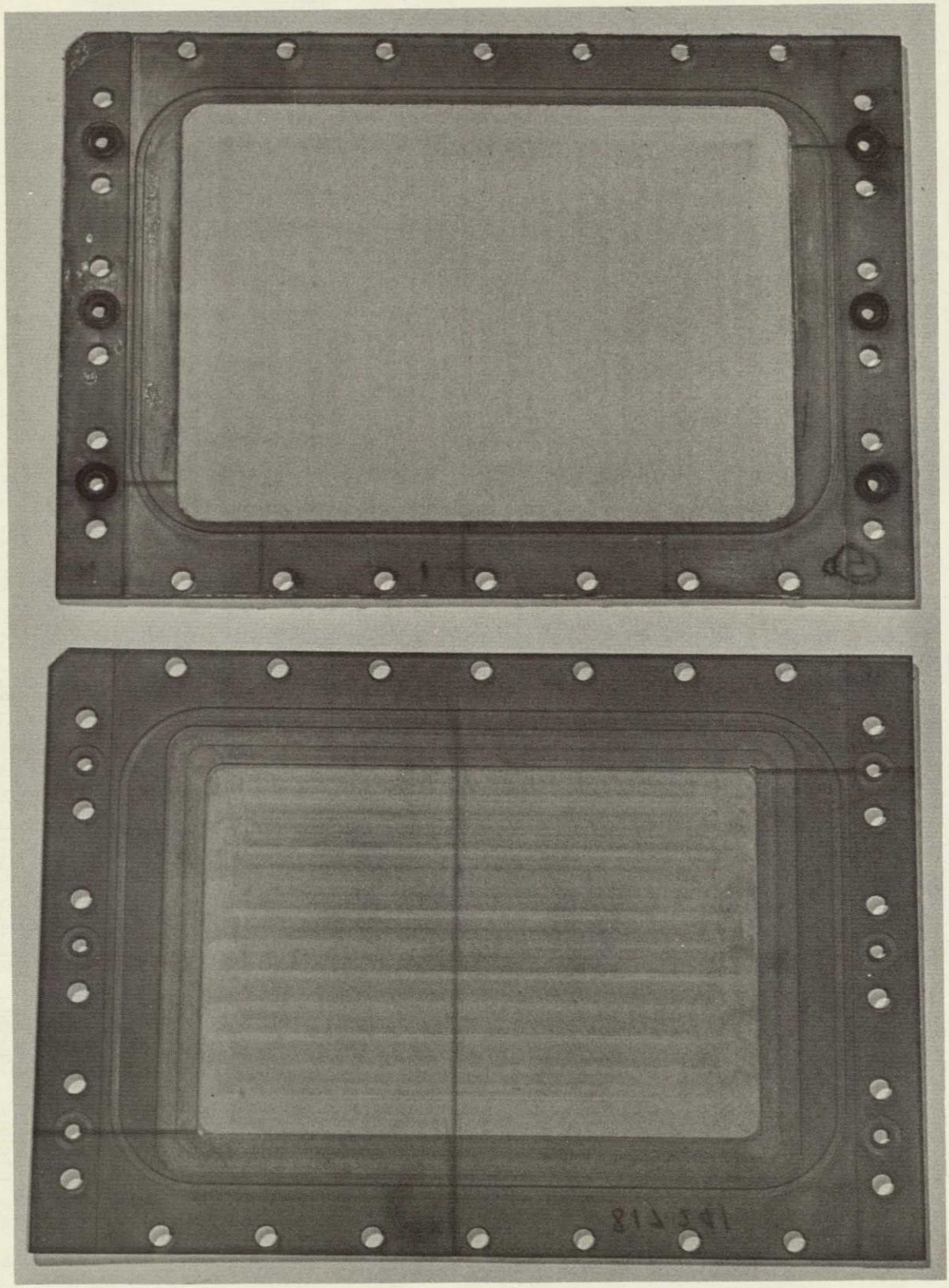

FIGURE C-8 COMPARISON OF NEW VERSUS WEM #1 POST-LIFE TEST H_2O PLATE (CAVITY SIDE)

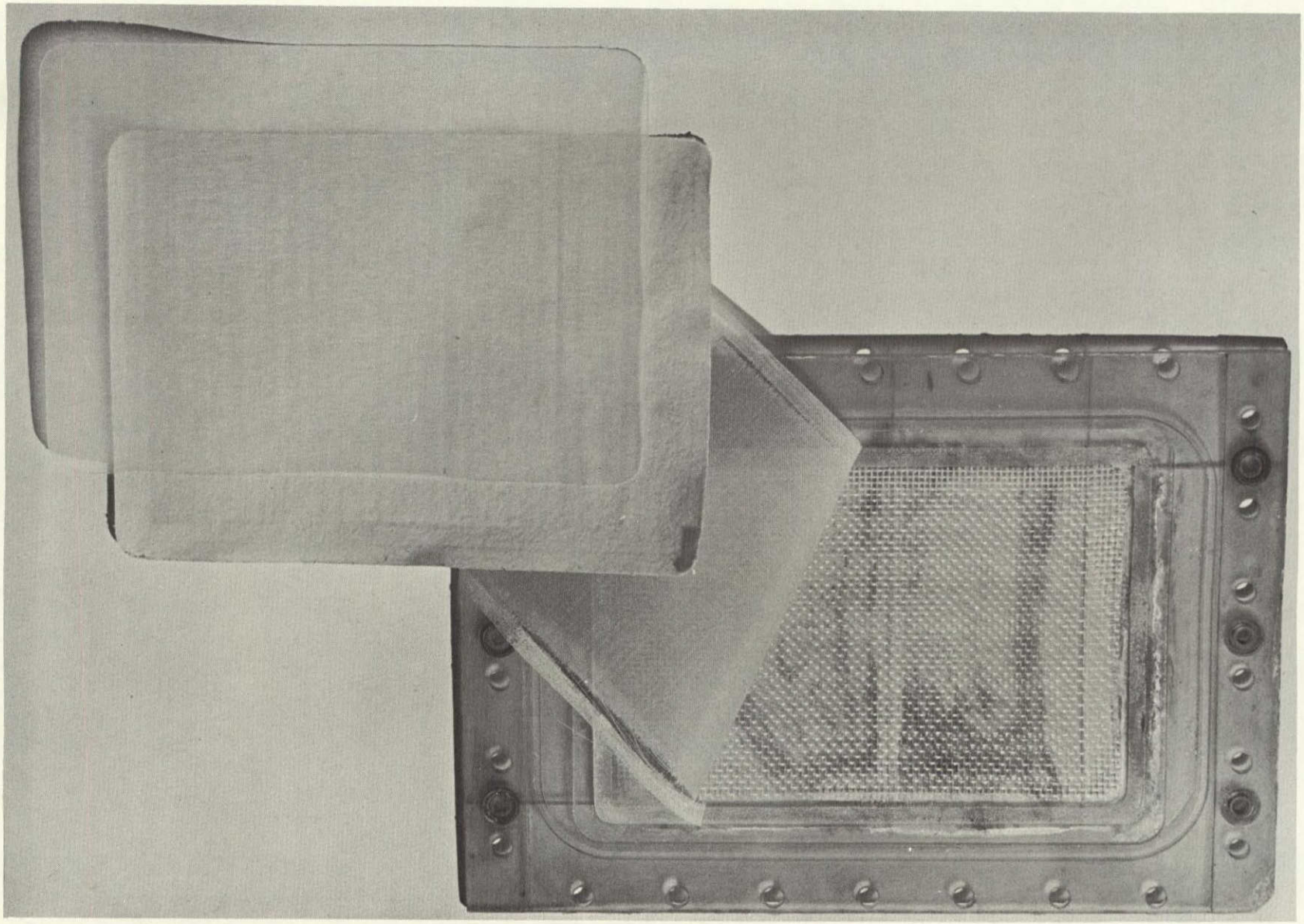

FIGURE C-9 WEM #1 H_2O PLATE SUBASSEMBLY COMPONENTS - POST-LIFE TEST CONDITION

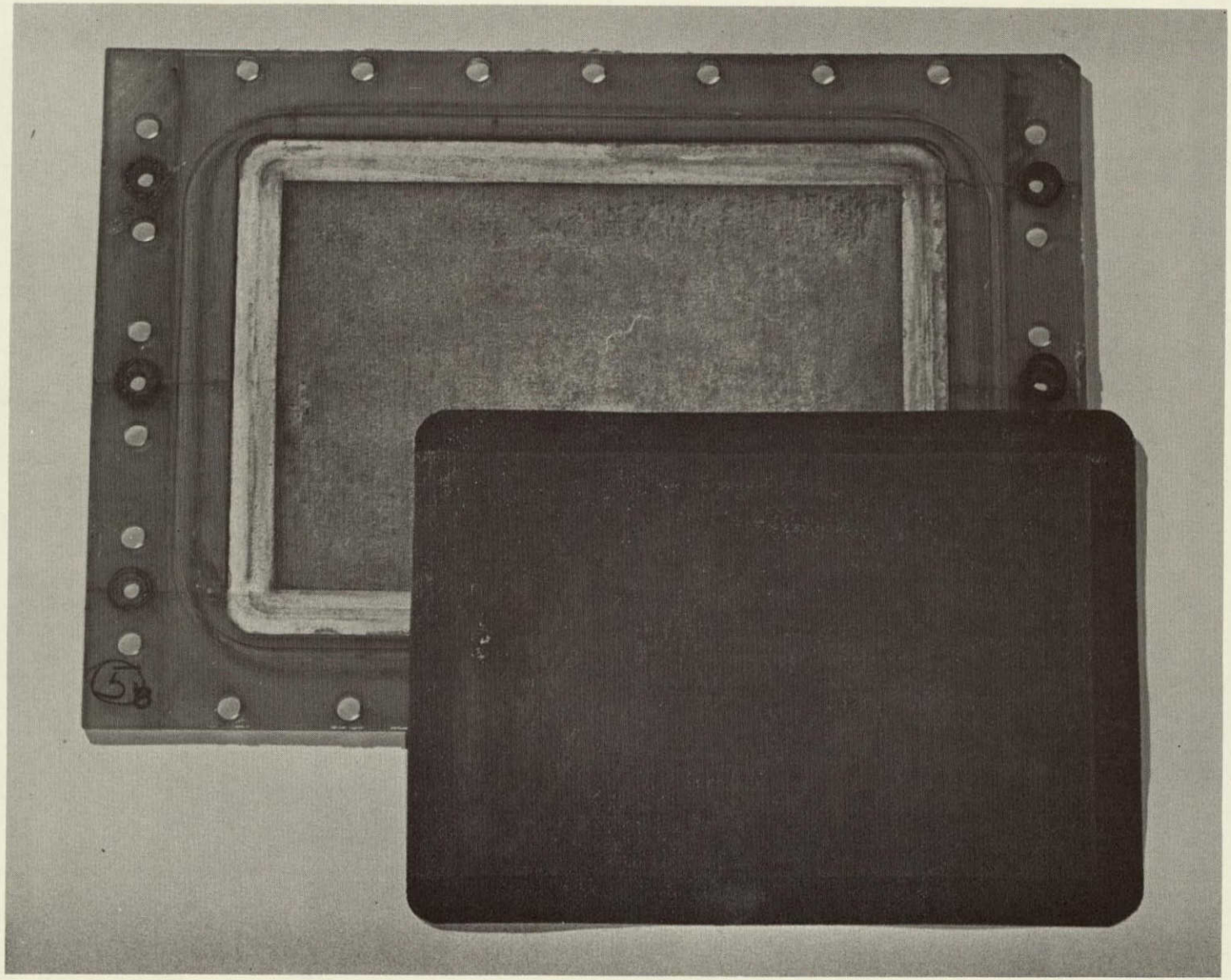

FIGURE C-10 WEM #1 HYDROGEN ELECTRODE MATRIX INTERFACE (TYPICAL POST-LIFE TEST CONDITION)

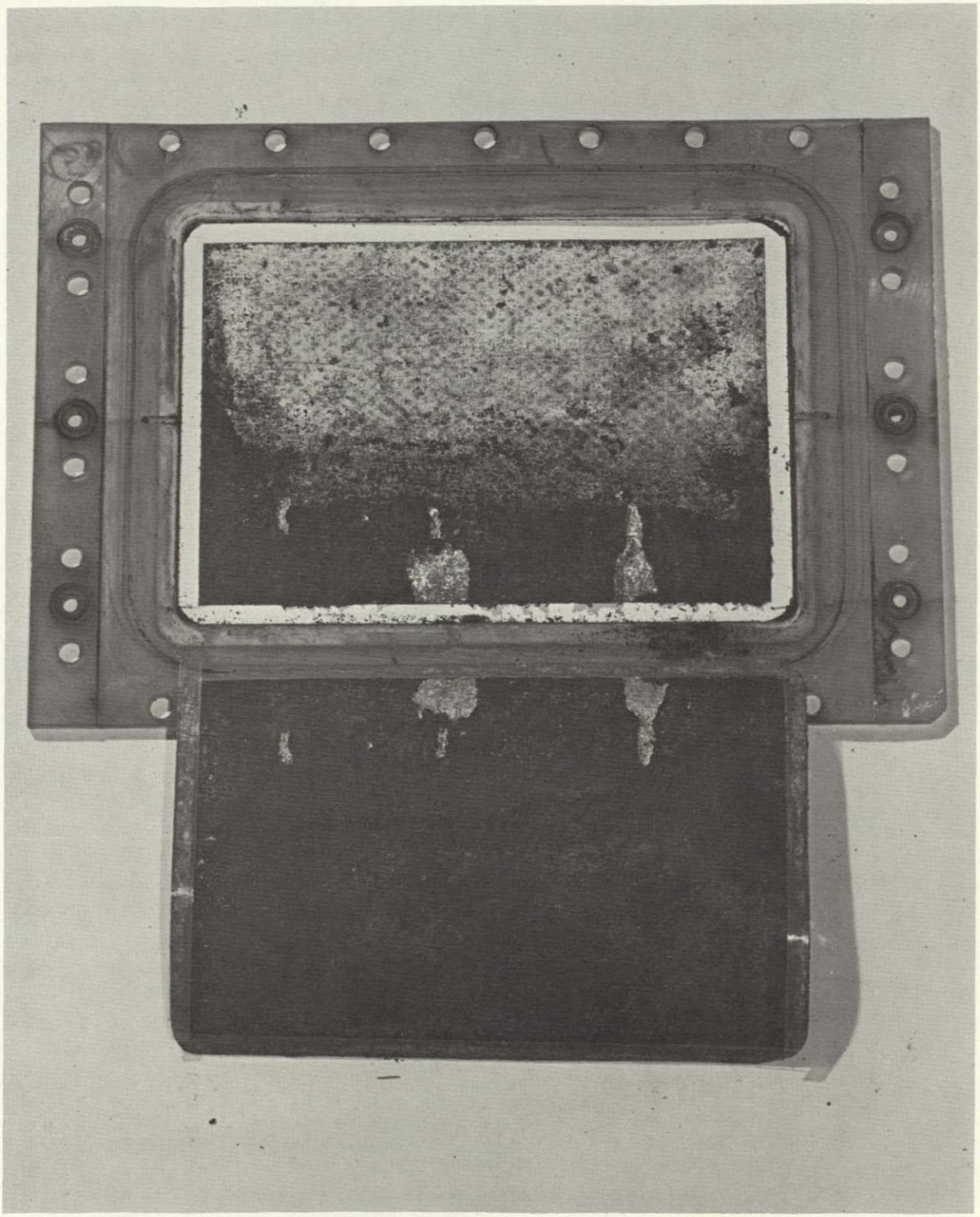

FIGURE C-11 WEM #1 OXYGEN ELECTRODE MATRIX INTERFACE
(TYPICAL POST-LIFE TEST CONDITION)

2333D

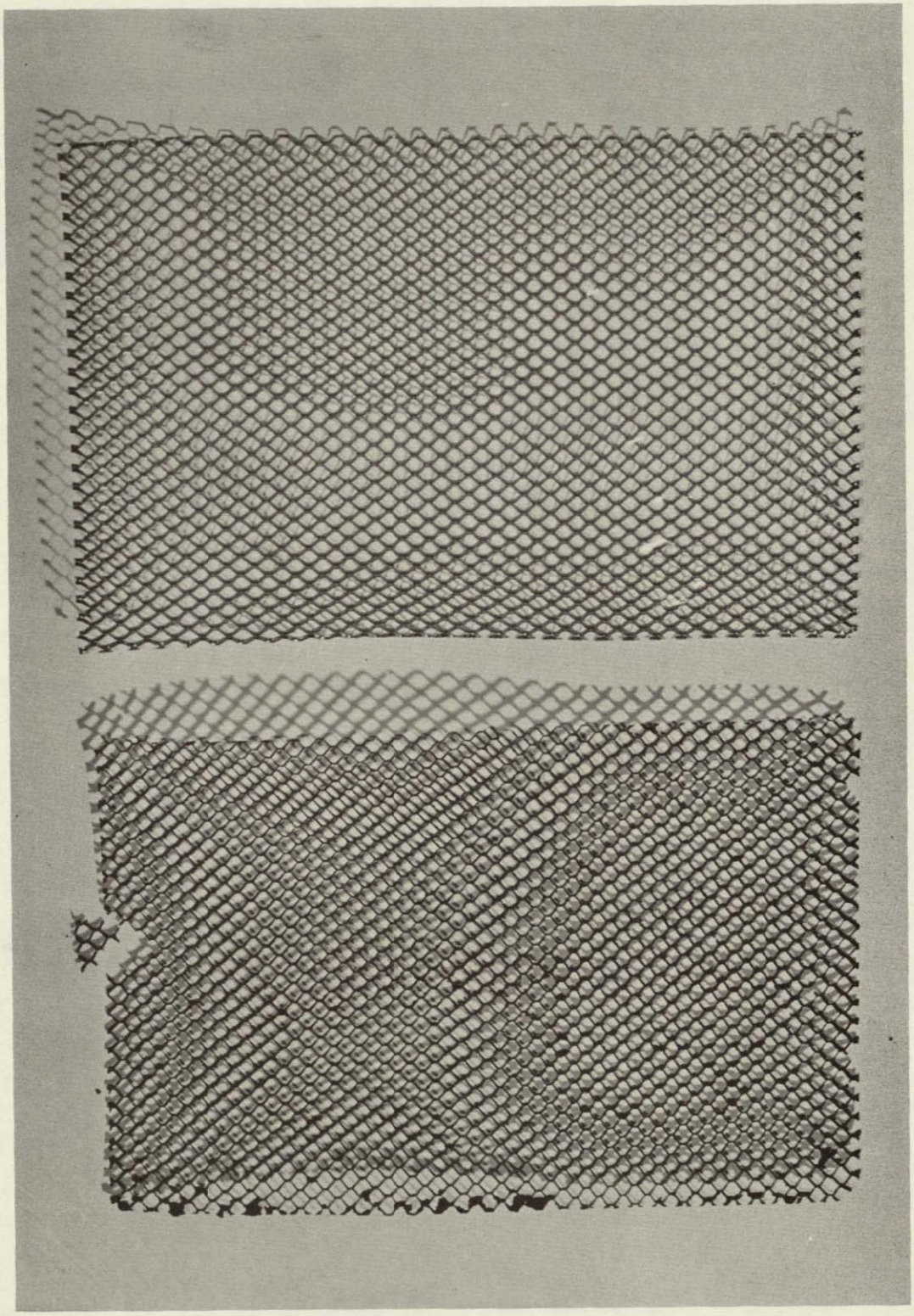

FIGURE C-12 COMPARISON OF NEW VERSUS WEM #1 POST-LIFE TEST OXYGEN CAVITY SPACER ELEMENT

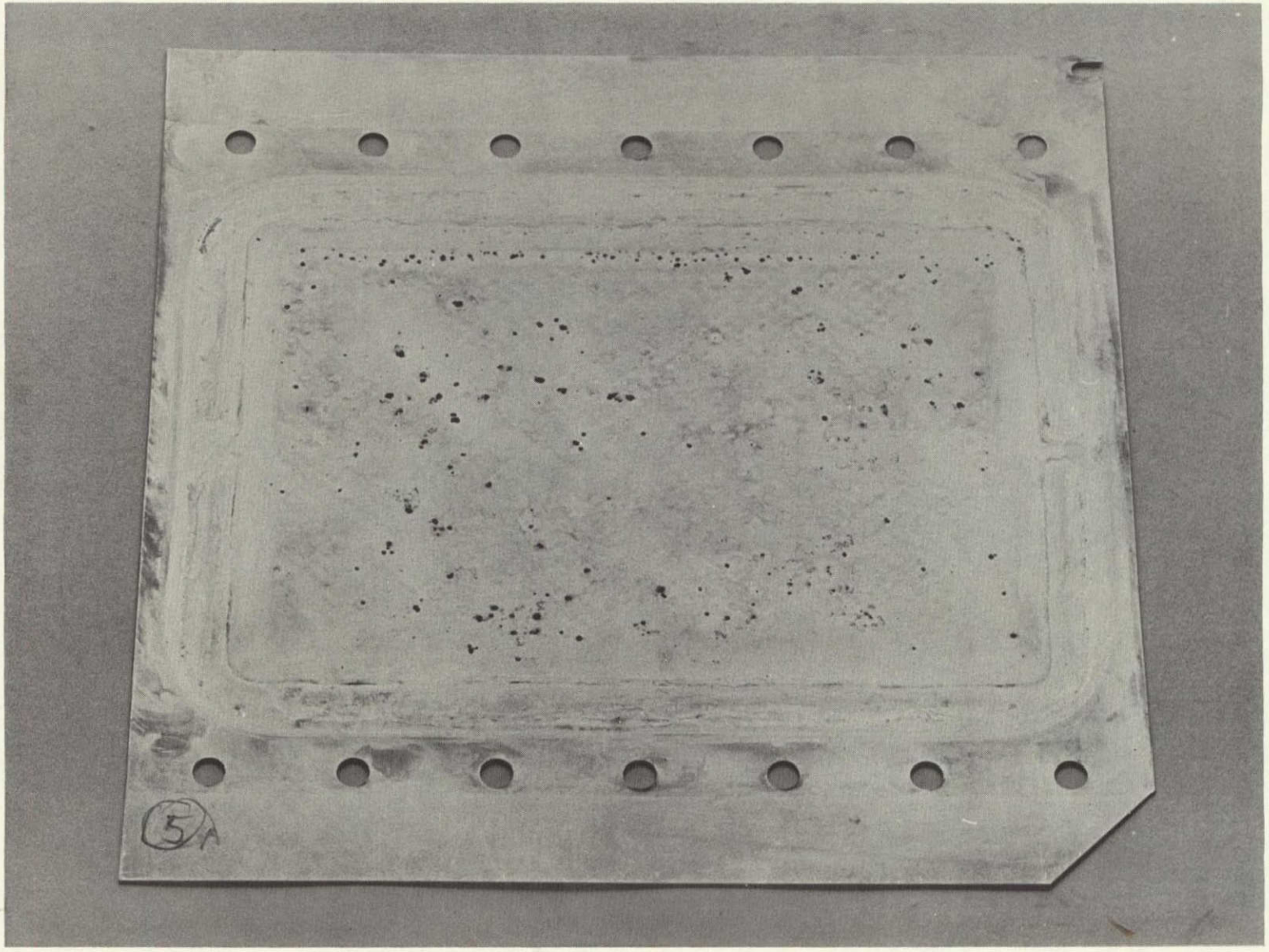

FIGURE C-13 WEM #1 PLAIN COLLECTOR PLATE APPEARANCE FOLLOWING POST-LIFE TEST CLEANING

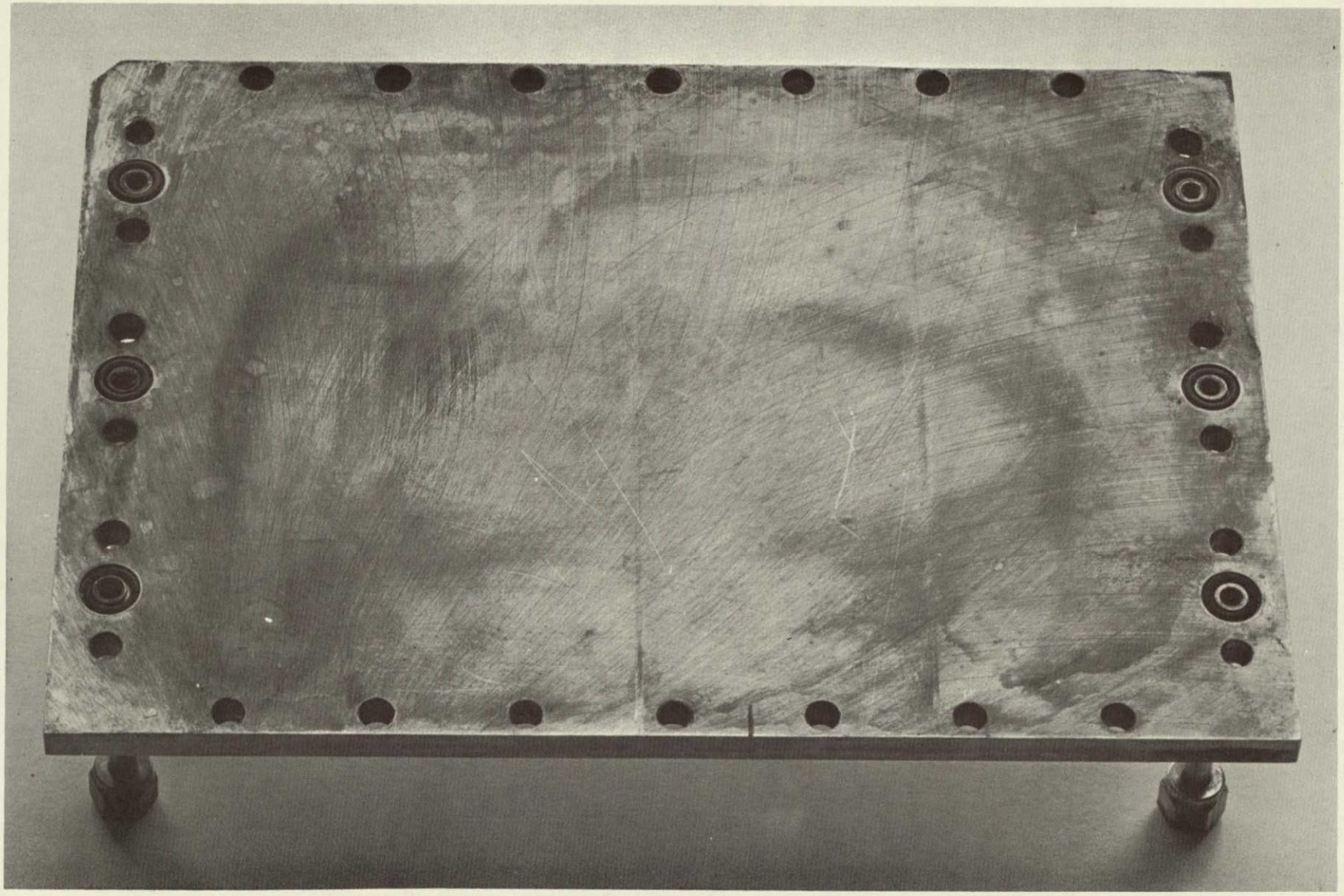

FIGURE C-14 WEM #1 STRUCTURAL ENDPLATE - POST-LIFE TEST CONDITION

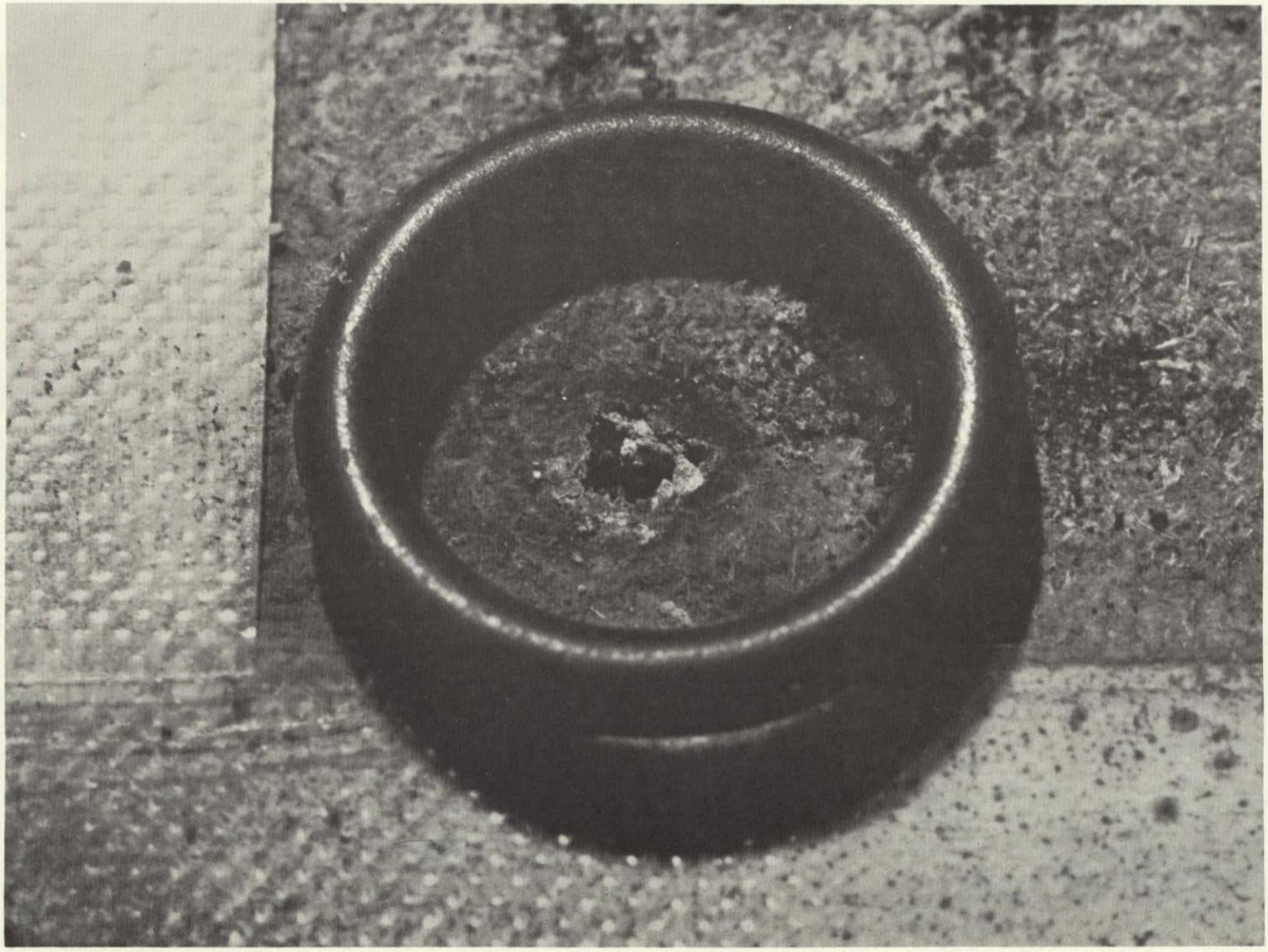

FIGURE C-15 EXPLODED VIEW - WEM #1 (CELL #1) H_2-O_2 MATRIX CROSSOVER FAILURE

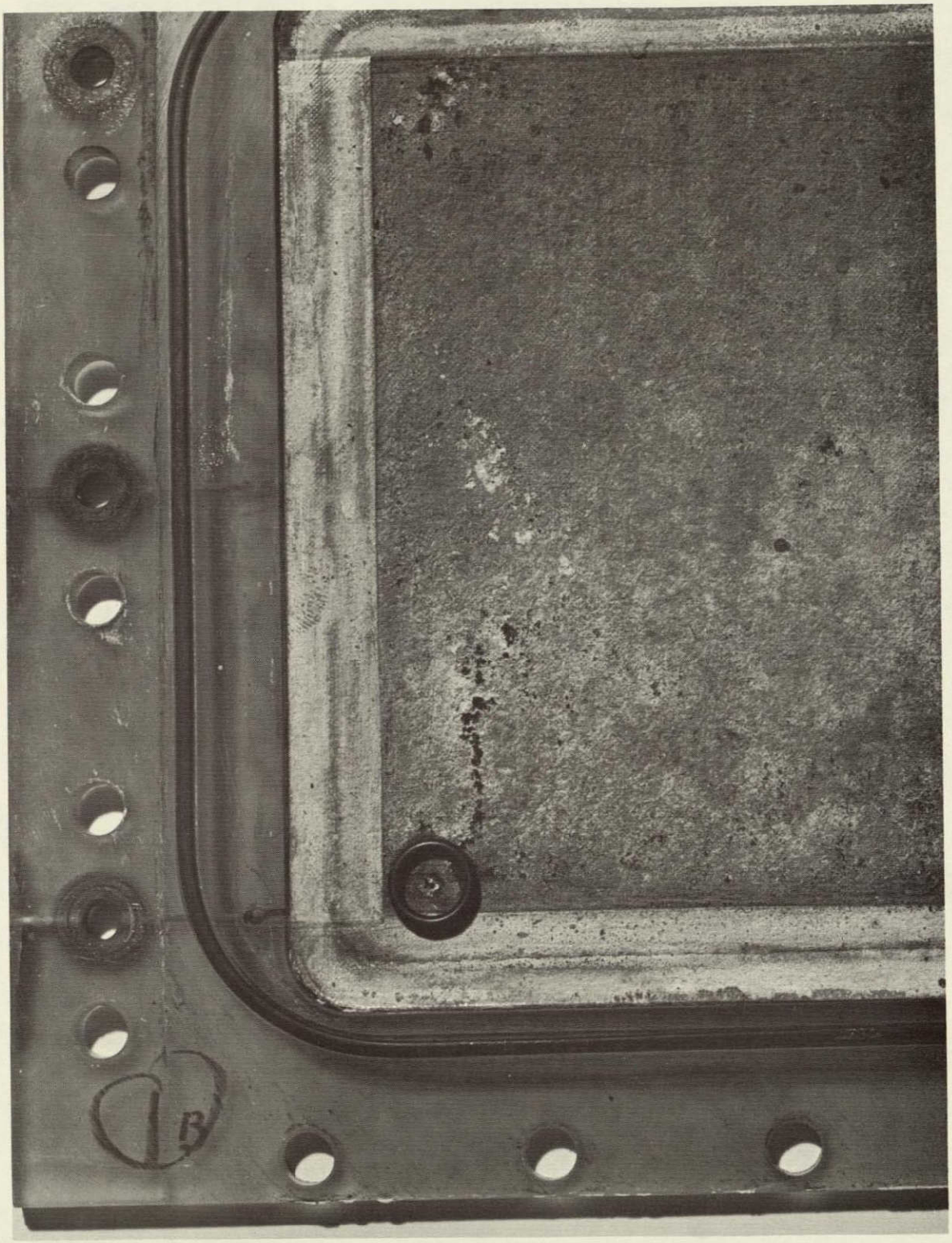

FIGURE C-16 A-16 NORMAL VIEW - WEM #1 (CELL #1)
H_2-O_2 MATRIX CROSSOVER FAILURE

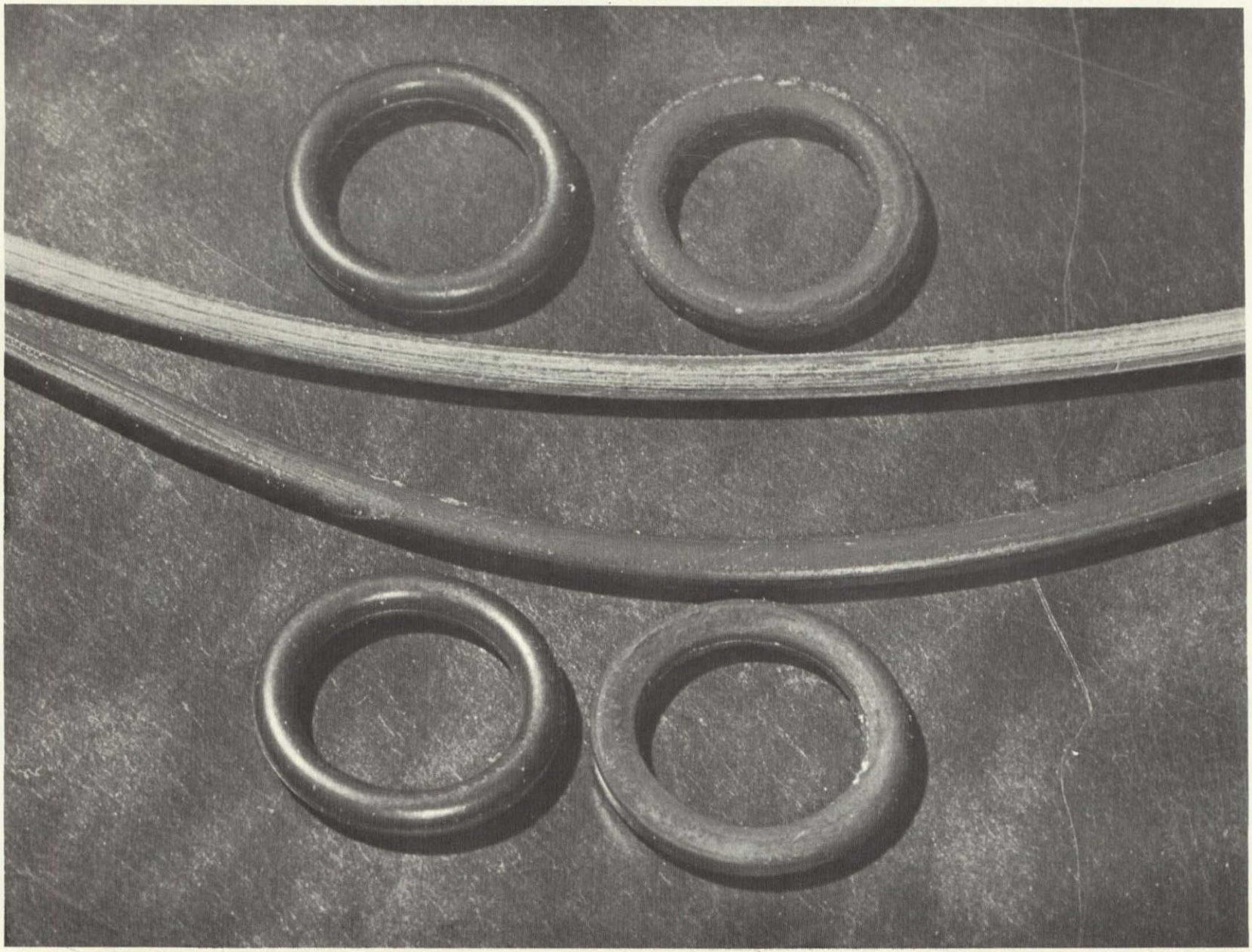

FIGURE C-17 COMPARISON - NEW VERSUS POST-LIFE TEST O-RING COMPONENTS (WEM #1)

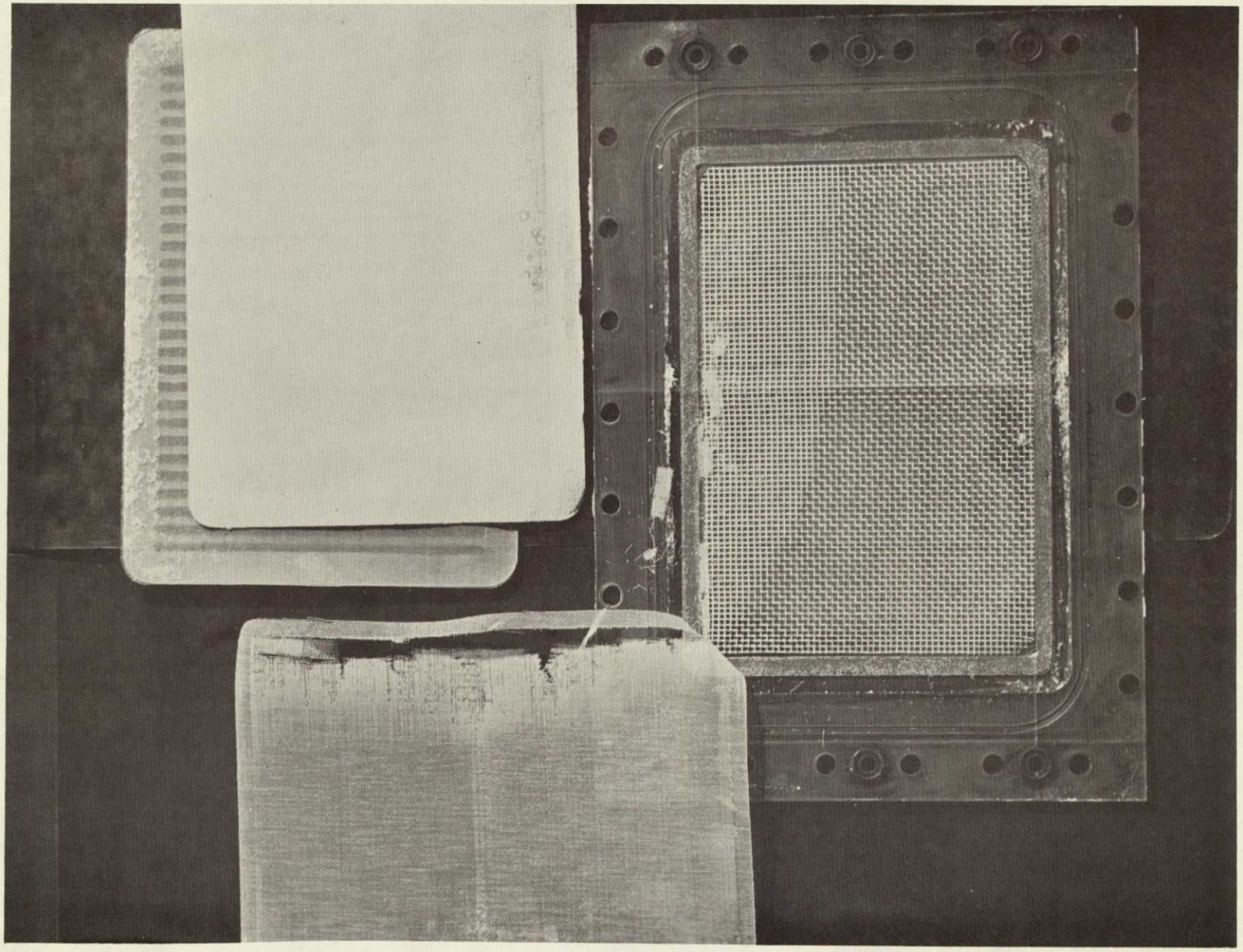

FIGURE C-19 WEM #1 (CELL #10) H_2O PLATE SUBASSEMBLY - MATRIX SUPPORT AND SPACER DAMAGE (POST-LIFE TEST)

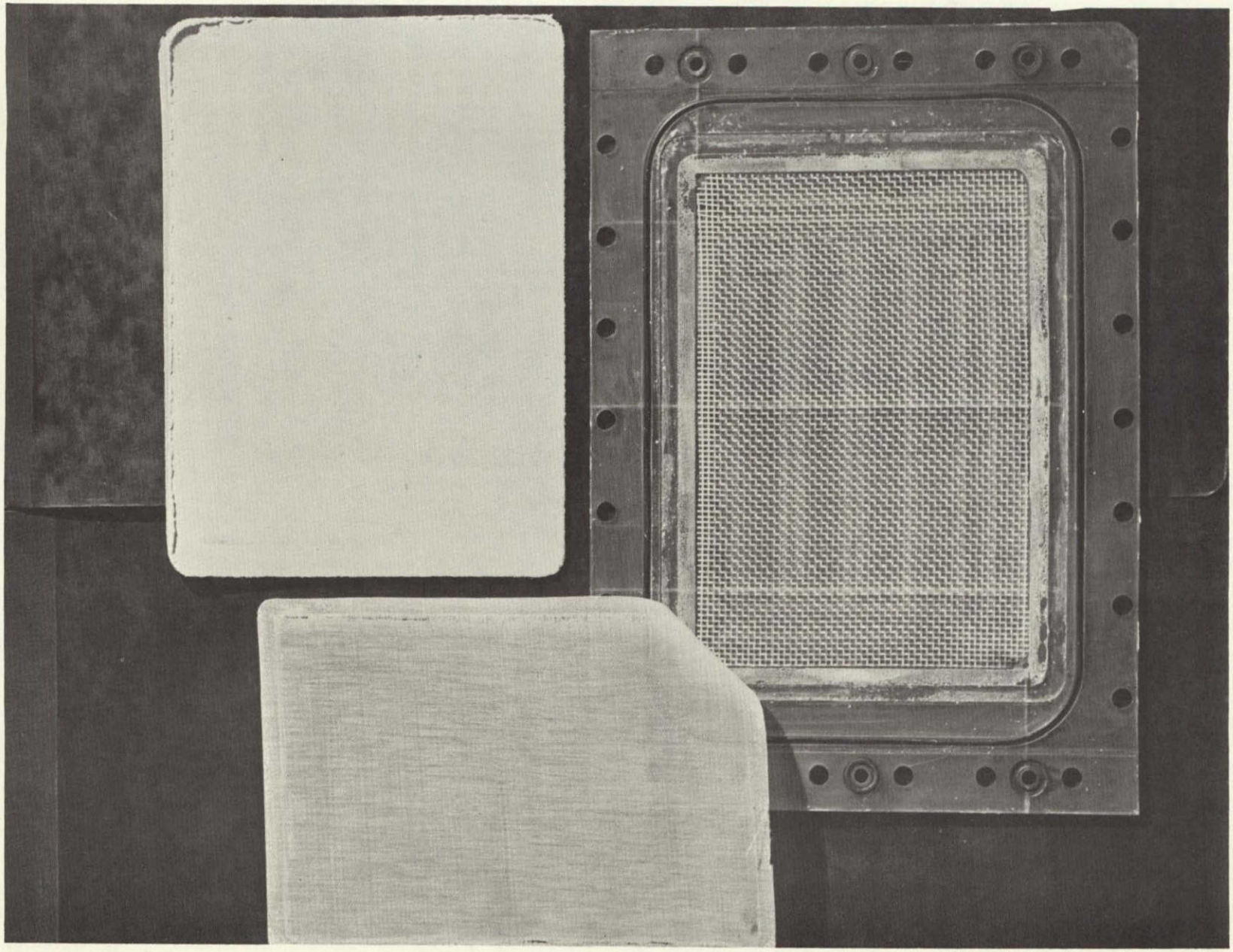

FIGURE C-18 | WEM #1 (CELL #4) H_2O PLATE SUBASSEMBLY - MATRIX SUPPORT DAMAGE (POST-LIFE TEST)

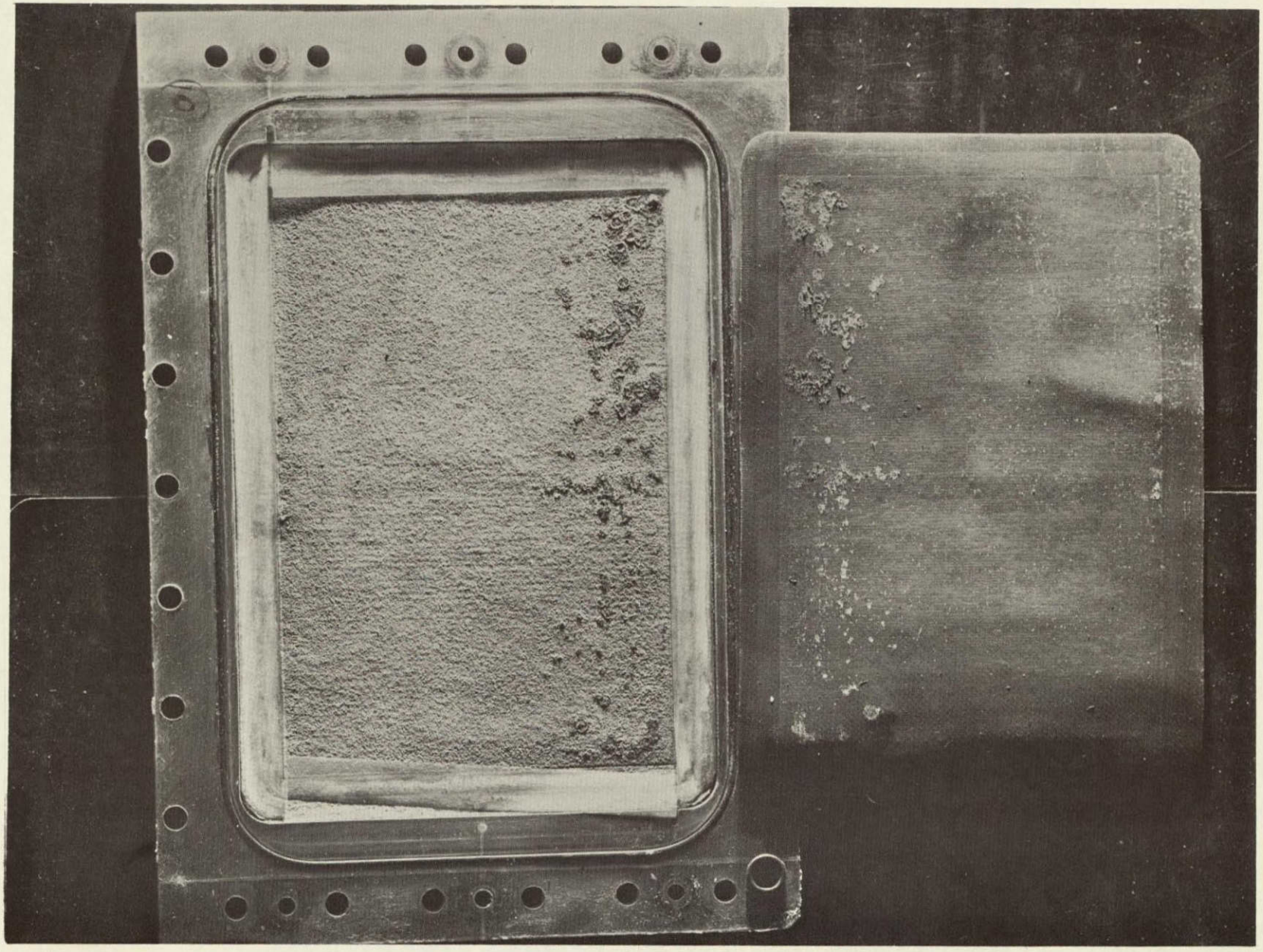

FIGURE C-20 WEM #1 (CELL #10) H_2 CAVITY - MATRIX AND ELECTRODE DAMAGE (POST-LIFE TEST)

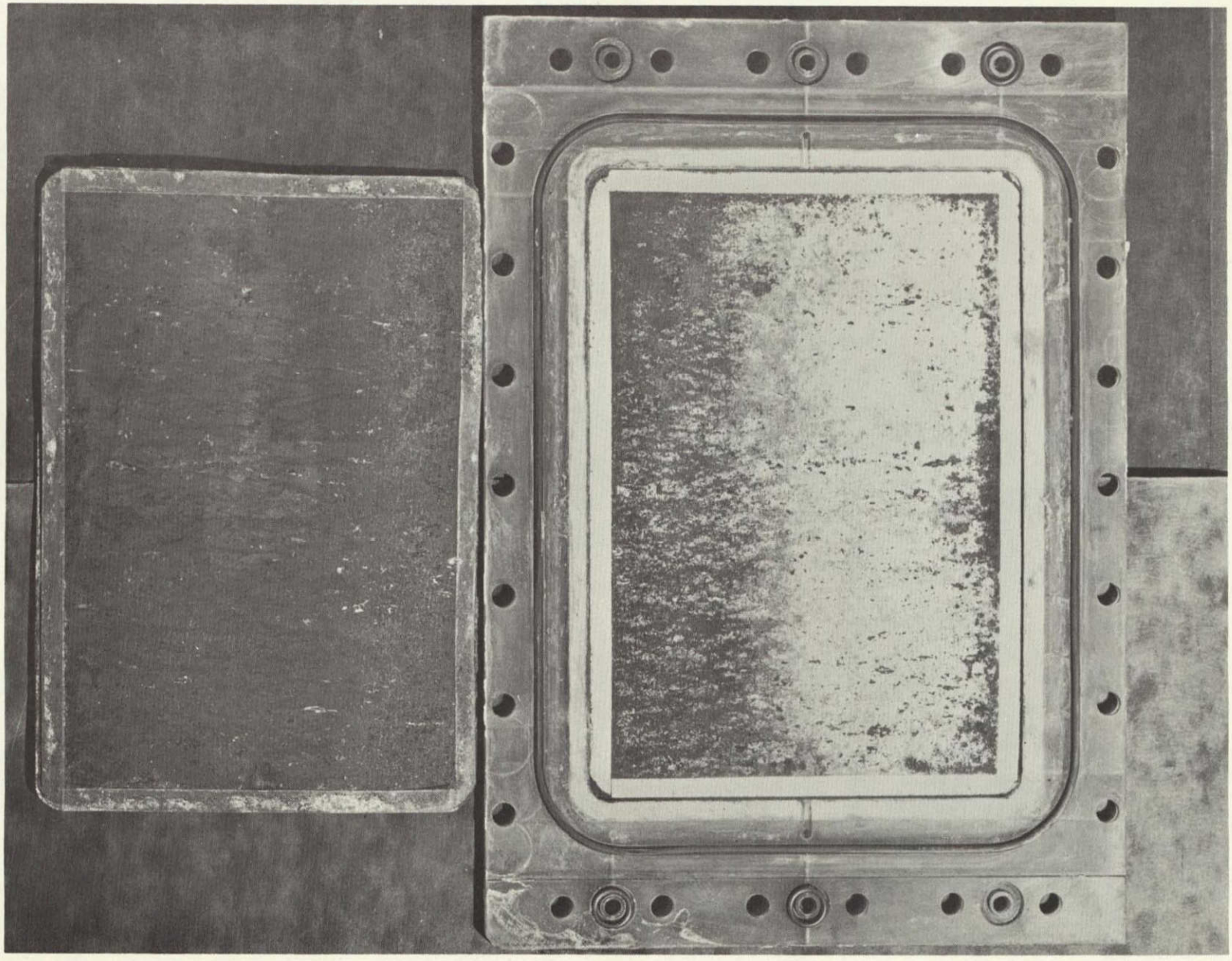

FIGURE C-21 A-21 WEM #1 (CELL #10) O_2 CAVITY - MATRIX AND ELECTRODE CORROSION (POST-LIFE TEST)

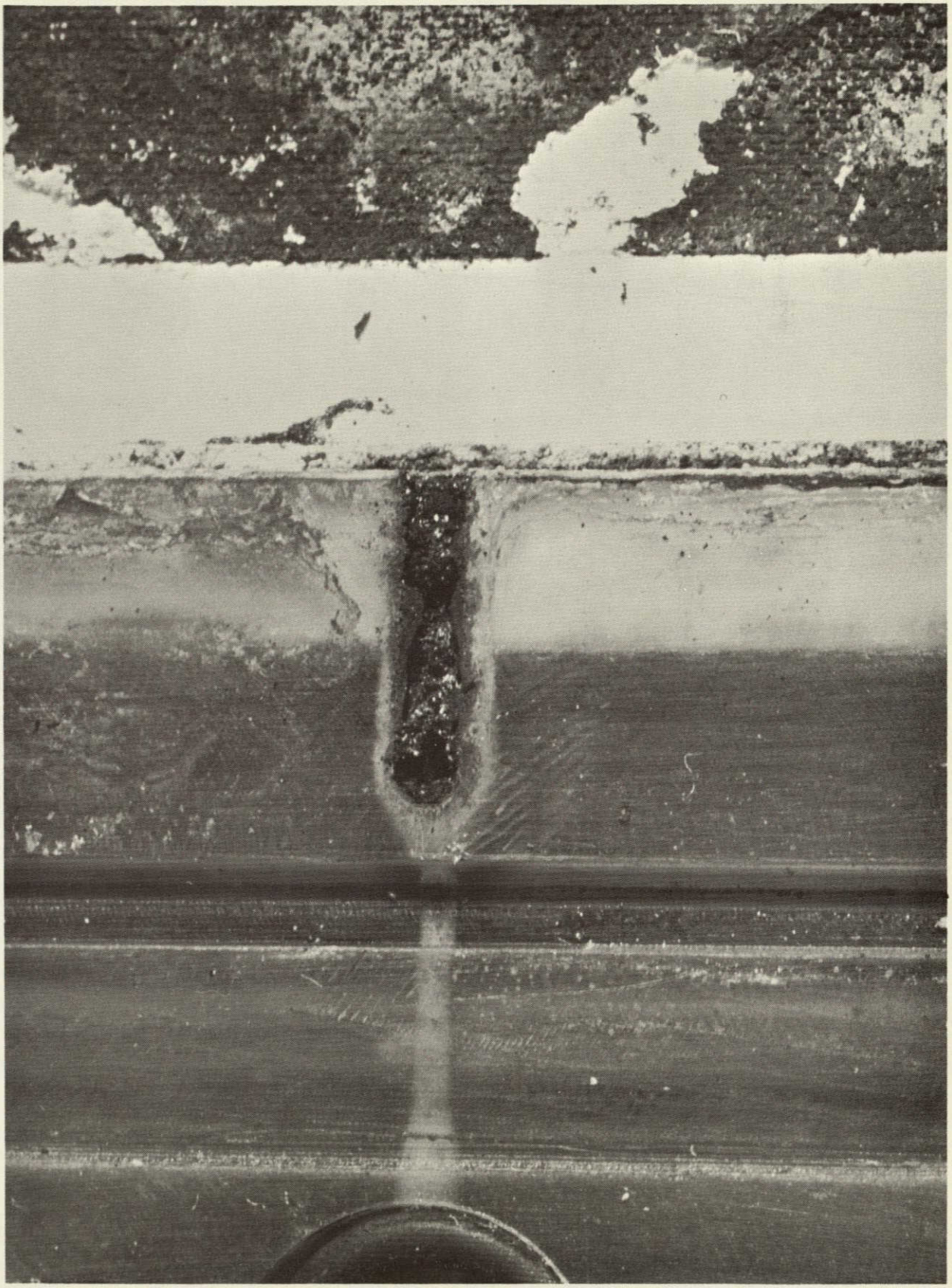

FIGURE C-22 WEM #1 (CELL #8) H_2-O_2 PLATE SUBASSEMBLY - GAS PORT DEPOSITS (POST-LIFE TEST)

2326D

TRW®

MECHANICAL PRODUCTS DIVISION